

Provenance of West Greenland Cretaceous and Paleocene sandstones and stream sediment samples based on U-Pb dating of Detrital zircon: data and results

Anders Scherstén, Martin Sønderholm & Agnete Steenfelt



GEOLOGICAL SURVEY OF DENMARK AND GREENLAND
MINISTRY OF THE ENVIRONMENT



GEUS

Provenance of West Greenland Cretaceous and Paleocene sandstones and stream sediment samples based on U-Pb dating of Detrital zircon: data and results

Anders Scherstén, Martin Sønderholm & Agnete Steinfeldt

Contents

Executive summary	4
Zircon provenance	4
Trace element in zircon	5
Stream sediments.....	5
Detrital heavy minerals	6
Whole-rock geochemistry.....	6
Introduction	7
Geological setting	8
The Nuussuaq Basin	9
Palaeogene offshore basins	12
Zircon provenance	14
Samples and methods.....	15
Heavy mineral CCSEM.....	16
Analytical techniques	17
Discordance.....	18
Data visualisation	19
Results and discussion	19
Itsaku	20
Upernivik Ø.....	22
Ikorfat.....	22
GRO#3	23
Patuut	24
Kingigtoq.....	25
Atarnikerdluk	26
Pingu.....	27
Grønne Ejland.....	27
Hellefisk-1	28
Qulleq-1	28
Summary	30
Stream sediments.....	30
Zircon trace elements	32
Heavy mineral CCSEM data.....	37
References	38
Appendix I – Cretaceous and Palaeogene samples	42
Itsaku, Svartenhuk Halvø.....	42
Upernivik.....	43
Upernivik.....	46
Ikorfat.....	50
GRO#3	51
Patuut	54
Kingigtoq, Disko.....	57
Atarnikerdluk.....	61
Pingu	64
Grønne Ejland.....	65
Hellefisk-1	66
Qulleq-1	69
Appendix II – Stream sediment samples	72
Appendix III – Standard reproducibility	118
Appendix IV – Software comparison	119
Appendix V – GIS data representattion	120

Executive summary

The extensive and very deep Jurassic/Cretaceous–Paleocene sedimentary basins offshore Disko and Nuussuaq have a significant petroleum exploration potential. At present, stratigraphic knowledge in this area is, however, almost non-existing and analogue studies from onshore areas and offshore exploration wells to the south are therefore crucial to understand the distribution and quality of possible source and reservoir rocks in the Disko–Nuussuaq offshore area. One of the main risk parameters in assessing leads in this region is the presence of an adequate reservoir rock. Tectonostratigraphic considerations suggest that several sand-prone stratigraphic levels are probably present but knowledge on their origin, regional dispersal pattern and reservoir quality is presently very little known both onshore and offshore.

A sediment provenance study including zircon provenance U-Pb dating and whole-rock geochemical analysis was therefore initiated by the Geological Survey of Denmark and Greenland with financial support from the Greenland Bureau of Minerals and Petroleum in preparation for the Disko West Licensing Round 2006. The main aim of this study is to try to:

1. Characterise the source areas and dispersal patterns for the various sandstone units of Cretaceous–Paleocene age in the Nuussuaq Basin and compare these with sandstone units in the West Greenland offshore exploration wells using advanced zircon provenance U-Pb dating (combined with preliminary zircon trace element analysis).
2. Detect possible changes in sediment source in time, e.g. local versus regional sources.
3. Investigate the quality of the various possible reservoir units using whole-rock geochemical analysis that potentially can provide information on sediment maturity, diagenetic processes, and, to a lesser extent, also provenance signatures.

Zircon provenance

Zircon provenance data has the potential to provide important constraints on sediment sources as their age distribution will reflect the ages of the eroded continental crust from which the sediments originate. It is clear from our work that zircon provenance data provide a powerful tool and, although the zircon age distributions in the sediments display a lot of similarities, significant differences have been observed.

65 samples (of which 4 were barren; 4262 zircon grains) from the Nuussuaq Basin and selected offshore wells were separated and analysed for their zircon age distribution. The results are in accordance with sediment origin from the Greenland Shield area. Exotic elements are relatively rare, which suggests that the system has received little input from distal sources. However, there are important deviations from this generalisation.

Samples from the Qulleq-1 and GRO#3 drill holes and samples from Upernivik carry Proterozoic components that appear to be exotic to West Greenland basement. This component is characterised by coupled peaks around 1.1 and 1.6 Ga. Both of these components are found in the crystalline basement in the Labradorian and Grenvillian orogenic terranes. Grenvillian (and Labradorian) rocks are known from north-western Labrador and Scotland – the latter have probably sourced the Krummedal supracrustal succession exposed in the forland of the East Greenland Caledonides. The Grenvillian component is generally absent in the analysed West Greenland samples, but where it is observed it tends to occur in the upper part of the stratigraphic sections. This suggests that this component was not sourced from reworked sediments overlying the Greenland Shield prior to rifting as we would expect it to be spatially and stratigraphically more widespread. We therefore conclude that a distal Grenvillian-Labradorian component was introduced to the

West Greenland Upper Cretaceous sediments. Notably, this component may prove to be important in understanding the sediment dispersal patterns in the basins offshore West Greenland if we can establish its origin in either the Labrador region or the East Greenland Caledonian foreland and its current spatial and temporal distribution. Further work is required to resolve these issues.

The stratigraphic results from samples collected on Itsaku on Svartenhuk Halvø illustrate the strength of zircon provenance analysis. At this locality a hiatus separates an Upper Albian to Lower Cenomanian deltaic succession (Kome and Atane Formations) from an Upper Campanian to Paleocene marine succession (?Kangilia Formation). Zircon from the Atane Formation shows distinctive Archaean and Palaeoproterozoic peaks between 3.0–2.7 Ga and 1.9 Ga, respectively. This is in accordance with the inference that these sediments formed in a delta fed from east or south-east. Zircon grains from the Kangilia Formation, on the other hand, have a unique signature represented by a single, narrow peak around 1870 Ma. This strikingly constrained distribution forms a perfect match with the 1869 ± 9 Ma date for the Prøven igneous complex situated immediately north of Svartenhuk Halvø. Although contemporaneous rocks are known from Canada to the west and may also be present beneath the Inland Ice to the north-east it, seems reasonable to infer that the sediments of the Kangilia Formation were derived from this unique source and that they are first generation sediment. Furthermore, it demonstrates a major change in the sediment transport direction in this region that may be related to a tectonic event in the basin during the Campanian.

Trace element in zircon

668 zircon grains from GRO#3, Itsaku, Upernivik, Grønne Ejland and Disko were re-analysed for their trace element composition. Trace elements substitution in zircon may be controlled by temperature or pressure and trace element characterisation of zircon populations can therefore potentially be used to separate zircon derived from different terranes that are of the same age. This method is, however, still debated and further research is therefore necessary before it can be used as a provenance tool. The results of our investigations have, however, demonstrated contrasting REE systematics between the 1870 Ma zircon populations of the Kangilia Formation at Itsaku and the regional Archaean zircon population. Although these two populations are initially identified through their age distribution contrasts, the example illustrates the potential in using zircon trace element abundances to provide additional constraints for solving provenance issues such as the origin of the Grenvillian signature from either the Canadian (Labrador) side or from East Greenland. However, much further research is required for zircon trace elements to reach its full potential.

Stream sediments

Detrital zircon grains from stream sediments were dated to obtain a relatively unbiased age map of the West Greenland basement that forms a source component benchmark for the Cretaceous and Paleocene sediments. 50 samples were selected for zircon separation. 100-200 grains were normally analysed when possible and 3928 spots gave meaningful data of which 3483 spots meets our 90% concordance criteria. The samples were divided into four subsets from their location south to north. These subsets form distinct age distributions were the southernmost area is dominated by Archaean peaks at ~2.8 and ~3.6 Ga. The ~2.8 Ga is dominated all subsets, while the 3.6 Ga peak quickly disappears. Subset two has a distinct ~1.9 Ga peak, which is present, albeit less pronounced, to the north. The overall age distribution is fitting well with those found in the Cretaceous–Paleocene sediments. Strikingly, however, the sediments typically carry all age components, which imply efficient mixing of the source components prior to sedimentation.

Detrital heavy minerals

Detrital heavy minerals were extracted and analysed for their size and compositional distribution. As with the stream sediments, this aims to create a source distribution map for provenance studies. Furthermore, these data are likely to contribute to ongoing prospecting efforts in Greenland and occasional occurrences of pyrope like garnet in some samples might be useful for diamond exploration as this mineral is an important indicator mineral for diamond source rocks.

Whole-rock geochemistry

204 whole-rock samples were analysed for their major and trace element composition. Results are difficult to interpret in a provenance sense, but a possible regional trend is southward increasing sediment maturity, and that the Atane Formation seems on average more mature than the Itilli Formation. Importantly, the Palaeogene samples from Hellefisk-1 have on average low $\text{Al}_2\text{O}_3/\text{SiO}_2$ contents (high maturity) and conforms with the hypothesis that the sediments are reworked from the Atane Formation. Furthermore, they do not appear to have significant volcanic contributions as evidenced by e.g. low Sc/Th ratios, indicating the possibility for high-quality reservoirs in the Palaeogene succession in the region.

Introduction

The extensive and very deep ?Jurassic/Cretaceous–Paleocene sedimentary basins offshore Disko and Nuussuaq have a significant petroleum exploration potential. At present, stratigraphic knowledge in this area is, however, almost non-existing and analogue studies from onshore areas and offshore exploration wells to the south are therefore crucial to understand the distribution and quality of possible source and reservoir rocks in the Disko–Nuussuaq offshore area (Figs 1, 2).

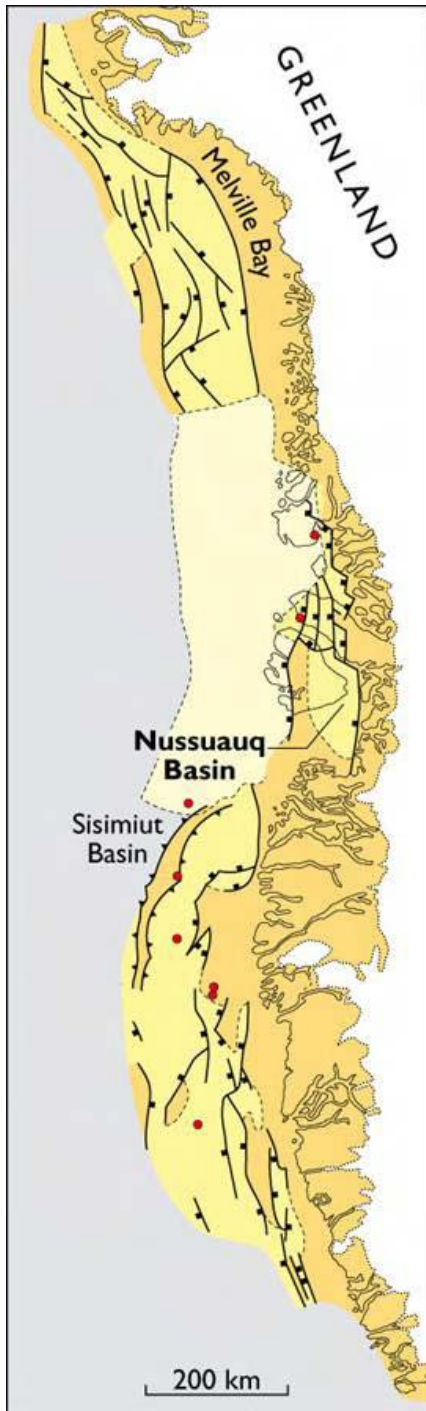


Fig. 1. Tectonic setting of the Nuussuaq Basin and other basins offshore West Greenland. **Red dots** show position of deep exploration and stratigraphic wells.

One of the main risk parameters in assessing leads in this region is the presence of an adequate reservoir rock. Tectonostratigraphic considerations suggest that several sand-prone stratigraphic levels are probably present but knowledge on their origin, regional dispersal pattern and reservoir quality is presently little known both onshore and offshore (Schiener 1975; Kirkegaard 1998a, b).

A sediment provenance study including zircon provenance U-Pb dating (combined with preliminary work on zircon trace element data) and whole-rock geochemical analysis was therefore initiated by the Geological Survey of Denmark and Greenland with financial support from the Greenland Bureau of Minerals and Petroleum in preparation for the Disko West Licensing Round 2006. The main aim of this study is to try to:

1. Characterise the source areas and dispersal patterns for the various sandstone units of Cretaceous–Paleocene age in the Nuussuaq Basin and compare these with sandstone units in the West Greenland offshore exploration wells using advanced zircon provenance U-Pb dating (combined with preliminary zircon trace element analysis).
2. Detect possible changes in sediment source in time, e.g. local versus regional sources.
3. Investigate the quality of the various possible reservoir units using whole-rock geochemical analysis that potentially can provide information on sediment maturity, diagenetic processes, and, to a lesser extent, also provenance signatures.

Geological setting

As a result of the opening of the Labrador Sea in late Mesozoic to early Cenozoic time a complex of linked rift basins stretching from the Labrador Sea to northern Baffin Bay developed along West Greenland (Fig. 1; cf. Chalmers & Pulvertaft 2001).

Two main phases of regional rifting and basin development have been documented during this time in the area; an episode of Early Cretaceous rifting, and a Late Cretaceous – Early Paleocene episode before sea-floor spreading started in mid-Paleocene time (Chalmers & Pulvertaft 2001). However, recently acquired seismic data across the Davis Strait and northern Labrador Sea combined with modelling of gravity and magnetic data have shown that deep sedimentary basins with unknown stratigraphy are widespread in the region (Chalmers *et al.* 2001), suggesting that initial rifting in the region may have occurred as early as during Jurassic or even Triassic time.

The most extensive outcrops of Mesozoic–Palaeogene rocks in the entire Labrador Sea – Davis Strait – Baffin Bay region are those of the Nuussuaq Basin in Disko – Nuussuaq – Svartenhuk Halvø area in central West Greenland (Fig. 2). The basin may be a southern extension of the basin complex in Baffin Bay – Melville Bay region (Fig. 1); the area between 68° and 73°N is, however, covered by Paleocene basalts and at present, little is therefore known about the deeper-lying successions in this region.

During the lower Paleocene (Danian) the area offshore southern West Greenland was subjected to major uplift and erosion. Sedimentation resumed in the late Danian, coevally with the major phase of Paleocene volcanism in the Disko–Nuussuaq area and continued into the Holocene with a major hiatus covering Oligocene in the north and mid-Eocene to mid-Miocene in the south (Fig. 3; Dalhoff *et al.* 2003).

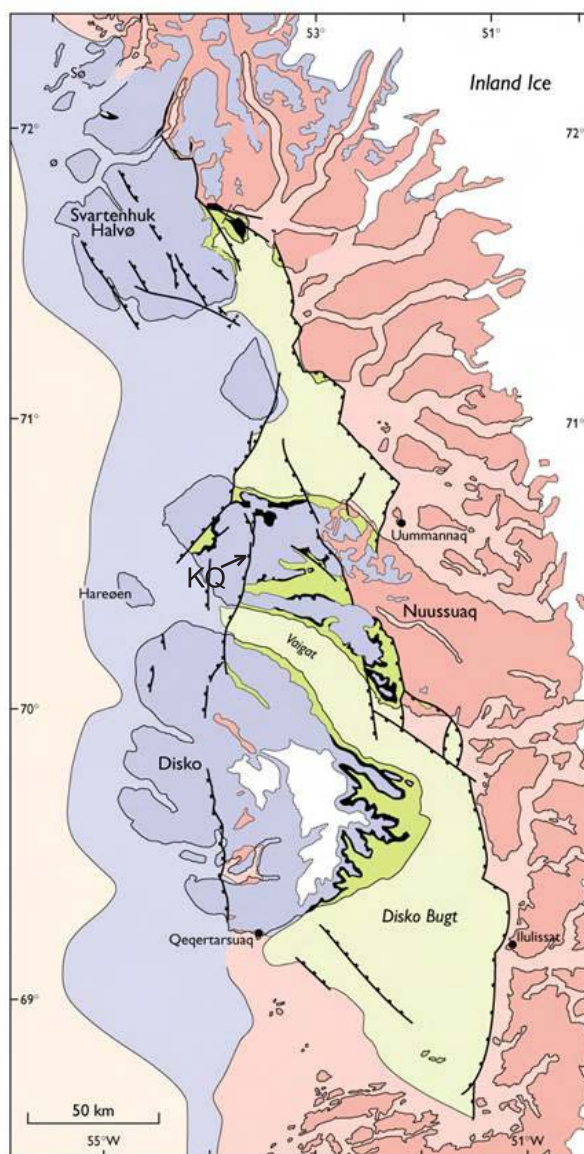


Fig. 2. Simplified geological map of the Nuussuaq Basin. **Pink:** Basement, **Green:** Cretaceous sediments, **Black:** Paleocene sediments, **Purple:** Paleocene volcanics, **Orange:** Palaeogene and Neogene sediments. **KQ:** Kuugannguaq–Qunnilik Fault.

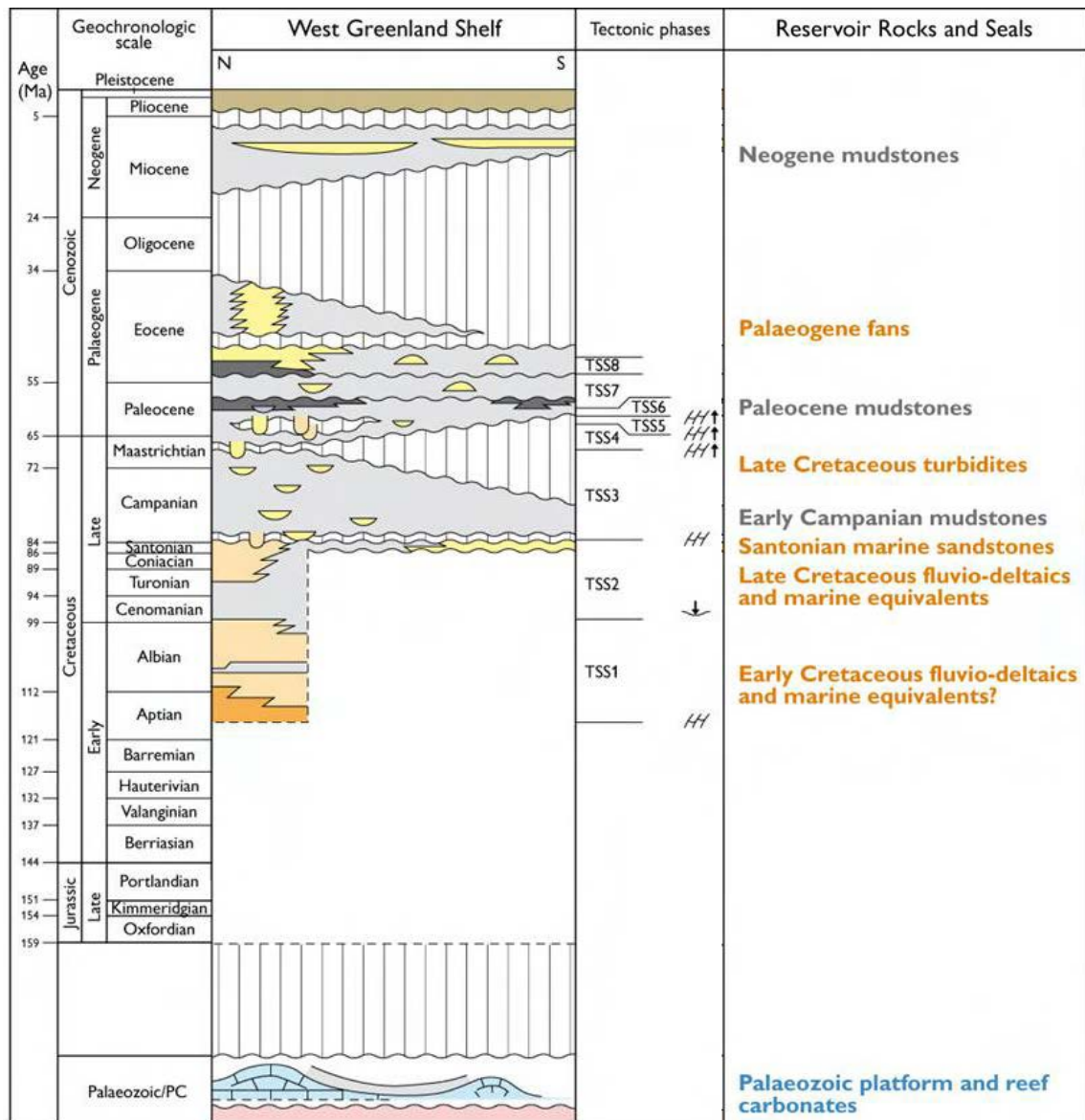


Fig. 3. Simplified stratigraphic scheme of the West Greenland basins showing tectonostratigraphic events (TSSs) recognised in the Nuussuaq Basin and related possible reservoir (orange text) and seal (grey text) units in the offshore basins.

The Nuussuaq Basin

The Cretaceous–Paleocene sedimentary succession of the Nuussuaq Basin onshore West Greenland are best known from eastern Disko and on Nuussuaq with minor, and less well known, outcrops in the northern part of the region on Qeqertarsuaq and Svartenhuk Halvø (Fig. 1, 2). The outcrops record a complex history of rifting, subsidence and uplift commencing with an earliest Cretaceous (or earlier) rift phase followed by a phase of thermal subsidence during the Cenomanian – Early Campanian. Resumed rifting began in the Early Campanian and grew in the Maastrichtian – Early Paleocene, culminating in the Early Paleocene (Fig. 3). The early of these later rift episodes was characterised by large-scale normal faulting, whereas the later episode was associated with continued extension and regional uplift (Dam & Søndersholm 1998; Chalmers *et al.* 1999; Dam *et al.* 1998a, 2000). The late phases were accompanied by widespread igneous activity and extrusion of a thick succession of flood basalts (Figs 3, 4; Pedersen *et al.* 2006, and references therein).

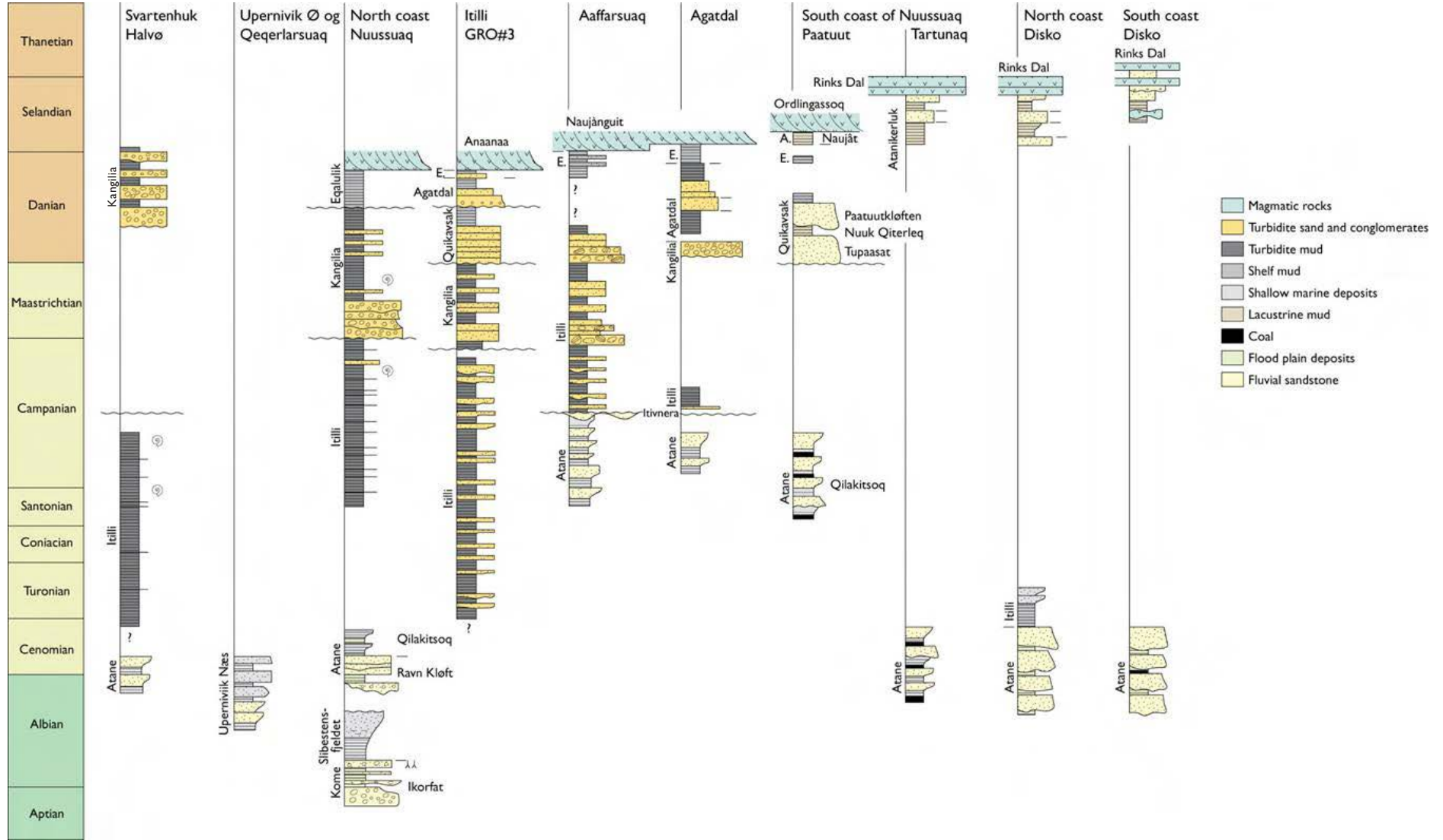


Fig. 4. Proposed lithostratigraphic scheme for the Nuussuaq Basin (after Dam *et al.* in prep.).

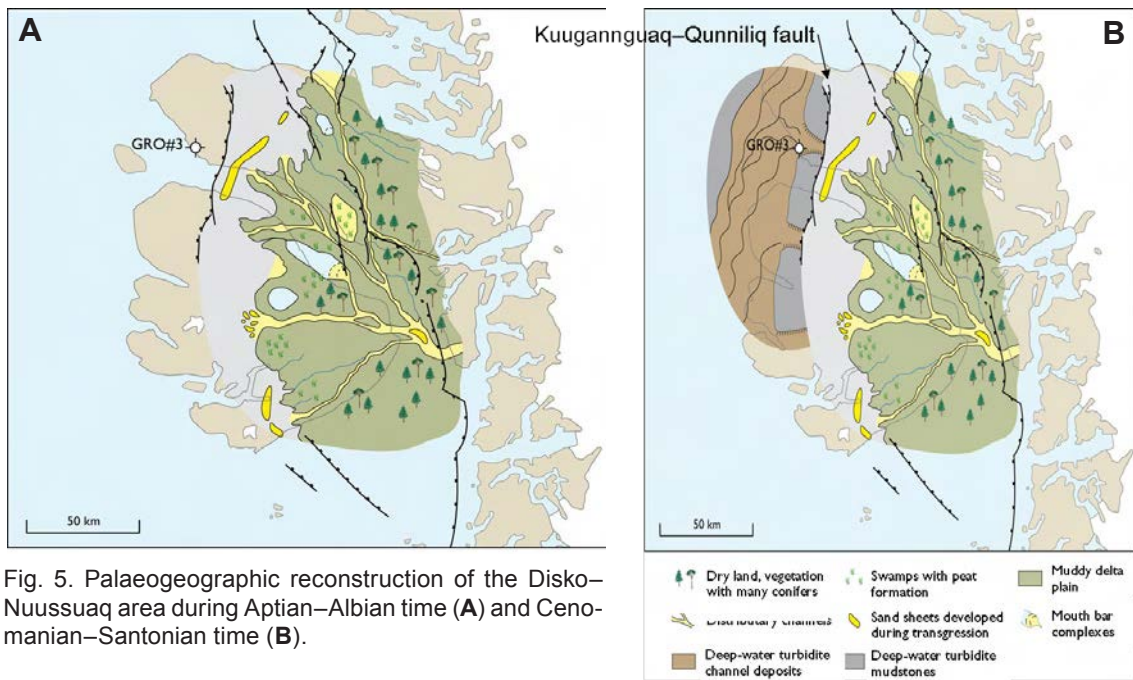


Fig. 5. Palaeogeographic reconstruction of the Disko–Nuussuaq area during Aptian–Albian time (A) and Cenomanian–Santonian time (B).

The exposed part of the succession in the Nuussuaq Basin can be divided into eight tectono-stratigraphic sequences (TSS; Fig. 3); the early rift episode includes two TSSs and the late episode six TSSs. These sequences are mainly related to tectonic events marking discrete basin-fill phases (Dam *et al.* 2006).

TSS 1. The oldest sediments exposed in the Disko–Nuussuaq Basin of TSS 1 represent a syn-rift phase of Late Albian age. It is dominated by fan-delta, wave- and fluvial dominated, shallow marine and deltaic deposits of the Kome Formation and the lower part of the Atane Formation. Locally discrete angular unconformities are present. The Kome Formation reflects local deposition controlled by basement highs, whereas the Atane Formation records deposition in a fluvial- and wave-dominated delta that fanned out to the west and north-west from a point east of Disko (Fig. 5A; Pedersen & Pulvertaft 1992). These sandstone-dominated deposits may be regionally present also in the offshore areas. It would be expected that reworking of the fluvial sandstones in the shallow marine environments occurring to the west and north-west would increase reservoir quality in these areas. The deepest parts of the Nuussuaq Basin (and the coeval offshore basins) probably contains syn-rift sediments of Jurassic (or older) age.

TSS 2. Following the initial rifting phase a long period of thermal subsidence that spans the Cenomanian/Turonian – earliest Campanian occurred (TSS 2). It is initiated with a major flooding surface represented by offshore and deep marine deposits of the Itilli Formation overlain by fluvio-deltaic deposits (upper Atane Formation). The transition from offshore and fluvio-deltaic deposition in the eastern part of the basin into deep marine deposition was controlled by the N–S trending Qunnilik–Kuugannguaq Fault crossing Disko and Nuussuaq (Fig. 5B). On Svartenhuk Halvø contemporaneous deep-water water deposition in a slope setting is recorded by a thick turbidite succession assigned to the Itilli Formation (Dam & Sønderholm 1994; Dam *et al.* 2000). This unit comprises marine anoxic shales, presumably of Cenomanian–Turonian age, that possibly are the source for the marine Itilli oil type (Dam *et al.* 1998b). Possible reservoir rocks in the offshore basins are probably related to various sand-prone, deep-water turbidite facies. Widespread turbidite sandstone bodies of regional extent may, however, not be present since no major tectonic events causing erosion and re-distribution of sediments occurred during this phase.

TSS 3. In earliest Campanian time a new tectonic episode was initiated that lasted from the Early Campanian to the Paleocene (Dam *et al.* 2000). The early phase of this rifting episode (TSS3; Aaffarsuaq Member of the Itilli Formation) that lasted into the Maastrichtian was characterised by normal faulting, subsidence and syn-rift sedimentation. It resulted in the development of an angular unconformity and deltaic deposition gave way to catastrophic deposition in a footwall fan setting along N–S trending normal faults. In the eastern part of the region uplift resulted in significant erosion of previously deposited Atane Formation deposits, and it therefore expected that turbidite sandstone bodies of regional extent are present in the deep-water facies in the offshore basins to the west. Furthermore, the provenance data suggest the presence of an axial distribution system in the basin that has a different source than the Atane delta.

In Late Maastrichtian – Early Paleocene time the stress system in the region changed and extension took place along NW–SE trending faults. Later, large-scale igneous activity and subsequent magmatic underplating, resulted in regional uplift and erosion in the Paleocene.

TSS 4–6. In the latest Maastrichtian – earliest Paleocene three major tectonic phases have been recognised, each associated with incision of valley systems and submarine canyons.

The first, latest Maastrichtian phase (TSS 4; Kangilia Formation) gave rise to incision and filling of two major NW–SE trending submarine canyons. The second phase (TSS 5; Quikavsak Formation, Tupaasat and Nuuk Qiterleq Members) took place in earliest Paleocene and was associated with major uplift of the basin and valley incision into early Paleocene fault scars. This phase was characterised by catastrophic deposition. The third phase was associated with renewed uplift, and valleys were incised into the old valley system (TSS 6; Quikavsak Formation; Paatuutkløften Member). Crossing the Kuugannguaq–Qunnilik Fault the valleys pass into a major submarine canyon system. The sandy fill of this canyon system is referred to as the Agatdalen Formation. This phase was followed by very rapid subsidence and deposition of transgressive estuarine and shoreface deposits and culminated with the extrusion of picritic hyaloclastite breccias. The recurrent phases of uplift and incision of submarine canyons and valleys in Atane Formation deposits in the eastern outcrop area resulted in major redistribution of sandstones into the deep-water environments to the west and major turbidite sandstone bodies are thus suspected to be regionally present.

TSS 7–8. Extrusion of the volcanic succession can be divided into two phases and is related to continental break-up (Pedersen *et al.* 2006, and references therein). The first phase (TSS 7) is dominated by extrusion of olivine-rich basalts and picrites (Vaigat Formation) and later by more evolved, plagioclase-phyric basalts (Maligât Formation). As the volcanic front moved towards east, large lakes were formed between the volcanic front in the west, and the cratonic crystalline basement in east, giving rise to syn-volcanic lacustrine deposits (Atanikerluk Formation). Magmatic activity in the Nuussuaq Basin resumed with an Early Eocene episode of intrusion of dyke swarms and extrusion of basalts and sparse comendite tuffs (TSS 8).

Palaeogene offshore basins

During the Palaeogene sediment input to the offshore basins south of the Disko–Nuussuaq area was predominantly from the north possibly from the major river system flowing out of central Greenland that also sourced the Nuussuaq Basin during the Cretaceous and earliest Paleocene time. Lesser amounts came from the mainland of Greenland to the east, and

minor amounts from the west. The sediments were deposited in environments that ranged from fresh-water/marginal marine to upper bathyal. Proximal environments are probably generally sand-prone. Basin-floor fans, syn-tectonic wedges and turbidite channel complexes that could act as reservoirs have been identified throughout the region (Dalhoff *et al.* 2003). Although the earliest phases of sedimentation were coeval with volcanism to the north the Palaeogene sandstones in the Hellefisk-1 well show clear affinities to the Atane Formation sandstones based on the zircon age signature. Furthermore, whole-rock geochemical data show that contribution from volcanic sources to the sandstones was negligible.

Zircon provenance

Constraining sediment provenance through detrital zircon U-Pb age dating is well established and highly successful (Fedó *et al.* 2003 and references within). An important breakthrough is the realisation of high throughput micro-beam technologies such as ion probe or laser ablation (LA) based mass spectrometry, which enables acquisition of less biased sample suites that cover a greater area (Williams & Claesson, 1987; Jackson *et al.* 2004). LA-ICP-MS is particularly promising as it combines low cost and extraordinary speed with suitable accuracy and precision (Frei *et al.* 2006). A sample is assumed to reflect the different source components that fed the sediments, and if different sources have different age structures, their relative contribution can be assessed. In principle, their relative contribution should be reflected by their relative occurrence in the sediment, but that assumes, for example, equal relative zircon abundances in all the source rocks, that preservation of each zircon contribution is the same and that there is no sampling bias. Such assumptions are rarely possible to comply with, and the relative zircon age distribution cannot simply be inverted to represent the relative source contributions. Nevertheless, the likelihood of identifying an age component in a sample is a function of its relative presence in the population and the size of the sample (i.e. n dated zircon grains). The more zircon grains that are analysed in any given sample, the more likely that all present age components are identified. This relationship can be described as

$$P = (1-f)^n \quad (1)$$

where P is the probability for finding a single component in the population, f is the relative abundance of any given component in the population and n is the number of dated grains (Fig. 6; Dodson *et al.* 1988). However, 117 grains have to be dated for a 95% confidence level that **all** present components are identified in a worst-case population (Vermeesch 2004). We have been aiming for 100 grains or more when possible, but a number of samples yielded considerably fewer grains, or even no grains in four cases. In some cases, the available grains were generally too small to analyse for our 20-30 μm spot size.

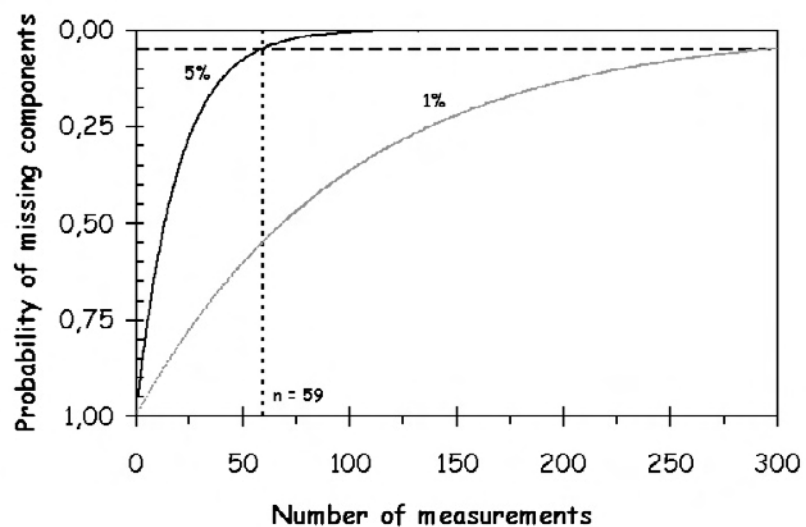


Fig. 6. The likelihood of missing a present component as a function of the number of dated grains and the frequency of the component in a detrital zircon sample (equation. 1). For a 95% confidence ($P = 0.05$) of identifying all components in a sample (horizontal dashed line), a 5% component abundance requires at least 59 grains to be dated, while a 1% component abundance requires 298 grains to be dated.

Samples and methods

65 samples have been separated for zircon. 22 of these were separated at Lund University, Sweden, according to the method described by Söderlund & Johansson (2002), which yield >90% of the zircon present in the rock. The remaining 43 samples were separated at GEUS through panning in plastic gold pans. These have a set of distinct ribbons that efficiently trap heavy minerals such as sulphides, oxides, phosphates and zircon. Oxides such as magnetite are removed with a hand magnet. The heavy mineral residue is further separated through swirling in ethanol over a strong Nd-magnet, which creates a gradient between zircon, sulphides (mainly pyrite) and phosphates (mainly apatite). Zircon is then hand picked from the final sample. The method is under development, but already yields varied populations of grains. These include variably coloured and rounded grains. Some grains maintain more euhedral shapes, which may suggest an adjacent provenance, while well-rounded grains may be derived from a more distal source. Complex multifaceted (twinning) zircon grains are also present.

Development work is under way to produce clean enough zircon samples such that the hand-picking can be excluded. The reason is two-fold, firstly, handpicking is a potential source of bias as the picker may preferentially pick large euhedral grains, which are easier to detect. Secondly, handpicking is a time consuming bottle-neck in large provenance projects such as this. Zircon separates that are clean enough to pour onto the mount will minimise picking bias and save substantial amounts of time.

The separated zircon grains are moulded into epoxy and polished to expose a central cross-section of each grain. The mount is scanned on a flatbed scanner so that individual grains can be located. Prior to loading the mount into the instrument it is cleaned in an ultrasonic bath and with ethanol to remove surface Pb contamination. The grains are analysed with GEUS' Element2 Laser-Ablation Sector Field Inductively Coupled Plasma Mass Spectrometer (LA-SF-ICP-MS), which produces accurate and precise age dates (Frei *et al.* 2006).

The laser ablation microprobe uses a focused laser to ablate a small amount of a sample contained in an air-tight sample cell. The ablated material is transferred to a mass-spectrometer in a carrier gas via Tygon[®] tubing for analysis. For the spot diameter (30 μm) and ablation times (35 s) used in this study, the ablated masses of zircon were approximately 150-300 ng.

Gerdes & Zeh (2006) and Frei *et al.* (2006) describe the analytical method in detail, but a brief summary is given here. We use a NewWave Research[®]/Merchantek[®] UP213 laser ablation unit that is equipped with a frequency quintupled ND-YAG laser, which emits a beam wavelength of 213 nm. The pulse duration is 5 ± 2 % RSD. We use a repetition rate of 10 Hz and a nominal energy output of 44 %, corresponding to a laser fluency of 8 J/cm². All data were acquired using a 30 μm diameter single spot. Samples and standards were mounted in a low-volume ablation cell specially developed for U-Pb-dating (Horstwood *et al.* 2003). Helium is used to flush the sample cell and is mixed downstream with the Ar sample gas of the mass-spectrometer, which yields a washout time < 15 s.

The ablated material is introduced into the GEUS' Element2 (ThermoFinnigan[®], Bremen) single-collector double focusing magnetic sector ICPMS, which is equipped with a fast field regulator for increased scanning speed. The total acquisition time for each analysis is 90 s of which the first 30 s are used to determine the gas blank. The instrument is tuned to give large,

stable signals for the ^{206}Pb and ^{238}U peaks, low background count rates (typically around 150 counts per second for ^{207}Pb) and low oxide production rates ($^{238}\text{U}^{16}\text{O}/^{238}\text{U}$ generally below 2.5 %). ^{202}Hg , $^{204}(\text{Pb} + \text{Hg})$, ^{206}Pb , ^{207}Pb , ^{208}Pb , ^{232}Th , ^{235}U and ^{238}U intensities were determined through peak jumping using electrostatic scanning in low resolution mode and with the magnet resting at ^{202}Hg . Each peak was determined at four slightly different masses and integrated sampling and a settling time of 1 ms for each isotope. Mass ^{202}Hg was measured to monitor the ^{204}Hg interference on ^{204}Pb where the $^{202}\text{Hg}/^{204}\text{Hg} \equiv 4.36$, which can be used to correct significant common Pb contributions. The laser induced elemental fractionation and the instrumental mass bias on measured isotopic ratios were corrected through standard-sample bracketing using the GJ-1 zircon (Jackson *et al.* 2004). Samples were analysed in sequences were an initial six standards are followed by ten samples, then three standards, followed by ten samples, three standards, and so on. The Plisovice zircon standard (Aftalion *et al.* 1989) has been used as an external reproducibility check, and yield long-term 2σ RSD precisions (n=109) of 2 %, 2.3 % and 1.1 % for the $^{206}\text{Pb}/^{238}\text{U}$, $^{207}\text{Pb}/^{235}\text{U}$ and $^{207}\text{Pb}/^{206}\text{Pb}$ ratios respectively (Frei *et al.* 2006). Cross check of the GJ-1 standard is presented in Appendix III.

The raw data is corrected for instrumental mass bias and laser-induced U-Pb fractionation through normalisation to the GJ-1 zircon using the commercially available software GLITTER and our in-house software ZIRCHRON. Data agreement is sufficient for the level of precision required here and Pb-ages plot along a one-to-one slope (Appendix IV).. Data evaluation and presentation is done in Excel spreadsheets and take advantage of IsoplotEx v. 3.0 (Ludwig 1999) and AgeDisplay (Sircombe 2004).

Heavy mineral CCSEM

Mineralogical characterization of sediments is a prerequisite for the exploration and exploitation of valuable sediment occurrences, such as heavy mineral deposits, and for the interpretation of sediment provenance and depositional environment (e.g. Morton 1985; Morton & Hallsworth 1999; Copjakova *et al.* 2005; Oszczypko & Salata 2005). Mineralogical characterization comprises two main parameters, namely mineral assemblage and chemical composition of individual mineral groups, or even individual mineral grains. Over the years, it has proven useful to focus characterization on the heavy mineral fraction (here defined as mineral grains denser than 2.8 g/cm^3) because this fraction encompasses a group of diverse minerals, reflecting a large range in source rock compositions, and because nearly all valuable mineral commodities, such as the Ti-minerals (i.e. rutile, leucosene, and ilmenite), zircon, garnet, staurolithe, monazite etc, are found in this heavy fraction.

Conventional methods of mineralogical characterization are based on the use of mineral separates obtained by size, gravity, magnetic, and/or other separation methods. The separated individual mineral fractions obtained in this fashion are then analyzed using petrography, microscopy and chemical means such as XRF or electron microprobe analysis. These methods are generally tedious, time-consuming, and labor intensive resulting in high cost. Therefore, a labor and cost efficient alternative technology for rapid mineralogical characterization of the heavy mineral fraction in sediments is highly welcome.

The chemical and physical characterization of both supra- and submicron particles by computer controlled scanning electron microscopy (CCSEM) is already commonplace in envi-

ronmental and forensic sciences, as well as for the determination of the degree of liberation of ore minerals. For example, CCSEM has been used to identify and quantify potentially health damaging particles transported airborne (e.g. Sitzmann *et al.* 1999; Powell *et al.* 2002, Laskin *et al.* 2005) and deposited in soils (Kennedy *et al.* 2002; Langmi & Watt 2003). For the characterization of gun shot residue (e.g. Lundrigan 2004) and impurities in coal (Zygarlicke & Steadman 1990, and references therein) CCSEM has become the standard off-the-shelf technology and it is widely applied in the ore industry for mineral liberation analysis (e.g. Kahn *et al.* 2002; Gu 2003).

CCSEM is a fully automated particle analysis technique for the determination of chemical and physical properties of a large number of individual particles (Lee & Kelly 1980). CCSEM enables the precise and accurate determination of the modal abundances of individual mineral fractions (e.g. ilmenite, rutile, zircon, or garnet) and their average chemical composition (as well as their compositional variation). It comes therefore as a surprise that CCSEM has not been applied in sedimentological studies that often rely on mineralogical information obtained from a large number of individual mineral particles.

Analytical techniques

All sediment samples were processed as follows: depending on the visual contents of heavy minerals, 30 to 90g of sediment was split from the bulk, dried and washed on a 45 micrometer sieve. The fraction larger than 45 micrometer was then sieved through 710-micrometer screen and the fraction between 45 and 710 micrometer was passed through a centrifuge with CHBr_3 that has a density of 2.8 g/cm^3 . For CCSEM analysis the heavy mineral fraction was mounted in epoxy using a technique developed at the Geological Survey of Denmark and Greenland (GEUS) that ensures that the overwhelming majority of the grains do not touch each other (Frei *et al.* 2005a, b). The sample mounts obtained in this fashion are subsequently cut to obtain a representative section and polished.

The sediment samples contain between 1 and 38 wt.% heavy minerals, but since most sediment bodies are strongly heterogeneous with layers and/or streaks of heavy mineral-rich sand of various thicknesses and abundances we will not discuss the absolute contents of the heavy mineral fraction in individual samples.

The basic principles of CCSEM are reported by Lee *et al.* (1980), Huggins *et al.* (1980) and Zygarlicke & Steadman (1990) and the application of CCSEM for the mineralogical characterisation of heavy mineral sands is described in more detail by Frei *et al.* (2005a, b).

For CCSEM analysis of heavy mineral sand samples, the software of the scanning electron microscope (SEM) automatically generates randomly placed back-scattered electron (BSE) images (so called "frames", with a resolution of 1024×1024 pixels and with magnifications typically ranging from 30 to 100 times) within the pre-defined limits of the sample. Subsequently, for every BSE image generated, mineral grains are segmented from the background by grey-level thresholding. The binary images are processed by a "holefill" function which fills out minor voids and cracks to simplify the images for subsequent analysis. Because all grains are embedded in a non-touching fashion, none of the de-agglomeration, segmentation, or separation processes commonly used in automated particle size analysis (usually achieved by grain erosion; e.g. Gu 2003; Kahn *et al.* 2002) are necessary, and hence the entire grain surface is used for subsequent analysis.

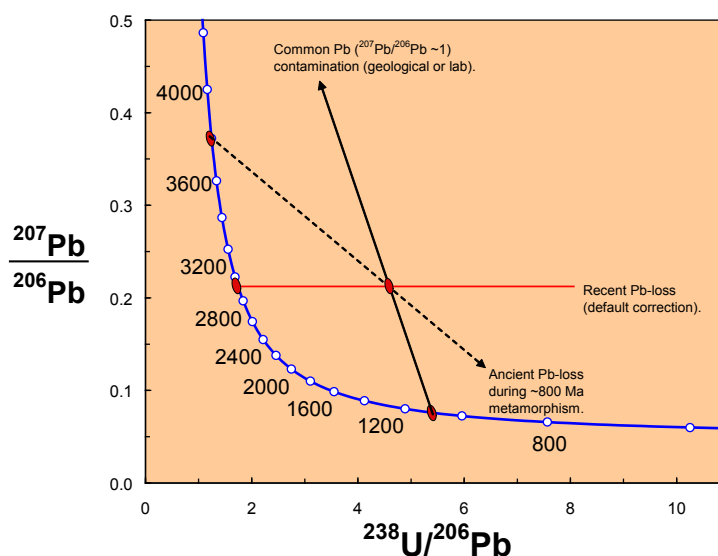
The processed binary images are utilized for the determination of grain size and shape parameters by image analysis and to control the beam for automated chemical analysis. Clusters of interconnecting pixels are recognized as individual grains and the electron beam scans across each grain for 10 seconds in order to acquire energy-dispersive X-ray (EDX) intensities for specified regions of interest. A guard region filter ensures omission of grains that are cross-cut by the margin of the generated images. For an average CCSEM session, about 64 to 100 frames per sample with 10–20 grains per frame are analyzed. Commonly > 1000 individual mineral grains per sample are analyzed in this fashion. For the purpose of this study, > 60,000 individual mineral grains have been analysed.

All data presented in this study have been acquired using a Philips XL 40 SEM equipped with a ThermoNoran System Six energy dispersive X-ray analysis system with integrated control of sample stage and electron beam. X-rays are counted on two energy dispersive X-ray detectors (ThermoNoran Pioneer and ThermoNoran Nanotrace) and count are summed up for subsequent calculation of element concentrations. The electron beam is generated using a tungsten filament operated at an accelerating voltage of 17 kV and a sample current of typically 50 to 60 μ A. The collected X-ray data are corrected for e.g. atomic number, absorption or fluorescence effects by the Proza correction scheme. Prior to analysis, all samples are carbon-coated to facilitate conductivity. Data reduction is performed using in-house developed software packages and the results are stored in a heavy mineral sands database.

Discordance

Zircon ideally incorporates U and Th but not their decay products, isotopes of Pb, into its crystal structure. Zircon that remains closed with respect to U-Th-Pb will plot along a so-called concordia curve as a function of their age. The concordia curve is characterised by increasing $^{206}\text{Pb}/^{238}\text{U}$, $^{207}\text{Pb}/^{235}\text{U}$ and $^{207}\text{Pb}/^{206}\text{Pb}$ ratios with increasing age (Fig. 7). The zircon may however, be displaced from the concordia curve through either incorporation of common Pb, through Pb-loss or mixing of different age domains. Common Pb contamination will increase the measured $^{207}\text{Pb}/^{206}\text{Pb}$ ratio, and is the easiest cause to identify, as it is associated with elevated ^{204}Pb (Fig. 7). Common Pb contamination is relatively rare and normally confined to polishing surfaces, mineral inclusions or fractures. Pb-loss or mixed age domains

Fig. 7. The Tera_Wasserburg concordia diagram illustrates three possible causes of zircon discordance, namely common Pb contamination, mixing of age domains (or ancient Pb-loss) and recent Pb-loss. A single discordant U-Pb zircon analysis is not readily interpreted as the Pb-loss history cannot be constrained through e.g. discordia trends



are more difficult to assess. A mixed age between two different age domains within a zircon grain may be avoided if all grains are examined in cathodoluminescence (CL) and backscattered electron (BSE) images, which are modulated by e.g. U and Th concentrations, which commonly vary between e.g. igneous cores and metamorphic rims. However, the penetration depth of the image is minute in comparison to the penetration of the laser beam, and a central inherited core that is not exposed at the polished surface would remain undetected in the CL or BSE images.

Ancient Pb-loss has the same effect on the zircon as do mixed ages, and the will be younger than the true age. Recent Pb-loss has no effect on the $^{207}\text{Pb}/^{206}\text{Pb}$ age and is assumed for all discordant data. Although assuming recent Pb-loss can be grossly incorrect, the $^{207}\text{Pb}/^{206}\text{Pb}$ age is a minimum age, which may sometimes be useful. The causes of discordance are several, and may vary infinitely as functions of e.g. relative proportions in mixed ages, and provide little or no useful additional information in a provenance study. We therefore use a arbitrarily chosen filtering criteria where all data that is more than $\pm 10\%$ discordant are discarded.

Data visualisation

Data are mainly presented in zircon $^{207}\text{Pb}/^{206}\text{Pb}$ age histograms, which also include a probability density distribution (Sircombe 2004) – see Appendices I, II and V. As discussed above, we filter away the data that is more than 10% discordant. We assume recent Pb-loss only in data $\leq 10\%$ discordant, and we exclusively use the $^{207}\text{Pb}/^{206}\text{Pb}$ ages, except for ages younger than 500 Ma, where we use the $^{238}\text{U}/^{206}\text{Pb}$ age. The reason for this is the small variation in $^{207}\text{Pb}/^{206}\text{Pb}$ for, which is visually evident in Fig. 7. The histograms only show the filtered data, but there are two probability density distributions (PDD; Sircombe 2004) presented in each diagram too; one dark grey that represents the filtered data and one light grey that includes all data. The PDD gives a visual impression of the likelihood of finding a zircon of a particular age within a sample. Contrary to the age histograms, the PDD takes the error of each analysis into count, which counters bin width effects, which can affect the histograms. The histograms exclusively use 100 Ma bin width for equal comparison of samples.

Visual comparison of different sample sets is useful and instructive, but a statistical test is desired to assess whether two samples are significantly different. The Kolmogorov-Smirnov (K-S) test provides a statistical method for testing if the cumulative distribution of two samples are similar or not. Importantly, the K-S test can only show if samples were not derived from the same source. K-S matrices are presented for each sample series and for selected groups. Two samples with a P-value that is < 0.05 are considered dissimilar, and thus likely to represent different sediment sources.

Results and discussion

4262 spot analyses in 65 samples yield a general trend with a strong dominance of Greenland Precambrian basement ages with peaks around 1.9, 2.5-3.2 and 3.6 Ga (Fig. 8). At face value, it seems as if there are few exotic components that were contributed to these sediments, although a small but significant Grenvillian component is present. Although there is a great deal of homogeneity between samples, there are also important differences and many samples lack one or several components, which is reflected in the K-S tests. It should

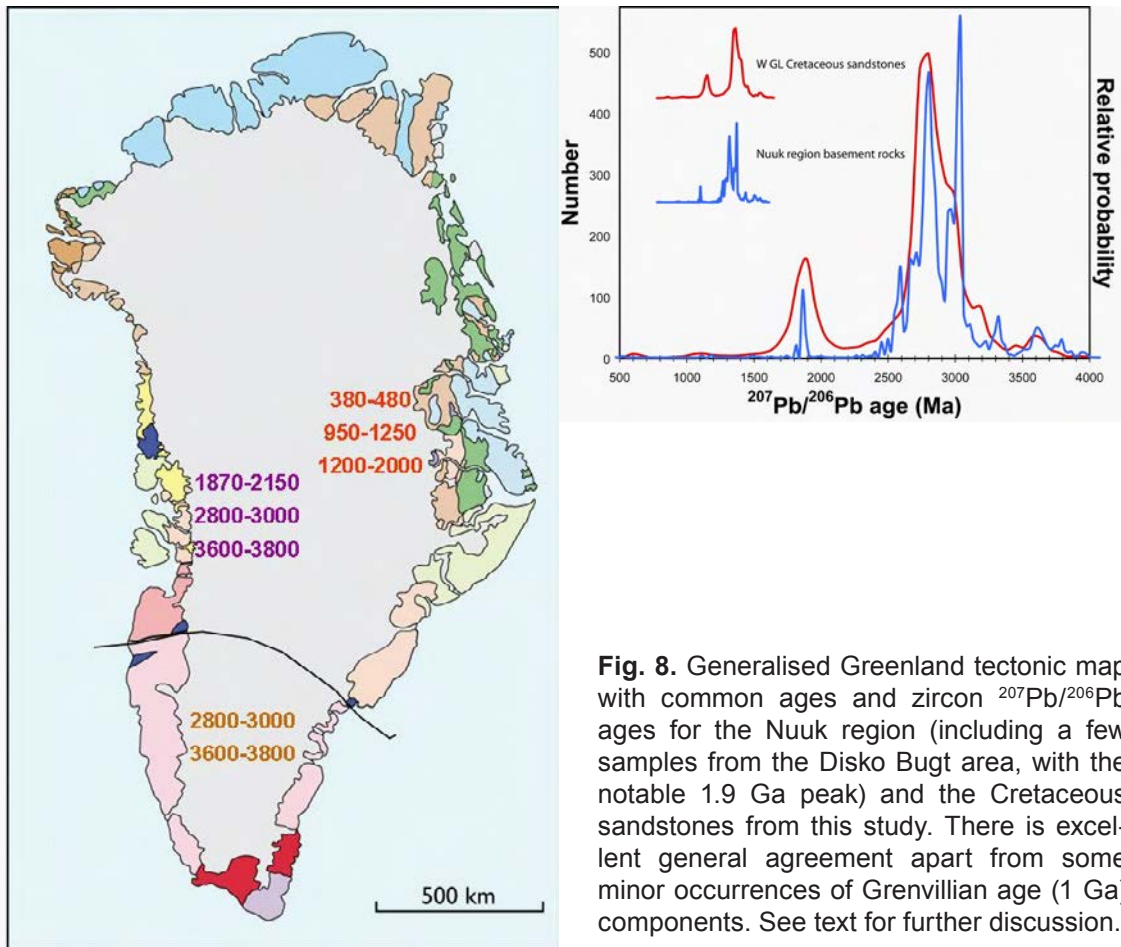


Fig. 8. Generalised Greenland tectonic map with common ages and zircon $^{207}\text{Pb}/^{206}\text{Pb}$ ages for the Nuuk region (including a few samples from the Disko Bugt area, with the notable 1.9 Ga peak) and the Cretaceous sandstones from this study. There is excellent general agreement apart from some minor occurrences of Grenvillian age (1 Ga) components. See text for further discussion.

be noted that some sample suites contain samples with few zircon grains that are <10% discordant, which may cause apparent differences as one or several components may be missed (Vermeesch 2004). In these cases, we treat the data conservatively and consider them a single population.

Itsaku

A set of 10 samples on Itsaku (Svartehuk Halvø) represent a stratigraphic column with the mid Cretaceous Kome/Atane Formation at the bottom and the Upper Cretaceous – Paleocene Kangilia Formation at the top. The two formations are separated by a hiatus. Zircon $^{207}\text{Pb}/^{206}\text{Pb}$ dates from the Kangilia Formation almost form a normal distribution, which is centred on 1870 Ma. However, it is slightly skewed and has a small tail towards Archaean ages (Fig. 9; Appendix I). Nevertheless, a source that is very homogenous with respect to zircon is required to produce such a tight distribution. The rocks of the Kome/Atane formation are in stark contrast to those of the Kangilia formation and display provenance components that include a smidge around 1 Ga, a well defined peak at 1.9 Ga and a wide Archaean palette between 2.5-3.6 Ga. The difference between the two formations is supported by the K-S test (Table 1). There are no significant differences within either formation, but they are distinctly different from each other; a conclusion that is readily drawn from their PDD profiles (Fig. 9). The Kome/Atane Formation is believed to have formed in a Mississippi style delta that was feed from southeast (Chalmers & Pulvertaft 2001). The strikingly constrained distribution of the Kangilia Formation requires a different source. In fact, the Kangilia zircon age distribution

forms a perfect match with the 1869 ± 9 Ma date for the Prøven igneous complex situated immediately north of Svartenhuk Halvø (Thrane *et al.* 2005). Although contemporaneous rocks are known from Canada to the west and may also be present beneath the Inland Ice to the north-east it, seems reasonable to infer that the sediments of the Kangilia Formation were derived from this unique source and that they are first generation sediment. Furthermore, it demonstrates a major change in the sediment transport direction from southeast to north in this region that may be related to a tectonic event in the basin during the Campanian. The Kangilia signature at Itsaku has hitherto not been found elsewhere.

Table 1. K-S P-values using error in the CDF for Itsaku sandstones

	463388	463390	463391	463392	463393	463394	463395	463397	463398	463399
463388		0.966	0.991	0.964	0.000	0.001	0.000	0.021	0.000	0.000
463390	0.966		0.285	1.000	0.000	0.000	0.000	0.000	0.000	0.000
463391	0.991	0.285		0.270	0.000	0.000	0.000	0.000	0.000	0.000
463392	0.964	1.000	0.270		0.000	0.000	0.000	0.000	0.000	0.000
463393	0.000	0.000	0.000	0.000		0.988	0.399	1.000	0.194	0.096
463394	0.001	0.000	0.000	0.000	0.988		0.599	1.000	0.262	0.271
463395	0.000	0.000	0.000	0.000	0.399	0.599		0.837	0.988	0.722
463397	0.021	0.000	0.000	0.000	1.000	1.000	0.837		0.640	0.389
463398	0.000	0.000	0.000	0.000	0.194	0.262	0.988	0.640		0.816
463399	0.000	0.000	0.000	0.000	0.096	0.271	0.722	0.389	0.816	

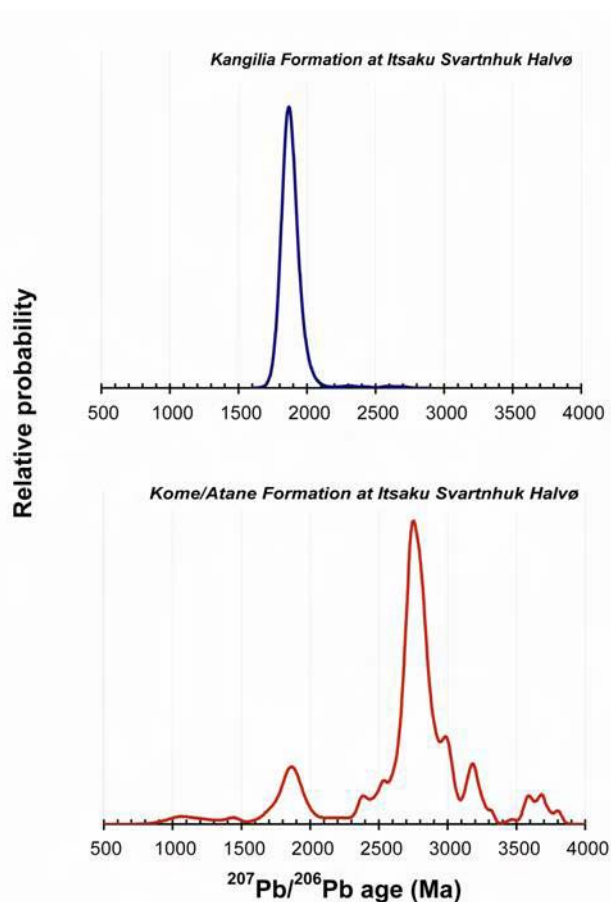


Fig. 9 Relative age distribution of zircon from the Kangilia formation (top) and Kome/Atane Formation (bottom) at Itsaku, Svartenhuk Halvø.

Upernivik Ø

Further south at Upernivik Ø, nine samples from the Upernivik Ø Formation are indistinguishable in the K-S test to the Kome/Atane Formation at Itsaku. However, an important difference to Itsaku is the presence of a peak at ~1.6 Ga. Collectively, the two peaks at ~1 and ~1.6 Ga respectively seems exotic to Greenland, while these ages are abundant in the Labradorian-Grenvillian (corresponding to Gothian-Sveconorwegian in the Baltic shield) orogens in Canada.

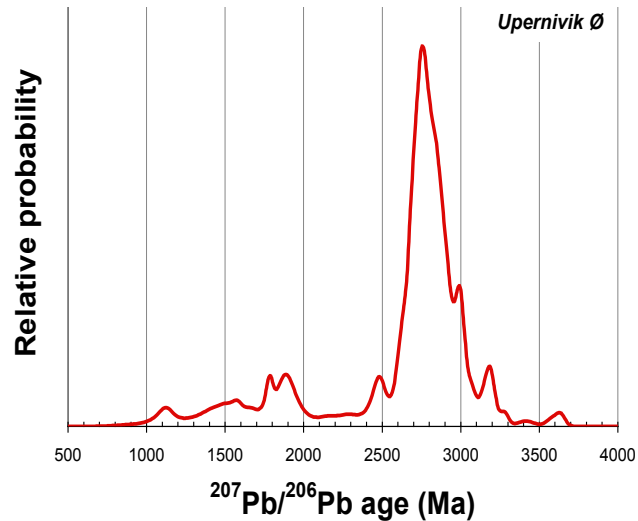


Fig. 10. Relative age distribution for Upernivik Ø. It matches well with the Kome/Atane Formation at Itsaku although Upernivik may show a slightly stronger Grenville component.

Ikorfat

A single small sample at Ikorfat only yielded 22 spots that pass the concordance criteria indicates that is dissimilar to all other suites (Fig. 11). This outcome likely stems from the slight displacement towards younger ages. However, it is premature to draw such a conclusion at this stage given the limited amount of data, and further work is required to confirm or dismiss the indication that it may represent a unique component.

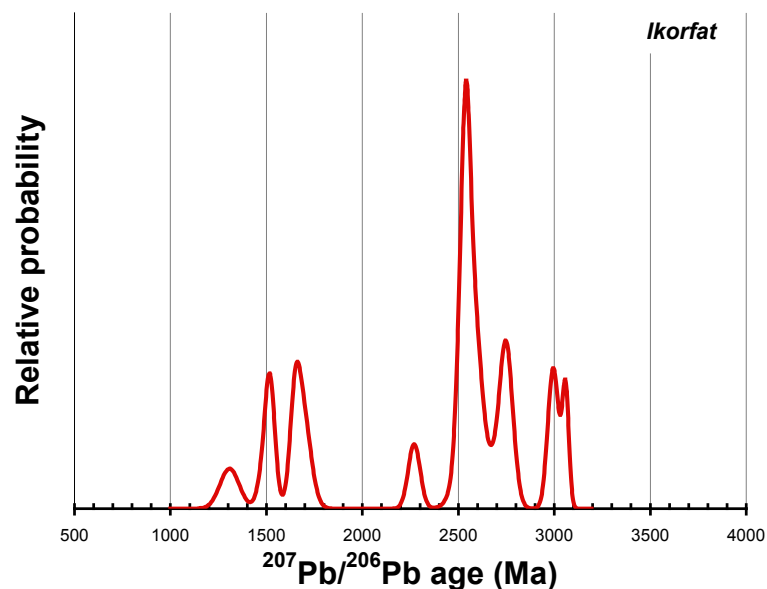


Fig. 11. Relative age distribution for Ikorfat. The K-S test yield a P-value that suggest it is dissimilar to all other sample suites. This is likely due to the relatively high abundance of late Archaean peaks. However, Ikorfat represents a small sample ($n=22$ <10% discordant data) that cautions against the validity of the conclusion.

GRO#3

The sample series at GRO#3 have been grouped according to their stratigraphic divisions; namely 2nd, 3rd, 4th and 5th sandstone units. Unfortunately a number of samples in the upper strata did not yield any zircon. None of the strata is significantly dissimilar and will be treated as a homogenous unit in the comparison with other sample suites (Table 2; Fig. 12). Like Upernivik, GRO#3 has a strong Labradorian-Grenvillian component present. It is unclear what the origin of this component is, but the fact that e.g. GRO#3 represents a deeper marine and seaward relative location may suggest an exotic origin. The component tend to be more pronounced in the upper strata of each section, which may support the exotic origin. If it was sourced from old reworked sediments, we would expect to find the component perhaps more generally admixed or more abundant in the lower strata rather than the opposite, which is observed.

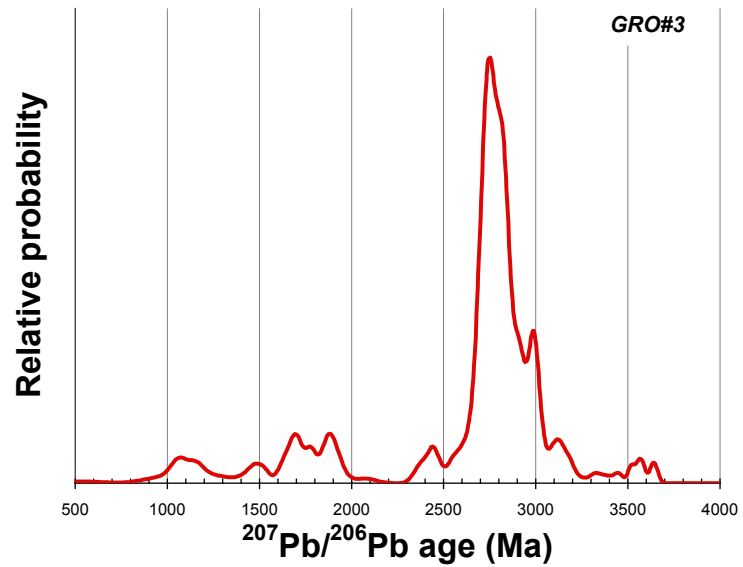


Fig. 12. Relative age distribution for GRO#3. GRO#3 has a significant Labradorian-Grenvillian component that may be of exotic origin. The four units that were examined here are indistinguishable from each other and are treated as a single group.

Table 2. K-S P-values using error in the CDF				
	2nd sst	3rd sst	4th sst	5th sst
2nd sst		0.777	0.475	0.426
3rd sst	0.777		0.914	0.646
4th sst	0.475	0.914		0.850
5th sst	0.426	0.646	0.850	

Patuut

The Patuut section runs through the Quikavsak Formation down through Atane Formation. The K-S test suggest that the two uppermost samples are dissimilar to the three in the bottom (Table 3), while sample GGU486829 is yielding good fits with all strata. A possible interpretation is that the two formations are sourcing subtly different components with an intermediate transition from one to the other. We therefore separate the upper Patuut from the lower, but assign sample GGU486829 to both groups, as it cannot be ascribed to one or the other. The Patuut samples do have some Palaeoproterozoic components, but lack Grenvillian ages (~1 Ga). It is clearly different from the Upernivik and GRO#3 sample suites, as well as the Atane Formation at Itsaku, but as we will see, similar to strata from nearby sample localities. As seen in Fig. 8, the patterns are not obviously dissimilar as the K-S test suggests, but there is a displacement of ages that seems to be significant (Fig. 13).

Table 3. K-S P-values using error in the CDF

	486827	486828	486829	486830	486831	486834
486827		0.998	0.695	0.000	0.000	0.000
486828	0.998		0.760	0.000	0.001	0.000
486829	0.695	0.760		0.387	0.675	0.638
486830	0.000	0.000	0.387		0.766	0.631
486831	0.000	0.001	0.675	0.766		0.347
486834	0.000	0.000	0.638	0.631	0.347	

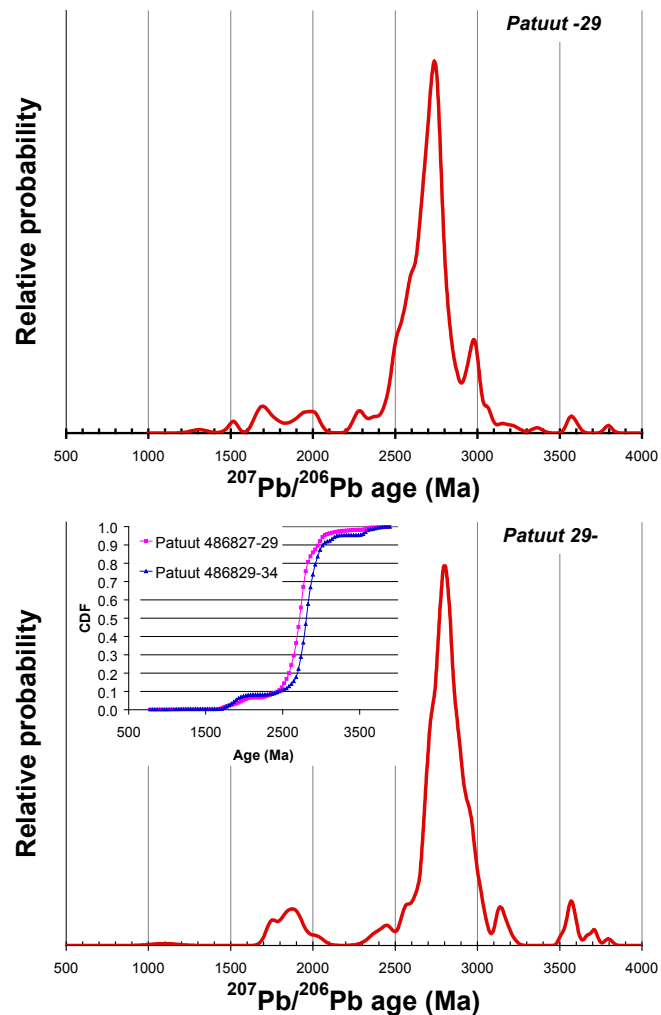


Fig. 13. Relative age distribution for Patuut. The probability density distributions are not obviously dissimilar as suggested by the K-S test. The inset cumulative distribution diagram shows that the outcome is due to a slight offset towards older ages in the lower Patuut section.

Kingigtoq

The sample suite at Kingigtoq contains a series of relatively small samples (i.e. <20 concordant $\pm 10\%$ zircon grains), and although there may be slightly different origin of some strata, we will consider them the same until there is firmer data to separate them on a fine scale. Overall the Kingigtoq sample display a typical pattern with a well defined Palaeoproterozoic peak around 1.9 Ga and a wide palette of Archaena ages, where some are lingering beyond a small peak at 3.5 Ga. The presence of Palaeo- to Eoarchaean ages is emerging as a ubiquitous component. Known outcrops of these ages are mainly known in the Isua-Nuuk region considerably farther south. Although Isua-Nuuk cannot be ruled out as the source of these components, the frequency of the age component may suggest a more proximal source or that ≥ 3.5 Ga rocks are more common than is currently known. It is plausible that such old rocks are present under the inland ice sheet. In any case, the component is in keeping with a sediment source from east-southeast (Chalmers & Pulvertaft, 2001).

	486707	486713	486718	486722	486727	486732	486739	486746
486707		0.475	0.852	0.042	0.733	0.640	0.594	0.443
486713	0.475		0.857	0.696	0.867	0.977	1.000	0.986
486718	0.852	0.857		0.253	1.000	1.000	0.941	0.891
486722	0.042	0.696	0.253		0.084	0.232	0.820	0.461
486727	0.733	0.867	1.000	0.084		0.974	0.847	0.925
486732	0.640	0.977	1.000	0.232	0.974		0.996	0.999
486739	0.594	1.000	0.941	0.820	0.847	0.996		0.972
486746	0.443	0.986	0.891	0.461	0.925	0.999	0.972	

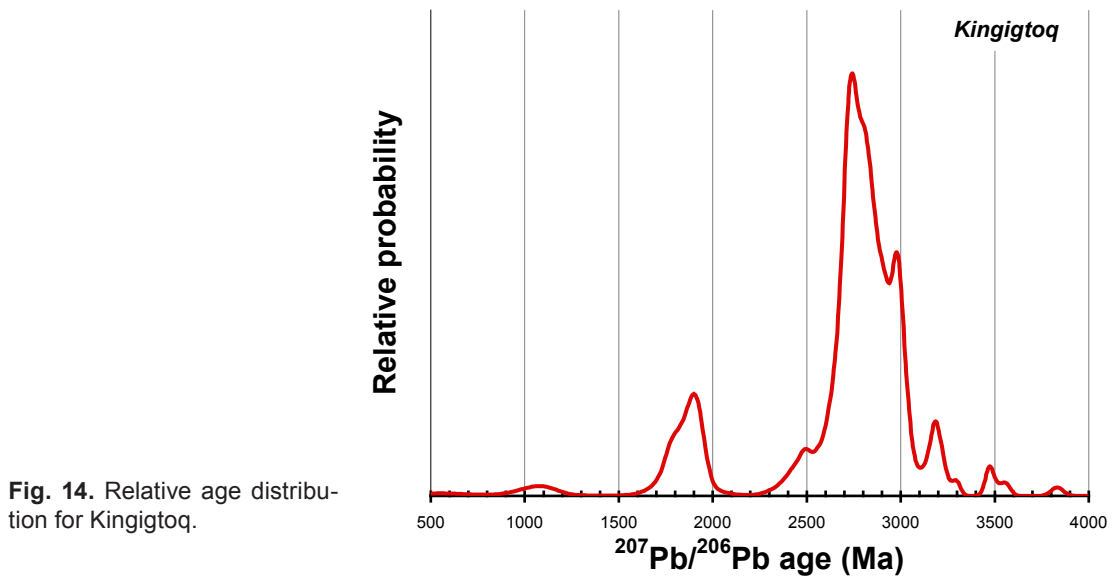


Fig. 14. Relative age distribution for Kingigtoq.

Atarnikerdluk

This sample set is very similar to that of Kongigtoq and lower Patuut. An interesting feature is the apparent disappearance of the 1.9 Ga Palaeoproterozoic component in the middle of the section, which is reflected in the low P-values for sample 486761 in Table 5. Given the total amount of 53 grains that fulfil the concordance criteria and the Dodson equation above, this component should probably have been detected, but as the sample is somewhat small we prefer to not separate it out at this stage. The significance of its absence remains unconfirmed at this stage, but if supported through a larger sample, it may represent an intermittent change in the sedimentary conditions (Fig. 15; Appendix I). N

	486748	486754	486761	486767	486772	486779
486748		0.779	0.001	0.318	0.472	0.728
486754	0.779		0.002	0.683	0.536	0.757
486761	0.001	0.002		0.126	0.042	0.000
486767	0.318	0.683	0.126		0.960	0.889
486772	0.472	0.536	0.042	0.960		0.910
486779	0.728	0.757	0.000	0.889	0.910	

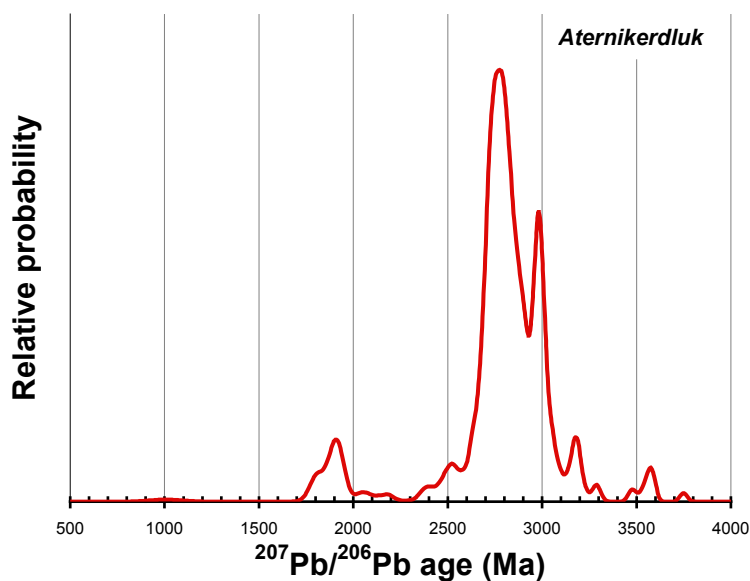


Fig. 15. Relative age distribution for Atarnikerdluk. The 1.9 Ga peak is not present in the middle of the section.

Pingu

Two samples from Pingu only amounts to 20 grains that fulfil the concordance criteria. Few constraints can therefore be drawn, but its 1.9, 2.7-3.4 and 3.6 Ga peaks are in good agreement with the expected age profile from the Greenland basement (Fig. 16). A striking observation is the occurrence of four 3.6 Ga grains in this limited population, which highlights its wide distribution and its relatively common occurrence.

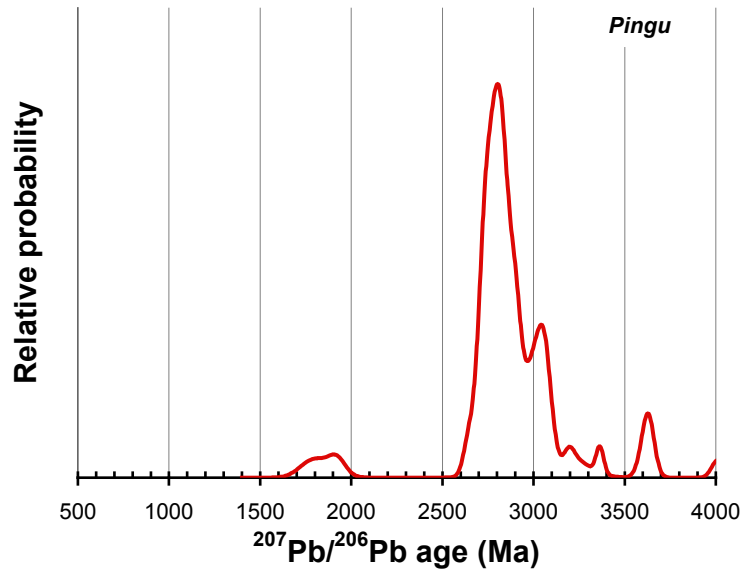


Fig. 16. Relative age distribution for Pingu. This is a very small sample that has to be treated accordingly, but it displays a typical Greenland basement provenance signature.

Grønne Ejland

Two samples from Grønne Ejland represent the most southern samples in the Disko Bugt area. They show great coherence with lower Patuut, Aternikerdluk, Kingigtoq, Pingu, and to a lesser degree, the Kome/Atane formation at Itsaku. Many of these samples belong to the Atane Formation, and there is good overall agreement, even though some locations, mostly along more westerly positions, record the Grenvillian-Labradorian age components.

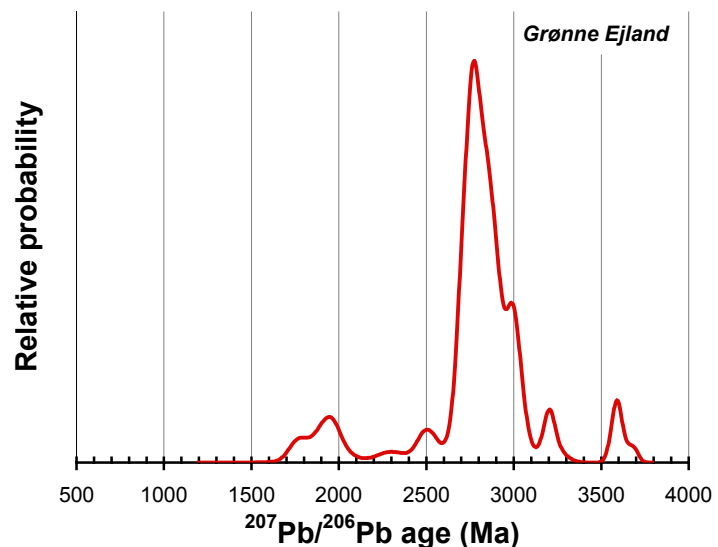


Fig. 17. Relative age distribution for Grønne Ejland.

Hellefisk-1

The Hellefisk drilling represents Palaeogene sediments that mainly constitute silt and sand. The sample suite is fairly homogenous with no systematic changes in the stratigraphic column (Table 6). It is strikingly similar to the Atane Formation, and its whole rock chemistry is rather mature. Its correspondence with the Atane Formation may suggest that they may have the same provenance or that Hellefisk is derived from reworked Atane Formation rocks. We prefer the former explanation based on its mature nature (e.g. low Al_2O_3/SiO_2 ratios), which is aided through reprocessing of previous sediments.

Table 6. K-S P-values using error in the CDF

	2610	2910	3300	3510	3990	4350	4770
2610		0.163	0.715	0.498	0.994	0.872	0.659
2910	0.163		0.001	0.030	0.220	0.028	0.421
3300	0.715	0.001		0.777	0.403	0.998	0.044
3510	0.498	0.030	0.777		0.310	0.942	0.112
3990	0.994	0.220	0.403	0.310		0.796	0.865
4350	0.872	0.028	0.998	0.942	0.796		0.244

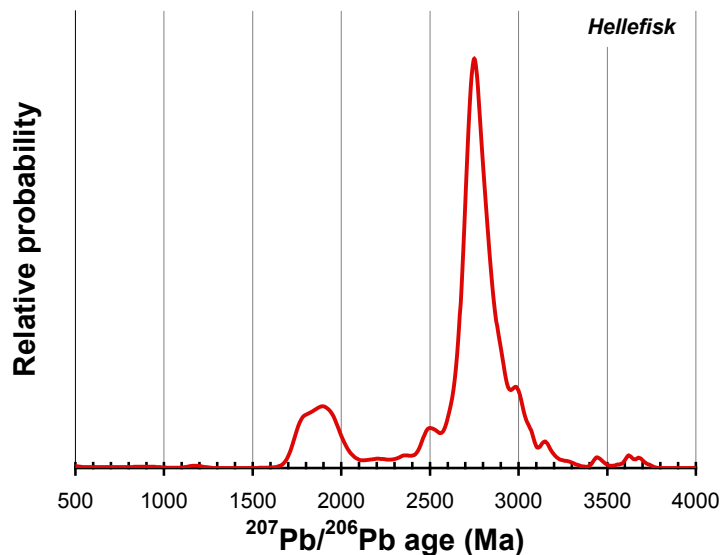


Fig. 18. Relative age distribution for Hellefisk-1.

Qulleq-1

Qulleq-1 is the most southern drilling, where our sample suite represents begins at 2610 m drill depth (Fig. 19). Qulleq-1 is rather similar to GRO#3 in its characteristics and it has a strong Grenvillian-Labradorian component (Fig. 19). A possible emerging pattern based on this data set is that the Grenvillian-Labradorian signatures are more abundant westward at any given latitude, and that it eventually disappears towards the east in the deltaic successions. It also seems to be more abundant towards south, but this inference hinges completely on the Qulleq-1 data set. Finally, it appears to weaken or even diminish downwards in each stratigraphic column (Fig. 20; Appendix I). This latter observation is noted in GRO#3, but particularly clear in the Qulleq-1 drilling. So much so, it is statistically significant in the K-S test (Table 7). In addition to the distribution pattern of the Grenvillian-Labradorian provenance signature, there is a sense of a zonation insofar that sample suites tend to yield high P-values along north-south lines.

Table 7. K-S P-values using error in the CDF					
	2610	2655	2700	2826	2919
2610		0.000	0.004	0.001	0.000
2655	0.000		0.343	0.622	0.099
2700	0.004	0.343		0.118	0.151
2826	0.001	0.622	0.118		0.957
2919	0.000	0.099	0.151	0.957	

Fig. 19. Relative age distribution for Qulleq-1 2610 m.

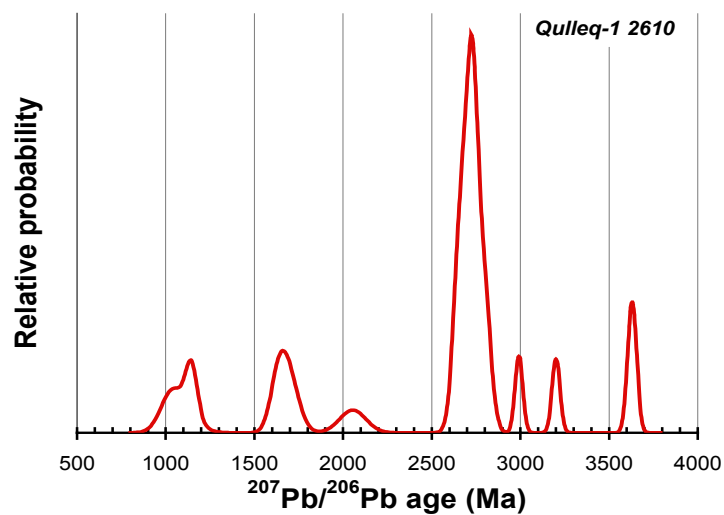
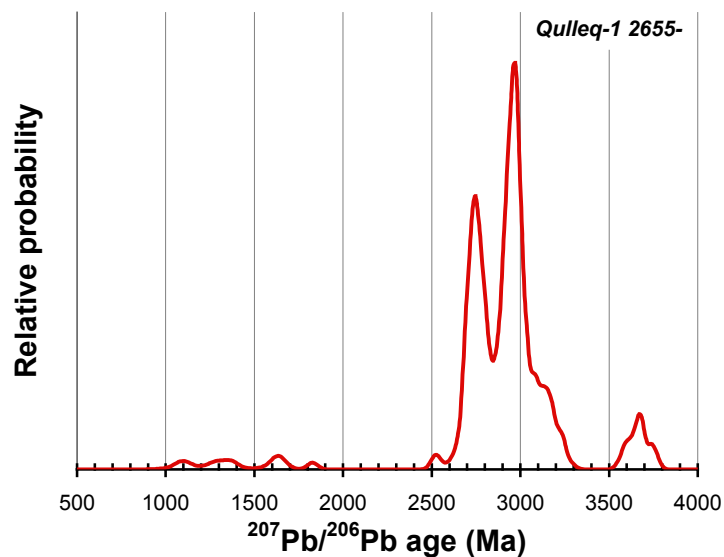


Fig. 20. Relative age distribution for Qulleq-1 2655- m.



Summary

It seems clear from these results that zircon U-Pb provenance is a powerful tool that yield useful results on both regional and local scale. The overall pattern in the Cretaceous-Palaeogene sediments in West Greenland is a typical Greenland Precambrian basement signature with abundant peaks at 1.9, 2.7-3.0 and 3.6 Ga, which largely reflect the continental crust evolution in Greenland. There are few exotic components, which may suggest a relatively closed system with respect to influx of zircon bearing components.

The overall transport direction is in accordance with sedimentary models that suggest deltaic successions mainly fed from east to southeast. A striking example that illustrates the power of the method and a flip in the depositional environment is the Kangilia Formation at Itsaku. A single, narrow peak around 1870 Ma represents it. This strikingly constrained distribution forms a perfect match with the 1869 ± 9 Ma date for the Prøven igneous complex situated immediately north of Svartenhuk Halvø. Although contemporaneous rocks are known from Canada to the west and may also be present beneath the Inland Ice to the north-east it seems reasonable to infer that the sediments of the Kangilia Formation were derived from this unique source and that they are first generation sediment. Furthermore, it demonstrates a major change in the sediment transport direction in this region that may be related to a tectonic event in the basin during the Campanian.

A small but significant peak at ~1100 Ma suggests a distal component that is not readily explained by derivation from the West Greenland basement. This component seems to be associated with a 1600–1700 Ma occurrence. Two possible sources can explain the dual peaks; an East Greenland or a Canadian. If an East Greenland origin is favoured, it might be expected that this signature is associated with Caledonian ages between 380 and 480 Ma, which have not yet been identified. Given the large number of grains analysed it should be expected that even a very small contribution would have been detected (cf. Vermeesch 2004). Furthermore, the 1100 Ma component seems to be absent in the onshore, deltaic facies and appears to be found only in the deep-water facies in both onshore and offshore samples. This, in conjunction with an absence of a 1900 Ma peak in the southernmost offshore well Qulleq-1 is most easily fit with a transport model along the Greenland west coast from south towards north.

Stream sediments

Detrital zircon grains from stream sediments were dated to characterise the local age distribution of catchment areas. The purpose is two-fold, firstly it aims at obtaining a relatively unbiased age map of the West Greenland basement and secondly, it forms a source component benchmark for the Cretaceous and Palaeogene sediments. The approach is the same as for the sediments and we filter data that is more than 10% discordant. Up to ~300 grains were picked from 50 samples although three were barren, and two lost in the analytical process due to instrumental problems. 100-200 grains were normally analysed when possible and a total of 3928 spots gave meaningful data of which 3483 spots meets the concordance criteria. The sample set was divided into four subsets according to their GGU numbers as the series are geographically separated (Table 8). Subsets are organised from south to north. The first subset is from the southernmost part of the study area just north of the Godthåbsfjord. Archaean gneisses that range from 3850 to 2600 Ma (Hollis *et al.* 2006) are

expected to dominate this area. Further north, the Archaean basement was reworked during the Nagssugtoqidian-Rinkian orogens, which adds a magmatic and metamorphic age peak at 1900 Ma (Connelly *et al.* 2000).

Table 8. Geographical subdivision of stream sediment samples

Subset	Samples
1	301730 – 309416
2	368216 – 382034
3	330765 – 330963
4	501009 – 501551

Subset 1 is dominated by Archaean peaks, which is entirely expected (Fig. 21). There are two apexes that have their loci at ~2800 and 3650 Ma respectively. There are hints of an Eoarchaean component as old 3900 Ma, but that remains to be confirmed by more detailed work. In subset 2, the fairly pronounced occurrence of >3600 Ma ages, seen in subset 1, is almost gone. In fact, most samples lack the component entirely, and tend to have fairly unimodal age profiles (e.g. 380987; Appendix II). Sample 368273 (Appendix II) stand out with significant peaks between 3500-3700 Ma. Subset 2 displays a well defined, albeit broad, peak has its apex at ~1900 Ma (Fig. 21), which is expected from the Nagssugtoqidian-Rinkian orogens (Connelly *et al.* 2000). The component is not present in some samples, but important in others (e.g. 381011; Appendix II). Subset 3 is fairly unimodal with ages ranging between 2600-3000 Ma (Fig. 21). This is in accordance with less pronounced effects of the Nagssugtoqidian-Rinkian orogens. The pattern of subset 3 is more or less replicated in subset 4, but a slight bimodality with a poorly resolved ~2900 Ma component, which is hinted in all subset, is more strongly supported here (Fig. 21)

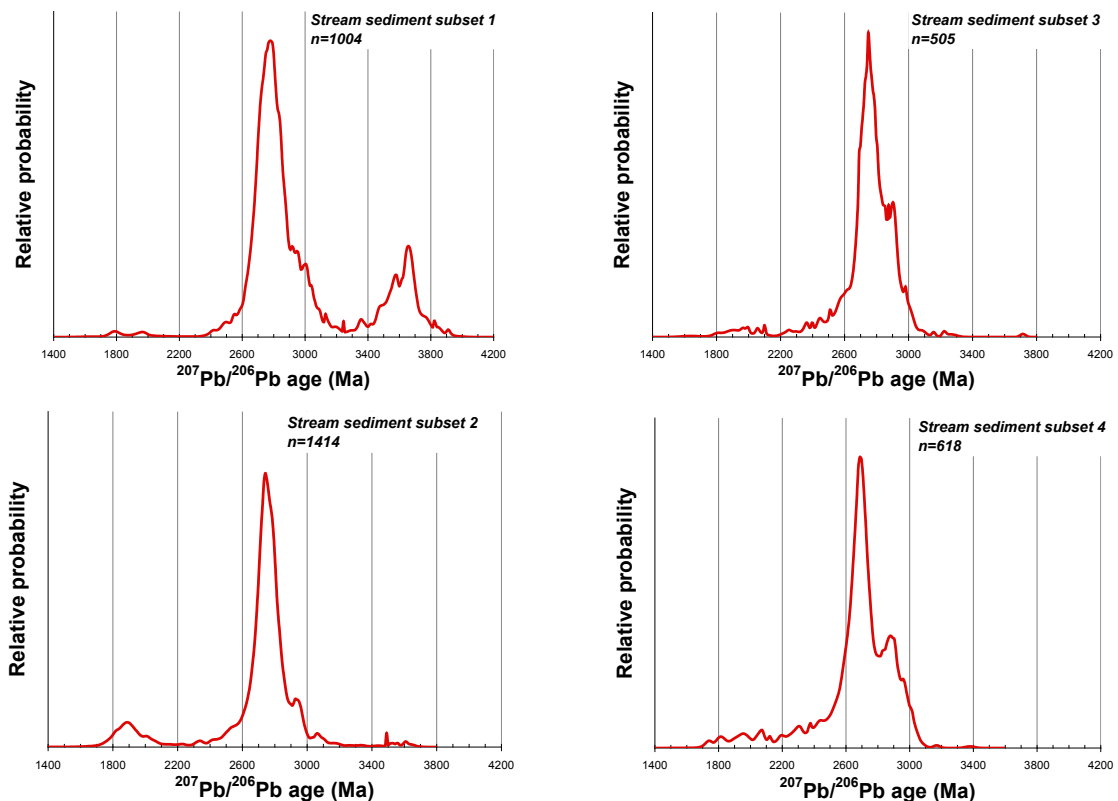


Fig. 21. Probability density distributions for stream sediment sample subsets.

Overall, the composite age distributions of the stream sediments conform with expectations, and map out known ages of tectonic events fairly well. It is also evident that the Cretaceous and Paleogene sediments reflect these components, but also require regional mixing of Proterozoic to Eoarchaeon components to explain their patterns (e.g. 463393; Appendix I).

Zircon trace elements

Zircon incorporated a number of trace elements in addition to U and Th, which enables zircon age dating. It may be hypothesised that their absolute or relative abundances will vary as functions of e.g. petrogenetic processes or source characteristics. A lot of focus has been devoted to zircon trace element geochemistry since the early nineties (Hinton & Upton, 1991), but its usefulness remains debated (Hoskin & Ireland, 2000; Belusova *et al.* 2006). We have re-analysed 668 grains for their trace element compositions to explore the potential in zircon trace elements. The data is available in the excel file 'Zircon trace element table.xls'. The data was acquired using the LA-SF-ICP-MS system described above, and the analytical procedure is principally similar to that described above. Concentrations were calculated assuming stoichiometric SiO₂ concentrations of 32.78 wt%, and all analyses were externally normalised to the NIST 610 glass.

There are no systematic correlations with age as is expected from a uniformitarian paradigm, and the intention is to identify process-specific characteristics that can be related to e.g. arc related magmatism versus late orogenic magmatism.

Focus in zircon trace element geochemistry has largely been on rare earth elements (REE), Ti and P substitution. REE are three valent except for reduced species of Eu²⁺ or oxidized species of Ce⁴⁺ and their decreasing ionic radius with increasing mass number is reflected by increasing compatibility into zircon. These properties are reflected such that typical zircon REE profiles have steep positive slopes, commonly with negative Eu-anomalies (Eu/Eu*) and positive (Ce/Ce*; Fig. 22), where at least the negative Eu/Eu* anomaly may be modulated by residual plagioclase during crustal melting to produce granite. It is notable in the current data set that there is no such thing as a typical zircon profile, and the data span a wide range of REE signatures (Fig. 23).

Interestingly, zircon tend to show less variation in their heavy REE concentrations than they do in their light REE. This leads to flatter slopes in more enriched samples, and another feature are the vanishing Eu/Eu* and Ce/Ce*. Unsurprisingly, REE is correlated with P (Fig. 24), which will balance the charge deficiency that the three valent REE produce when they substitute for Zr⁴⁺. Xenotime is a REE+Y phosphate that is isostructural with zircon, and it may be assumed that there is a solid solution series between xenotime and zircon. However, as seen in Fig. 24, there is REE+Y overabundance in many grains, and some other explanation is required for a large number of grains. One hypothesis may be an intermediate component between xenotime and another REE phosphate; monazite (Fig. 24). Xenotime and monazite have very contrasting REE slopes, where xenotime is the one similar to zircon. An added monazite component may thus, to some extent, explain the shallower slope in some of the REE enriched zircon grains (Fig. 25). It seems that many features of zircon REE geochemistry are not principally controlled by tectonic or petrogenetic signatures, which complicates its use in provenance studies as point source plutons may be envisaged to display a range of zircon compositions.

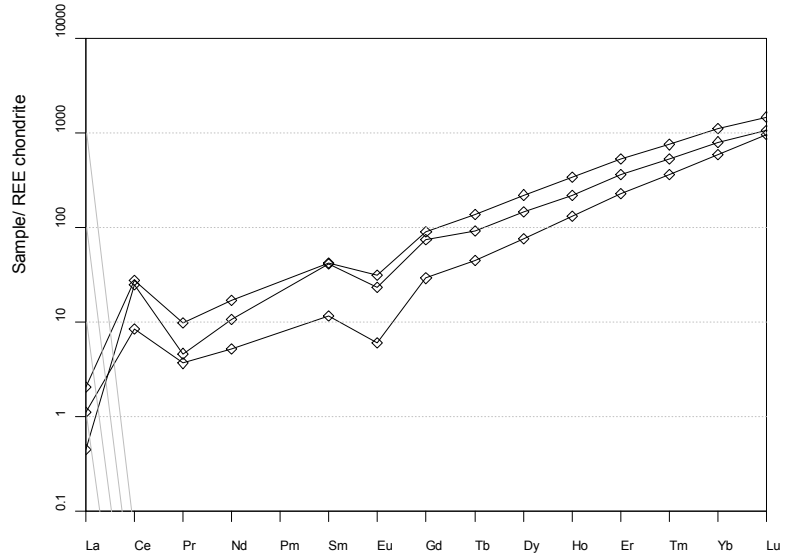


Fig. 22. Typical zircon profiles display steep positive slopes with positive Ce/Ce* and negative Eu/Eu* anomalies, respectively.

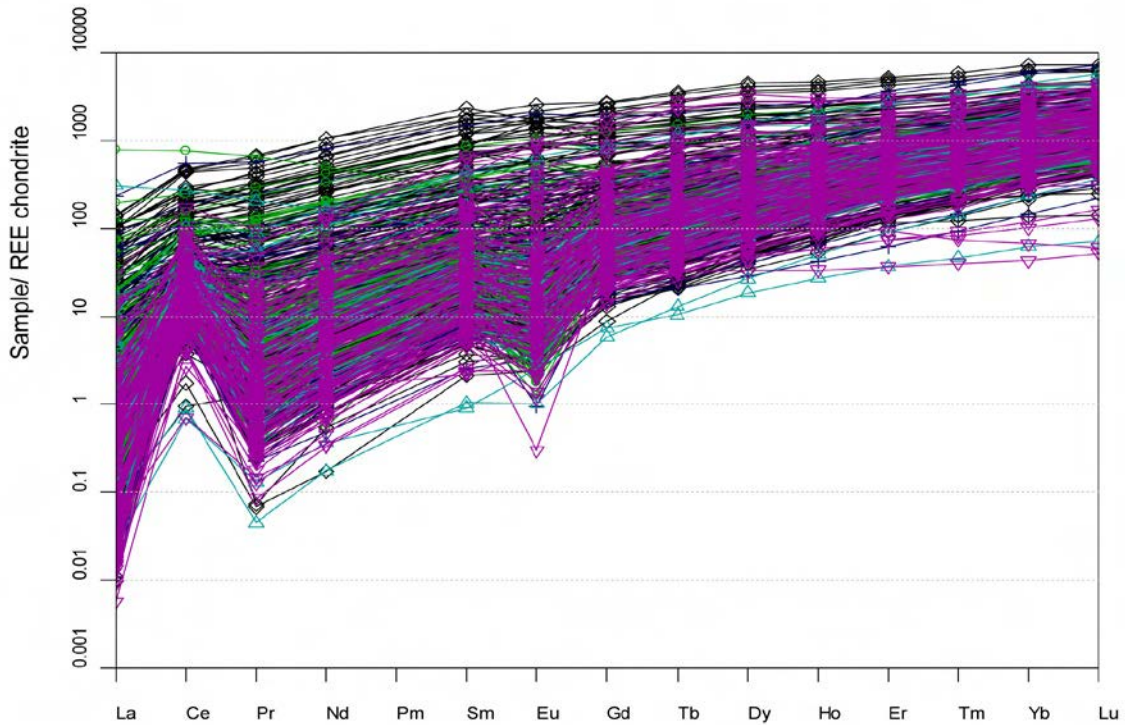
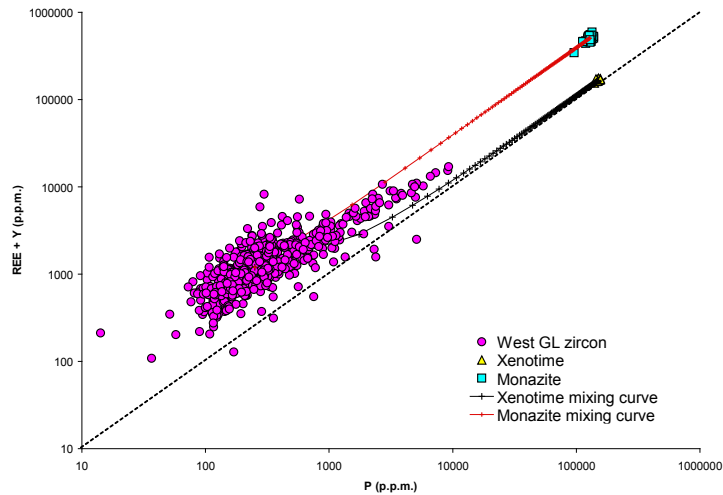


Fig. 23. All REE profiles (n=668) determined in this survey show a wide range.

It is notable that the current data set is derived from detrital zircon, and as such the grains are not easily grouped in more detail than their ages allow. Clearly that is insufficient for the purpose of fully understand how zircon trace element data may be utilised. However, the Kangilia Formation zircon at Itsaku are useful with respect to zircon trace elements in provenance studies. It may be argued on basis of the $^{207}\text{Pb}/^{206}\text{Pb}$ age structure that these grains were derived from a point source. We infer that this source is the Prøven igneous complex, which is exactly the same age as the detrital age distribution peak apex; namely 1870 Ma (Thrane

Fig. 24. P plotted against REE+Y, which are major components in xenotime and monazite. There is a clear positive correlation between P and REE+Y and most grains are overabundant in REE+Y with respect to xenotime. Mixing curves for median zircon-monazite and zircon-xenotime are plotted.



et al. 2005). On this assumption we treat these grains as a single population ($n=140$) that represent an average sample of the Prøven complex. These zircon grains cover the same range of correlated P and REE+Y variations as the entire sample set, which reinforces the notion that zircon REE systematics are foremost controlled by crystal chemical processes. However, they display two features that can be deduced on the notion that they represent a single population Firstly, it seems as if they may display somewhat lower Ce/Ce* for a given Eu/Eu* when contrasting them to all other grains (Fig. 26). This may reflect a more evolved source that has undergone plagioclase removal through crystal fractionation or as a melting residual during crustal melting. The latter solution may be more attractive as it is in keeping with a potentially unique feature of the Prøven complex as a late orogenic crustal melt that can be contrasted against the general syn-orogenic Archaean geological evolution.

A further possible test is Ti in zircon thermometry (Watson *et al.* 2006). This is based on the notion that Ti^{4+} substitute for Zr^{4+} when it is buffered ($a=1$). Here we note that Ti is positively correlated with P and that unreasonably high temperature estimates are obtained for zircon with elevated P content. It may be possible to obtain a correction for Ti overabundance due to P, but we prefer to filter that data out as such corrections will be associated with large errors and since we lack the necessary data set to obtain a correction factor. Zircon crystallisation temperatures were calculated for data that have less than 300 p.p.m. P, which we used as the cut-off value (Fig. 26). We then contrasted the Kangilia Formation zircon from Itsaku against all other grains in our data set. The average Kangilia temperature estimate is $845 \pm 93C^{\circ}$ (1σ ; $n=93$), A hint of a contrast is visible in Fig. 27, and a K-S test that assumes $93C^{\circ}$ 1σ external (analytical + geological as determined for Kangilia) reproducibility confirms that the Kangilia zircon thermometry is statistically different from the Archaean population, but indistinguishable from similarly aged Palaeoproterozoic zircon (Fig. 28).

The division of the zircon into these different groups implies that each population was derived in similar geological environments, which is reflected in their temperatures. Zircon grains that are similar in age to those of the Kangilia Formation were pooled into a separate Palaeoproterozoic group. Fig. 23 shows the cumulative distribution function (CDF) that takes account of assigned errors, and a matrix with P-values in the K-S test, and indicates that the Kangilia Formation is significantly different from the Archaean pool. On the other hand, it is not statistically dissimilar from the Palaeoproterozoic pool. Likewise, the Palaeoproterozoic pool is indistinguishable from the Archaean, possibly describing some transitional geological or pooling effect. Importantly, the Palaeoproterozoic component in

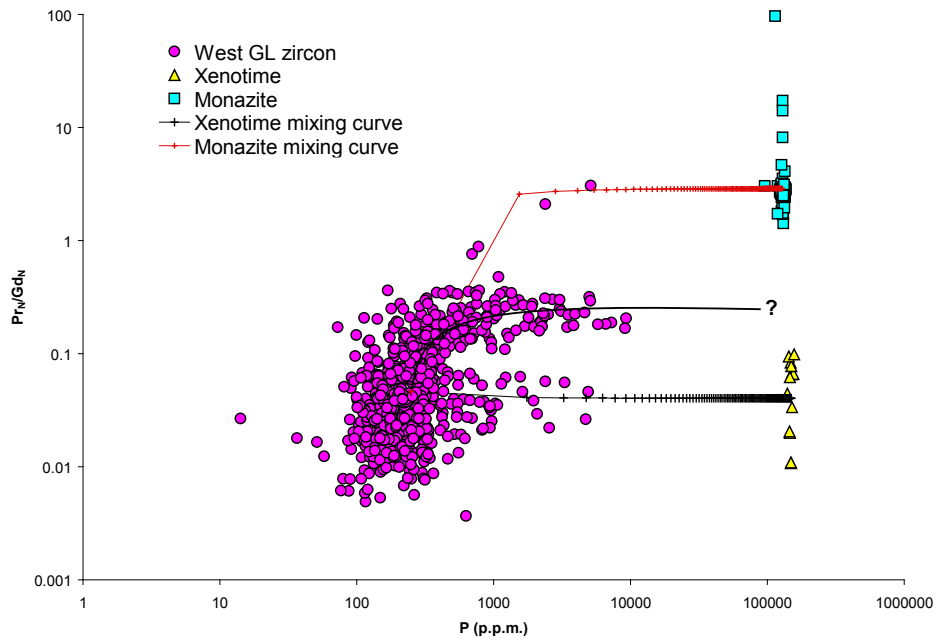


Fig. 25. P is plotted against chondrite normalised Pr_N/Gd_N ratios, which are reflecting the slope of the REE profile. A higher ratio corresponds to steeper negative slopes. Natural monazite and xenotime data are plotted for reference, and used to calculate mixing curves between median zircon-monazite and zircon-xenotime. Some zircon plot on either trend, but the bulk of the P-enriched grains form an intermediate trend. Note that these trends assumes a common explanation for all types of zircon as these are geologically unrelated.

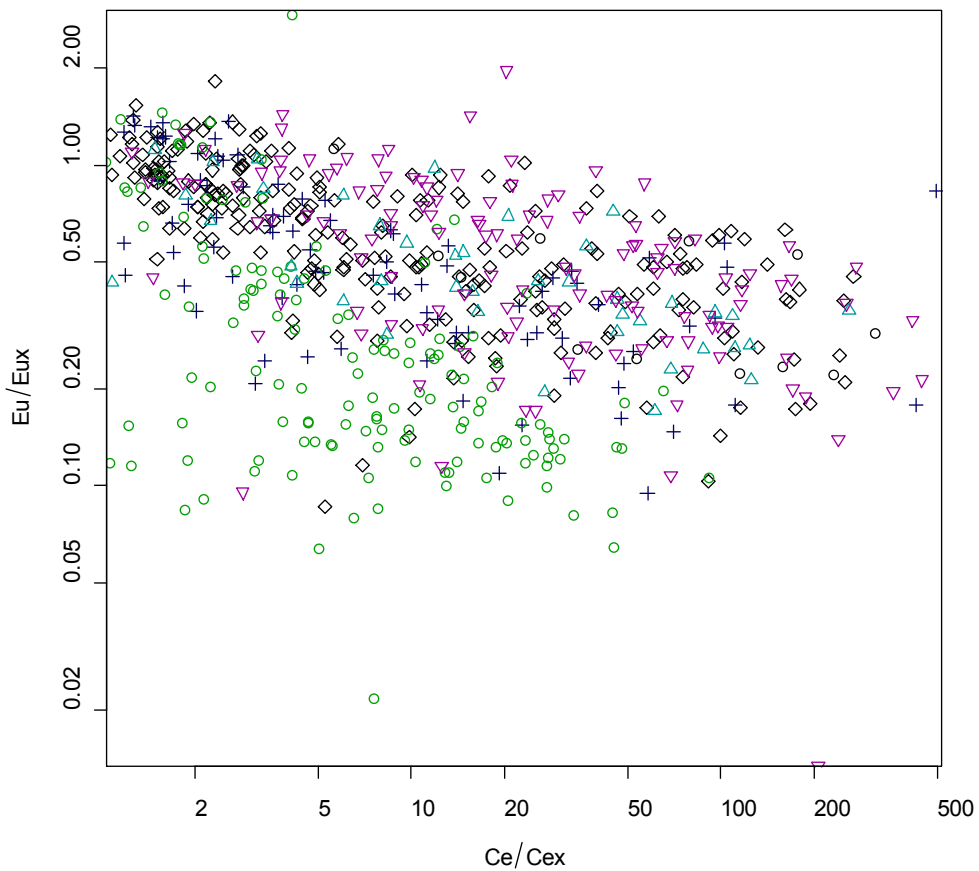


Fig. 26. Ce anomalies (Ce/Ce^*) plotted against Eu-anomalies (Eu/Eu^*) for all acquired data. Zircon that are assumed to be derived from the 1870 Ma Prøven complex plot along a steeper negative correlation with lower Ce/Ce^* for a given Eu/Eu^* .

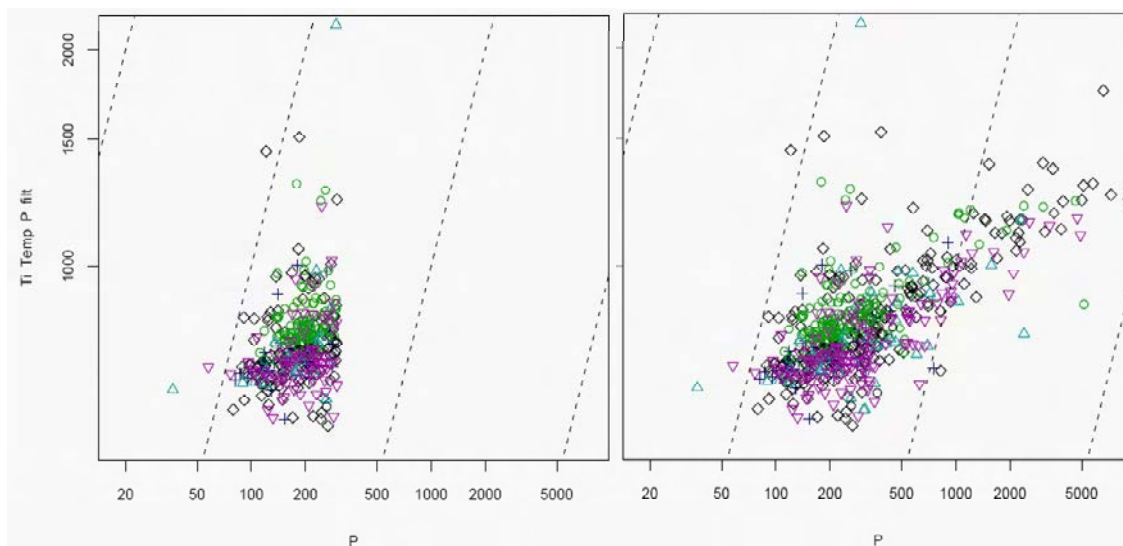
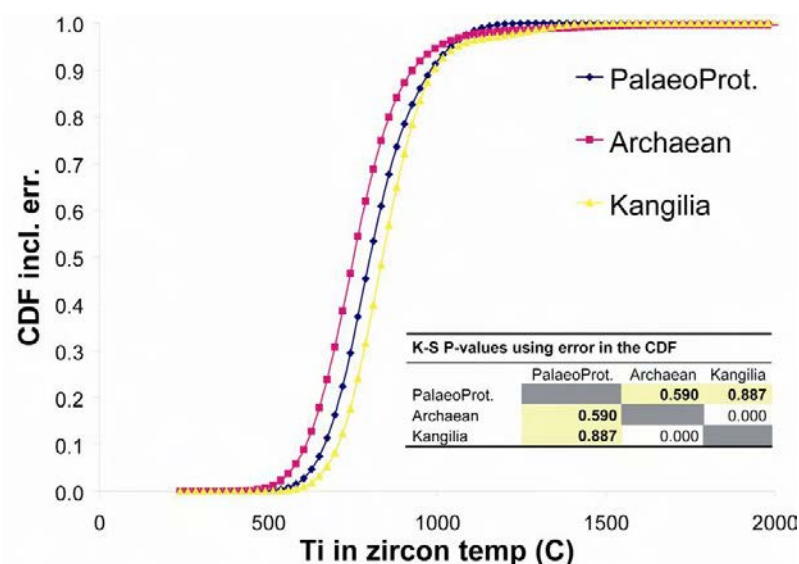


Fig. 27. P is plotted against Ti temperature for a filtered (left) and unfiltered data set. Many grains that yield unrealistically high temperature estimates are associated with elevated P contents.

Fig. 28. Ti in zircon thermometry for zircon from Kangilia Formation, which is assumed to be derived from the Prøven igneous complex. The Kangilia 1σ reproducibility ($\pm 90\text{ C}^\circ$) is the assigned error to each individual analysis.



samples that display a wide palette of both Archaean and Proterozoic ages may be the same as the point source component in Kangilia, or it may merely demonstrate the presence of other intrusions of the same type as that feeding the Kangilia Formation.

Our initial work on trace elements in zircon indicate the potential, but much further work is required. A problem is the necessary pooling of data, which may not always be justified as it is difficult to ascribe a zircon grain to a particular group. It is evident from the Kangilia Formation zircon, which we ascribe to a point source, that there may be great variability within a component, and two apparently dissimilar grains may in fact have been derived from the same source. Strictly speaking, each grain represents its own sample that has to be contrasted against all other. Additional constraints and a hierarchical pooling order may be useful in eventually ascribing individual grains to separate populations. A way forward may be pools that are defined by known provenance age components, that are then further divided on the basis of trace element geochemistry, other stable and radiogenic isotope systems such as oxygen and lutetium-hafnium.

Heavy mineral CCSEM data

The results of the CCSEM work is appended electronically on DVD. A first observation of this data set show interesting and systematic variations in garnet compositions (Fig. 28). Pyrope like garnet is found in the northernmost and southernmost parts of the study region. Pyrope is particularly interesting as its Cr-rich variety is an important indicator mineral for kimberlite, which is the main source rock of diamonds. The differences in garnet composition in the stream sediment has a twofold use. Firstly, as the catchment areas of these sediments are well constrained, the search for economically important occurrences of e.g. kimberlite is aided. Secondly, much like zircon, garnet is resistant to erosion and if geographically unique signatures can be mapped out in stream sediments, sediment provenance studies will see added constraints when used in conjunction with zircon ages. Further evaluation work of this large data set is needed, but is expected to yield interesting results.

References

- Aftalion, M., Bowes, D.R., Vřana, S. 1989: Early Carboniferous U-Pb zircon ages for garnetiferous perpotassic granulites, Blansky Les Massif, Czechoslovakia. *Neues Jahrbuch für Mineralogie, Monatshefte* **4**, 145-152.
- Belousova, E.A., Griffin, W.L., O'Reilly, S.Y. 2006: Zircon crystal morphology: trace element signatures and Hf isotope composition as a tool for petrogenetic modelling: Examples from eastern Australian Granitoids. *Journal of Petrology* **47**, 329-353.
- Chalmers, J. & Pulvertaft, T. 2001: Development of the continental margins of the Labrador Sea: a review. In: Wilson, R. *et al.* (eds) *Non-volcanic rifting of continental margins: a comparison of evidence from land and sea*. Geological Society (London) Special Publications **187**, 77-105.
- Chalmers, J.A., Christiansen, F.G., Søndersholm, M., Olsen, J.C., Myklebust, R. & Schönwandt, H.K. 2001: Geological information base growing on North Atlantic rift basins. Data developed for Greenland licensing. *Offshore* **61**(11), 87-89, 100
- Dalhoff, F., Chalmers, J.A., Gregersen, U., Nøhr-Hansen, H., Rasmussen, J.A. & Sheldon, E. 2003: Mapping and facies analysis of Paleocene-Mid-Eocene seismic sequences, offshore southern West Greenland. *Marine and Petroleum Geology* **20**, 935-986.
- Connelly, J.N., van Gool, J.A.M. & Mengel, F.C. 2000: Temporal evolution of a deeply eroded orogen: the Nagssugtoqidian Orogen, West Greenland. *Canadian Journal of Earth Sciences* **37**, 1121-1142.
- Copjakova, R., Sulovsky, P. & Paterson, B.A. 2005: Major and trace elements in pyrope-almandine garnets as sediment provenance indicators of the Lower Carboniferous Culm sediments, Drahaný Uplands, Bohemian Massif: *Lithos* **82**, 51-70.
- Dam, G. 2002: Sedimentology of magmatically and structurally controlled outburst valleys along rifted volcanic margins; examples from the Nuussuaq Basin, West Greenland. *Sedimentology* **49**, 505-532.
- Dam, G. & Søndersholm, M. 1994: Lowstand slope channels of the Itilli succession (Maastrichtian-Lower Paleocene), Nuussuaq, West Greenland. *Sedimentary Geology* **94**, 47-71.
- Dam, G. & Søndersholm, M. 1998: Sedimentological evolution of a fault-controlled Early Paleocene incised-valley system, Nuussuaq Basin, West Greenland. In: Shanley, K.W. & McCabe, P.J. (eds) *Relative role of eustasy, climate, and tectonism in continental rocks*. Society of Economic Paleontologists and Mineralogists Special Publication **59**, 109-121.
- Dam, G., Larsen, M. & Søndersholm, M. 1998a: Sedimentary response to mantle plumes: Implications from Paleocene onshore successions, West and East Greenland. *Geology* **26**(3), 207-210.

- Dam, G., Nøhr-Hansen, H., Christiansen, F.G., Bojesen-Kofoed, J.A. & Laier, T. 1998b: The oldest marine Cretaceous sediments in West Greenland (Umiivik-1 borehole) – record of the Cenomanian–Turonian Anoxic Event? *Geology of Greenland Survey Bulletin* **180**, 128-137.
- Dam, G., Nøhr-Hansen, H., Pedersen, G.K. & Sønderholm, M. 2000: Sedimentary and structural evidence of a new early Campanian rift phase in the Nuussuaq Basin, West Greenland. *Cretaceous Research* **21**, 127–154.
- Dam, G., Pedersen, G.K. & Sønderholm, M. 2006: Geological evolution of the sub-volcanic Cretaceous-Paleocene Nuussuaq Basin, West Greenland – an analogue to other sub-volcanic North Atlantic basins. FORCE Sedimentology Stratigraphy Group Seminar, 14–15 March 2005, Stavanger, Norway (unpublished abstract).
- Dam, G., Pedersen, G.K., Sønderholm, M., Midtgaard, H. & Petersen, A.K. in prep: Lithostratigraphy of the Nuussuaq Basin, West Greenland. *Geological Survey of Denmark and Greenland Bulletin*.
- Dodson, M.H., Compston, W., Williams, I.S., Wilson, J.F. 1988: A search for ancient detrital zircons in Zimbabwean sediments. *Journal of the Geological Society of London* **145**, 977–983.
- Fedo, C.M., Sircombe, K.N., Rainbird, R.H. 2003: Detrital zircon analysis of the sedimentary record. In: Hanchar, J.M., Hoskin, P.W.O. (Eds.), *Zircon. Reviews in Mineralogy and Geochemistry* **53**, 277-303.
- Frei D., Rasmussen T., Knudsen C., Larsen M., Whitham A. & Morton A. 2005a: Linking the Faroese area and Greenland: New methods and techniques used in an innovative, integrated provenance study. *Fróðskaparrit – Annales Societatis Scientiarum Færoensis* **43**, 96-108.
- Frei, D., Knudsen, C., McLimans, R.K. & Bernstein, S. 2005b: Fully automated analyses of the chemical and physical properties of individual mineral species in heavy mineral sands by Computer Controlled Scanning Electron Microscopy (CCSEM): *Proceedings of 2005 Heavy Mineral Conference*, 103-108.
- Frei D., Hollis J.A., Gerdes A., Harlov D., Karlsson C., Vasquez P., Franz G., Johansson L., & Knudsen C. 2006: Advanced *in-situ* trace element and geochronological microanalysis of geomaterials by laser ablation techniques. *Geological Survey of Denmark and Greenland Bulletin* **10**, 25-28.
- Gerdes, A., Zeh, A. 2006: Combined U-Pb and Hf isotope LA-(MC)-ICP-MS analyses of detrital zircons: Comparison with SHRIMP and new constraints for the provenance and age of an Armorican metasediment in Central Germany. *Earth and Planetary Science Letters* **249**, 47–61.
- Gu Y. 2003, Automated scanning electron microscope based mineral liberation analysis. *Journal of Minerals and Materials Characterization and Engineering* **2**, 33-41.
- Hinton, R.W., Upton, B.G.J. 1991: The chemistry of zircon: Variations within and between large crystals from syenite and alkali basalt xenoliths. *Geochimica et Cosmochimica Acta* **55**, 3287-3302.

Hollis, J.A., Frei, D. van Gool, J.A.M., Garde, A.A. & Persson, M. 2006: Using zircon geochronology to resolve the Archaean geology of southern West Greenland. *Geological Survey of Denmark and Greenland Bulletin* **10**, 49–52.

Horstwood, M., Foster, G.L., Parrish R.R. & Noble, S.R. 2003 Common-Pb corrected in situ U–Pb accessory mineral geochronology by LA-MC-ICP-MS. *Journal of Analytical Atomic Spectrometry* **18**, 837–846.

Hoskin, P.W.O., Ireland, T.R. 2000: Rare earth element chemistry of zircon and its use as a provenance indicator. *Geology* **28**, 627–630.

Huggins, F.E., Kosmick, D.A., Huffman, G.P. and Lee, R.J. 1980, Coal mineralogy by SEM analysis. *Scanning Electron Microscopy* **1**, 531–540.

Jackson, S., Pearson, N.J., Griffin, W.L. & Belousova, E.A. 2004: The application of laser ablation – inductively coupled plasma – mass spectrometry to in situ U-Pb zircon geochronology. *Chemical Geology* **211**, 47-69.

Kahn, H., Mano, E.S. & Tassinari, M.M.M.L. 2002, Image analysis coupled with SEM-EDS applied to the characterization of a partially weathered Zn-Pb ore. *Journal of Minerals and Materials Characterization and Engineering* **1**, 1–9.

Kennedy, S.K., Walker, W. & Forslund, B. 2002, Speciation and characterization of heavy metal contaminated soils using computer controlled scanning electron microscopy. *Environmental Forensics* **3**, 131–143.

Kierkegaard, T. 1998a: Evaluation of the diagenetic alterations in the core of the GANT#1 well, Tunorsuaq, West Greenland Danmarks og Grønlands Geologiske Undersøgelse Rapport **1998/7**, 53 pp.

Kierkegaard, T. 1998b: Diagenesis and reservoir properties of Campanian-Paleocene sandstones in the GANT-1 well, western Nuussuaq, central West Greenland. *Geology of Greenland Survey Bulletin* **180**, 31–34.

Langmi, H.W. & Watt, J. 2003: Evaluation of computer-controlled SEM in the study of metal-contaminated soils. *Mineralogical Magazine* **67**, 219–231.

Laskin, A., Wietsma, T.W., Krueger, B.J. & Grassian, V.H. 2005: Heterogeneous chemistry of individual mineral dust particles with nitric acid: A combined CCSEM/EDX, ESEM, and ICP-MS study. *Journal of Geophysical Research* **110**, p. D10208–D10222.

Lee, R.J. & Kelly, J.F. 1980: Overview of SEM-based automated image analysis. *Scanning Electron Microscopy* **1**, 303 only.

Lundrigan, N. 2004: Gunshot residue technology. *Law and Order* **20**, 66–68.

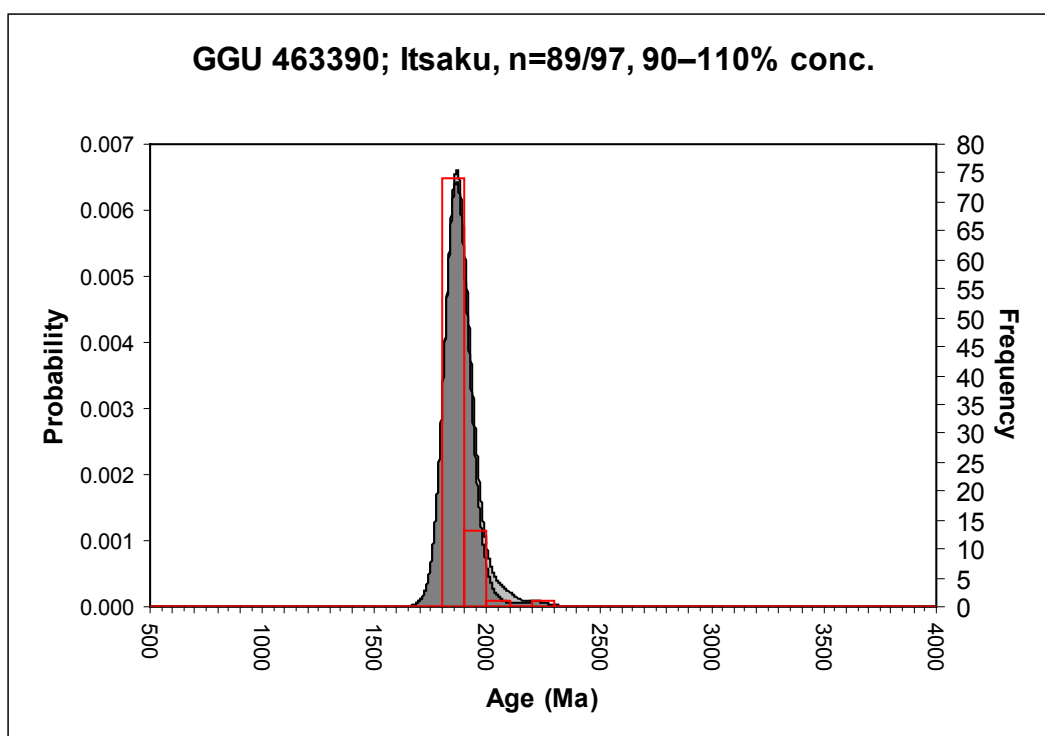
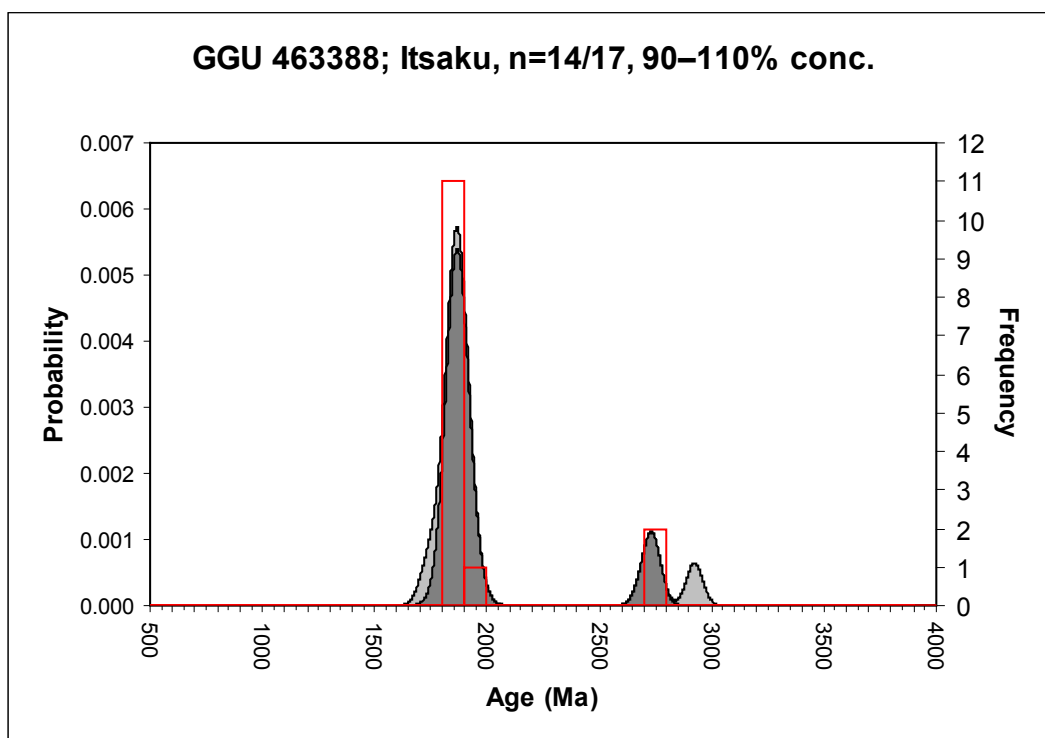
Morton, A.C., 1985: A new approach to provenance studies: electron microprobe analysis of detrital garnets from Middle Jurassic sandstones from the Northern North Sea. *Sedimentology* **32**, 553–566.

- Morton, A.C. & Hallsworth, C.R. 1999: Processes controlling the composition of detrital mineral assemblages in sandstones: *Sedimentary Geology* **124**, 3-29.
- Oszczypko, N. & Salata, D. 2005: Provenance analyses of the late Cretaceous - Palaeocene deposits of the Magura Basin (Polish Western Carpathians) - evidence from a study of the heavy minerals: *Acta Geologica Polonica* **55**, 237–267.
- Pedersen, G.K. & Pulvertaft, T.C.R. 1992: The nonmarine Cretaceous of the West Greenland Basin, onshore West Greenland. *Cretaceous Research* **13**, 263–272.
- Pedersen, A.K., Larsen, L.M., Pedersen, G.K. & Dueholm, K.S. 2006: Five slices through the Nuussuaq Basin, West Greenland. *Geological Survey of Denmark and Greenland Bulletin* **10**, 53–56.
- Powell, J.W.D., Hunt, A. & Abraham, J.L. 2002: Anthropogenic vanadium-chromium-iron and cerium-lanthanum-iron particles in settled urban house dust: CCSEM identification and analysis. *Water, Air and Soil Pollution* **135**, 207-217.
- Pulvertaft, T.C.R. & Chalmers, J.A. 1990: Are there Late Cretaceous unconformities in the onshore outcrops of the West Greenland Basin? *Rapport Grønlands Geologiske Undersøgelse* **148**, 75–82.
- Schiener, E.J. 1975: Sedimentological notes on sandstones from Nûgssuaq, central West Greenland. *Rapport Grønlands Geologiske Undersøgelse* **69**, 35-44.
- Sircombe, K.N., 2004: AgeDisplay: an Excel workbook to evaluate and display univariant geochronological data using binned frequency histograms and probability density distributions. *Computers and Geosciences* **30**, 21-31.
- Sitzmann, B., Kendall, M., Watt, J. & Williams, I. 1999: Characterization of airborne particles in London by computer controlled scanning electron microscopy. *The Science of the Total Environment* **241**, 63-73.
- Söderlund, U., Johansson, L. 2002: A simple way to extract baddeleyite (ZrO₂). *Geochemistry, Geophysics, Geosystems* **3**, DOI: 10.1029/2001GC000212.
- Thrane, K., Baker, J., Connelly, J., Nutman, A., 2005: Age, petrogenesis and metamorphism of the syn-collisional Prøven Igneous Complex, West Greenland. *Contributions to Mineralogy and Petrology* **149**, 541-555.
- Watson, E.B., Wark, D.A., Thomas, J.B. 2006: Crystallisation thermometers for zircon and rutile. *Contributions to Mineralogy and Petrology* **151**, 413-433.
- Williams I.S., Claesson, S. 1987: Isotopic evidence for the Precambrian provenance and Caledonian metamorphism of high grade paragneisses from the Seve Nappes, Scandinavian Caledonides: II. Ion microprobe zircon U-Th-Pb. *Contributions to Mineralogy and Petrology*, **97**, 205-217.
- Zygarlicke, C.J. & Steadman, E.N. 1990: Advanced SEM techniques to characterise coal minerals. *Scanning Microscopy* **4**, 579-590.

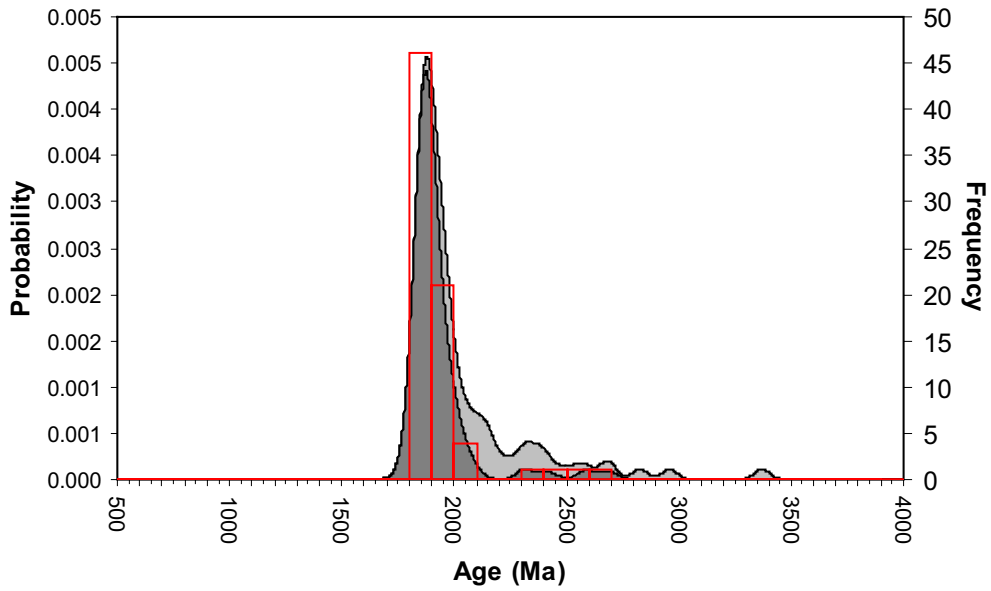
Appendix I – Cretaceous and Palaeogene samples

Compilation of all zircon U-Pb samples, which have been ordered from north to south, and from top to bottom at each respective location.

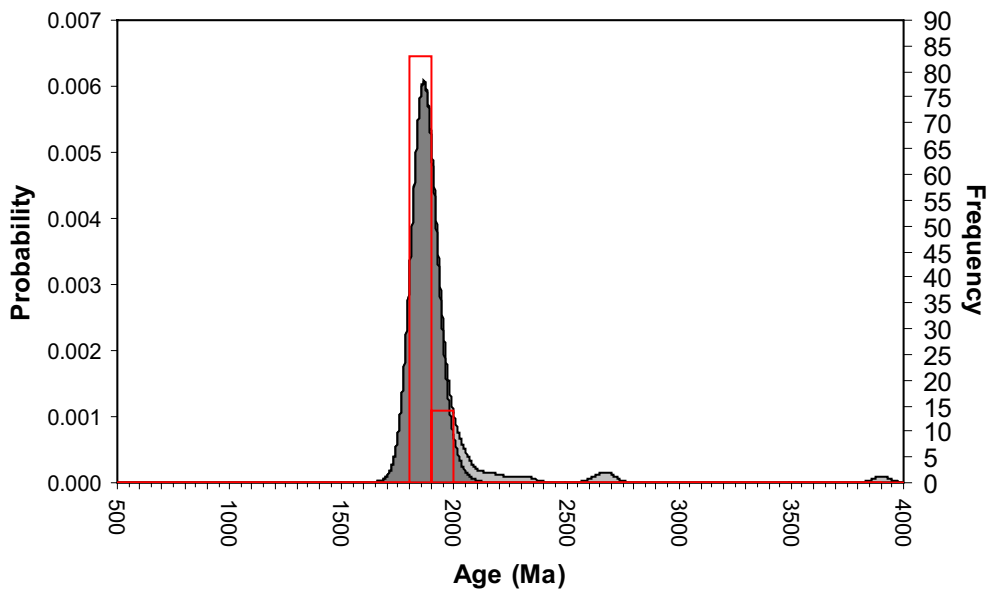
Itsaku, Svartenhuk Halvø

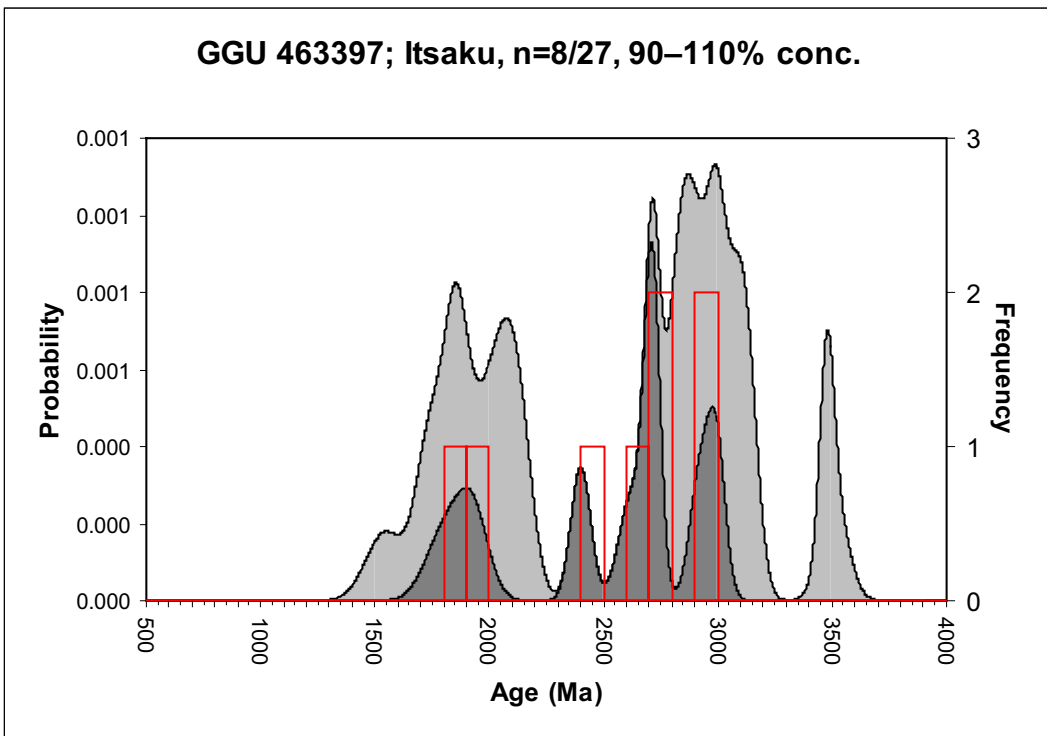
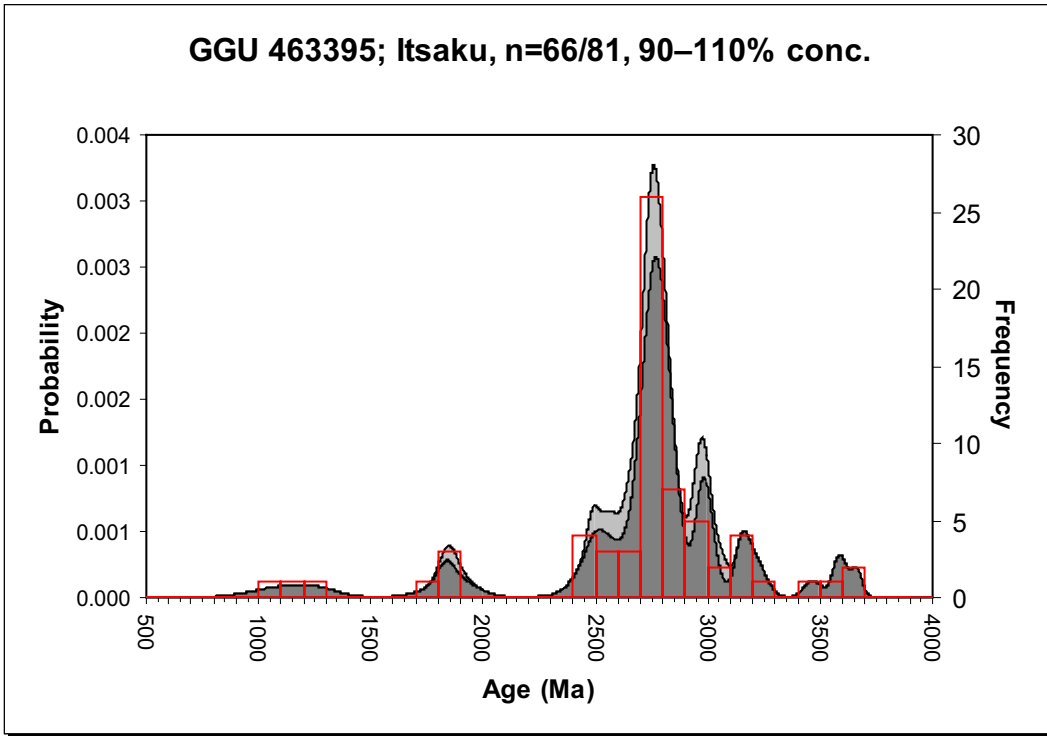


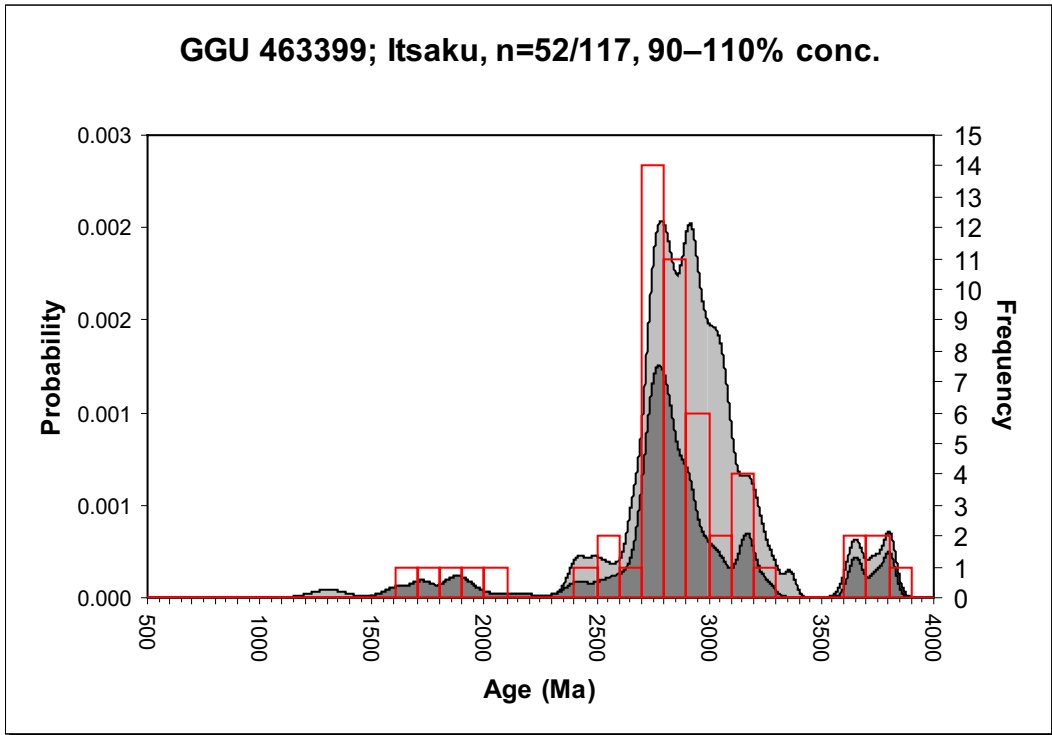
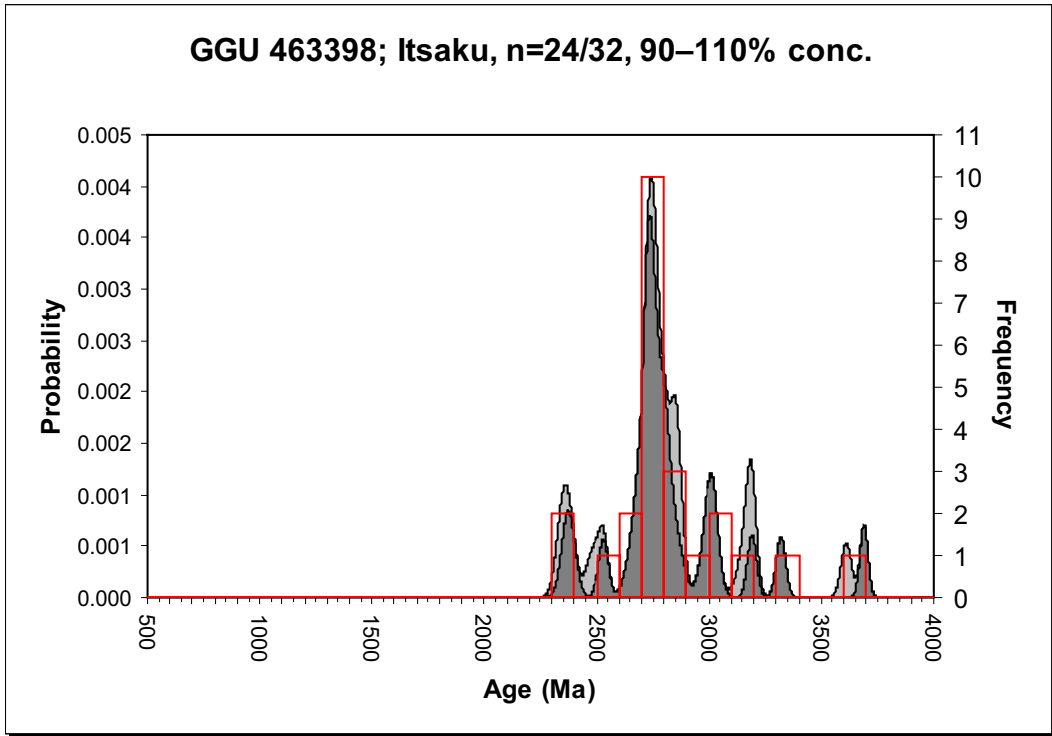
GGU 463391; Itsaku, n=75/106, 90–110% conc.



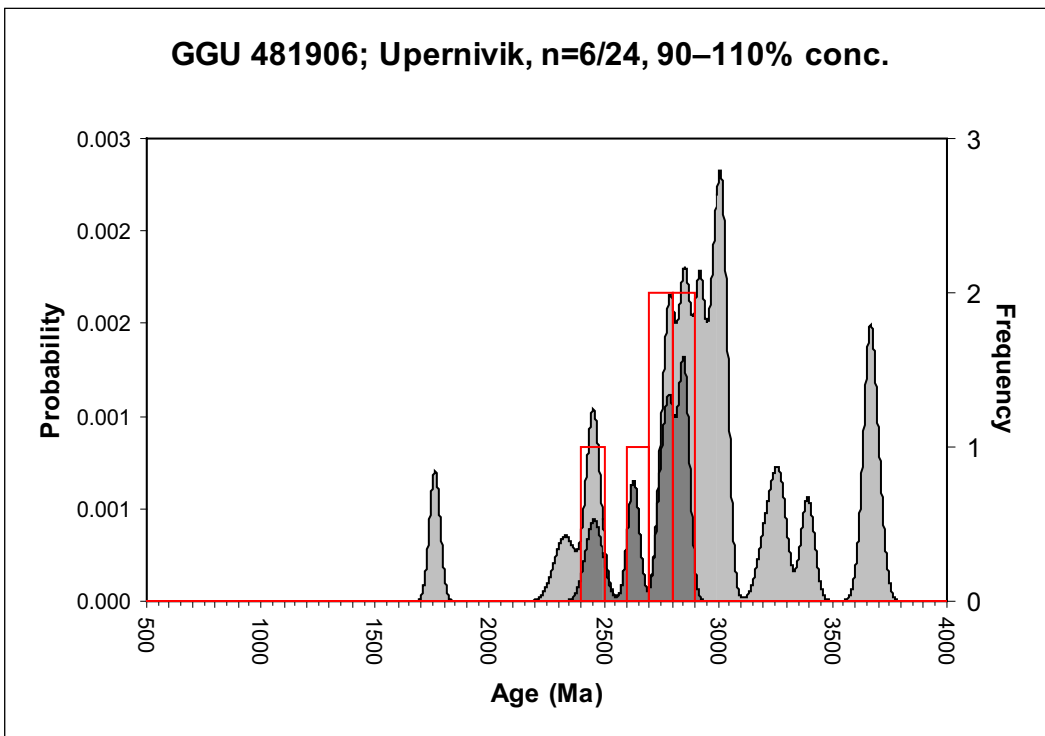
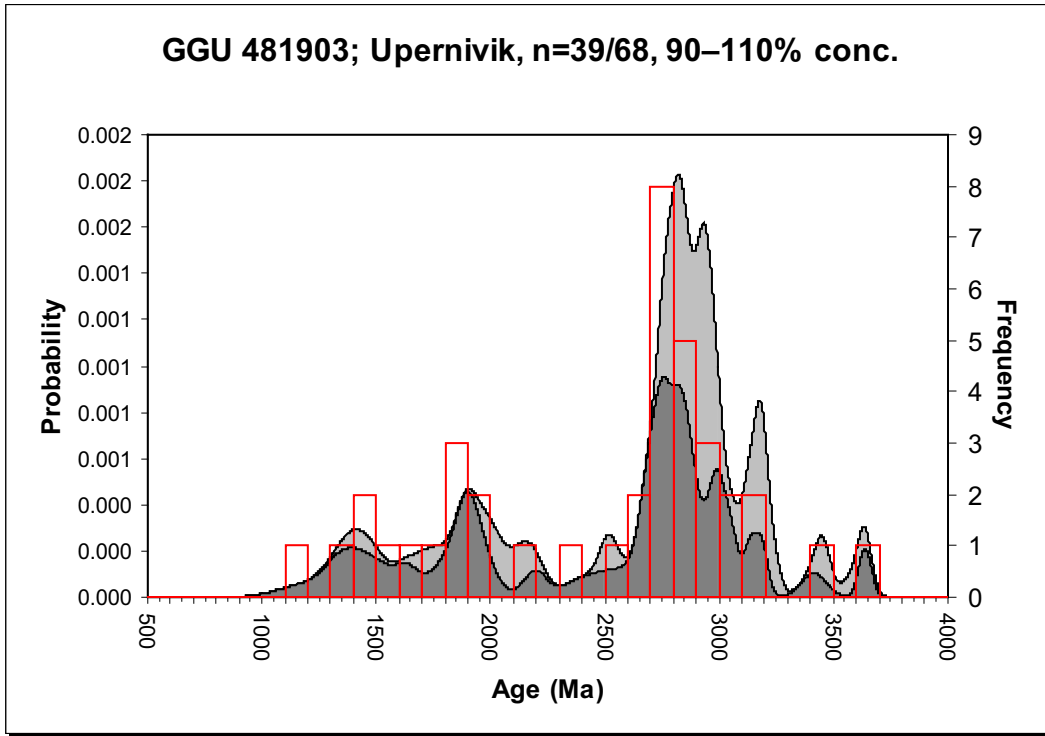
GGU 463392; Itsaku, n=97/109, 90–110% conc.

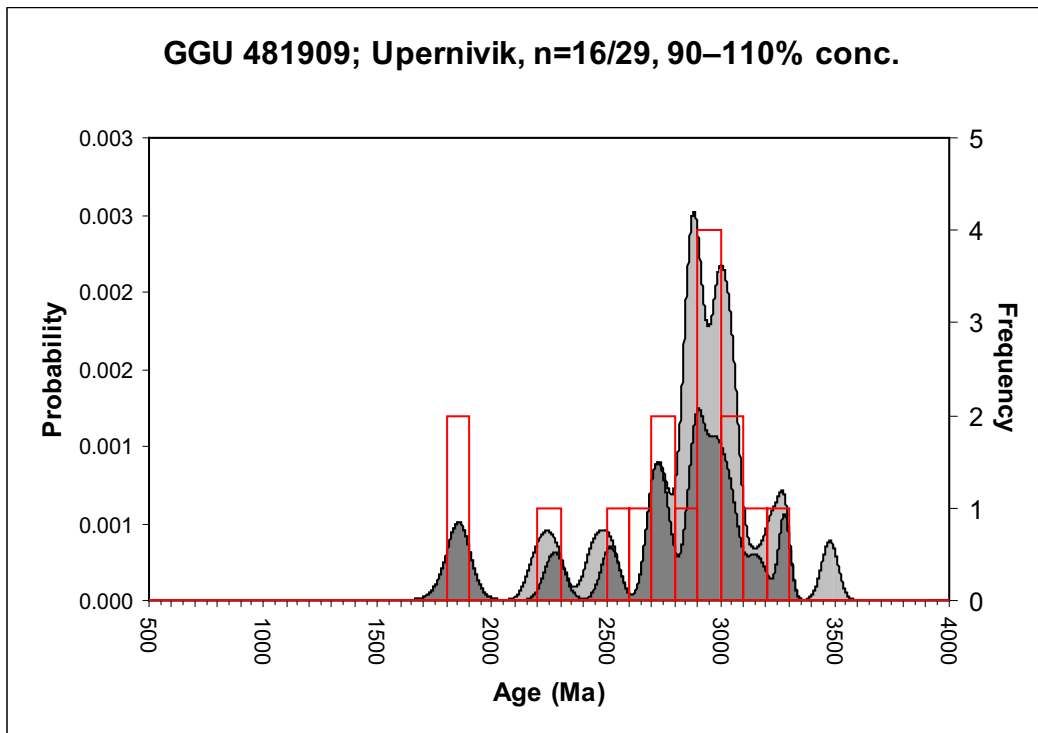
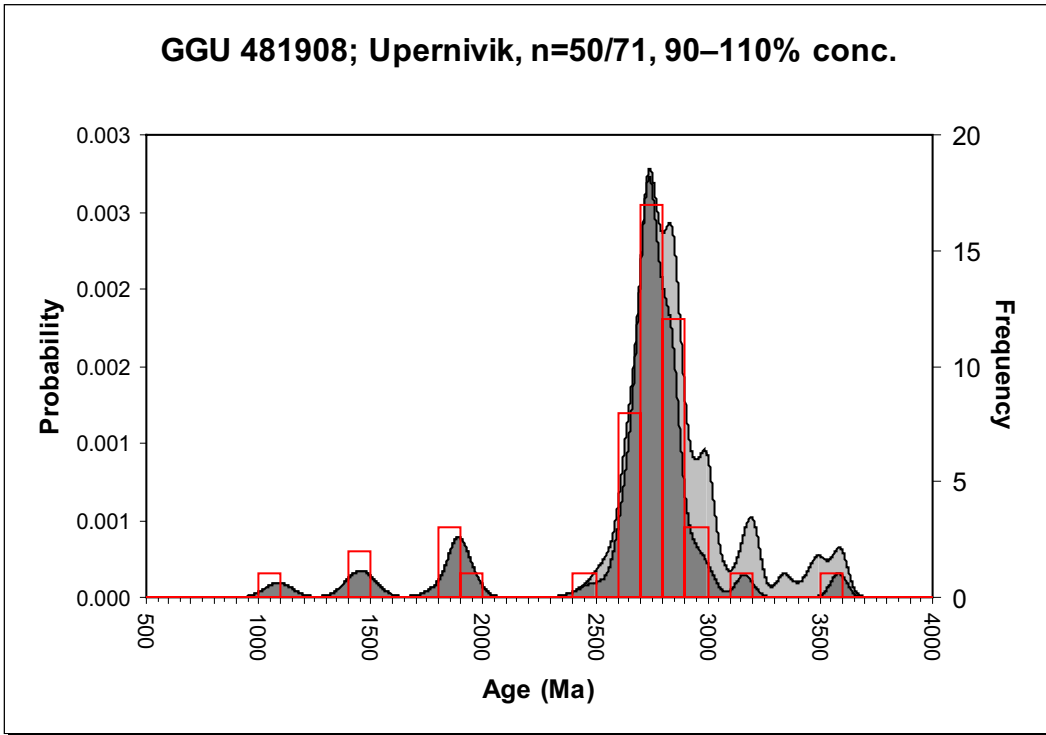




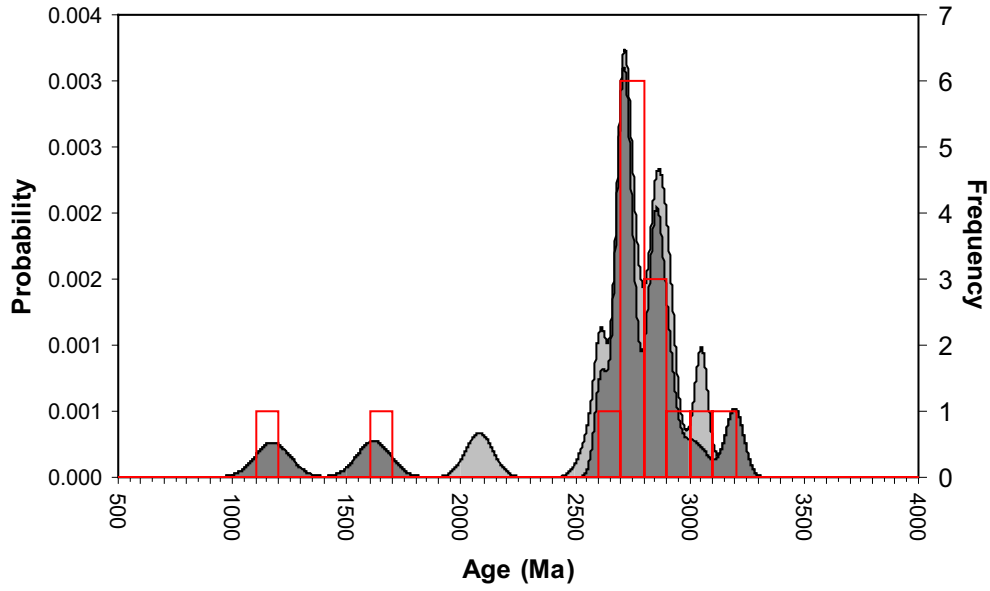


Upernivik

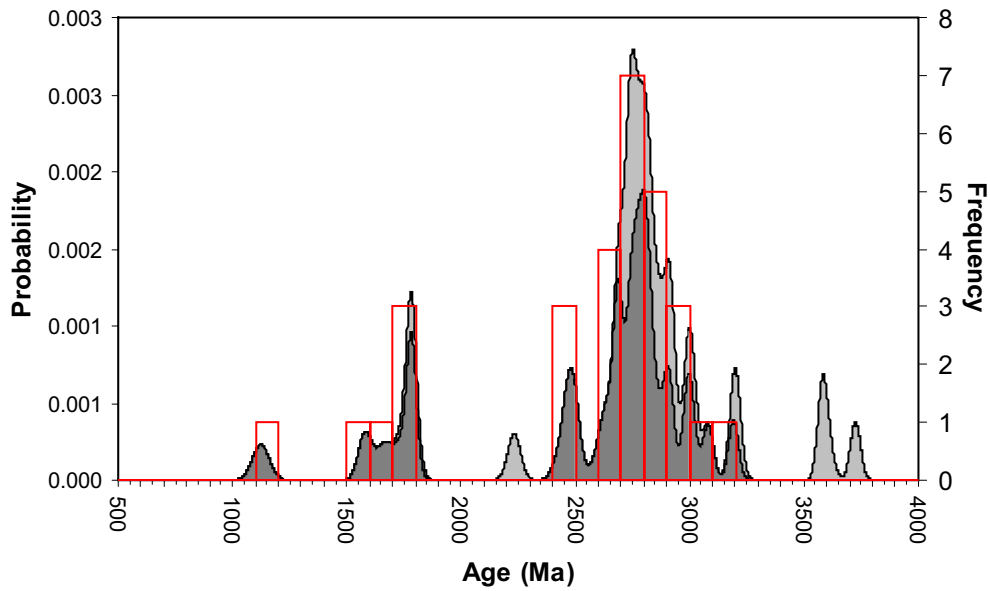




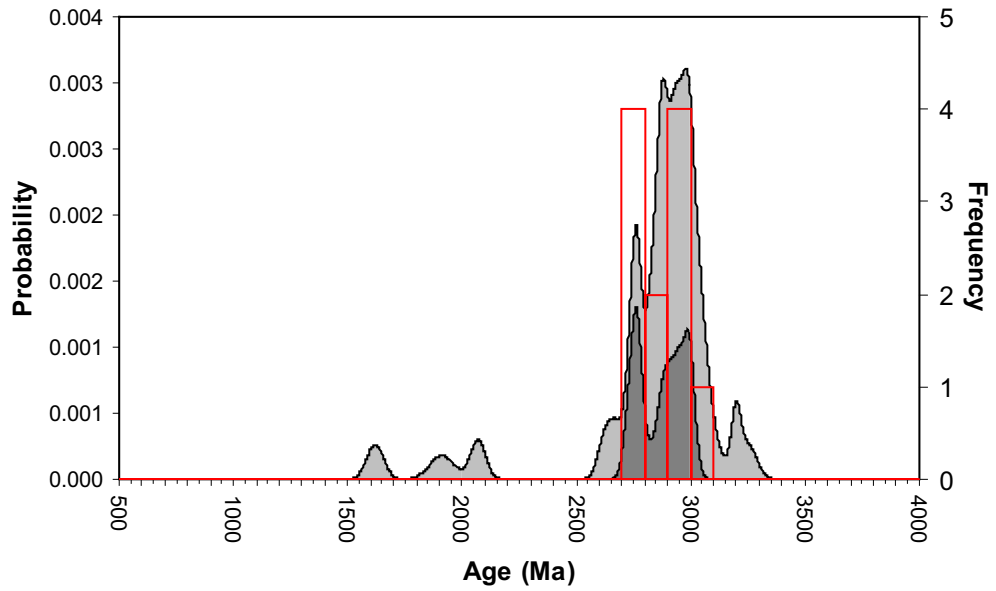
GGU 481910; Upernivik, n=15/20, 90–110% conc.



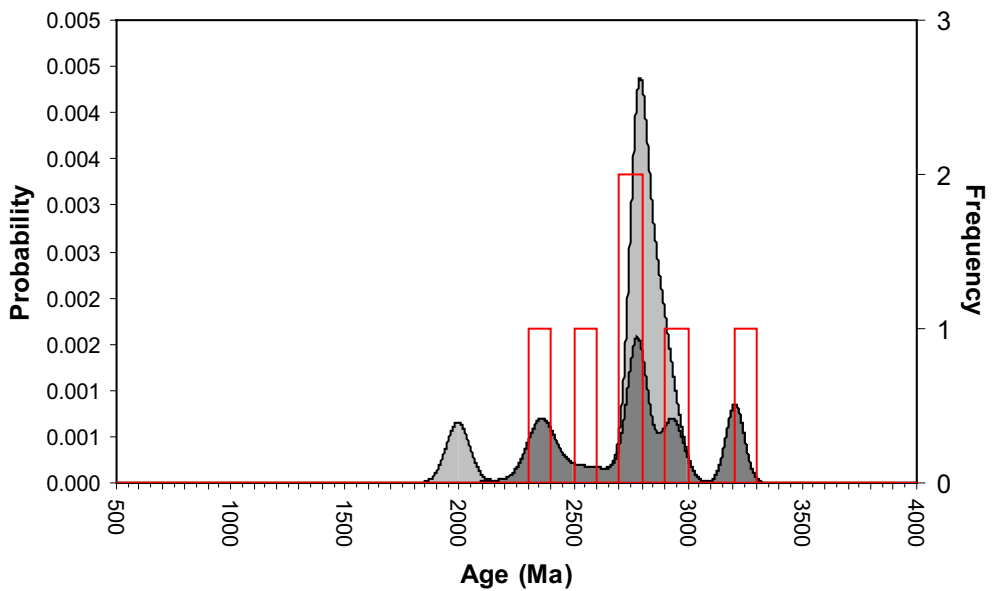
GGU 481912; Upernivik, n=30/47, 90–110% conc.



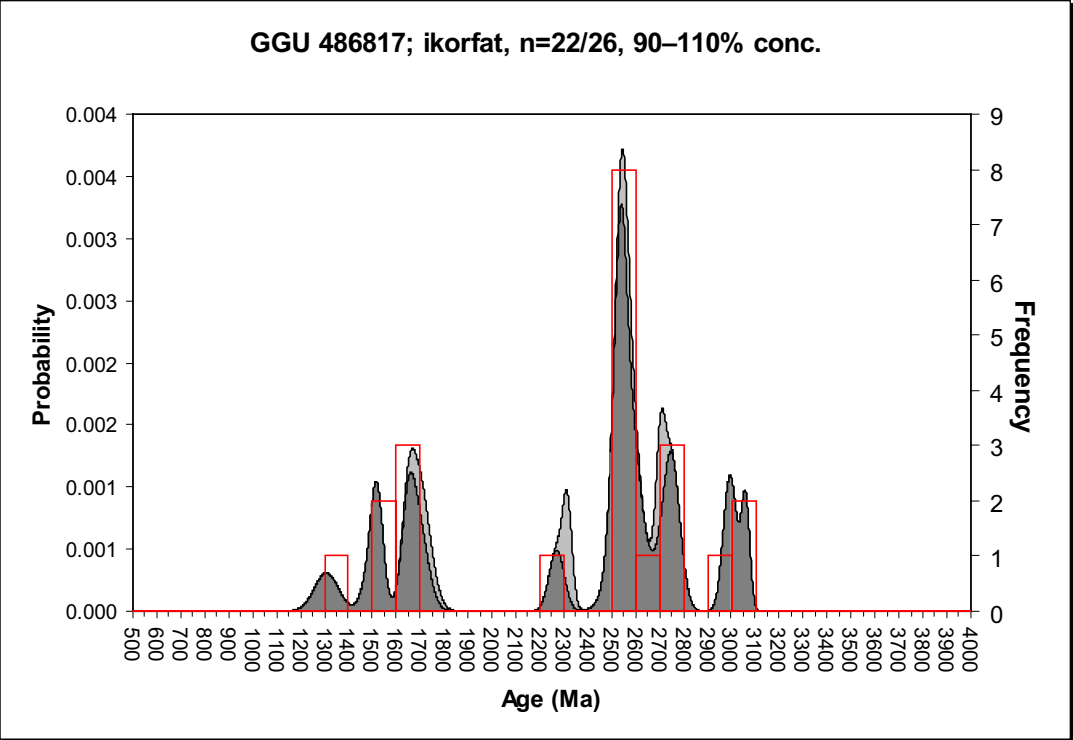
GGU 481913; Upernivik, n=11/41, 90–110% conc.



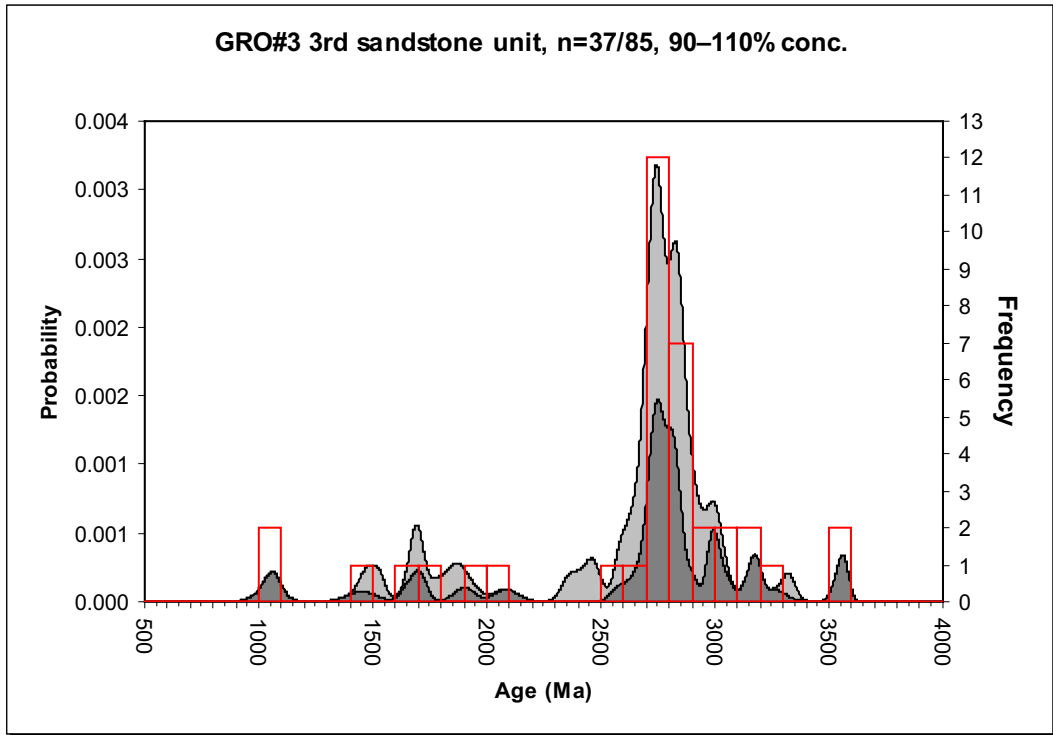
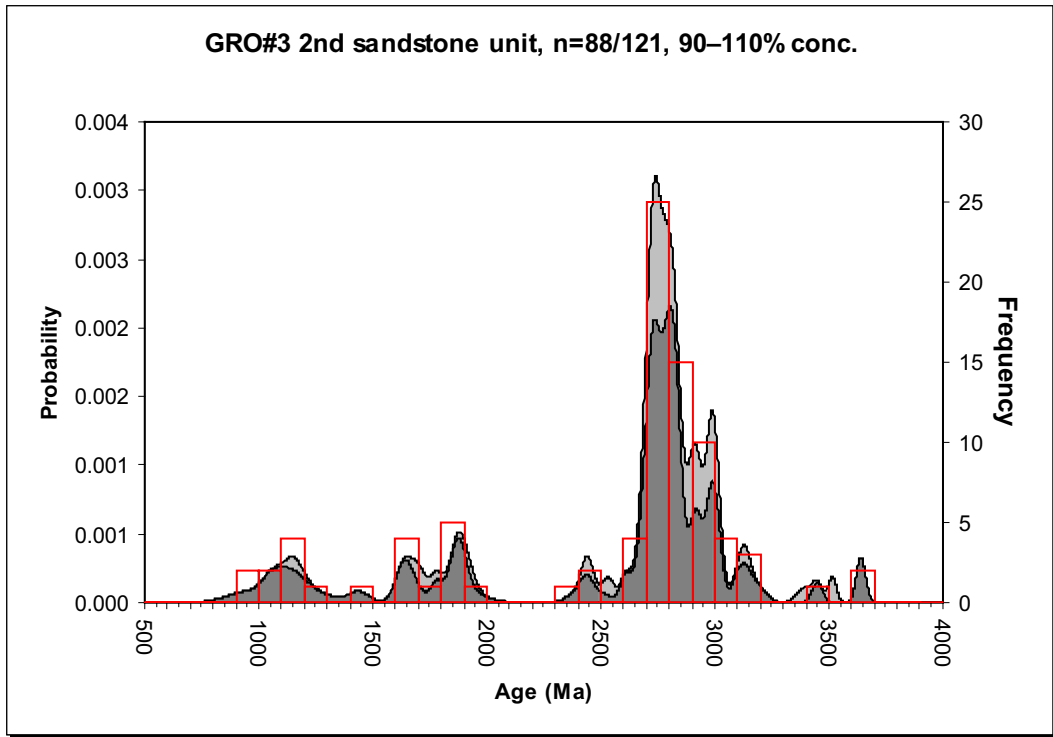
GGU 481914; Upernivik, n=6/12, 90–110% conc.

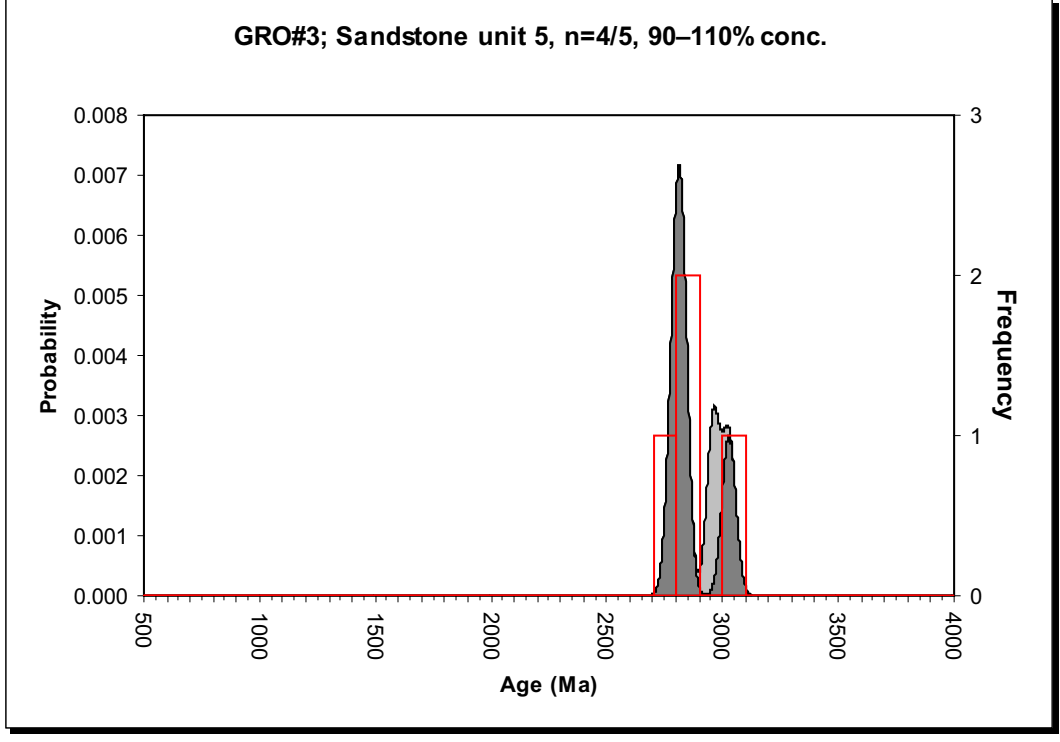
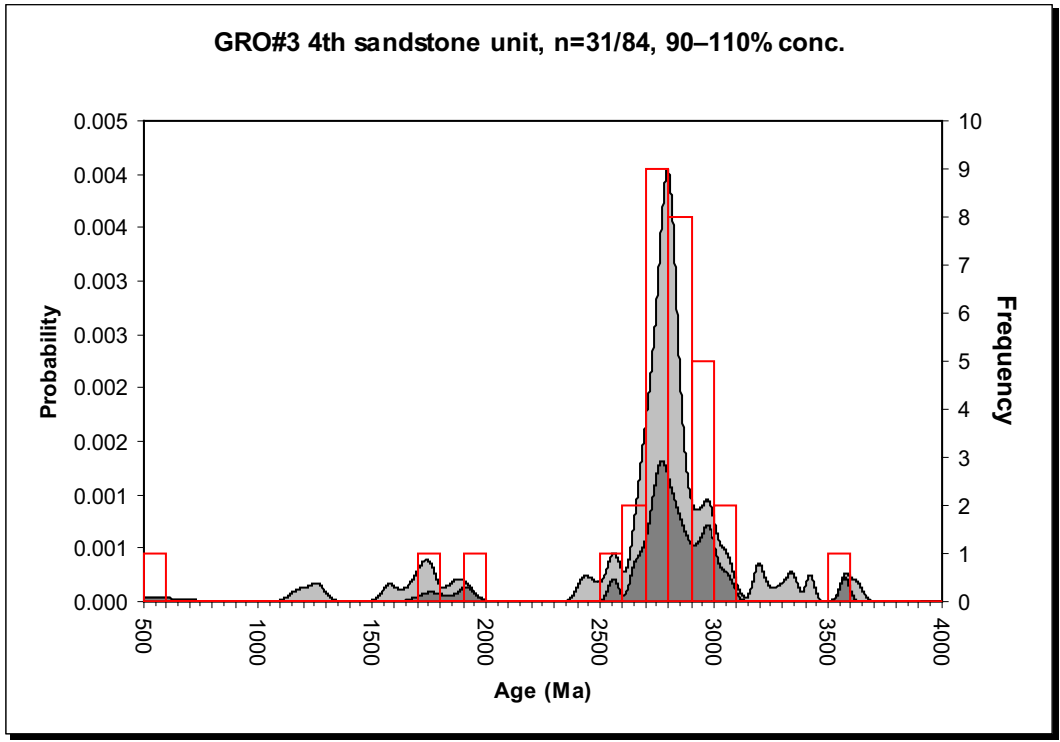


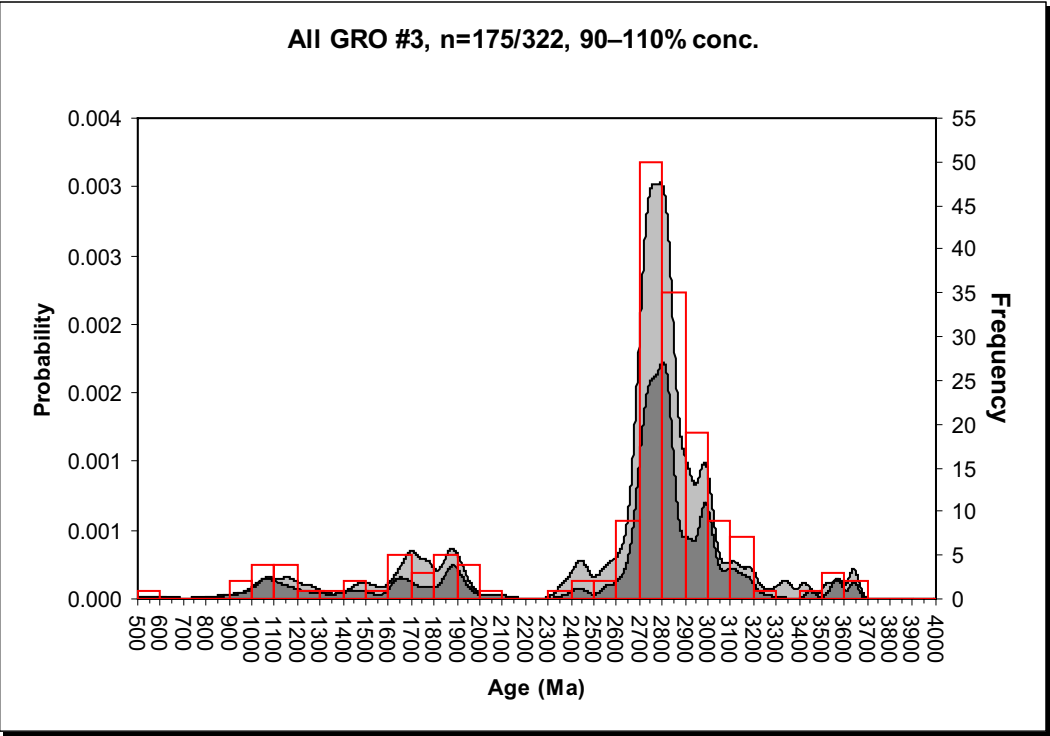
Ikorfat



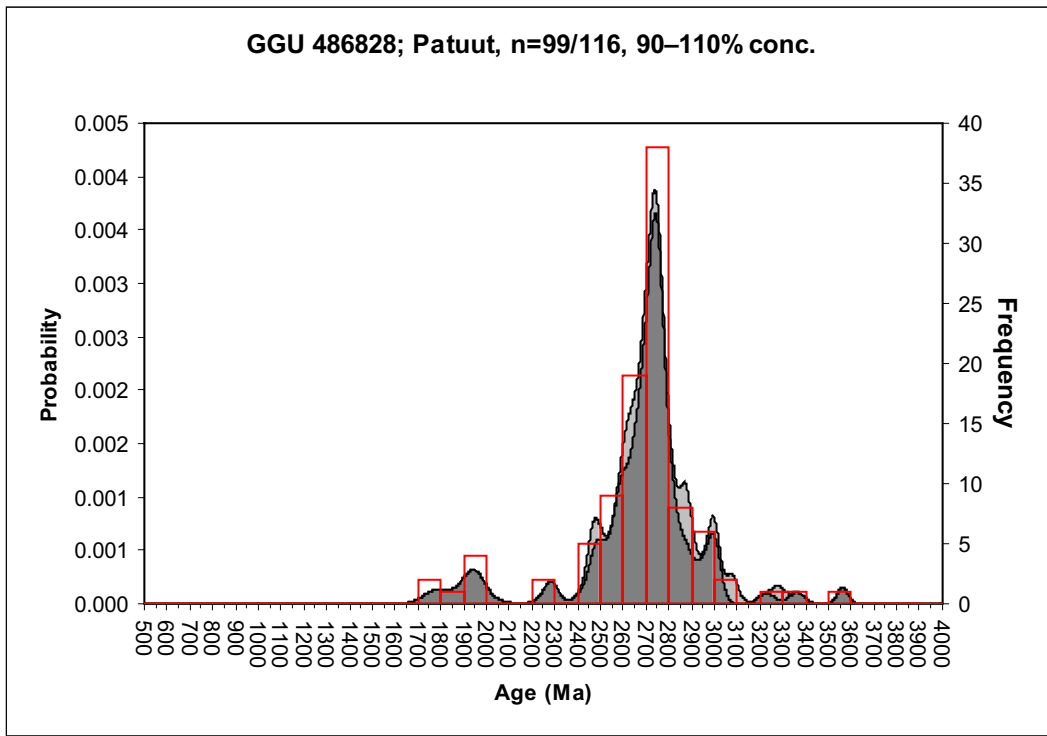
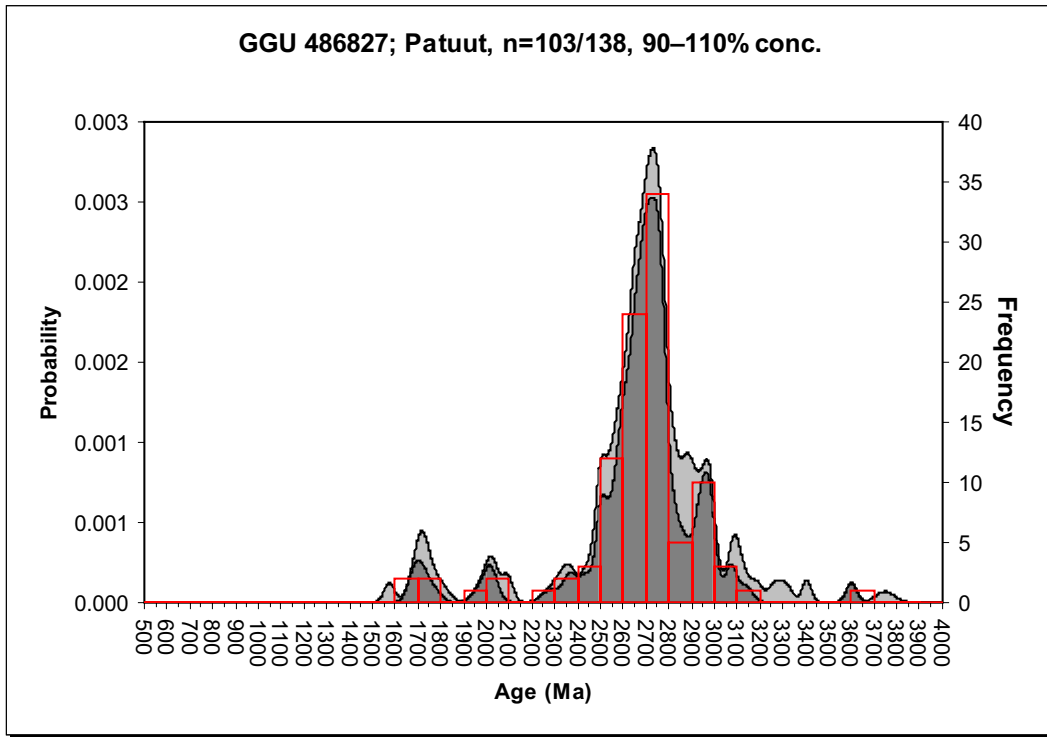
GRO#3

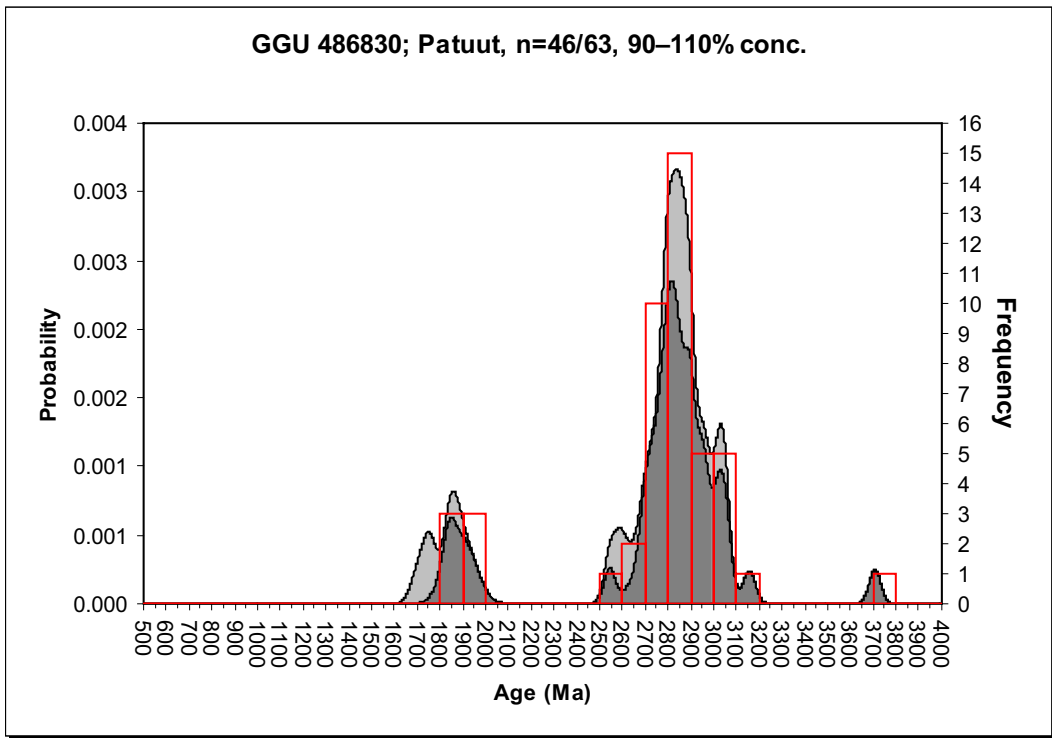
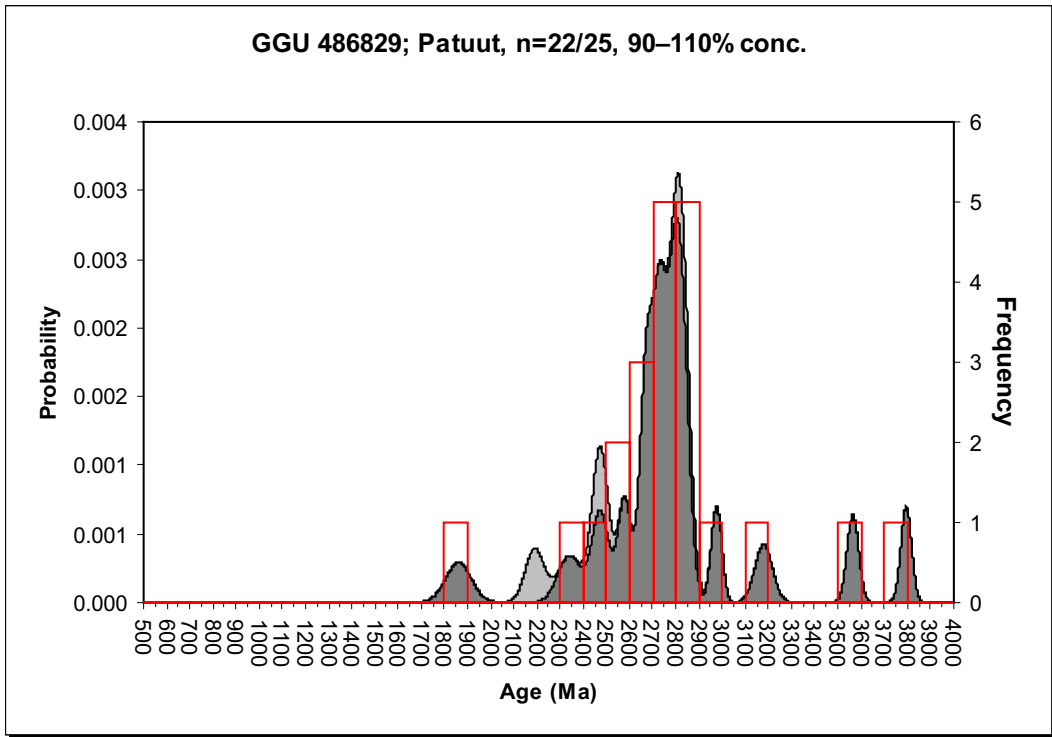




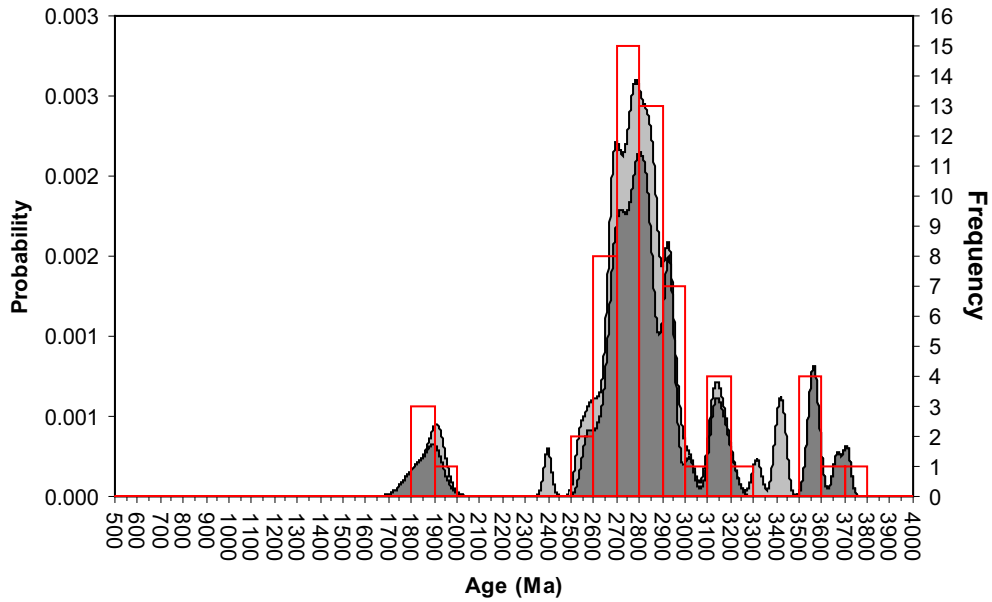


Patuut

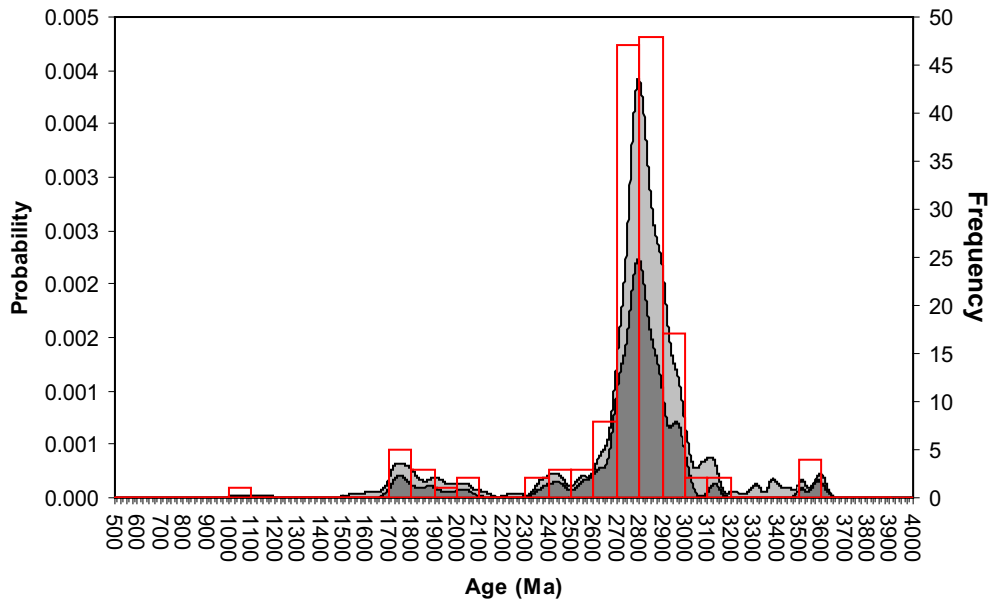




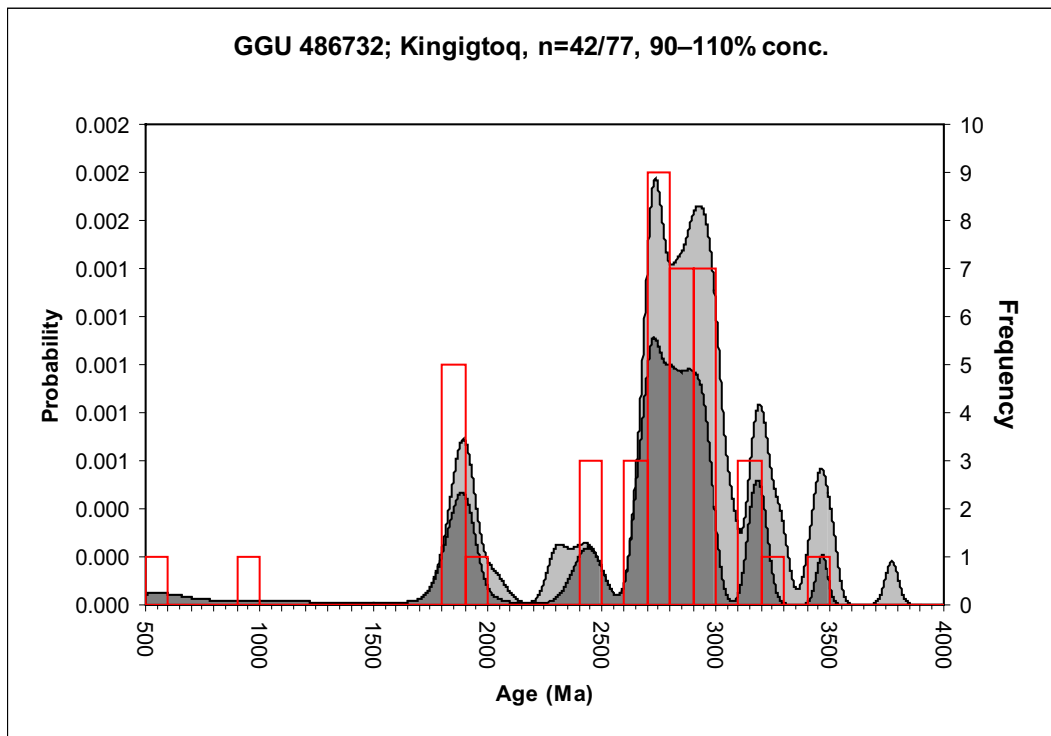
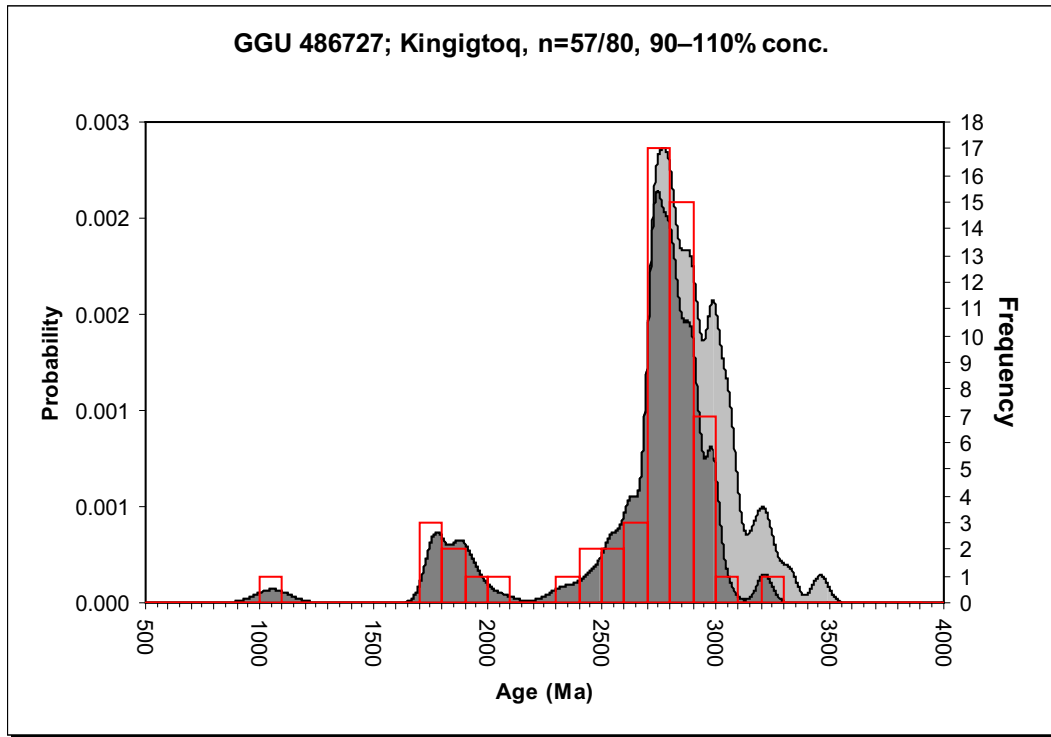
GGU 486831; Patuut, n=61/82, 90–110% conc.

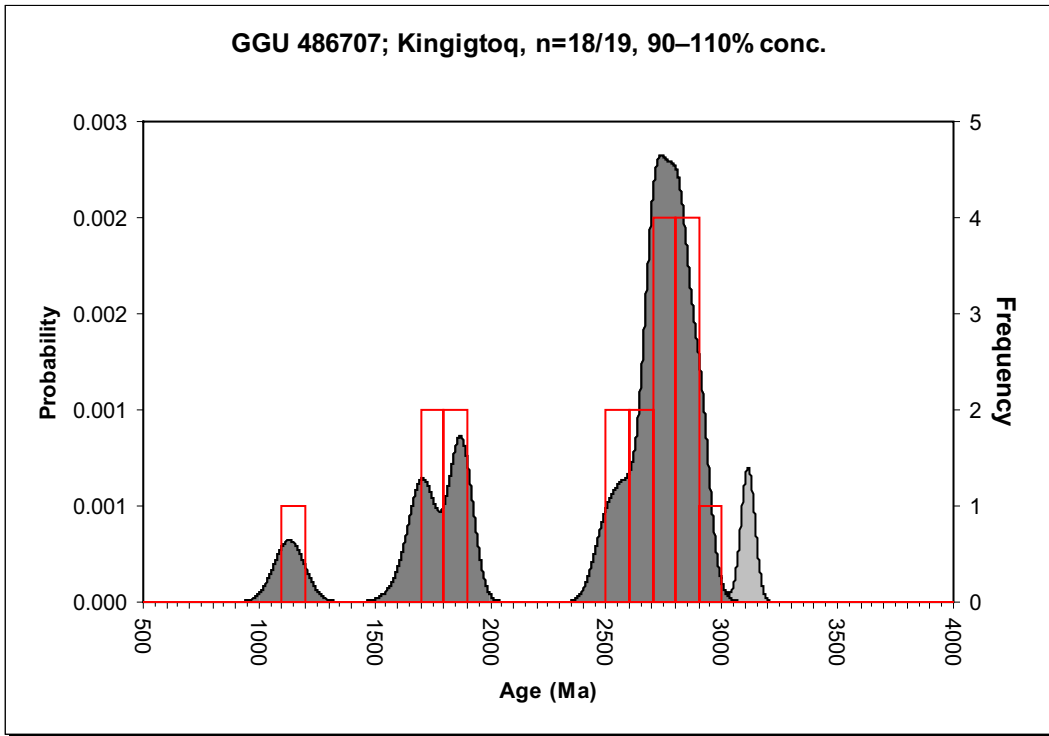
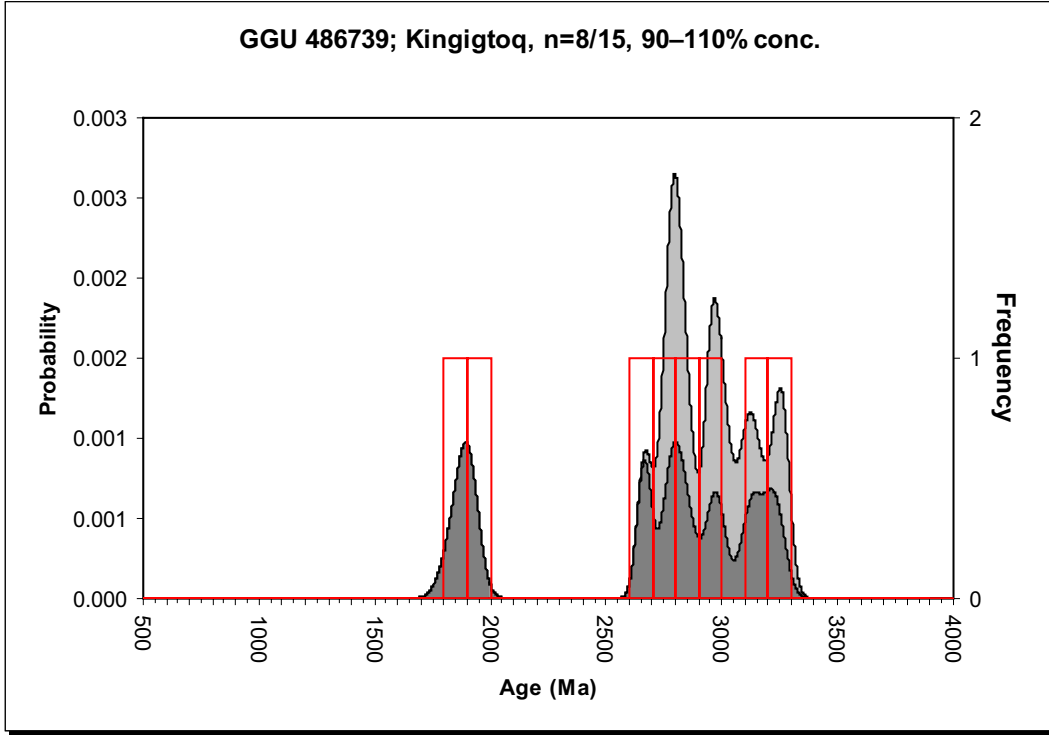


GGU 486834; Patuut, n=148/272, 90–110% conc.

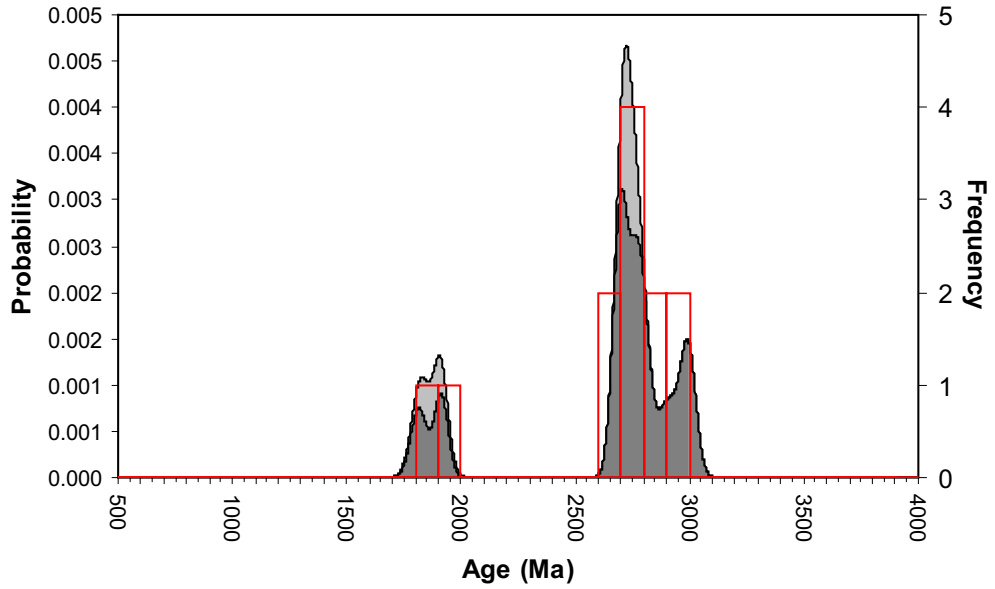


Kingigtoq, Disko

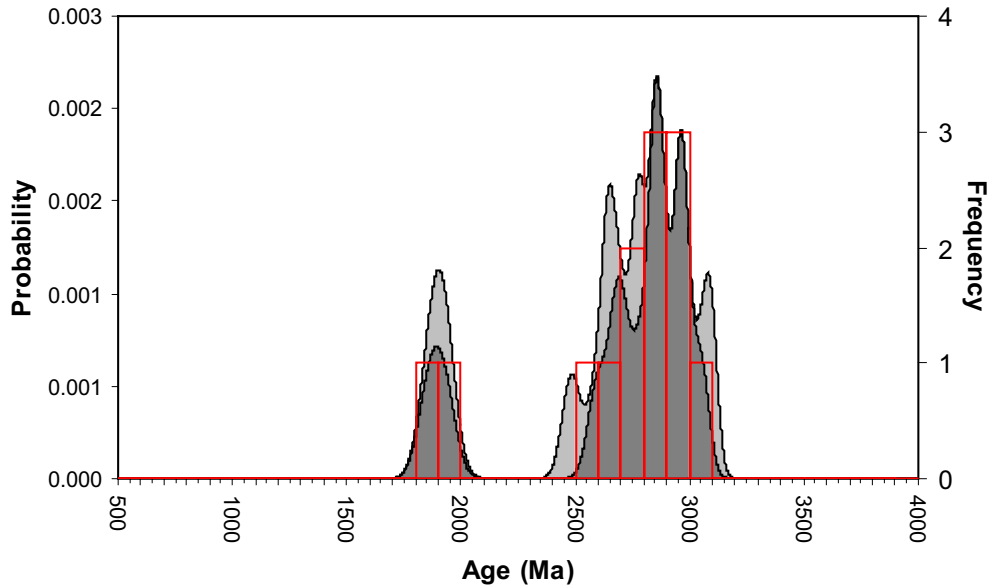




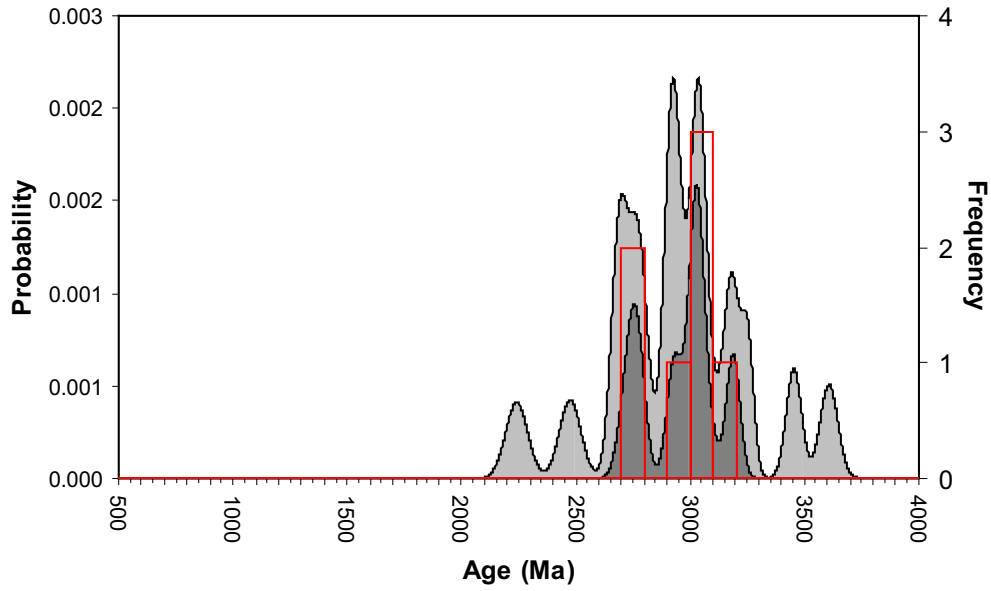
GGU 486718; Kingigtoq, n=12/15, 90–110% conc.



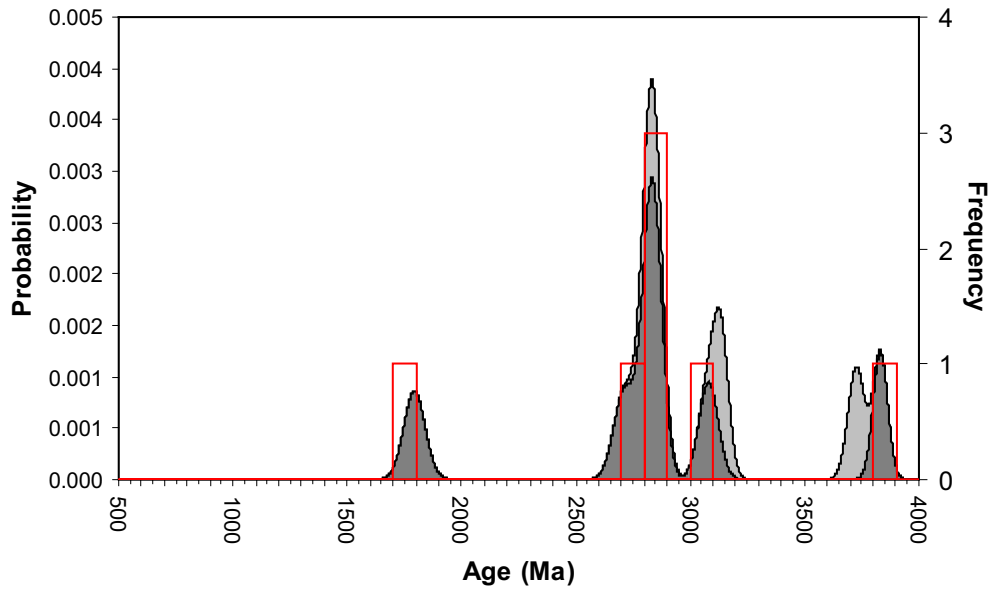
GGU 486746; Kingigtoq, n=13/18, 90–110% conc.



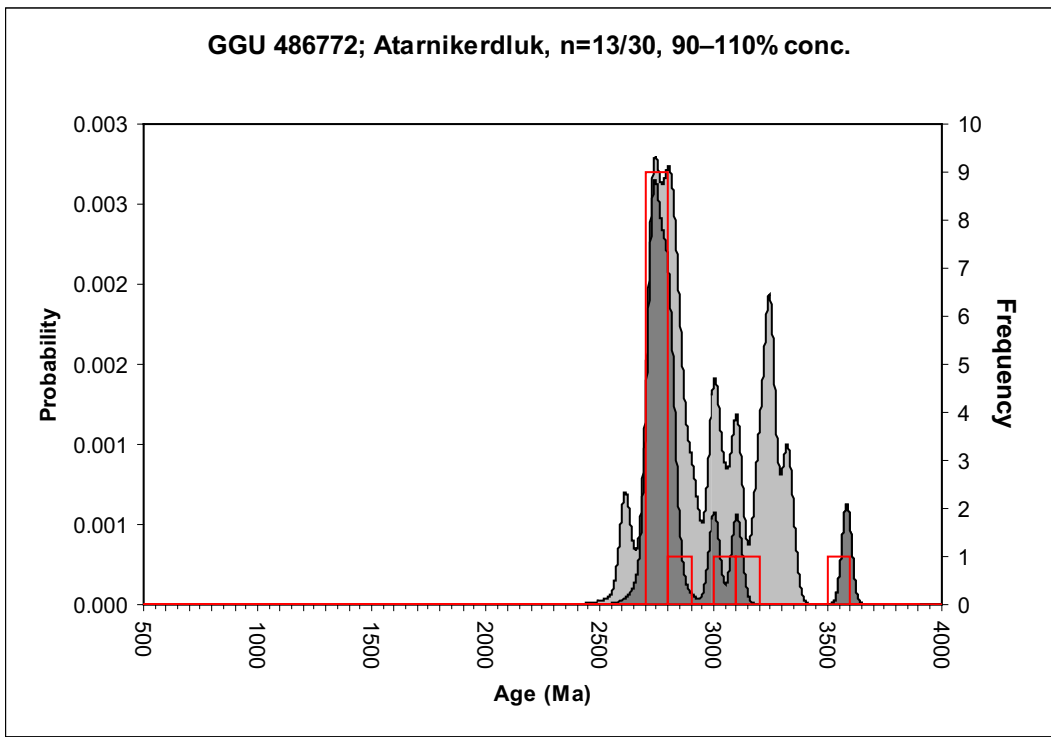
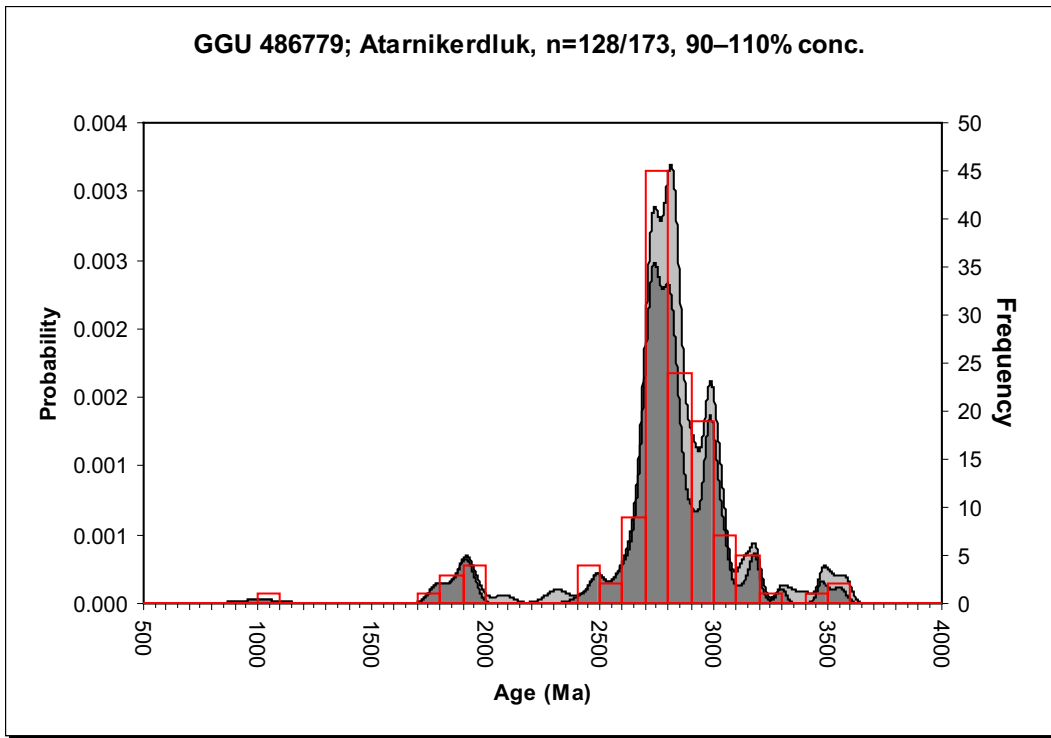
GGU 486722; Kingigtoq, n=7/20, 90–110% conc.

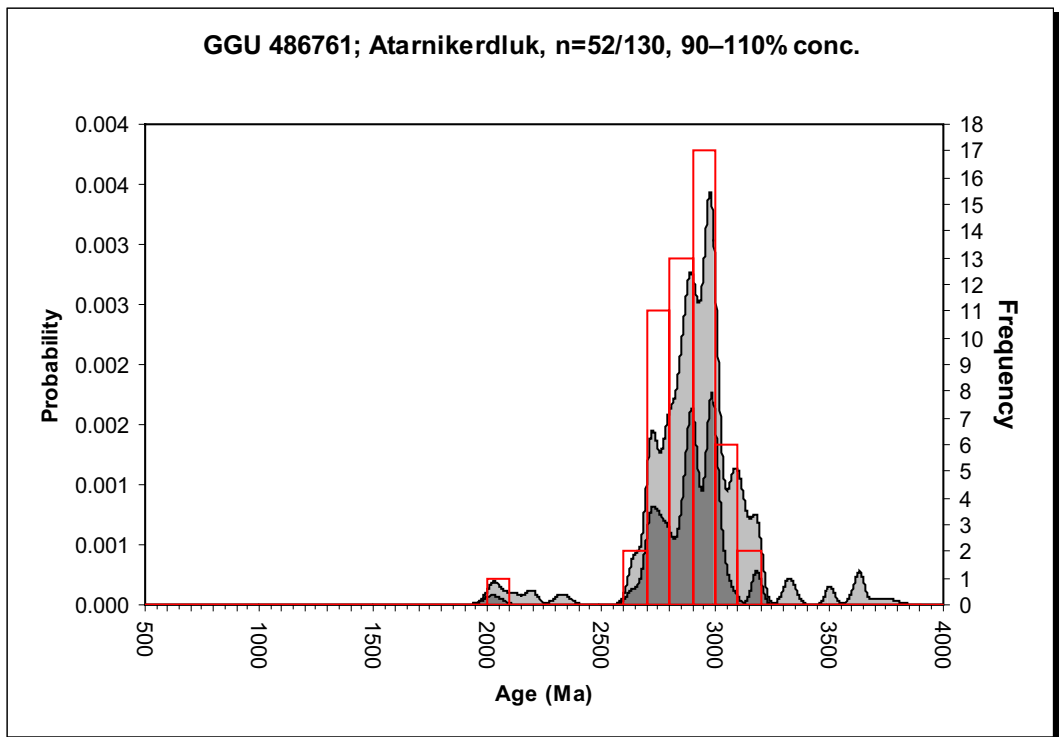
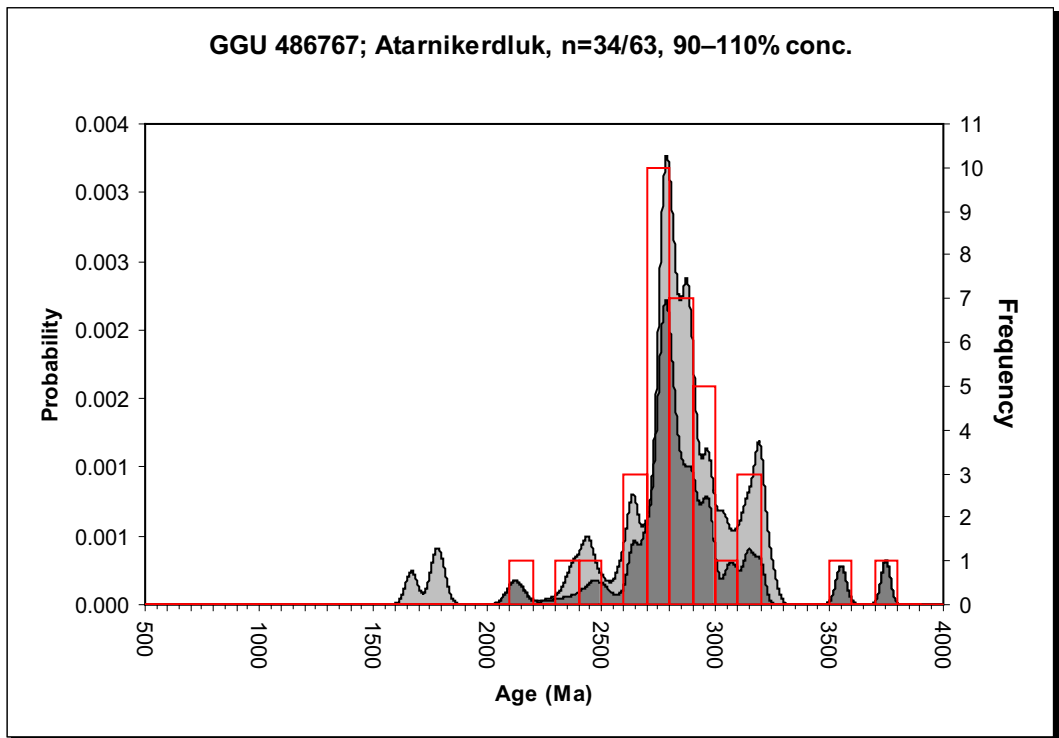


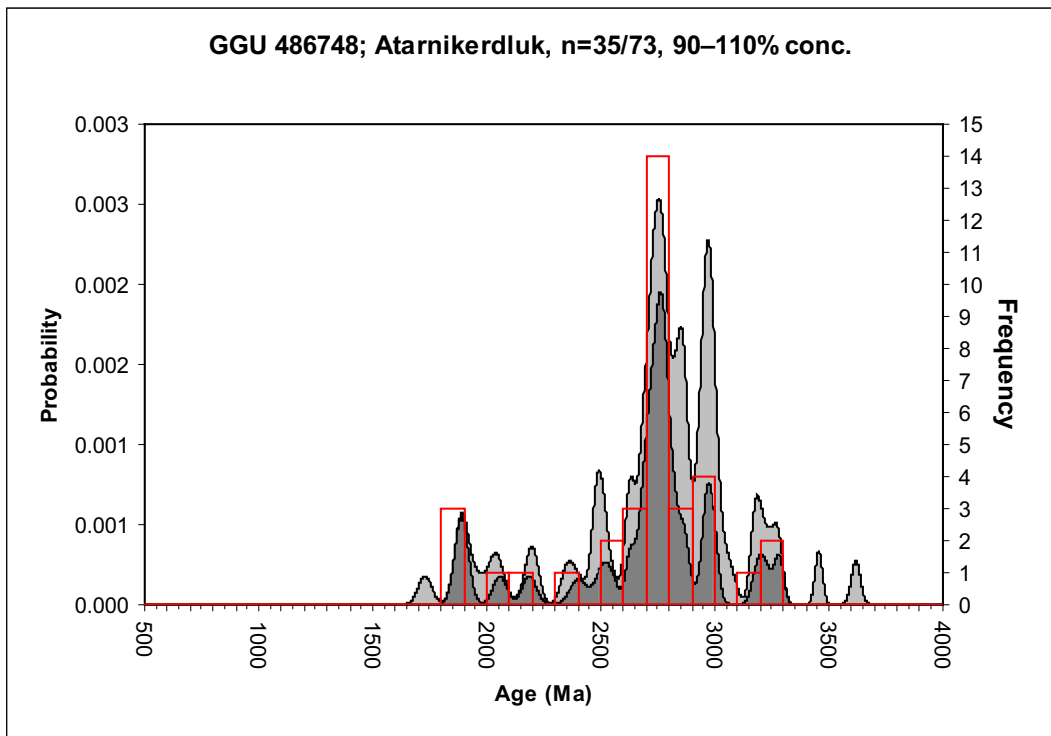
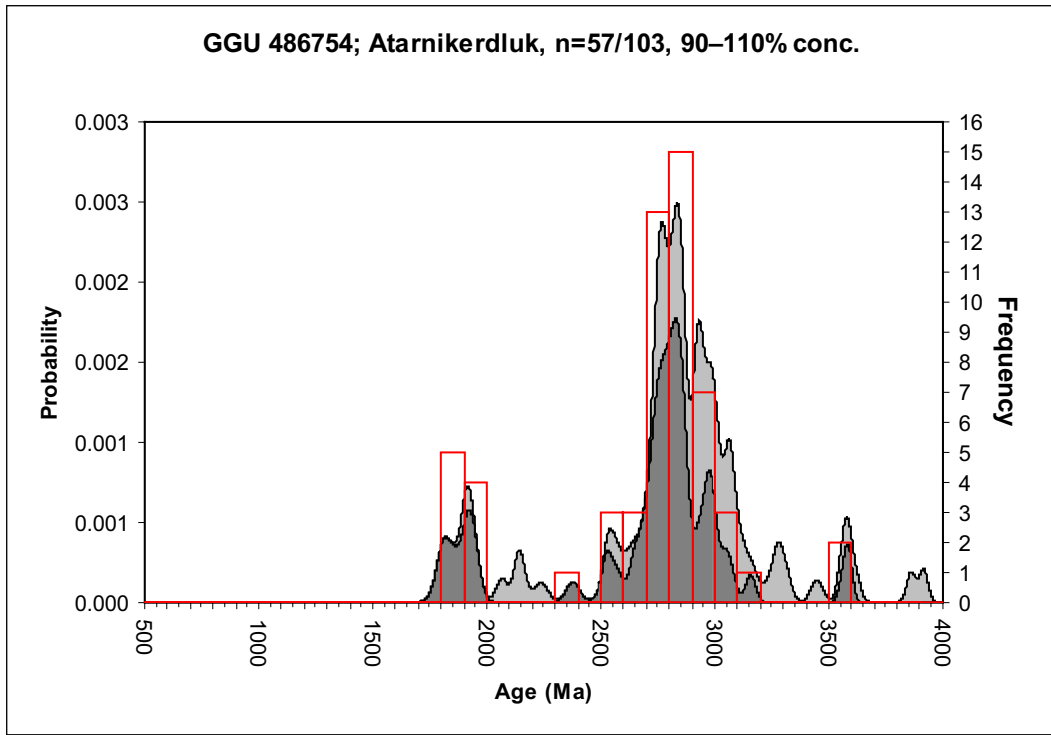
GGU 486713; Kingigtoq, n=7/10, 90–110% conc.



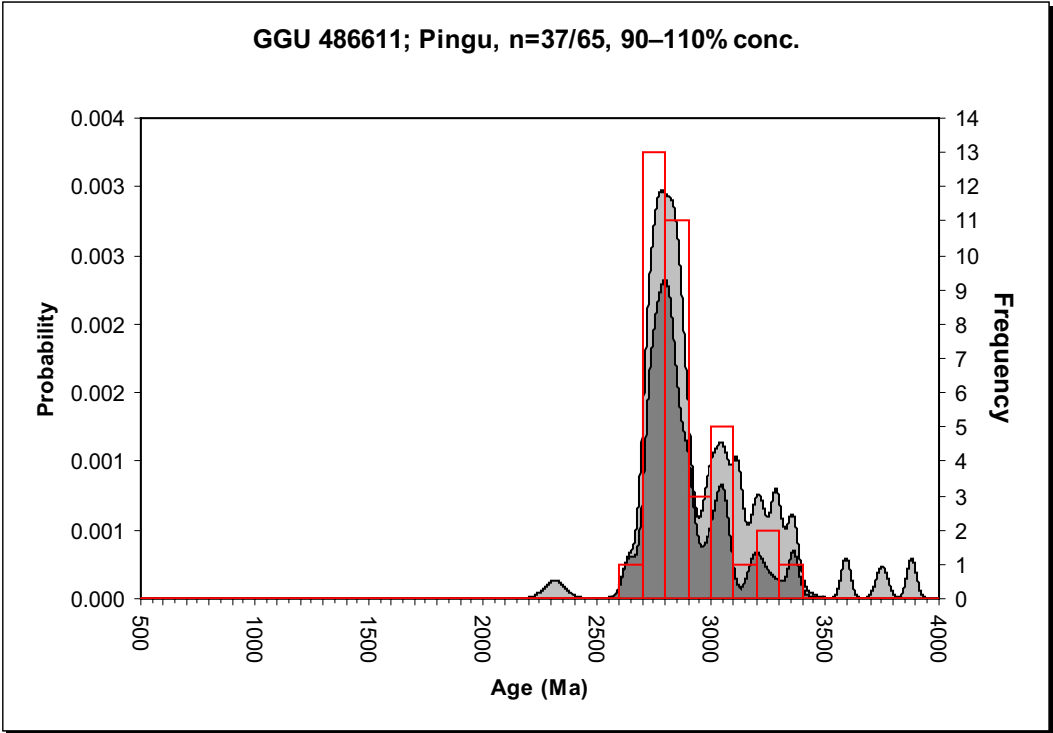
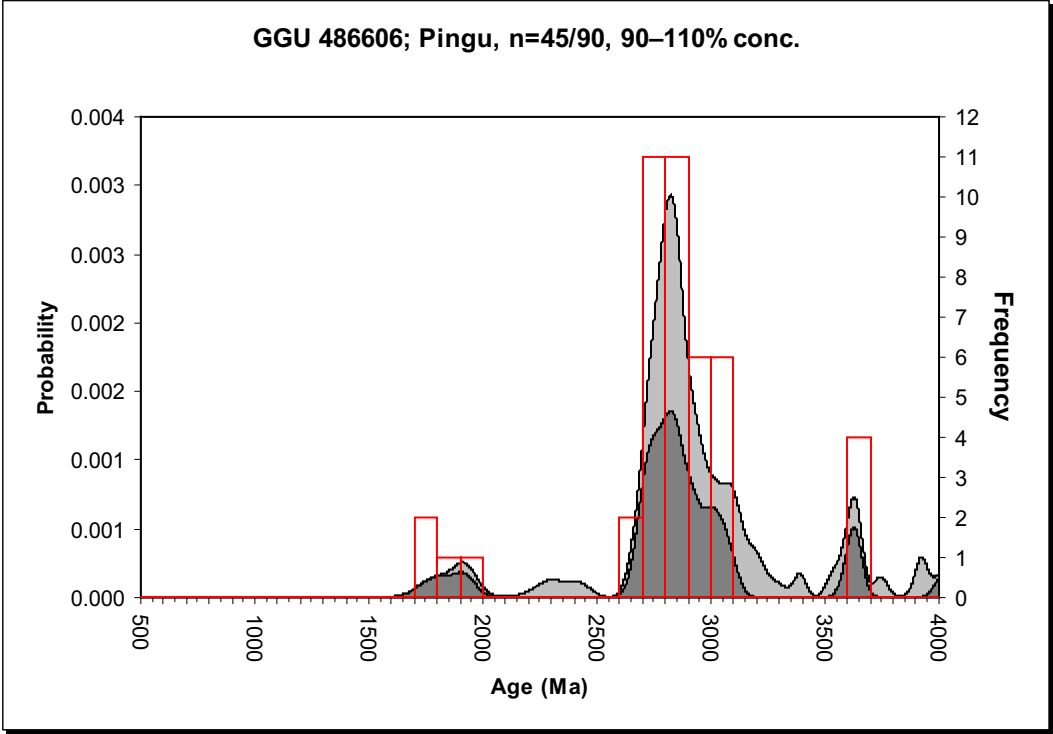
Atarnikerdluk



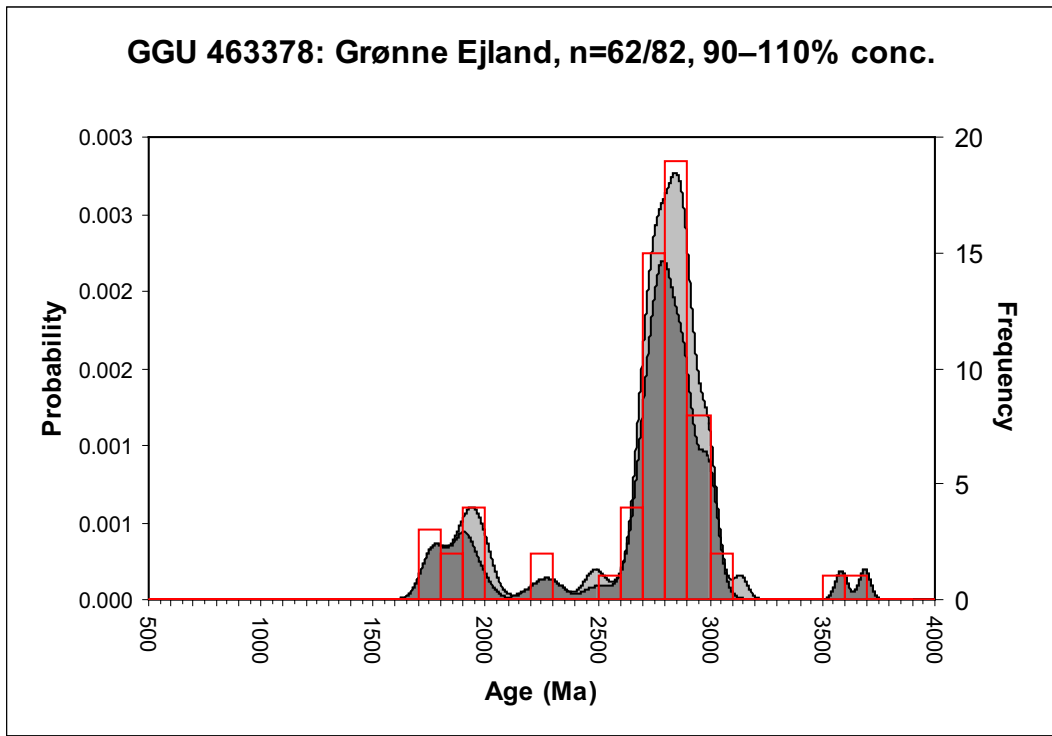
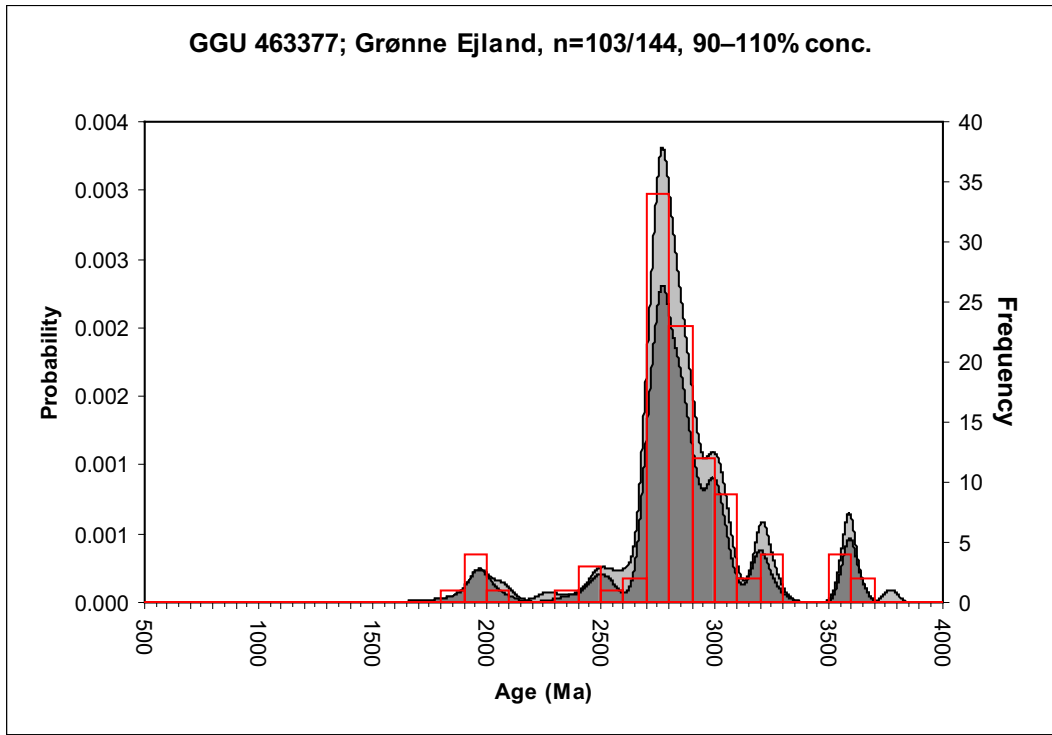




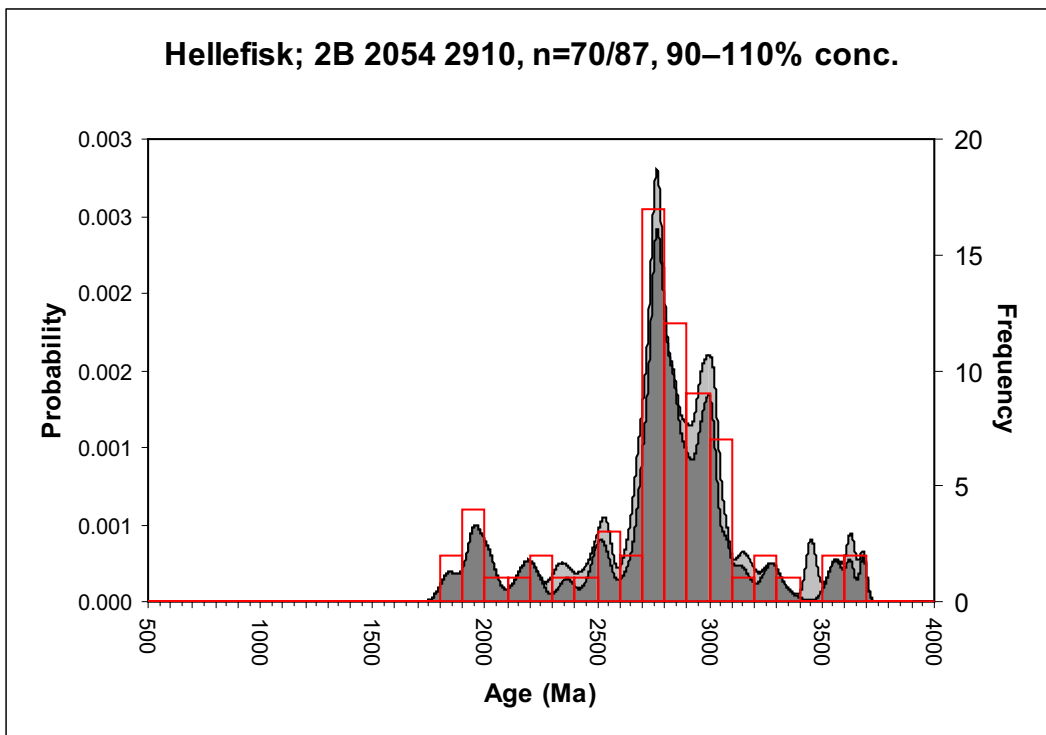
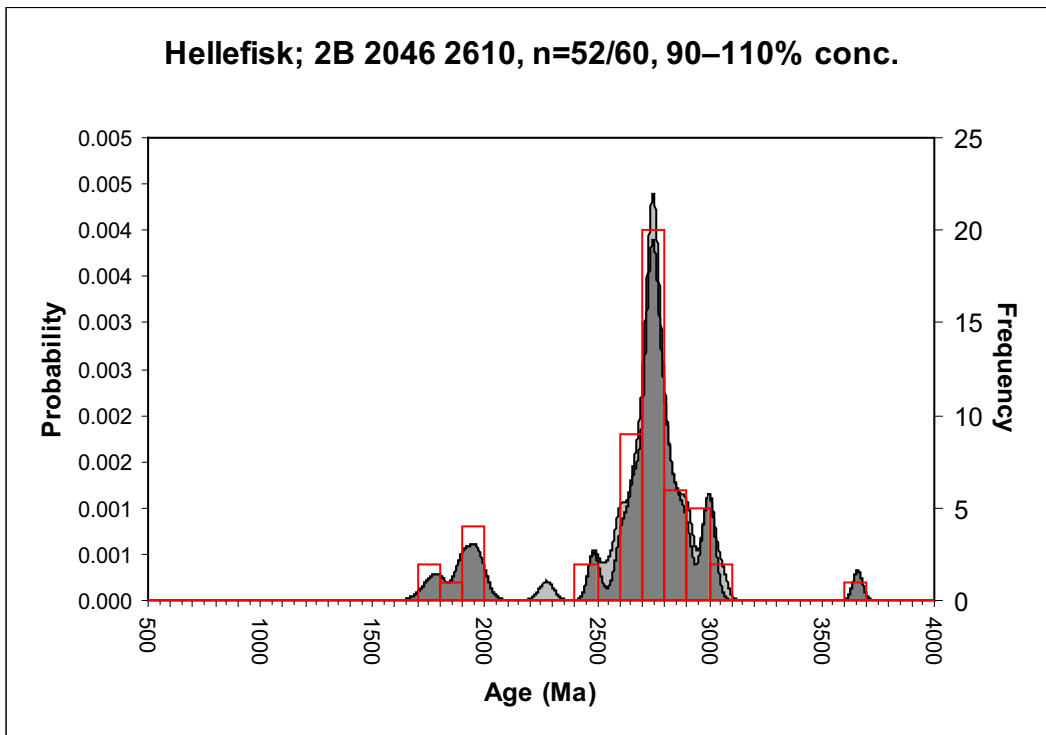
Pingu

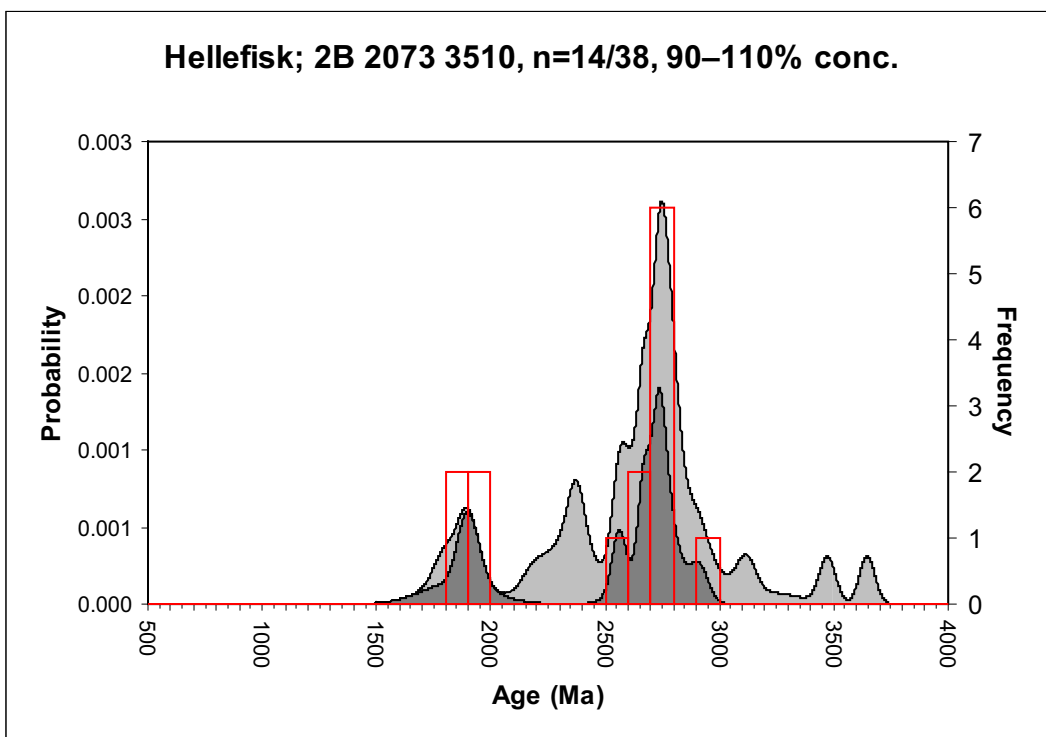
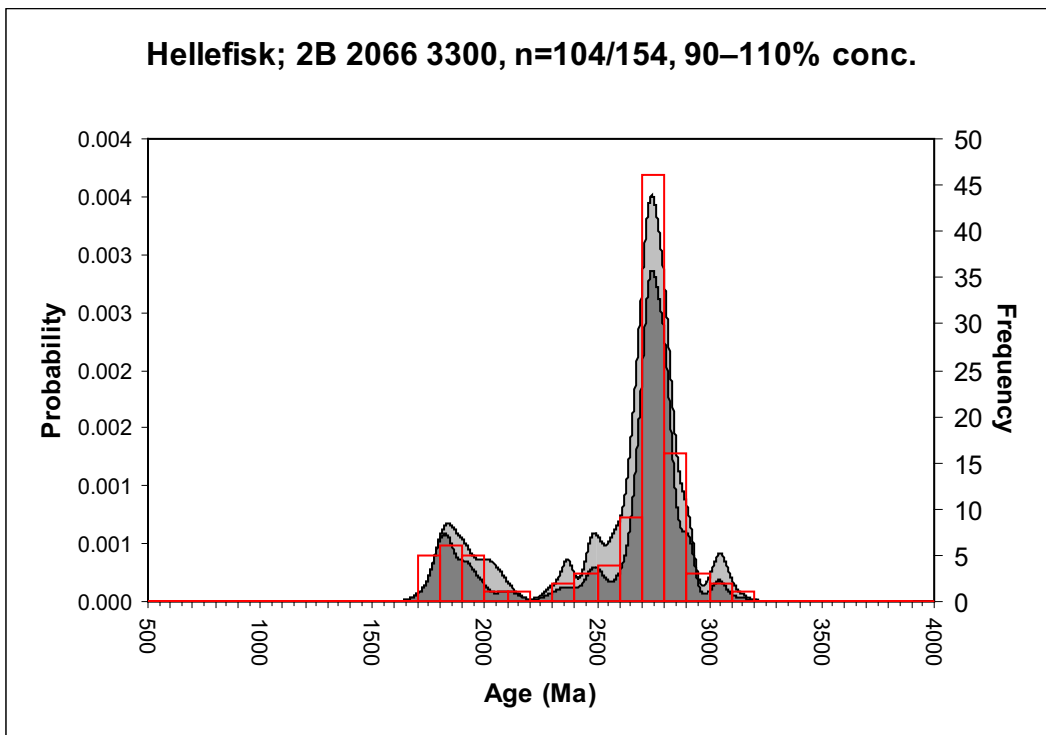


Grønne Ejland

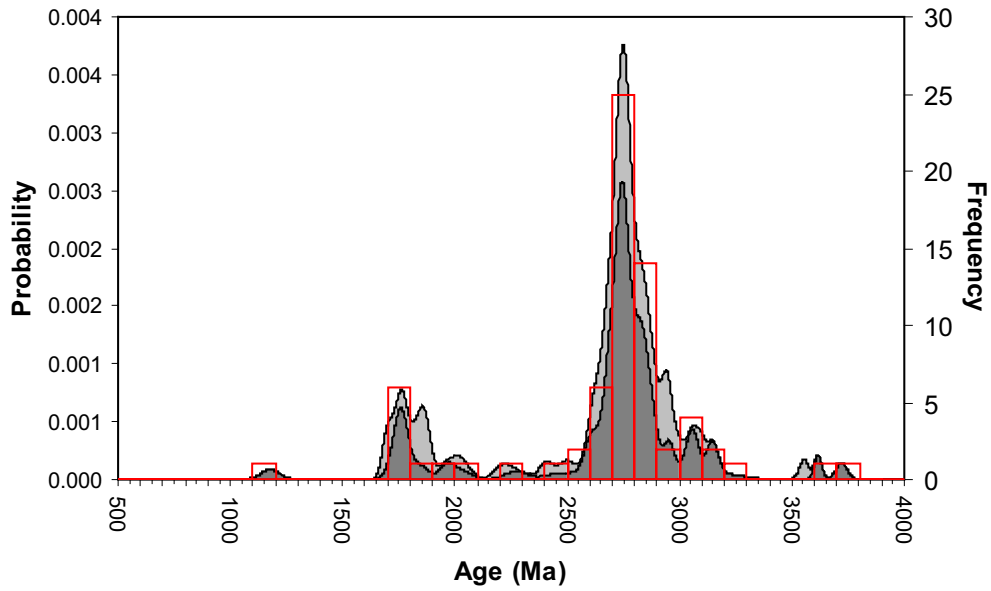


Hellefisk-1

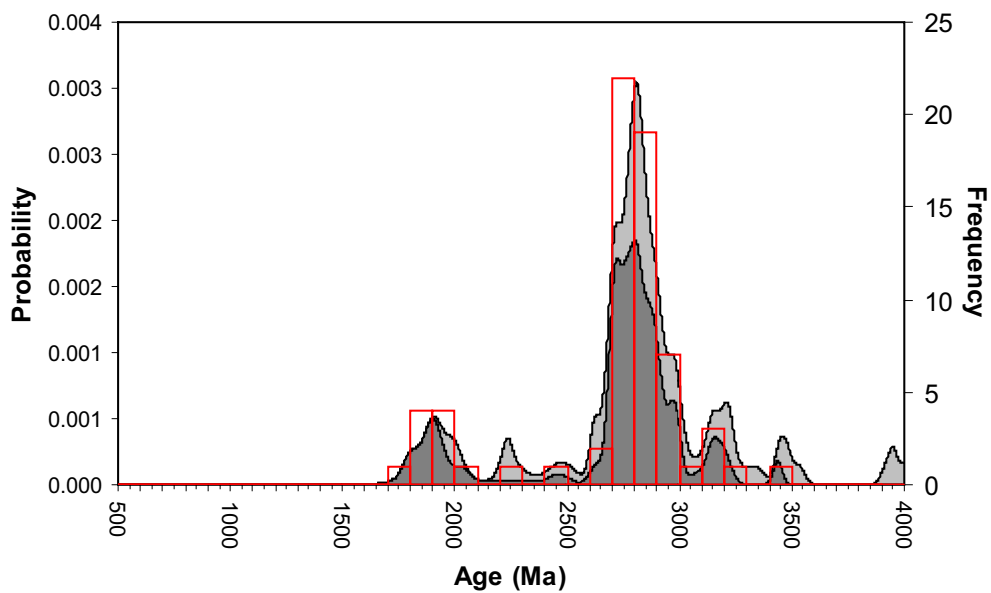




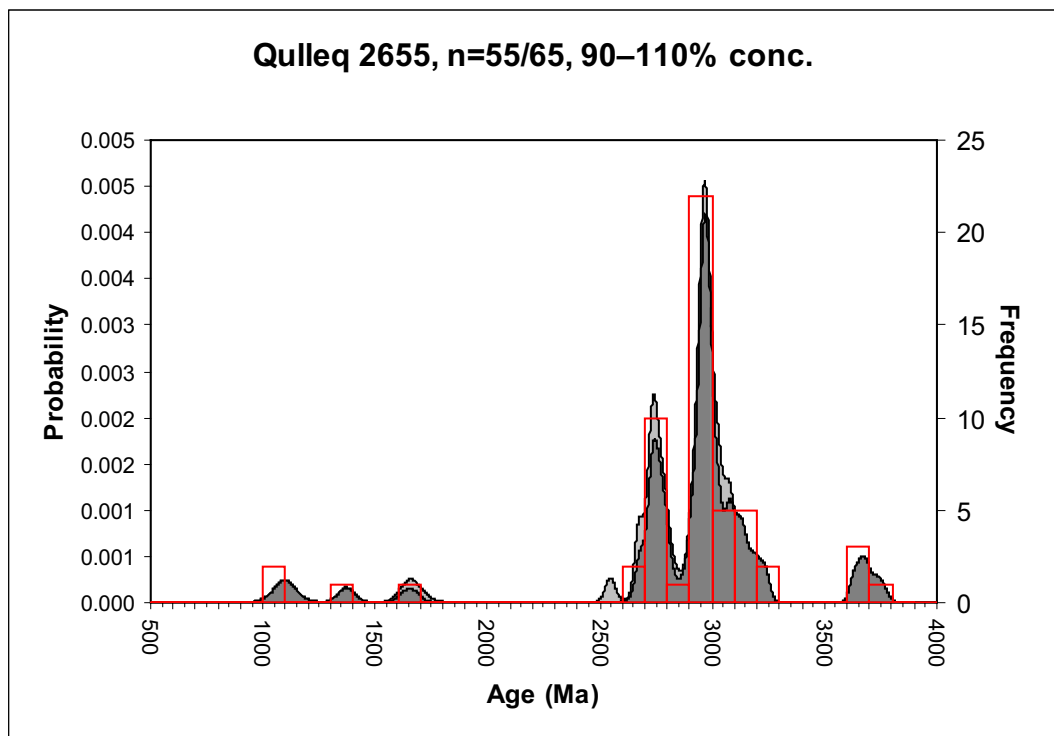
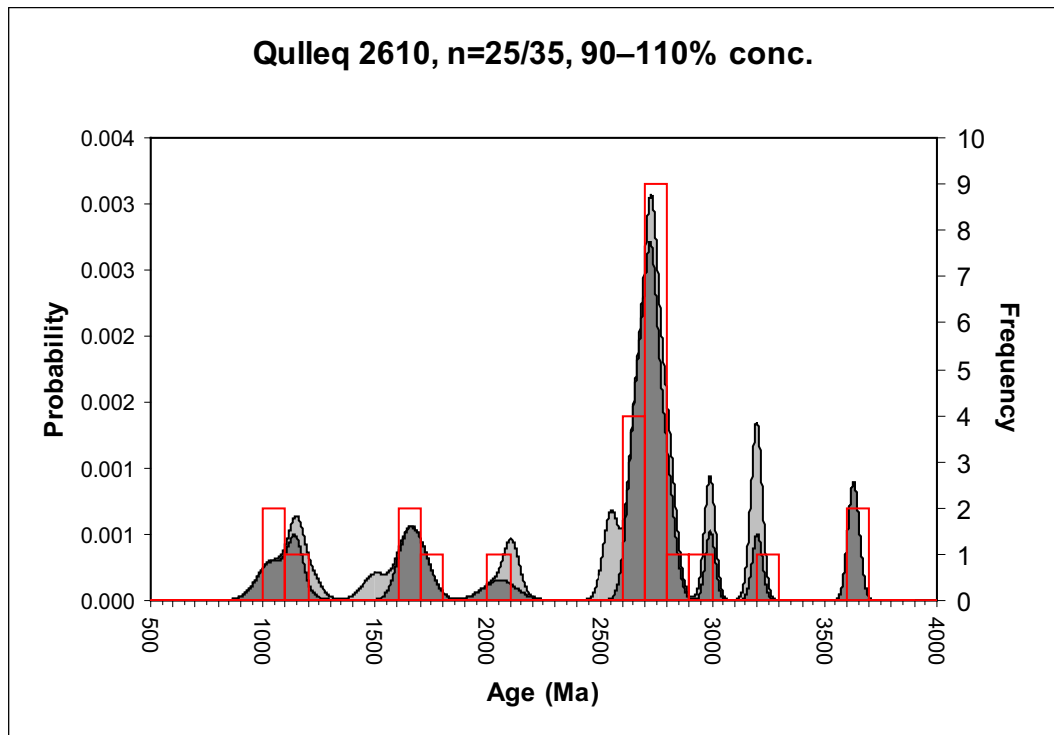
Hellefisk; 2B 2089 3990, n=70/113, 90–110% conc.

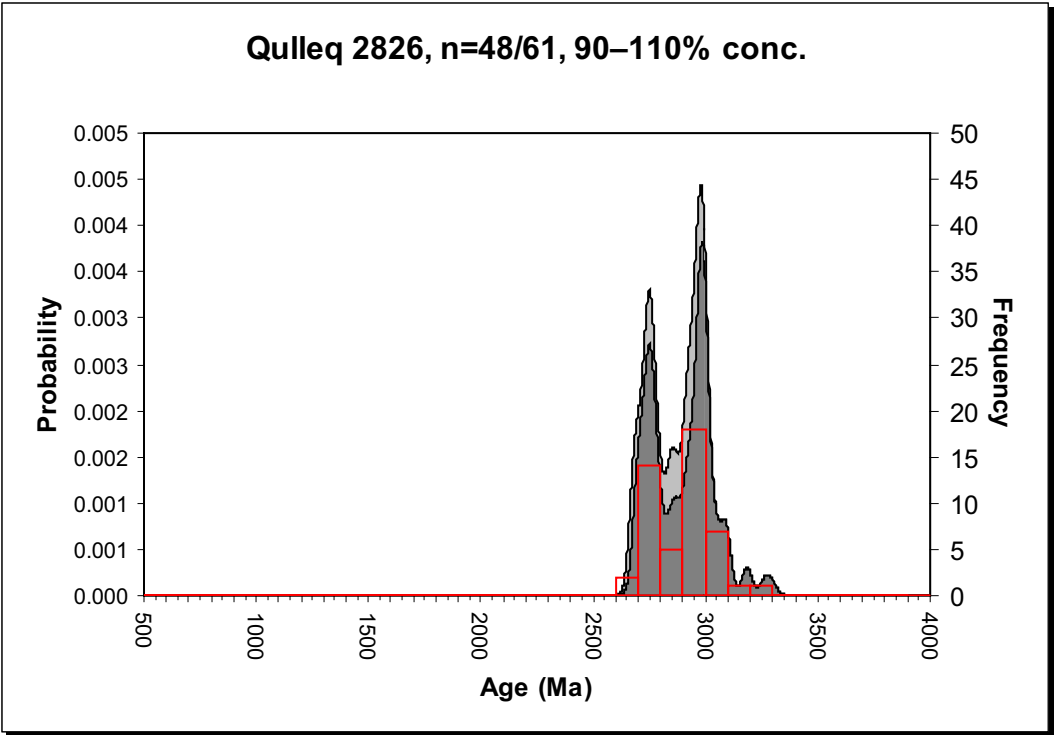
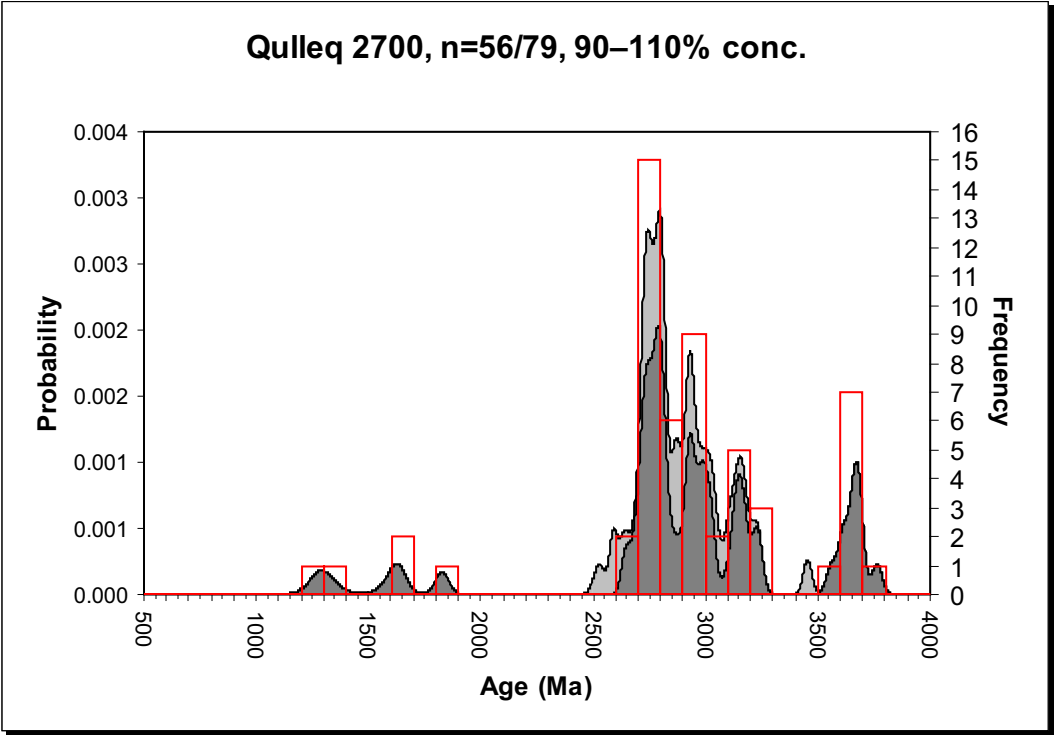


Hellefisk; 2B 2159 4770, n=68/114, 90–110% conc.

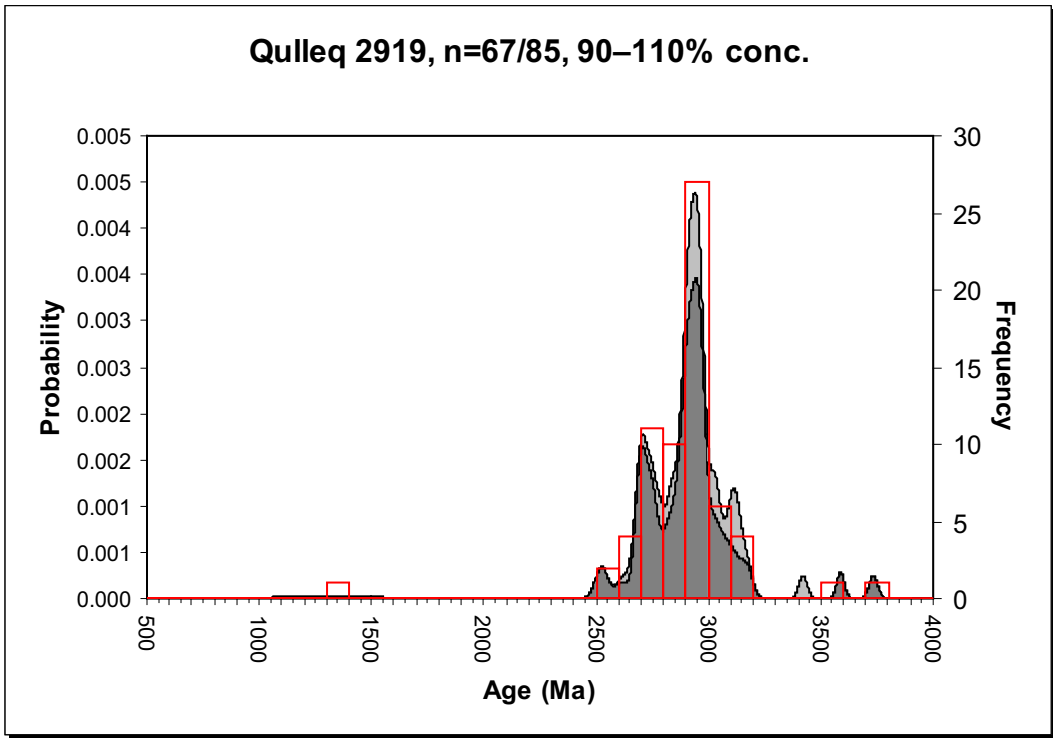


Qulleq-1





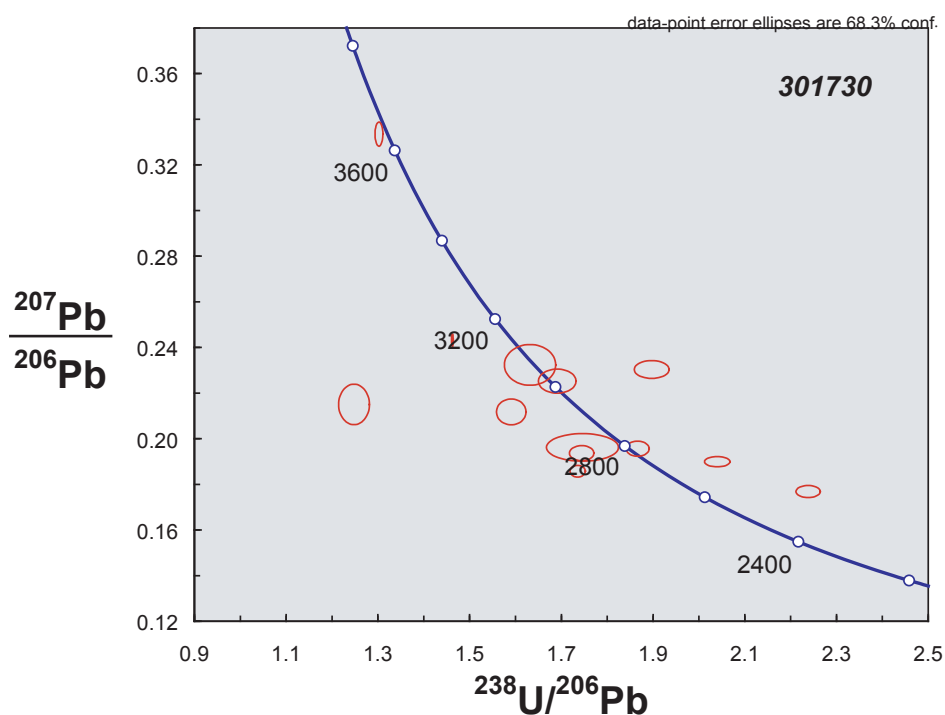
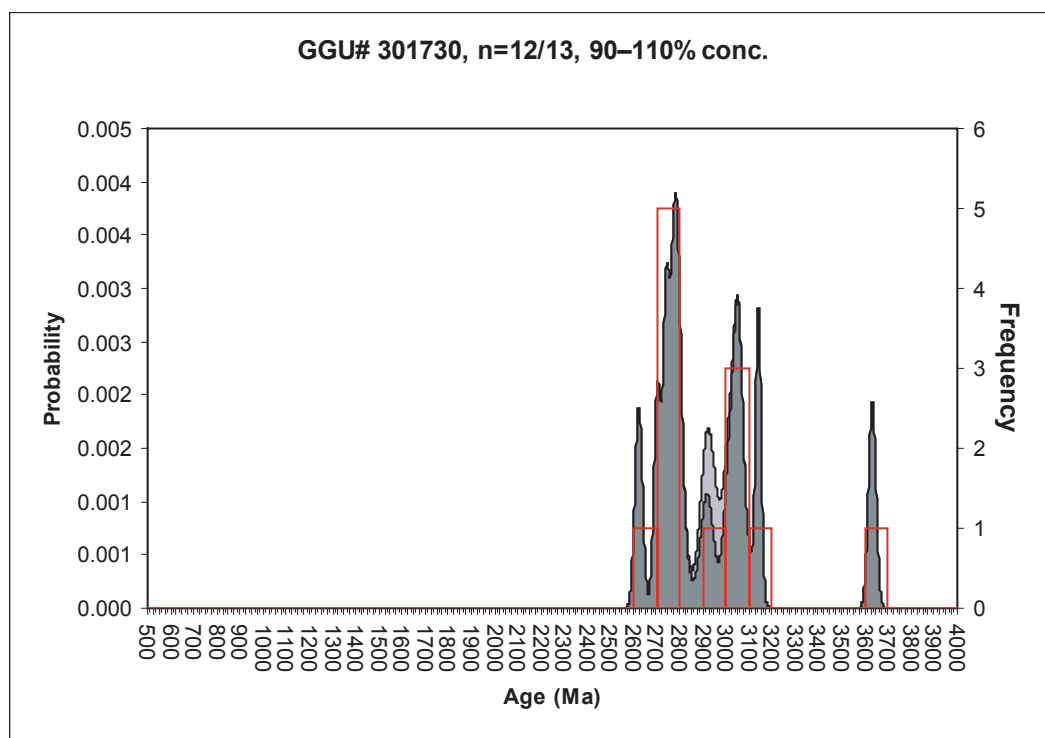
Qulleq 2919, n=67/85, 90–110% conc.



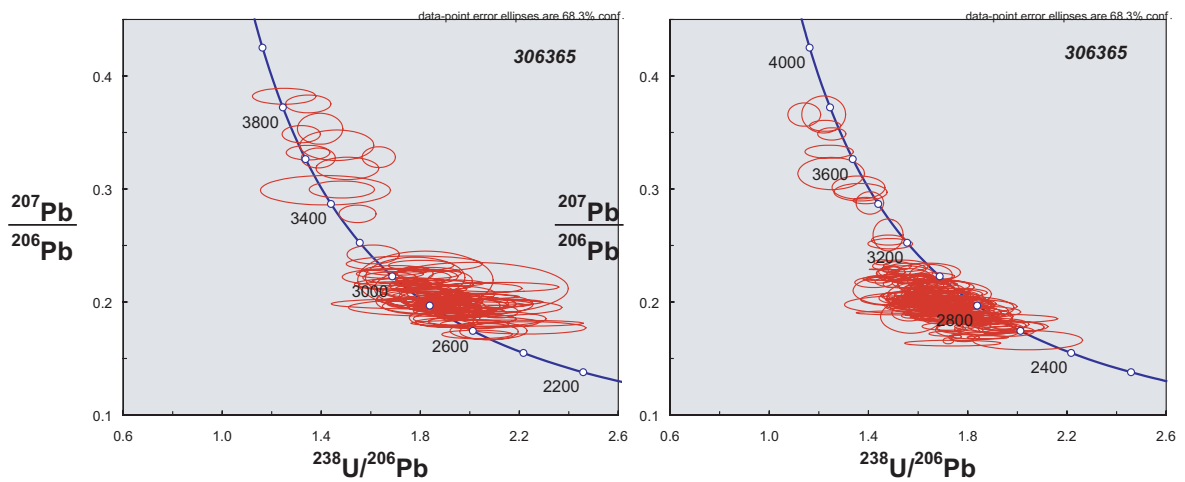
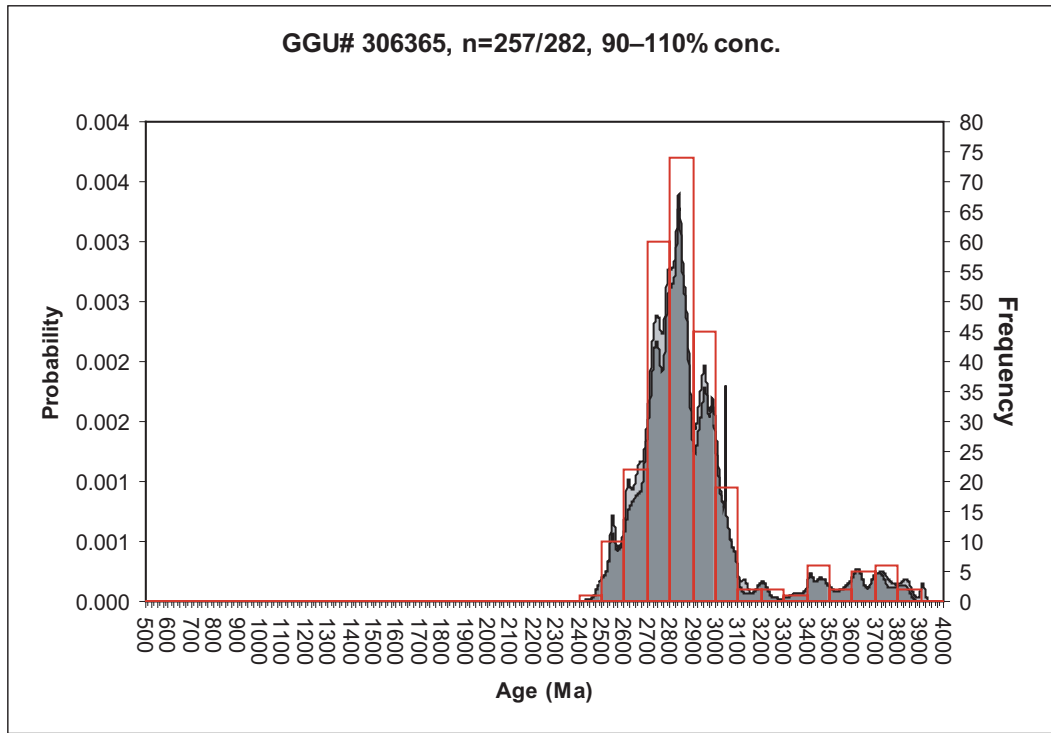
Appendix II – Stream sediment samples

Compilation of all stream-sediment zircon U-Pb samples organised by GGU sample number.

301730

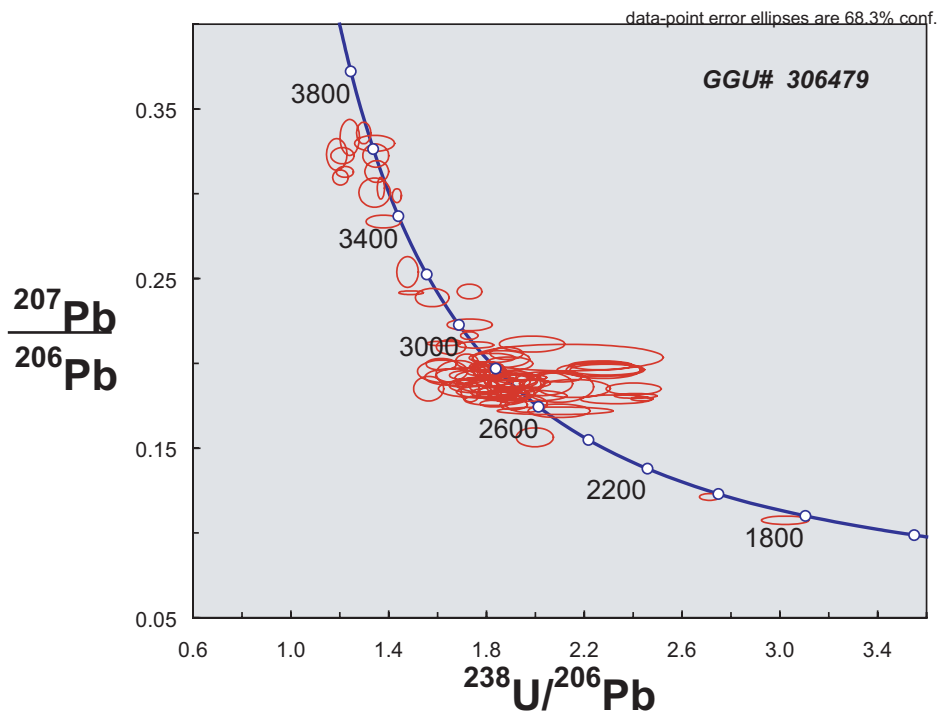
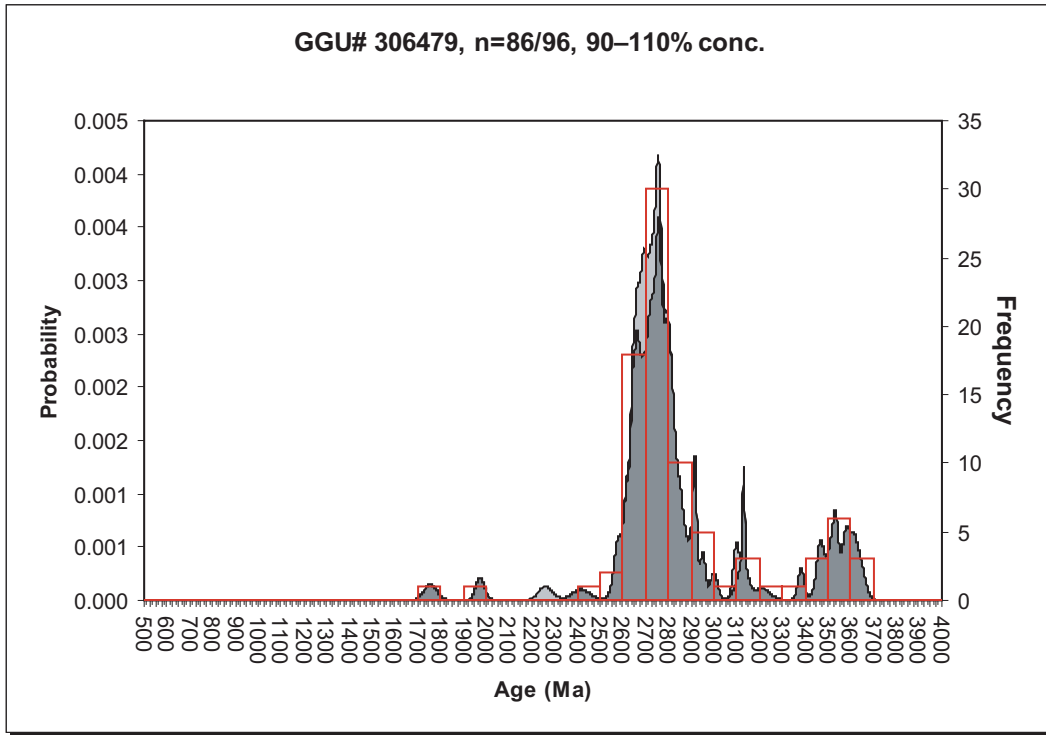


306365

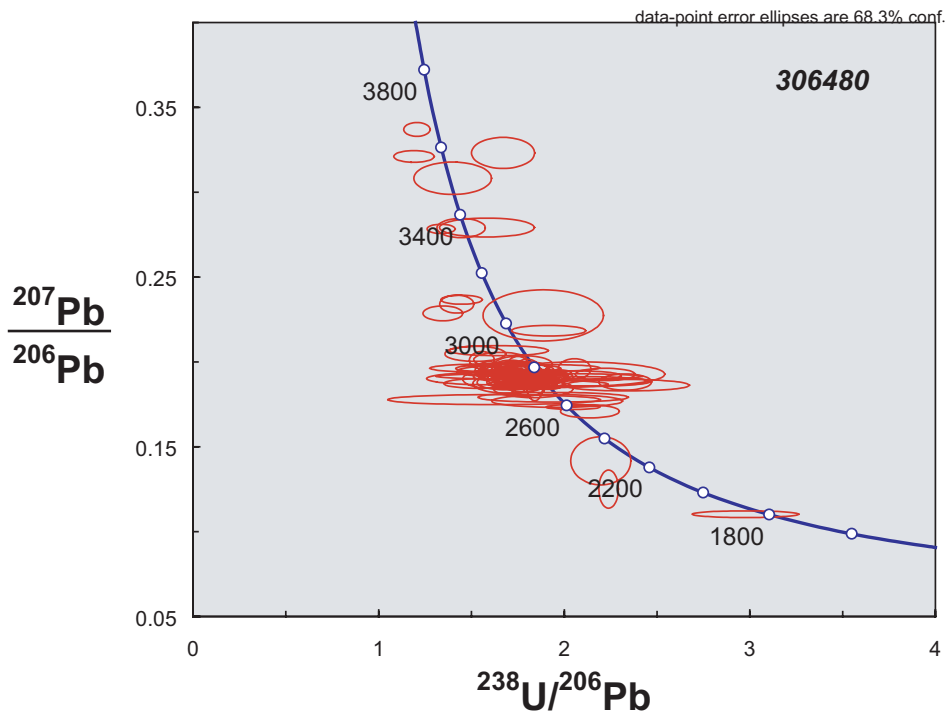
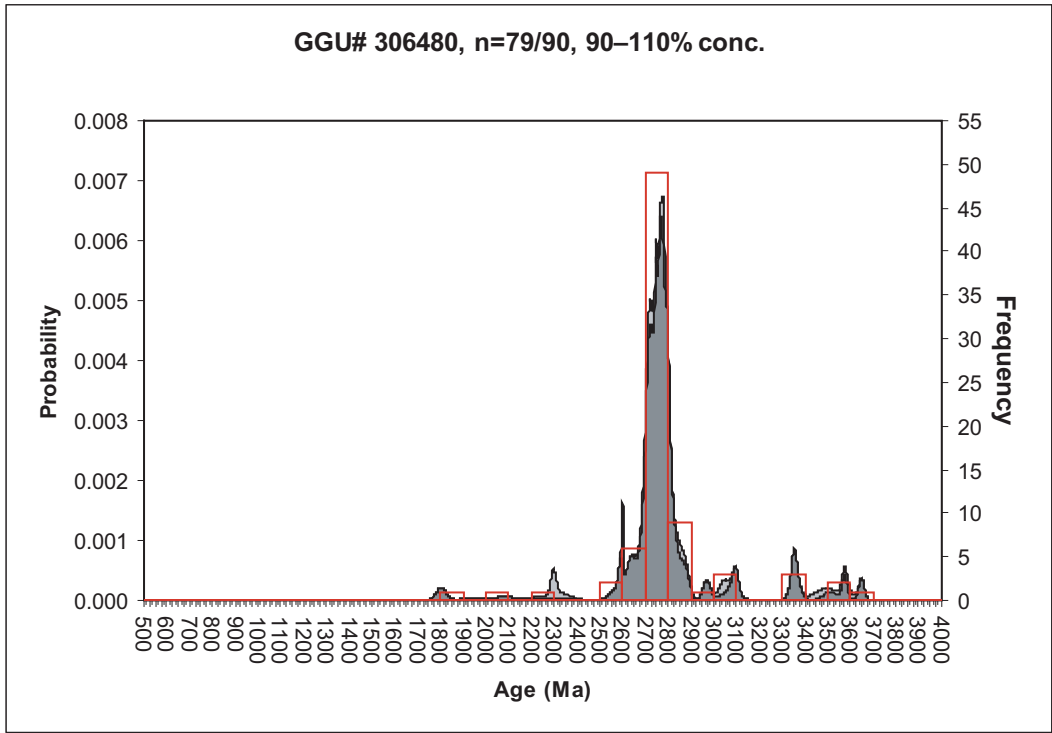


The sample had to be split into two as the plotting program could not handle all the data point. The lower left diagram represents the normal discordant part of the data set and the lower right diagram represents the reversely discordant part.

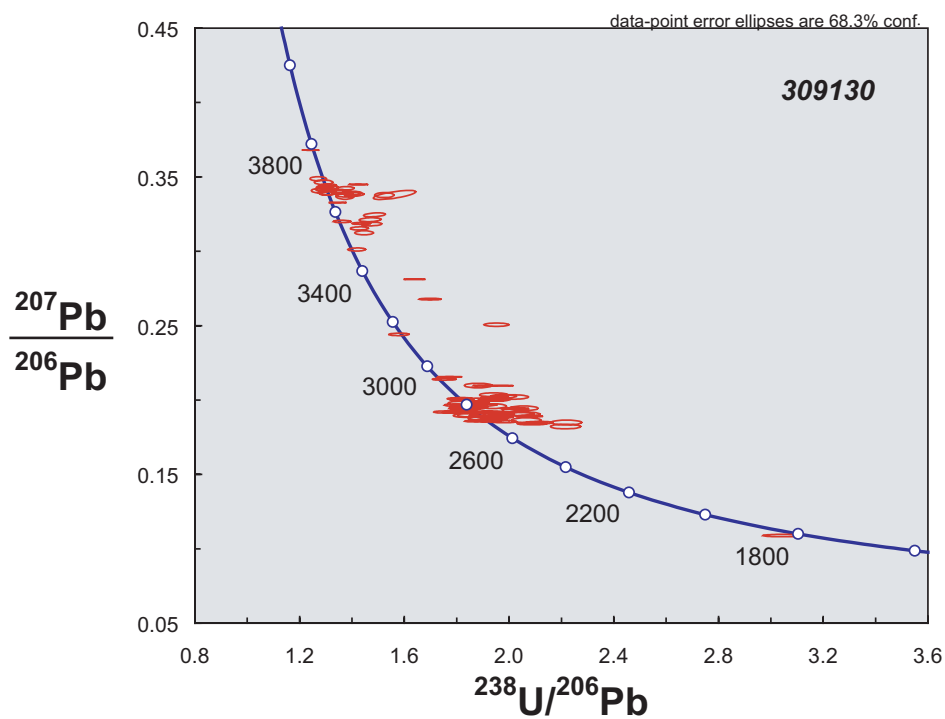
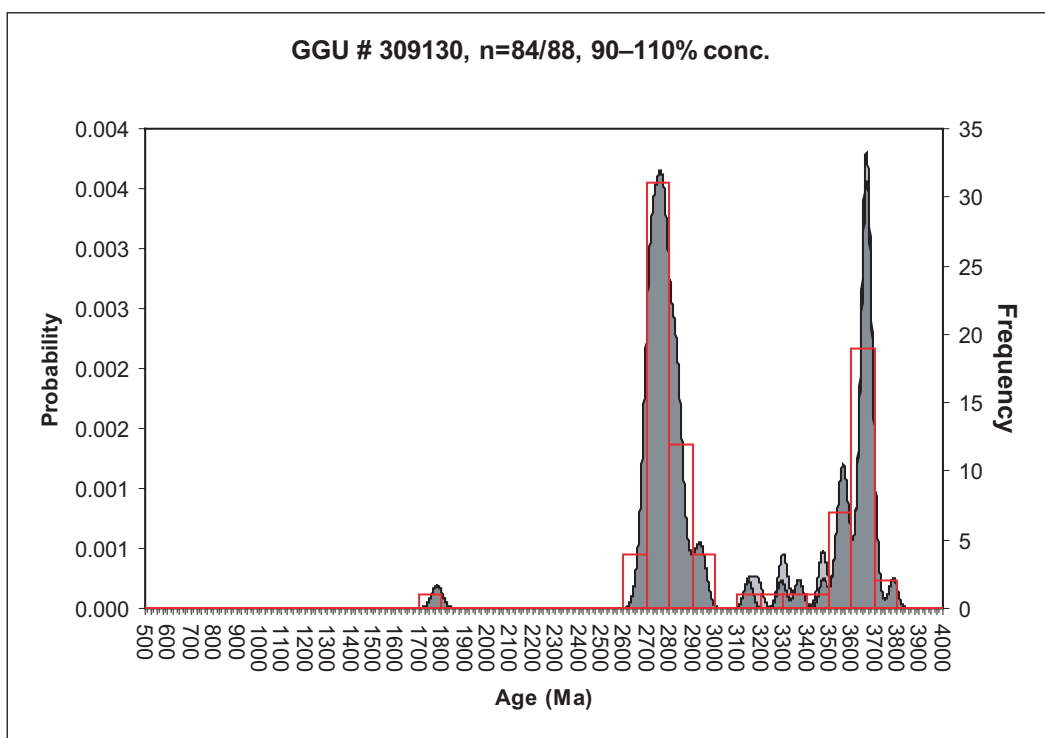
306479



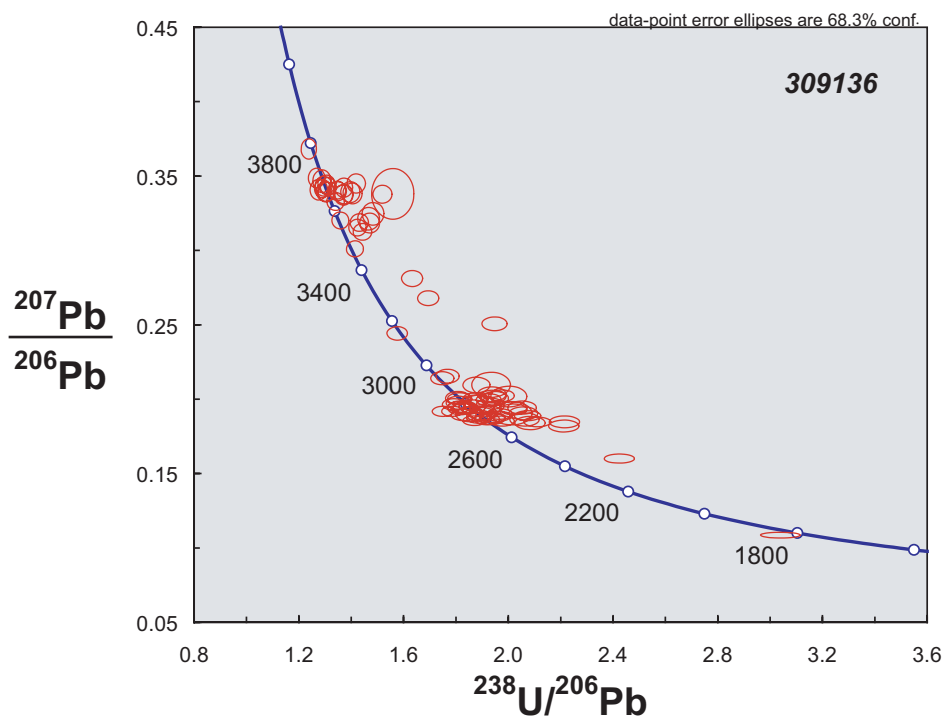
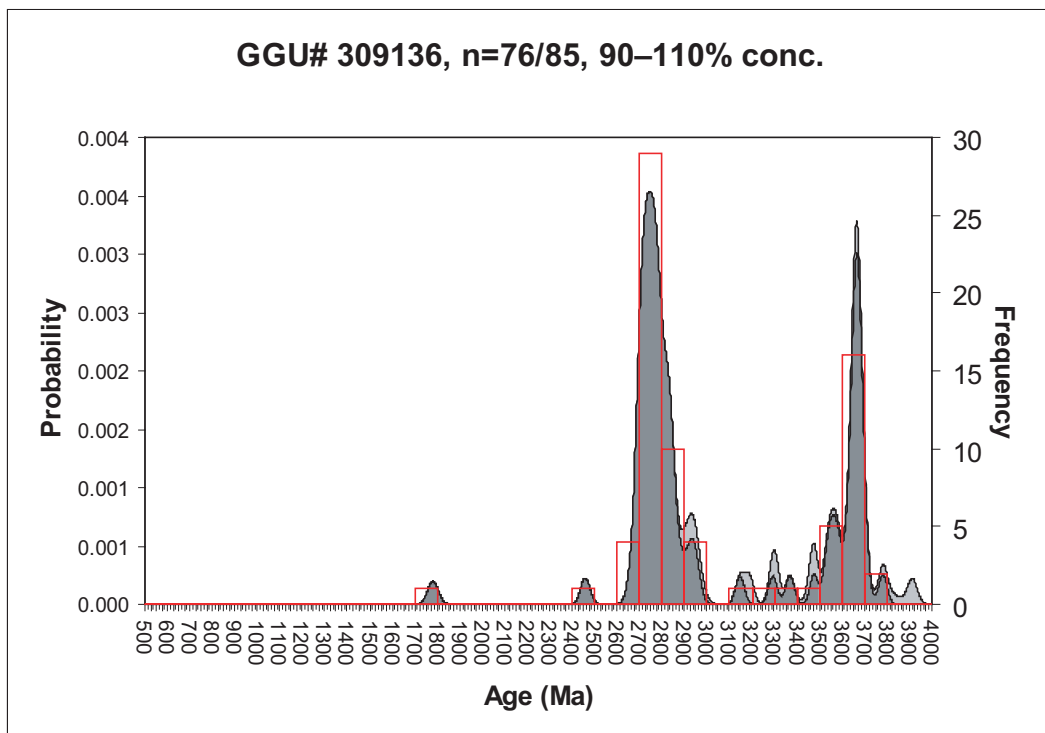
306480



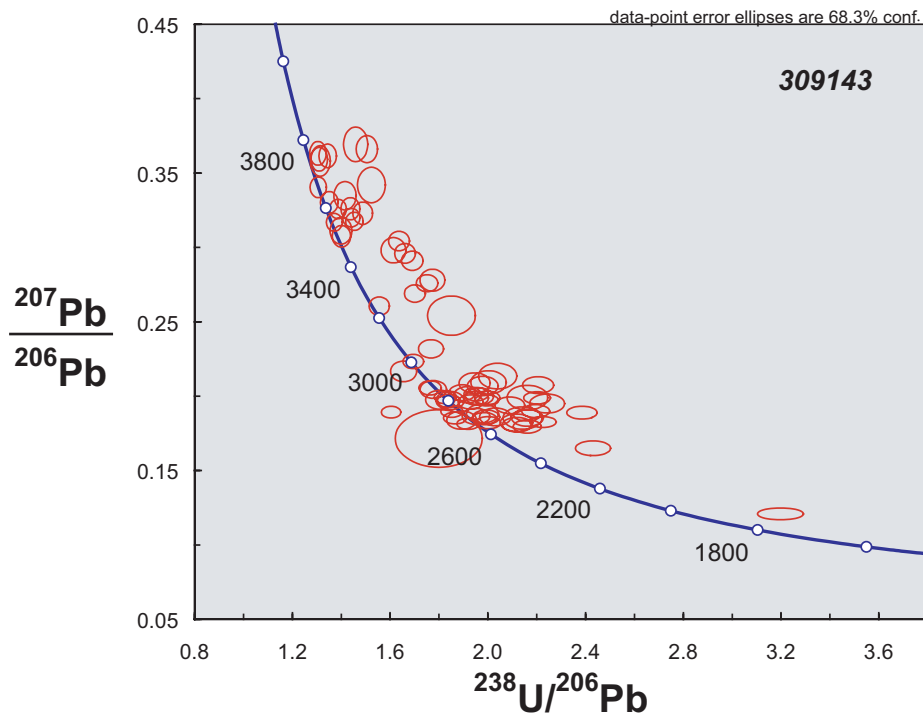
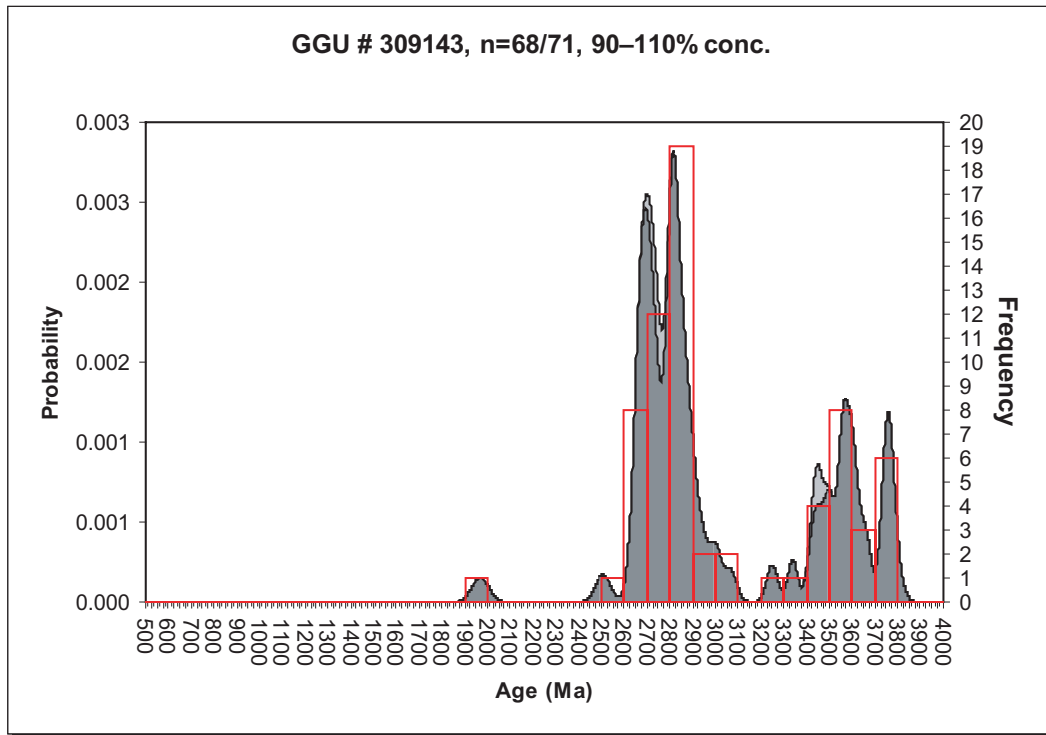
309130



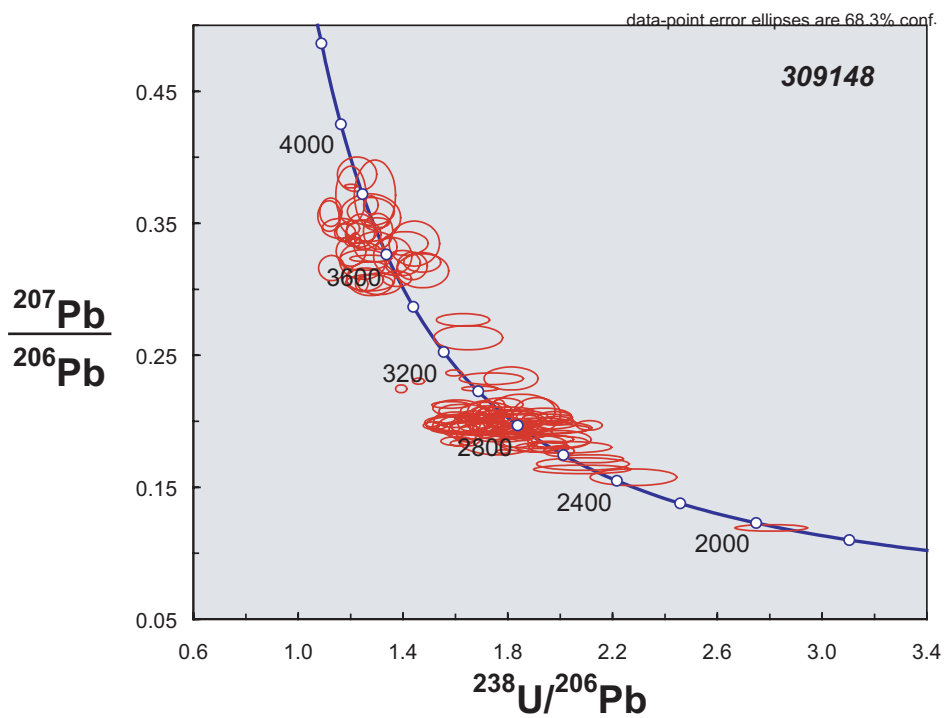
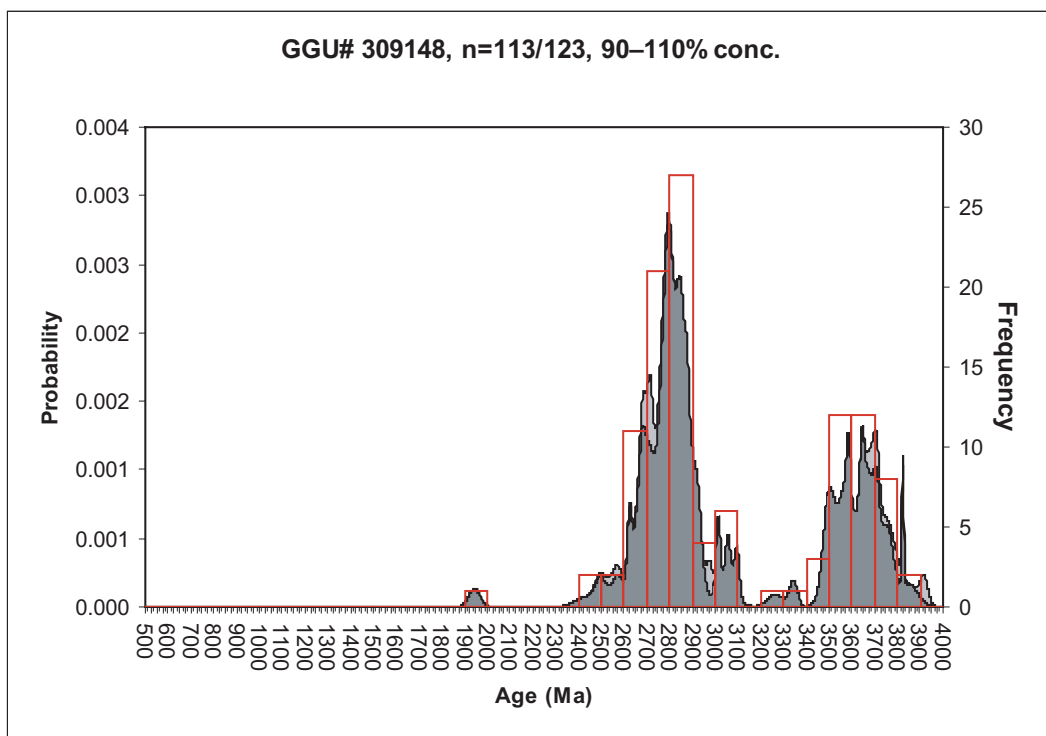
309136



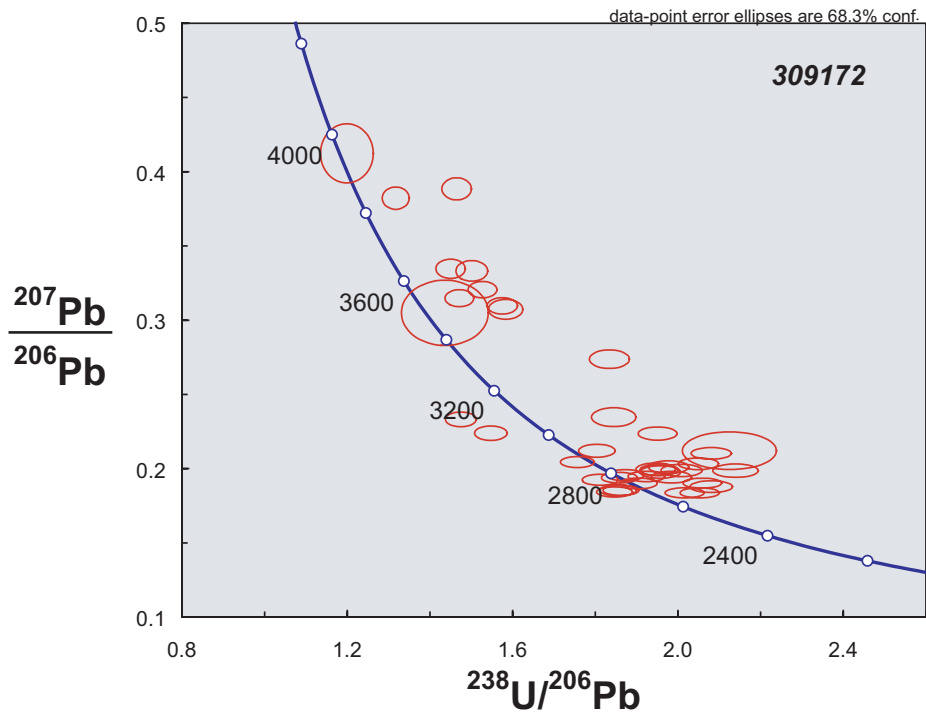
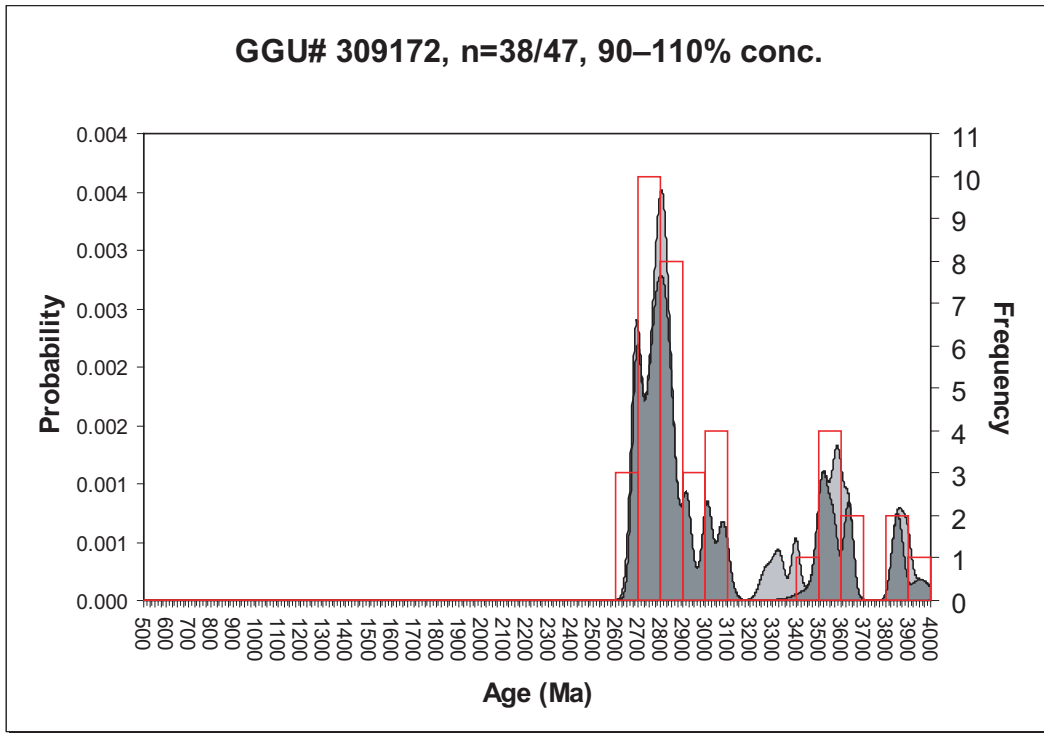
309143



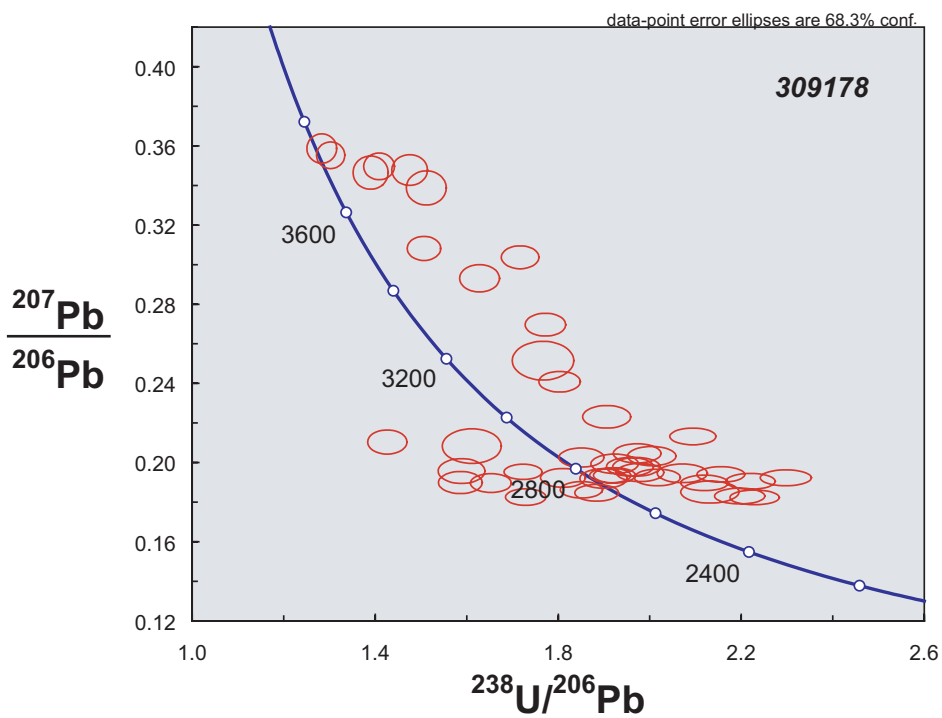
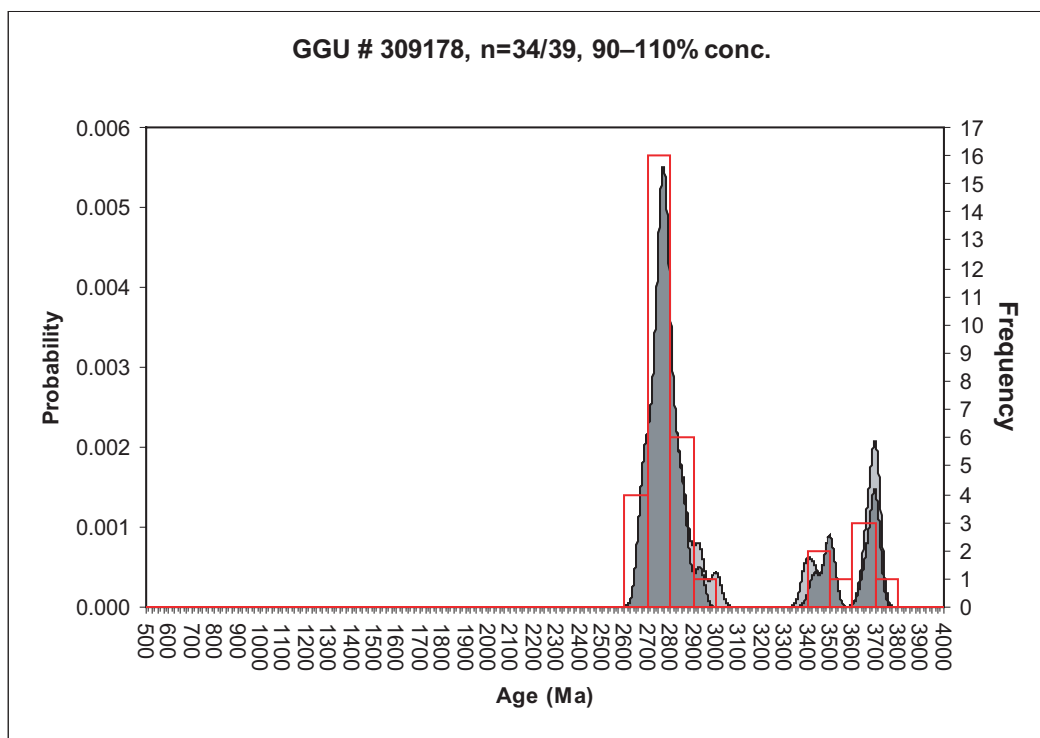
309148



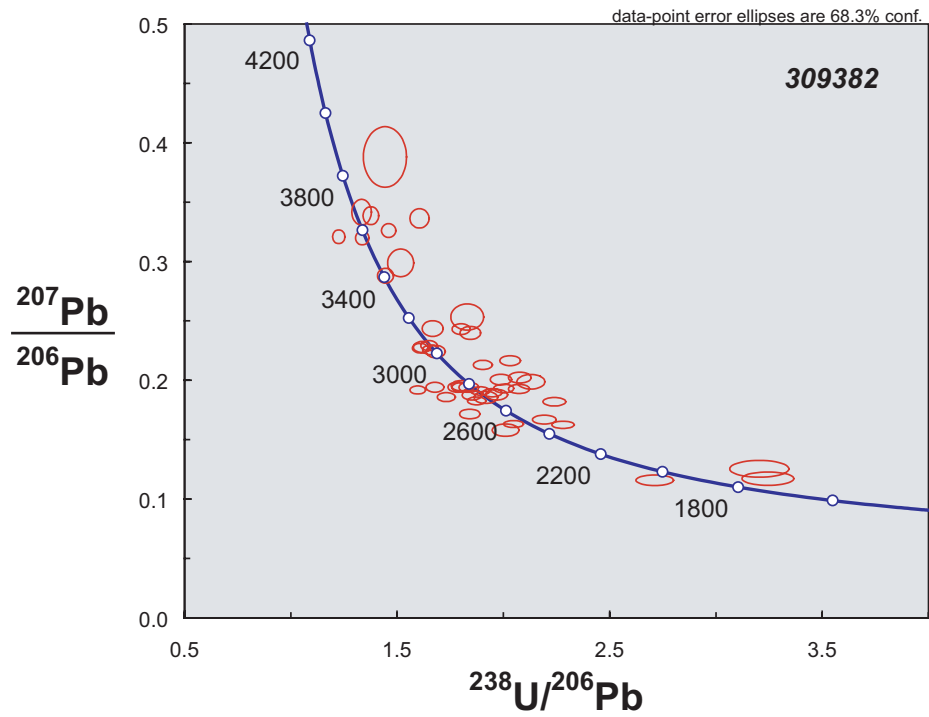
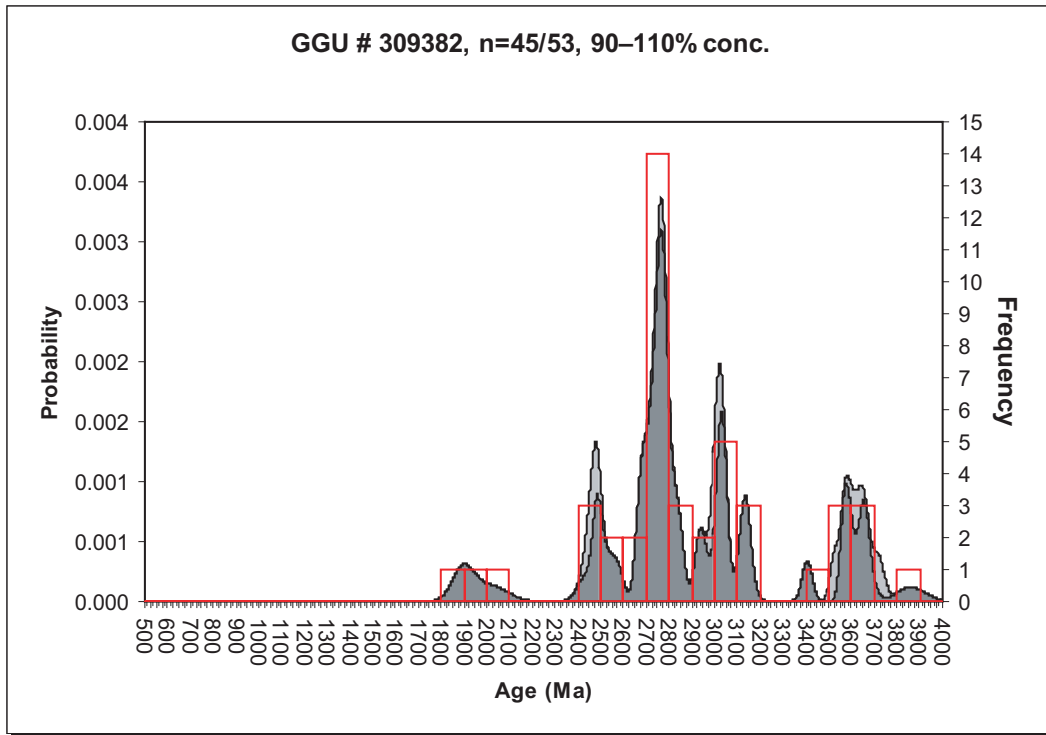
309172



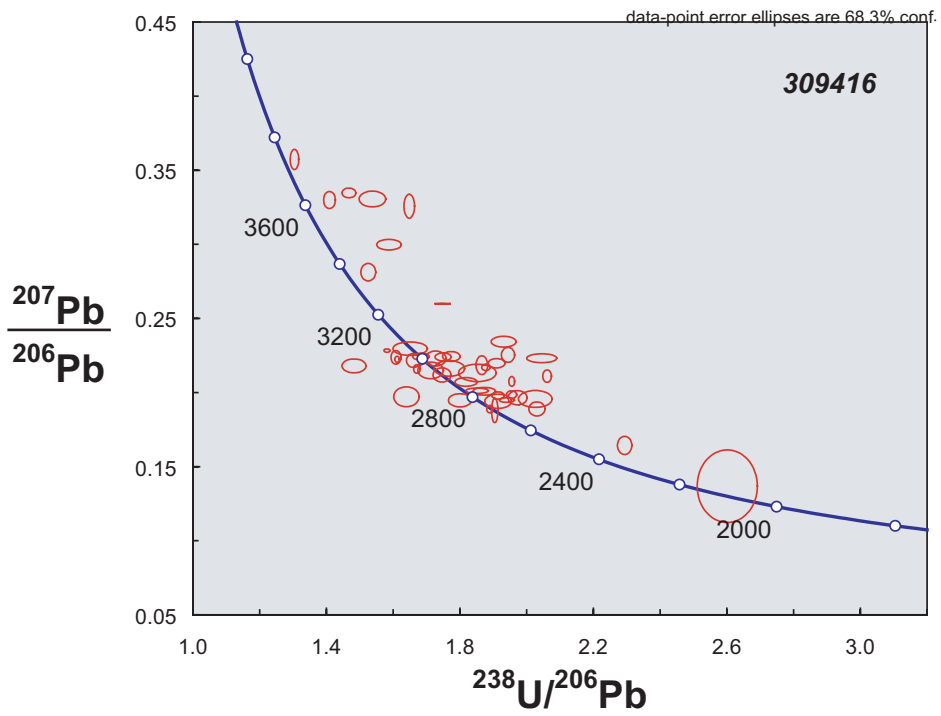
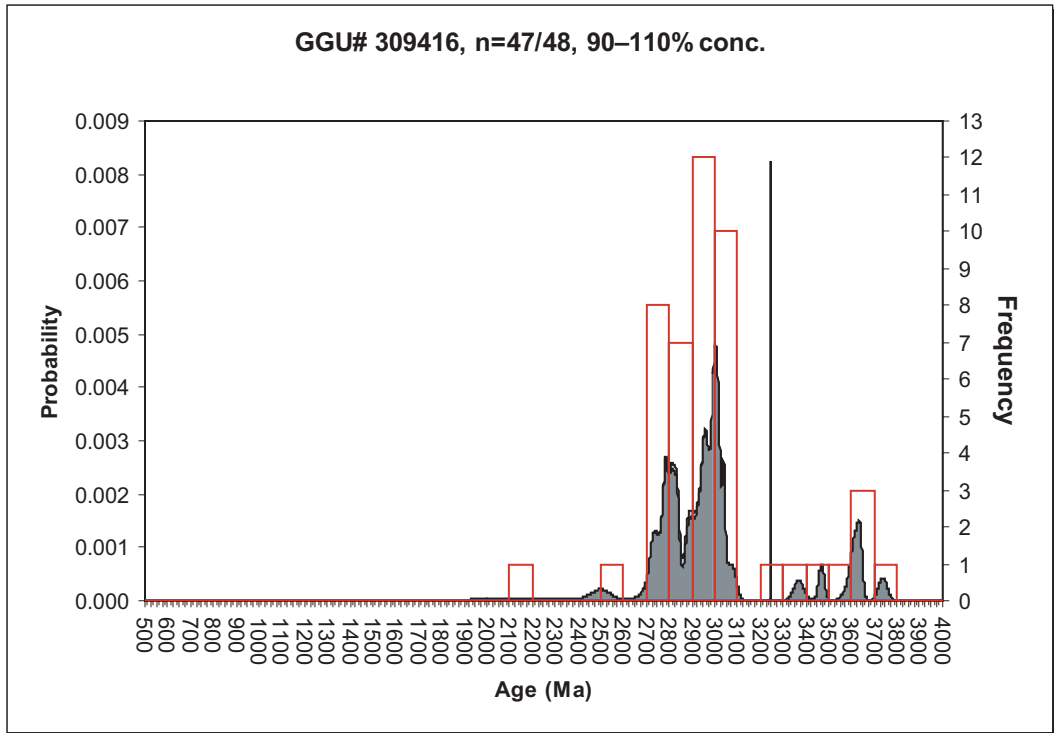
309178



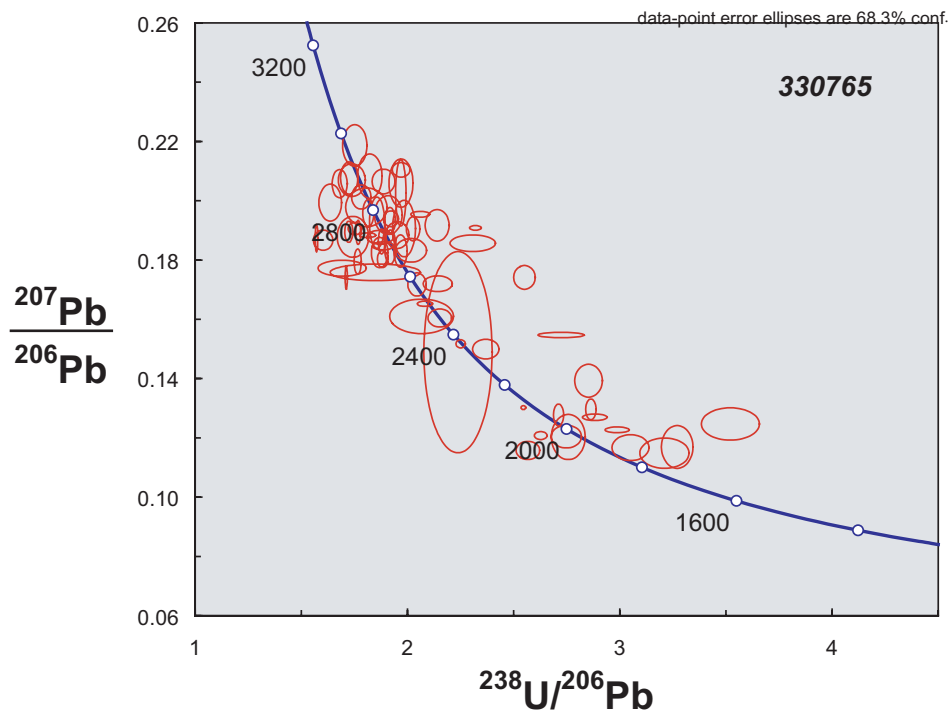
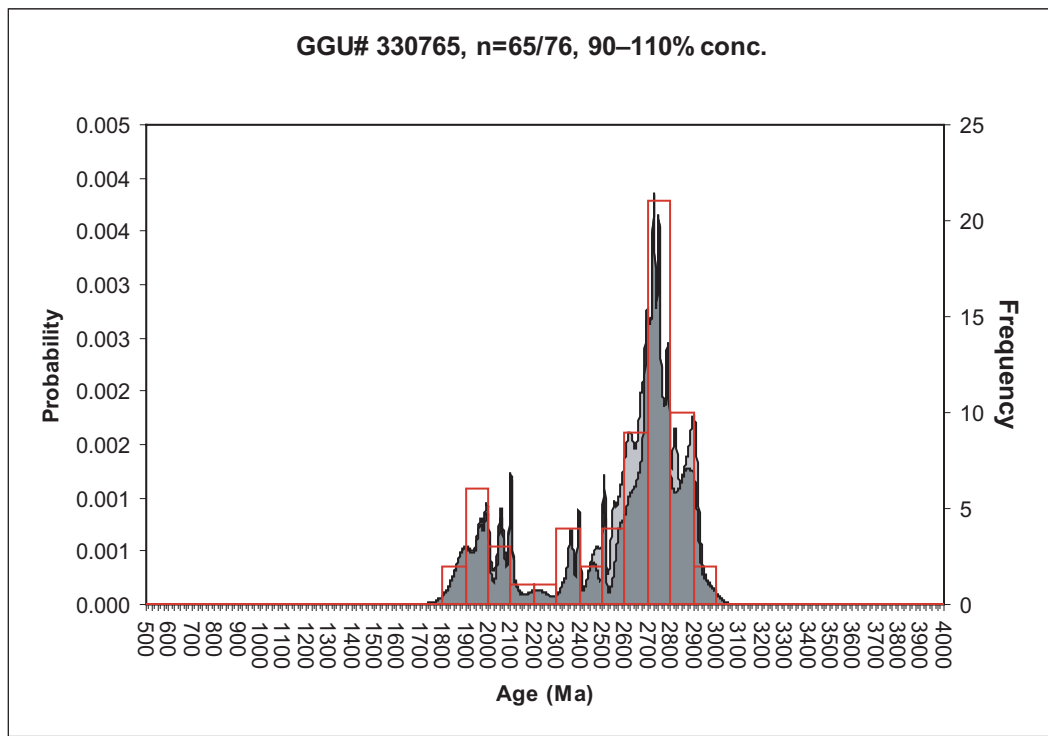
309182



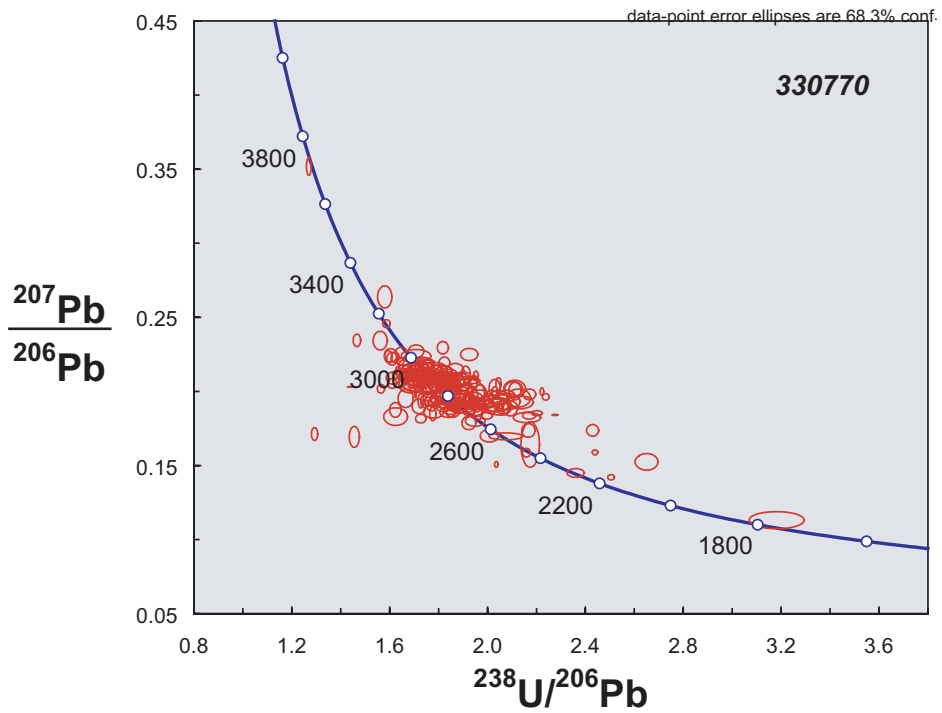
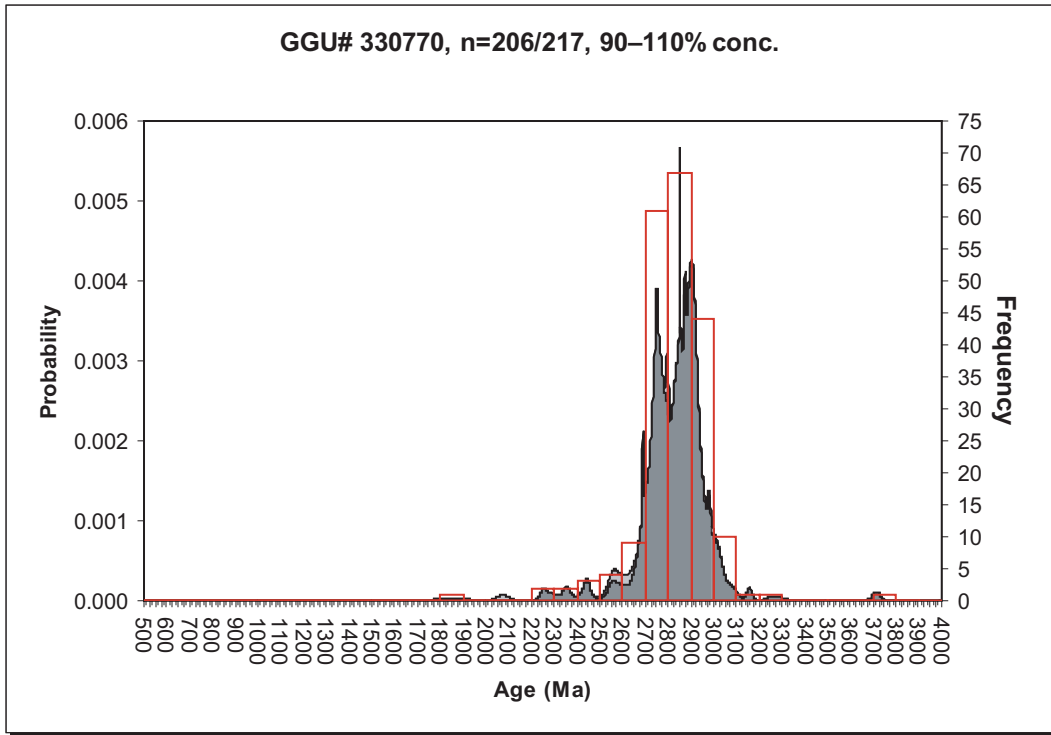
309416



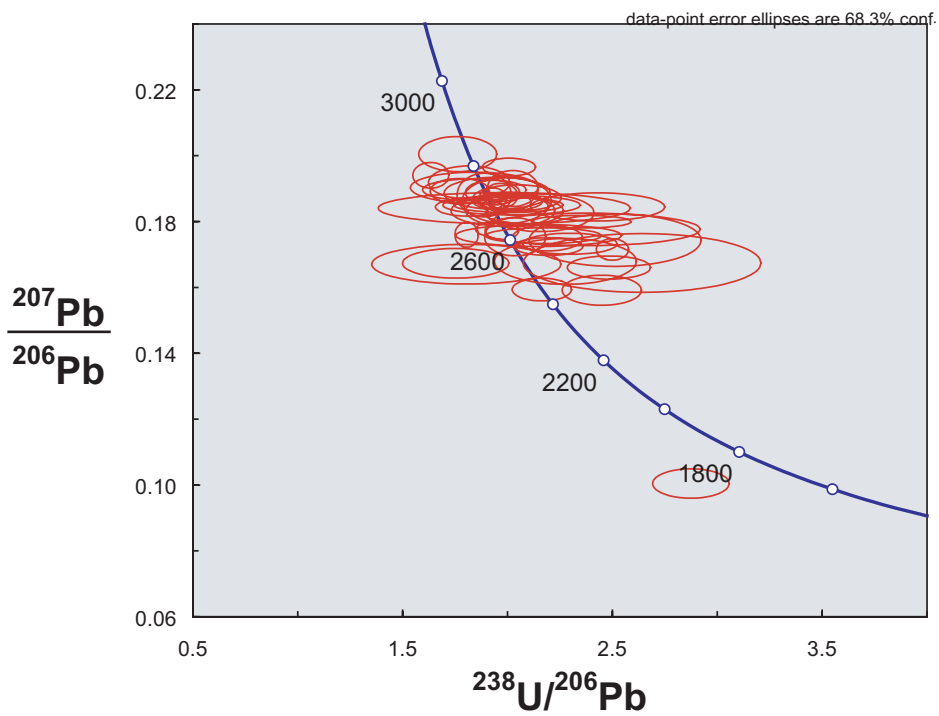
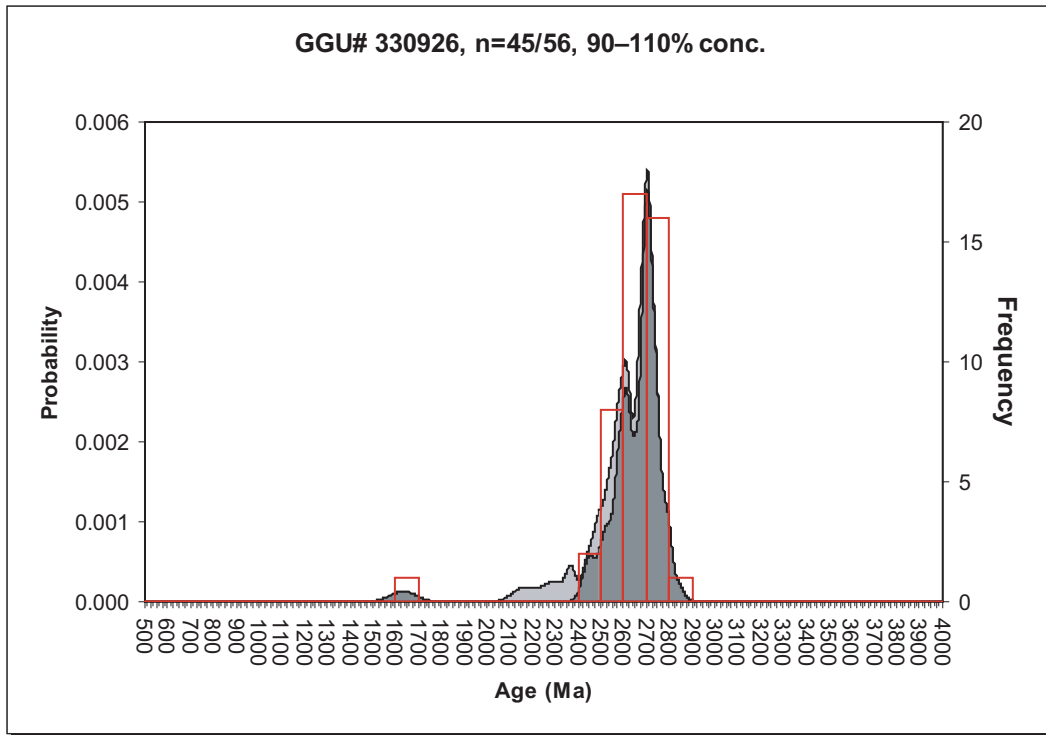
330765



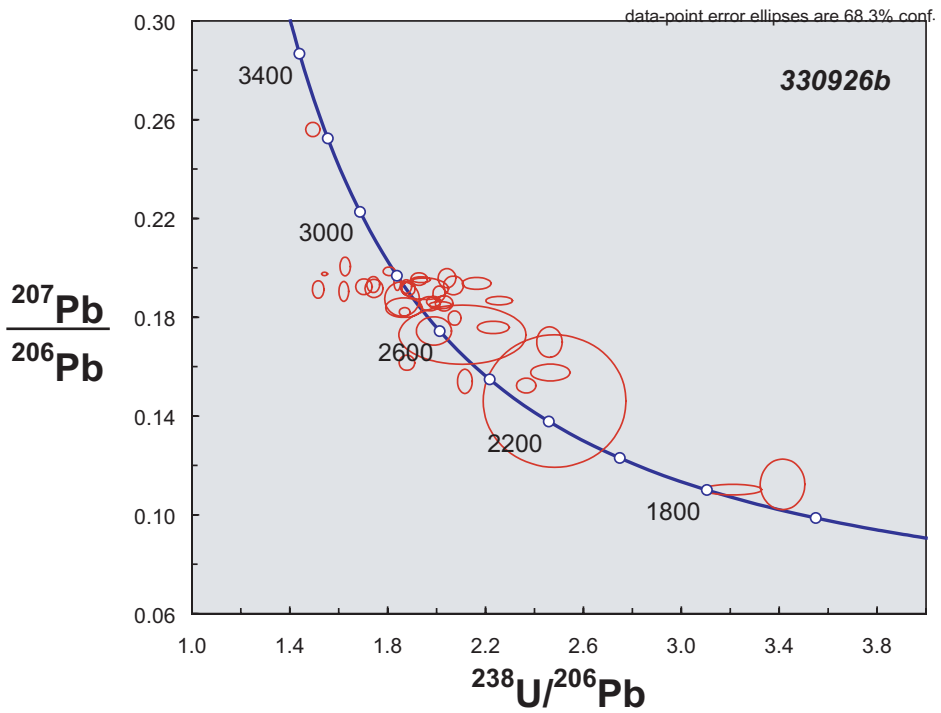
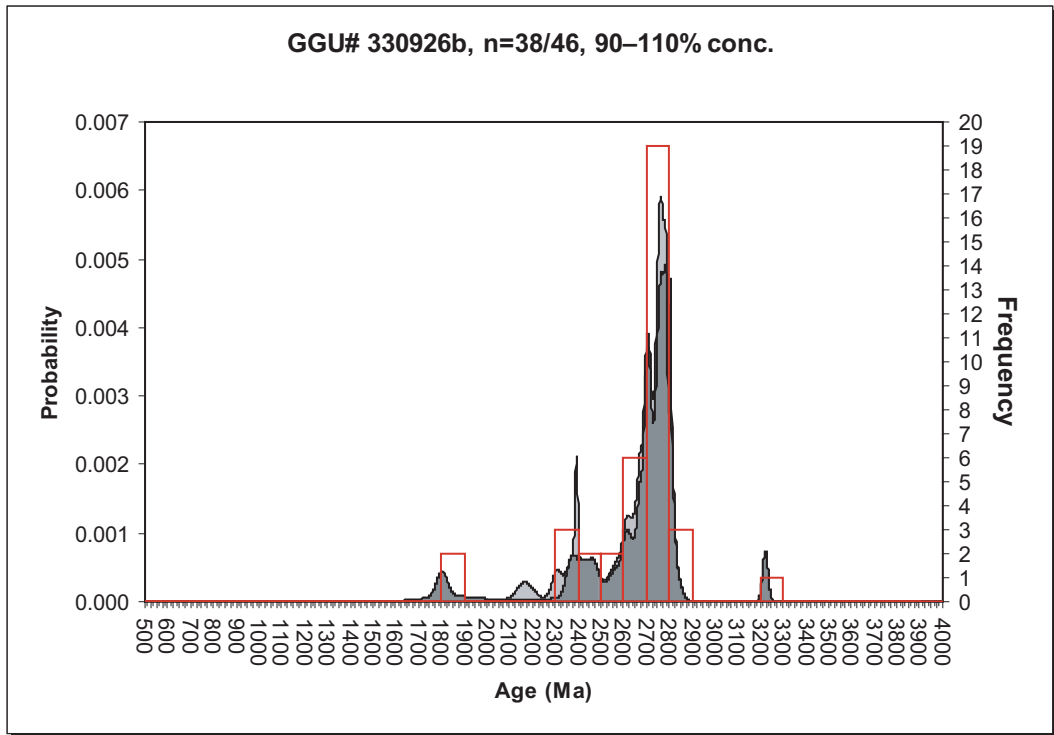
330770



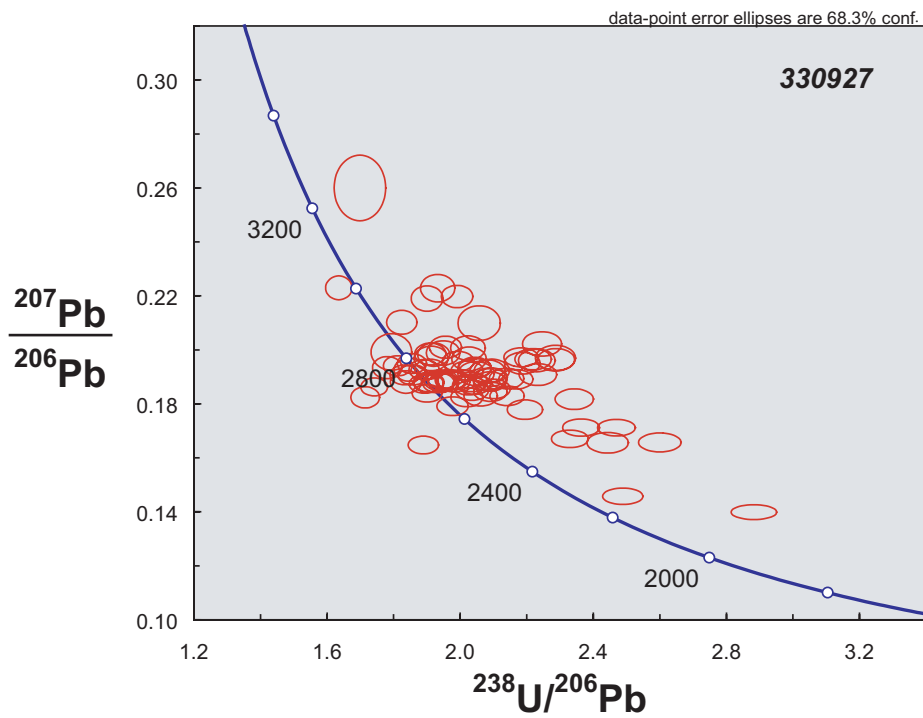
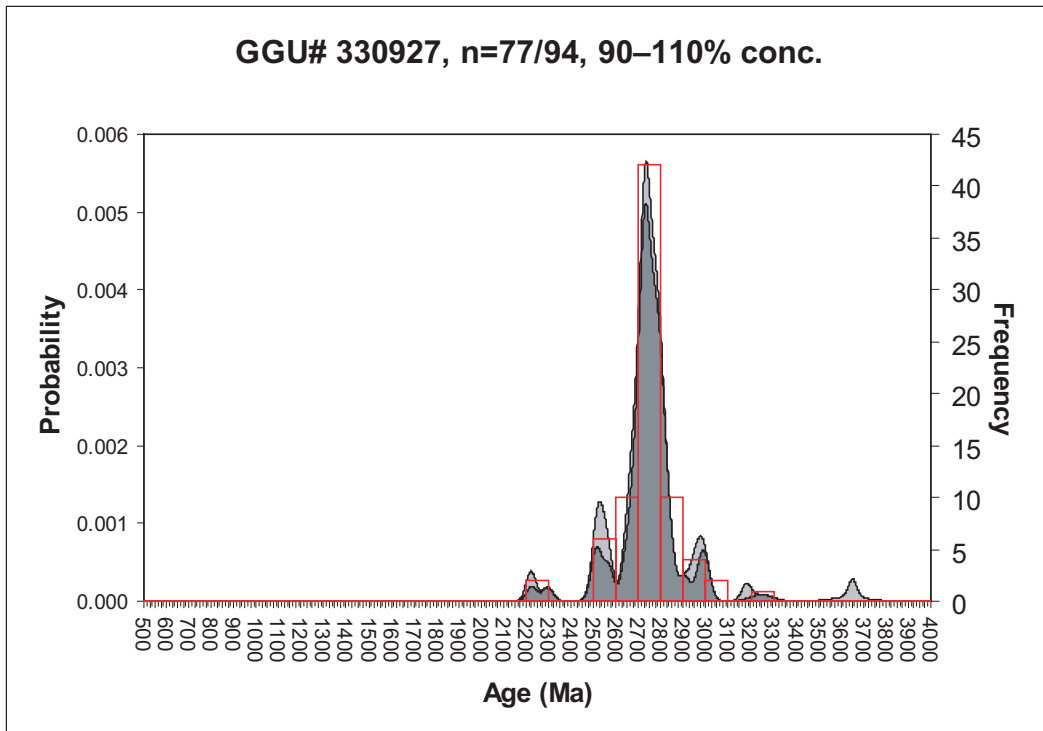
330926



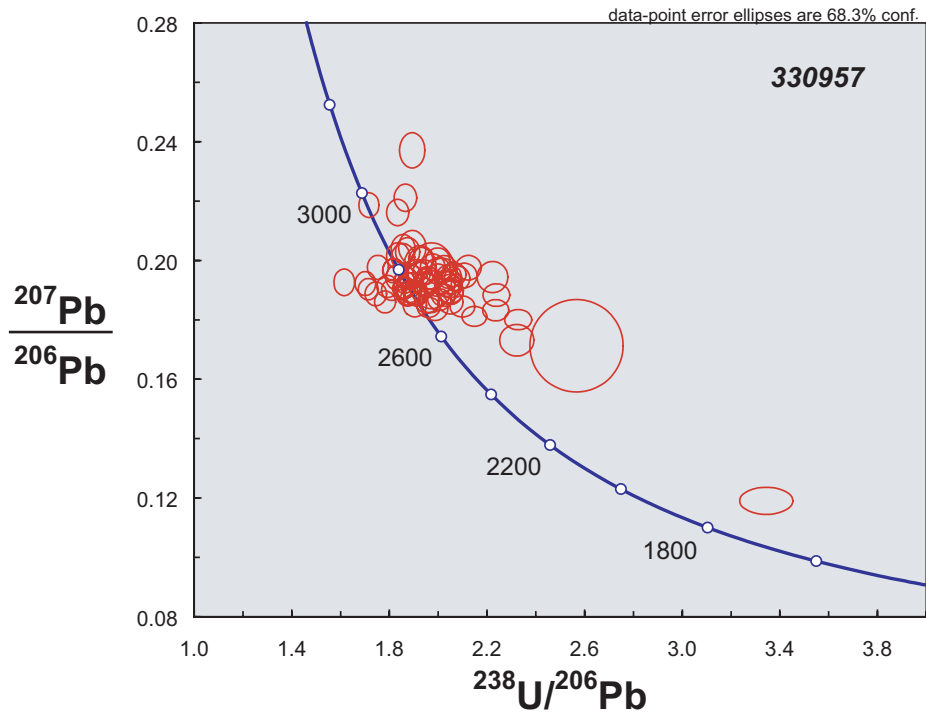
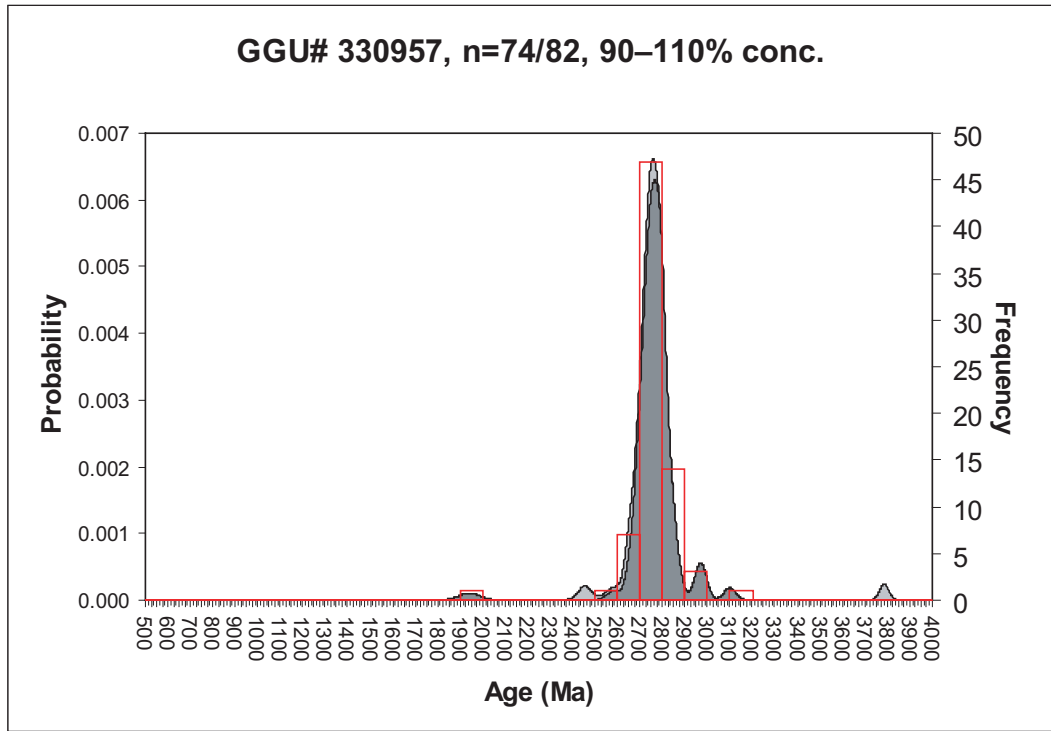
330926b



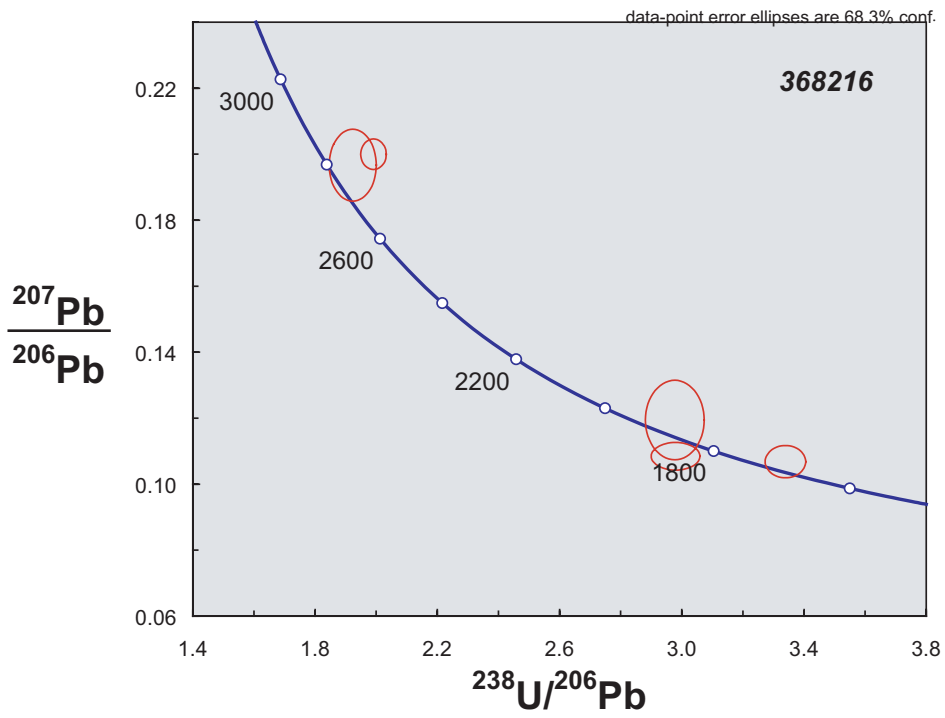
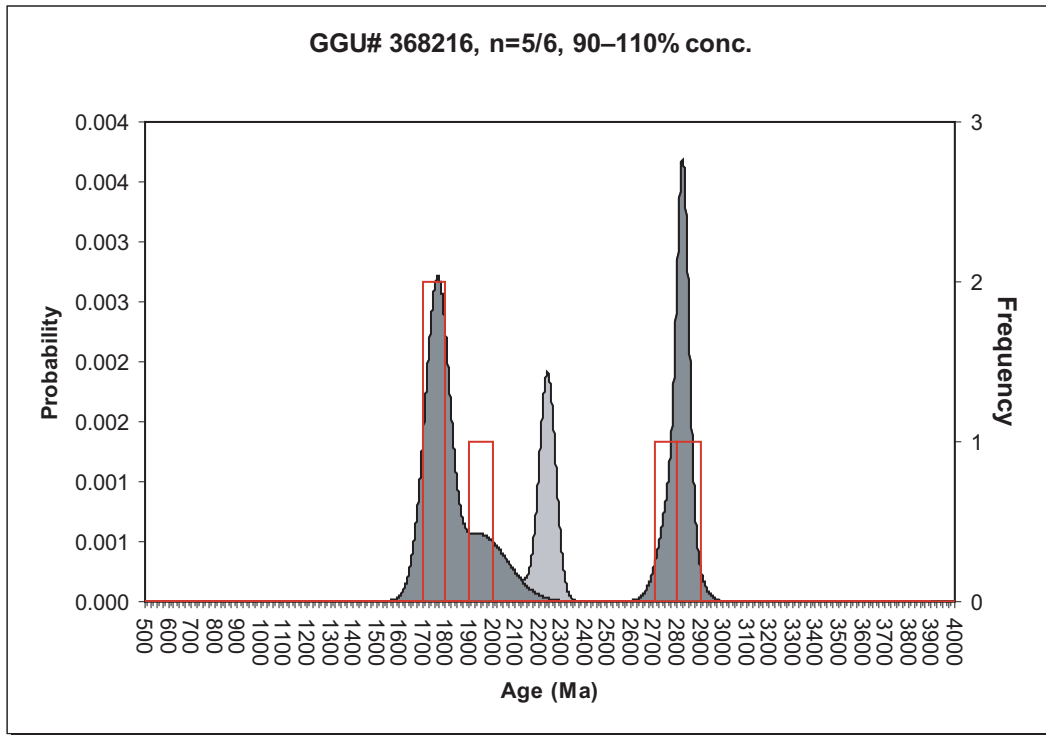
330927



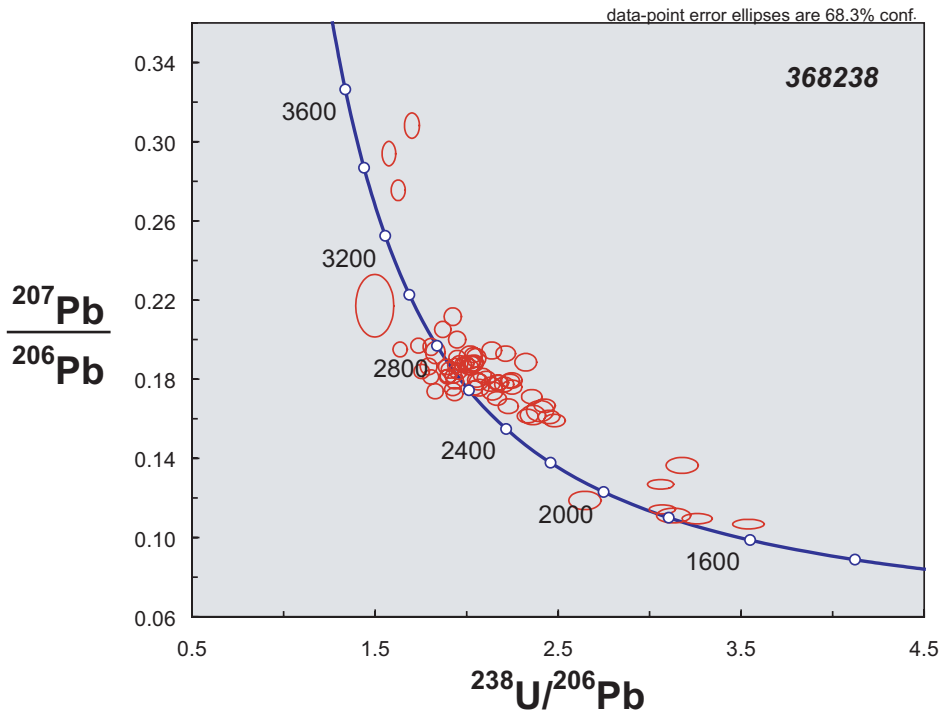
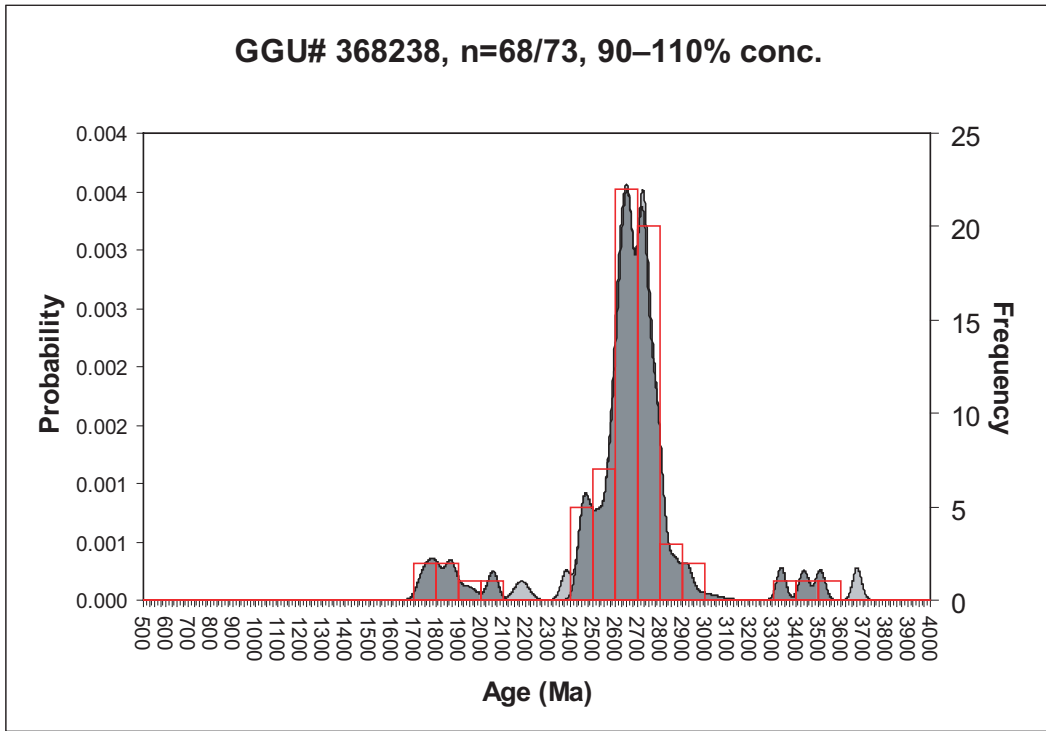
330957



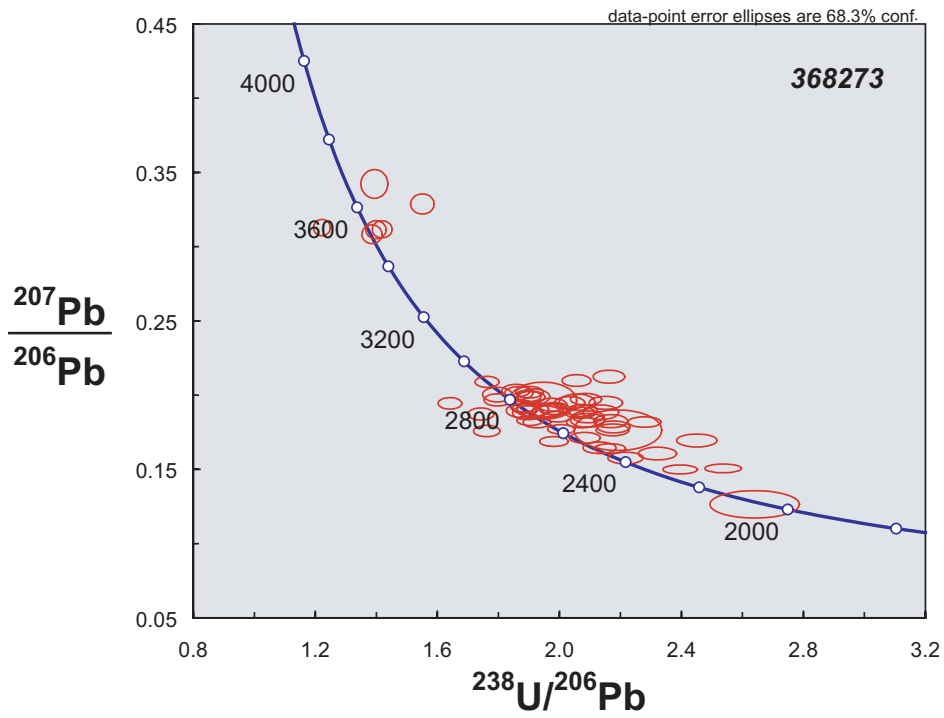
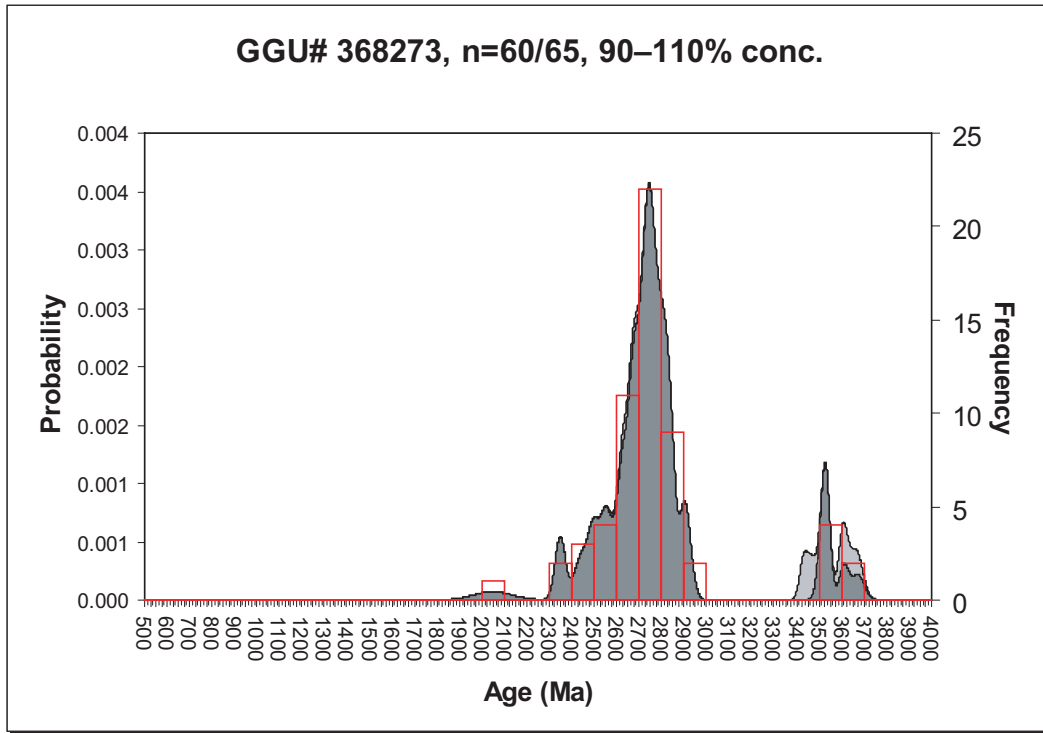
368216



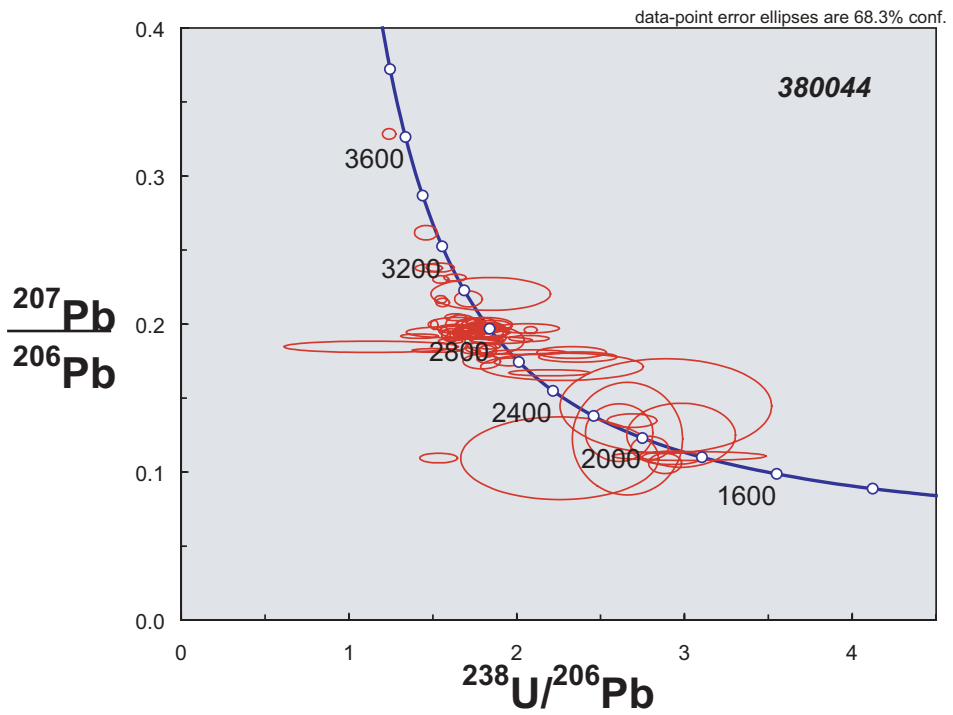
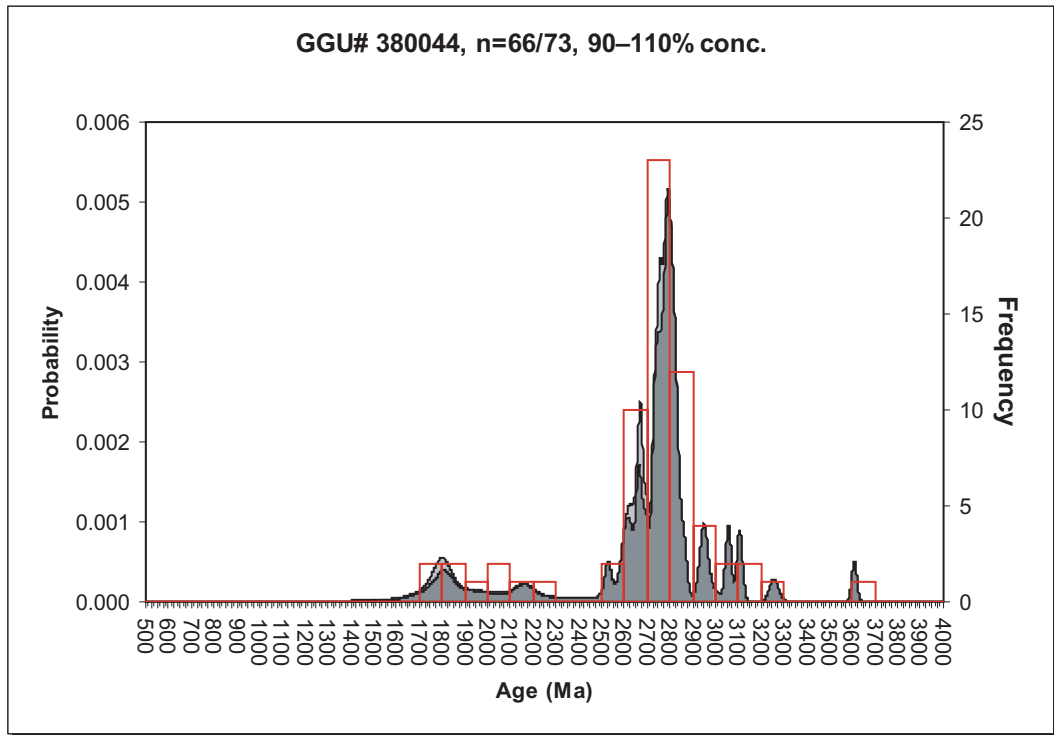
368238



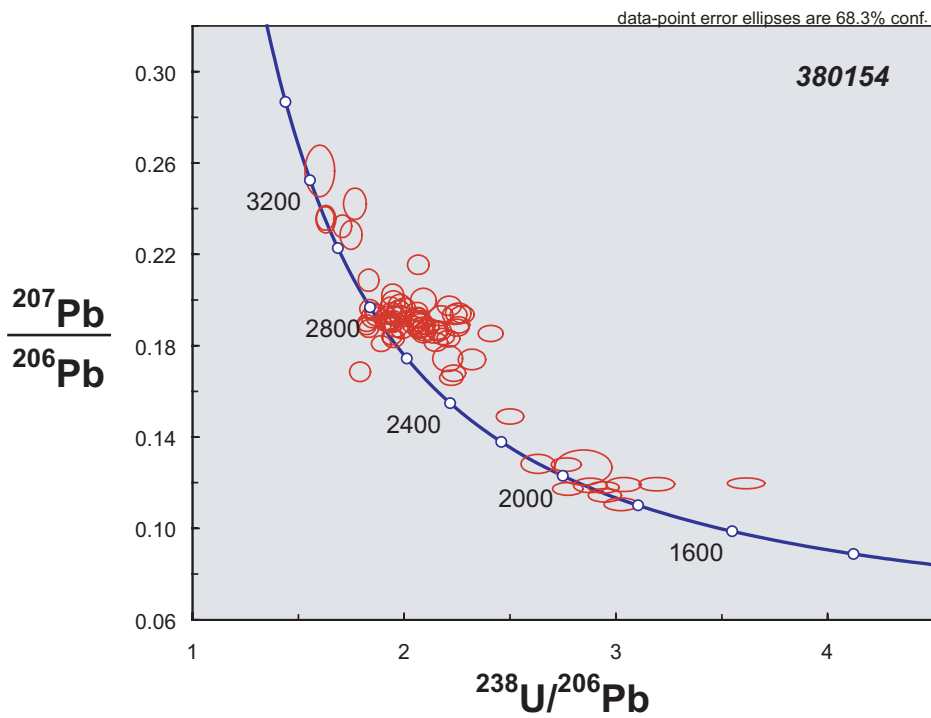
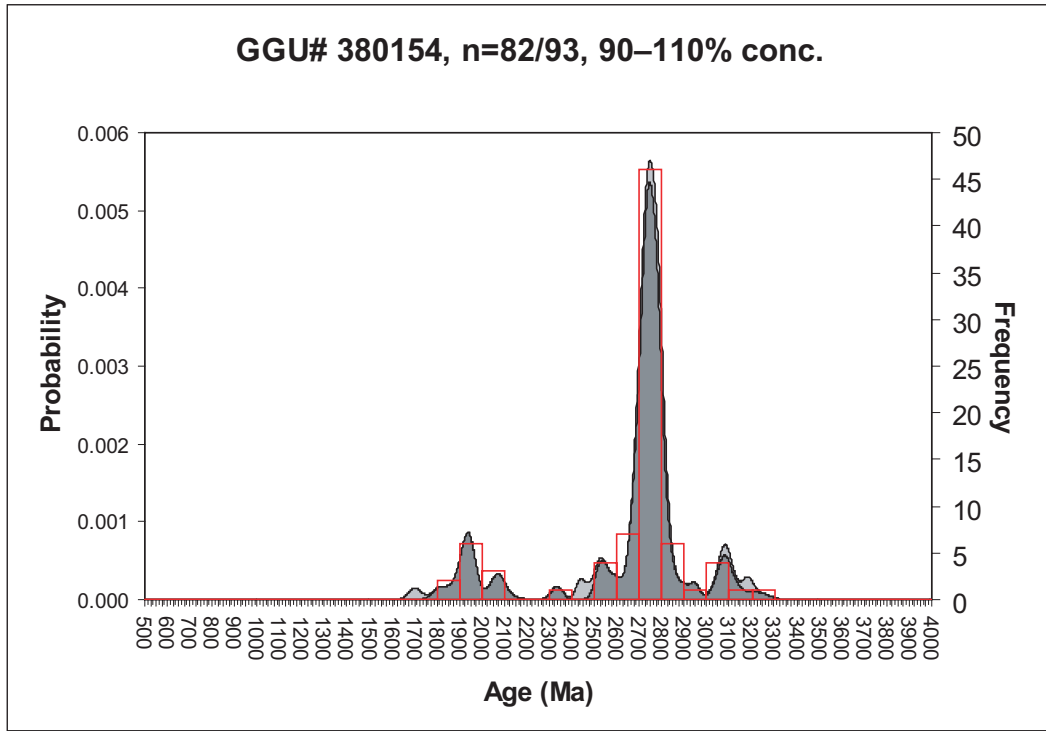
368273



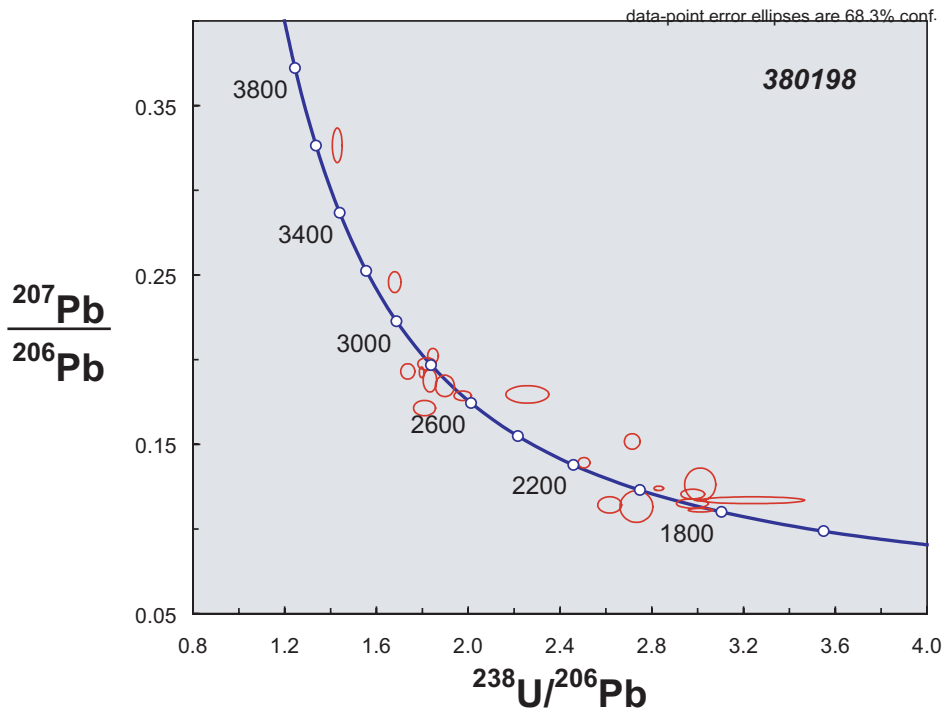
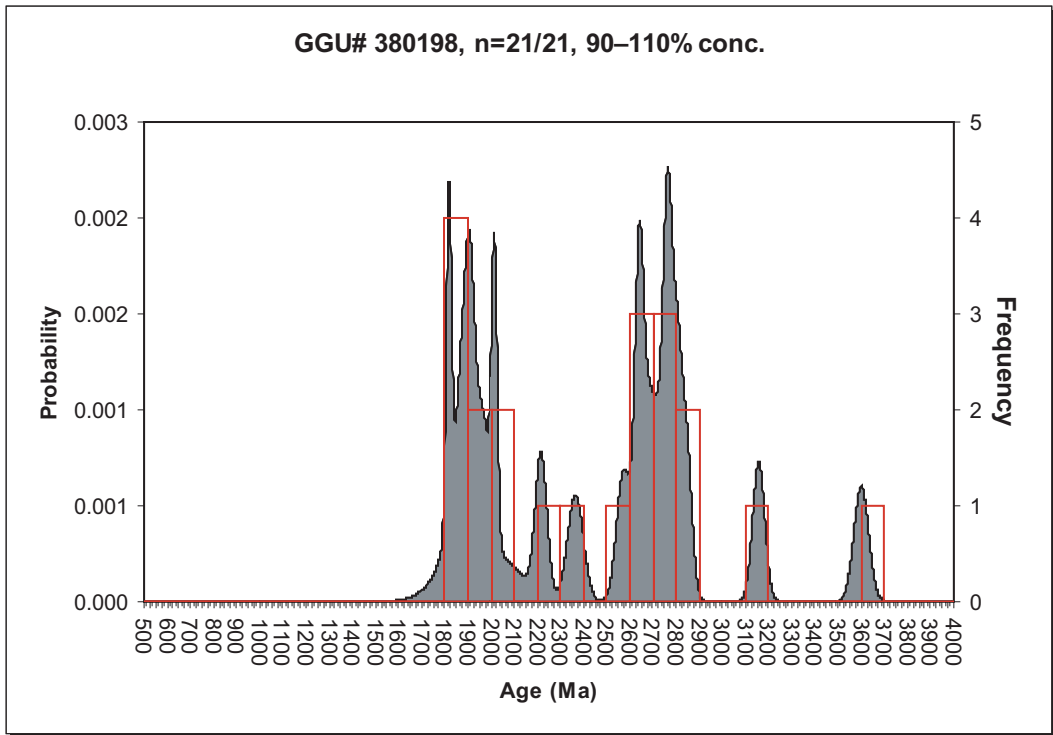
380044



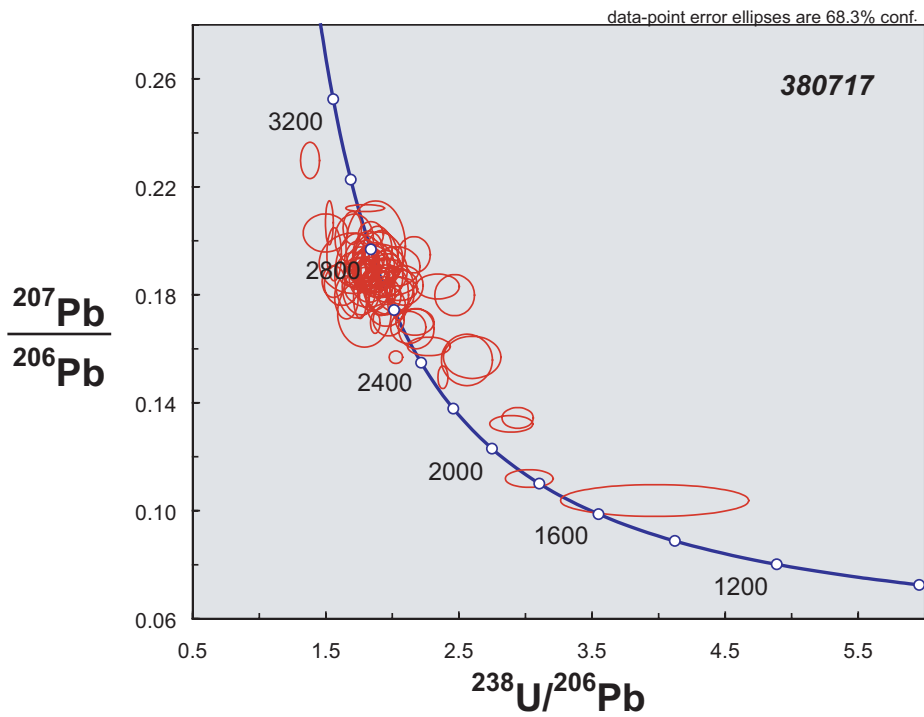
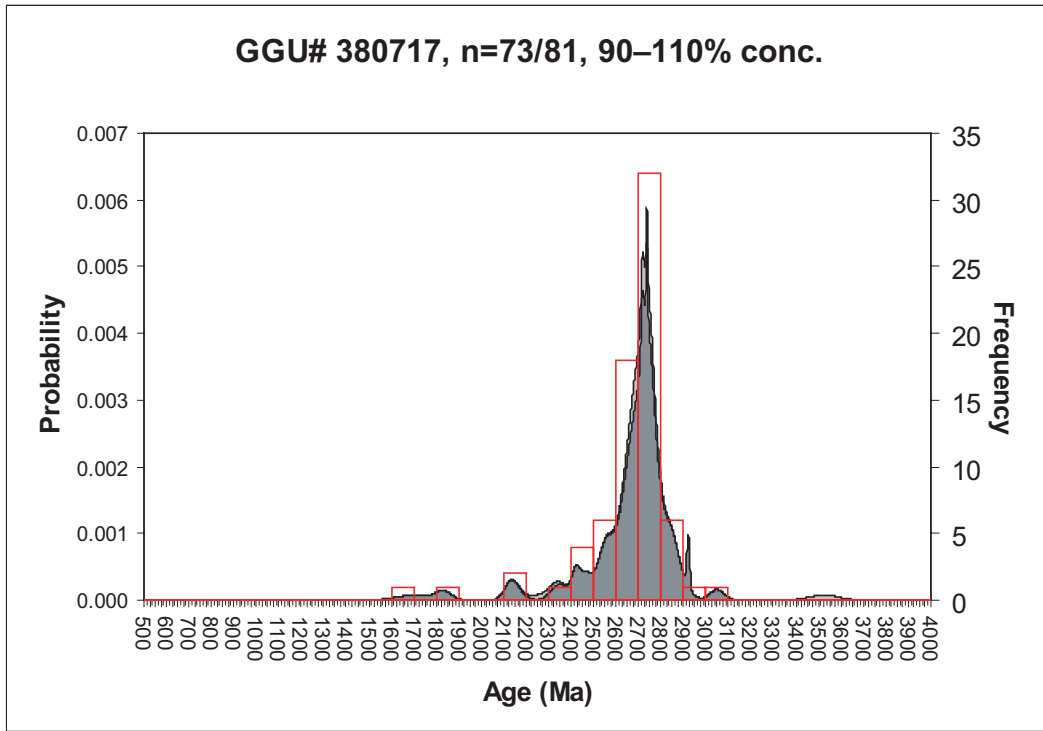
380154



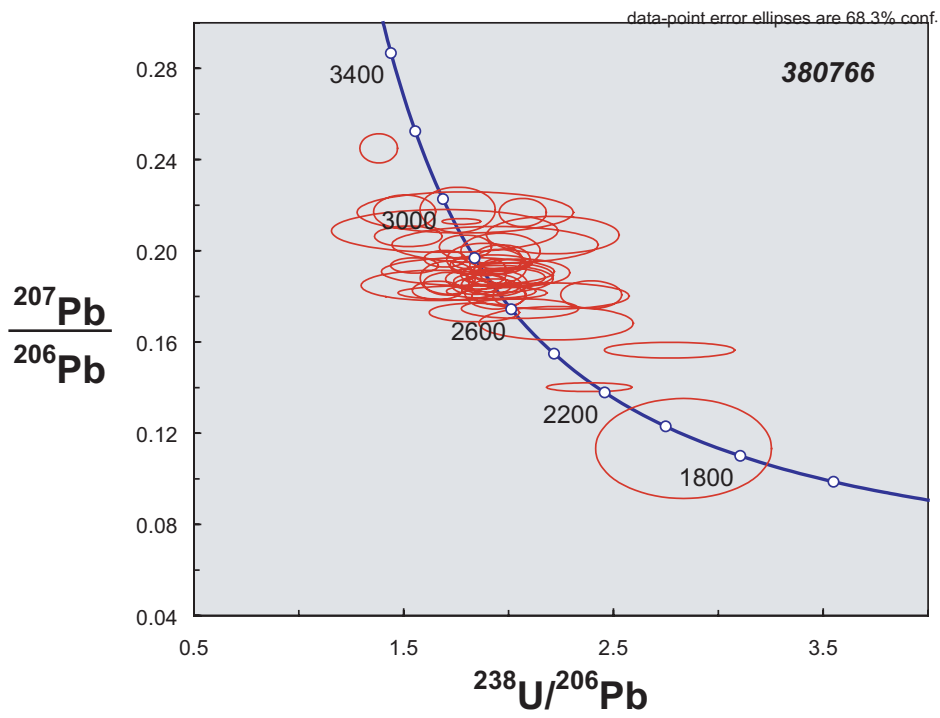
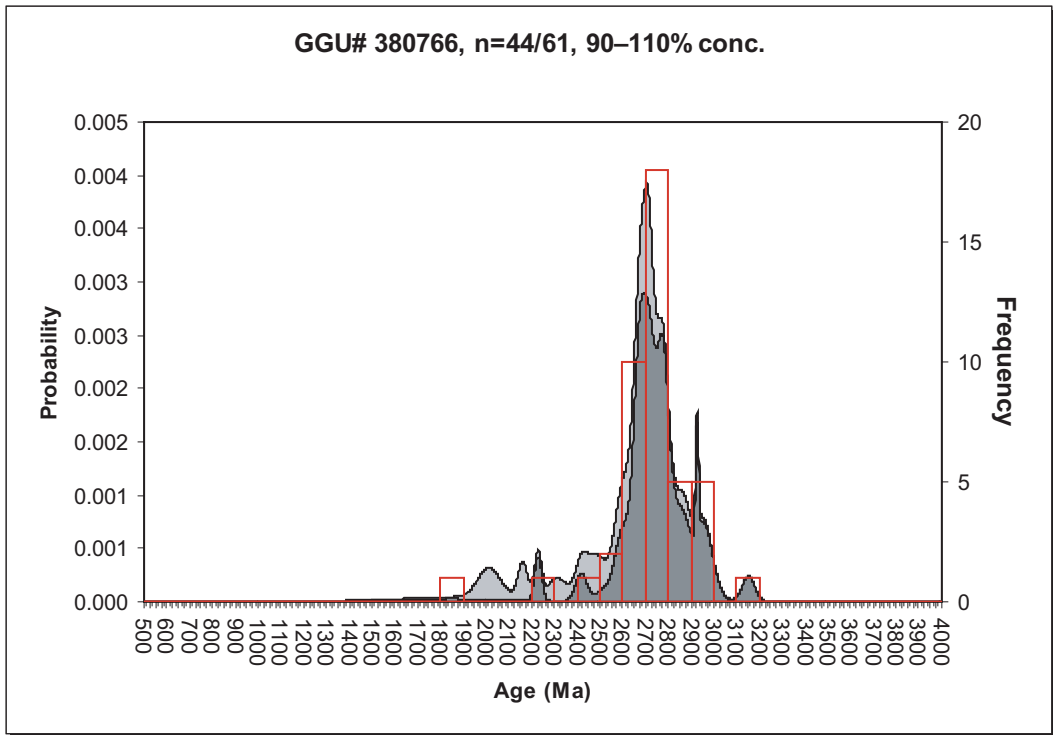
380198



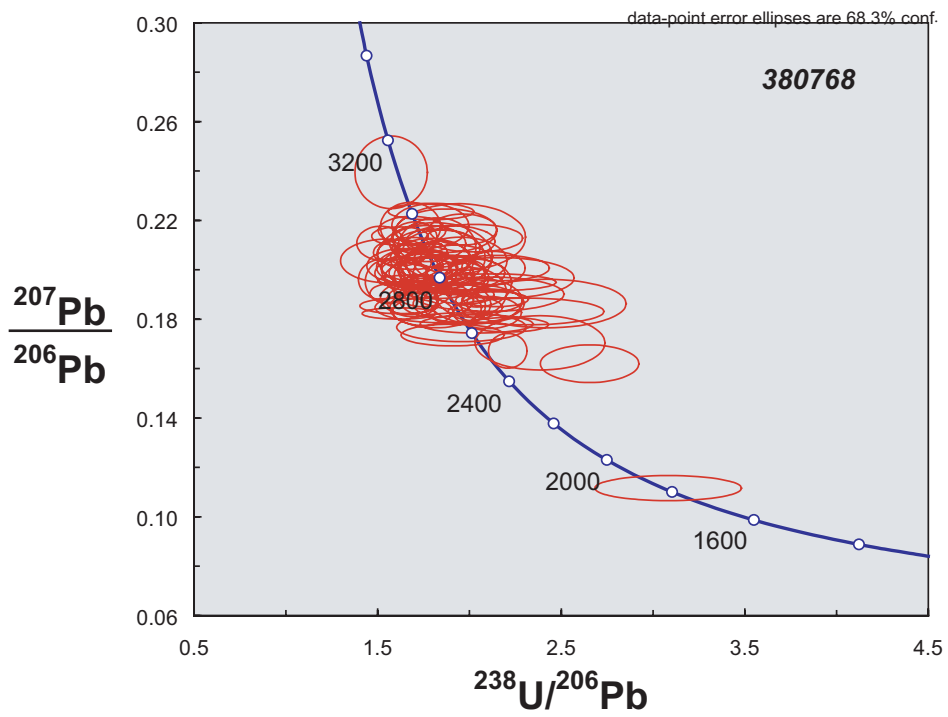
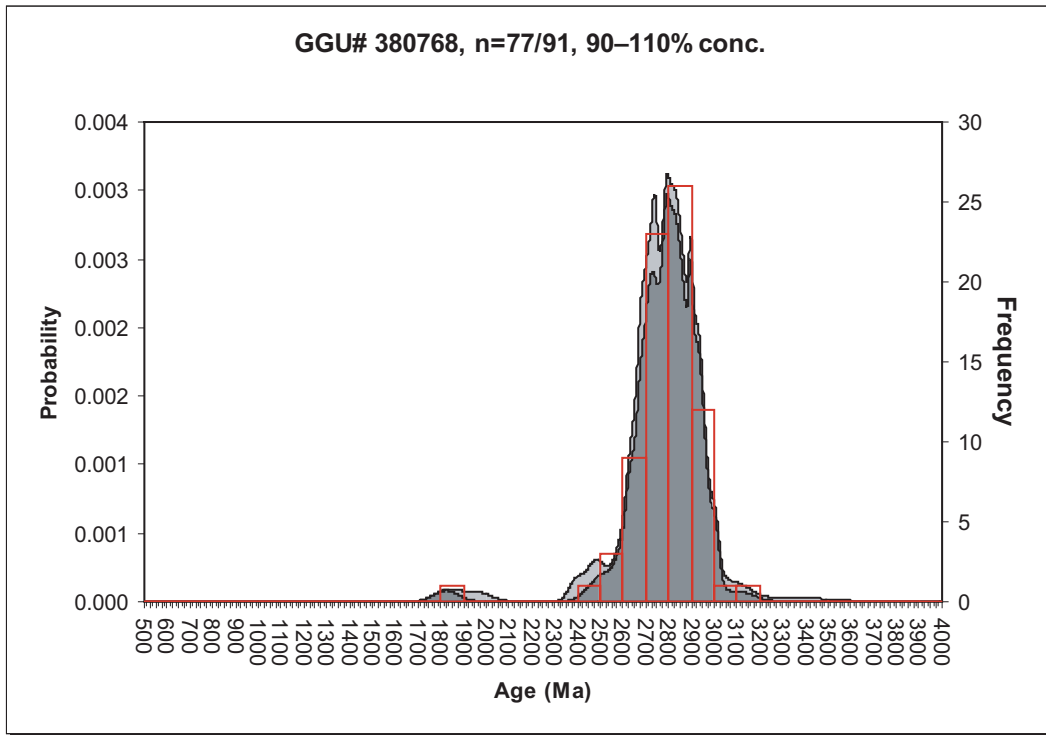
380717



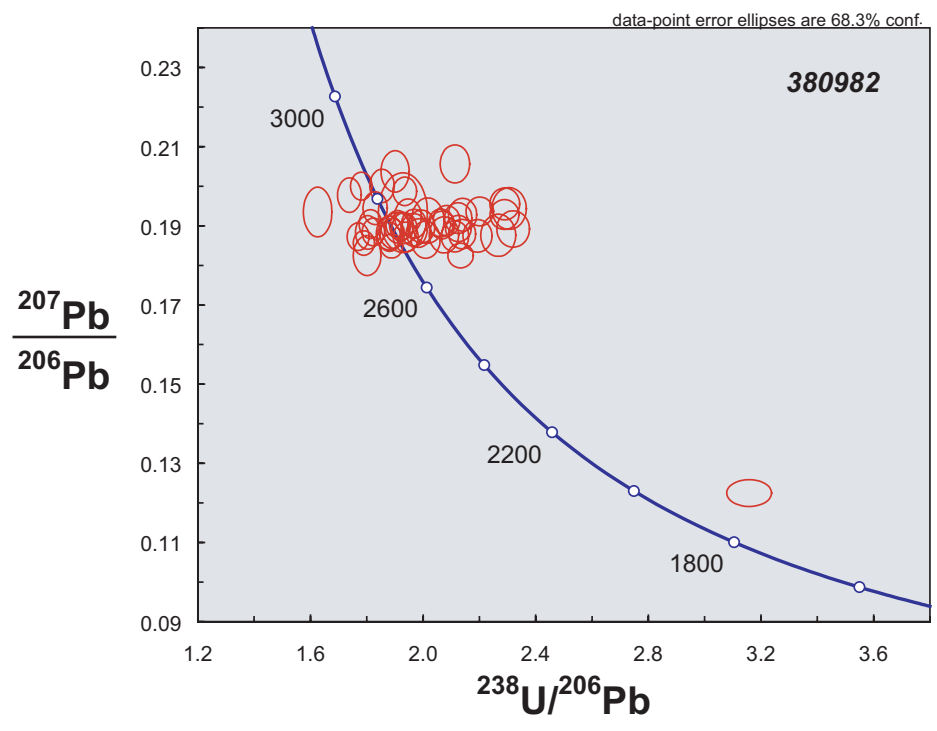
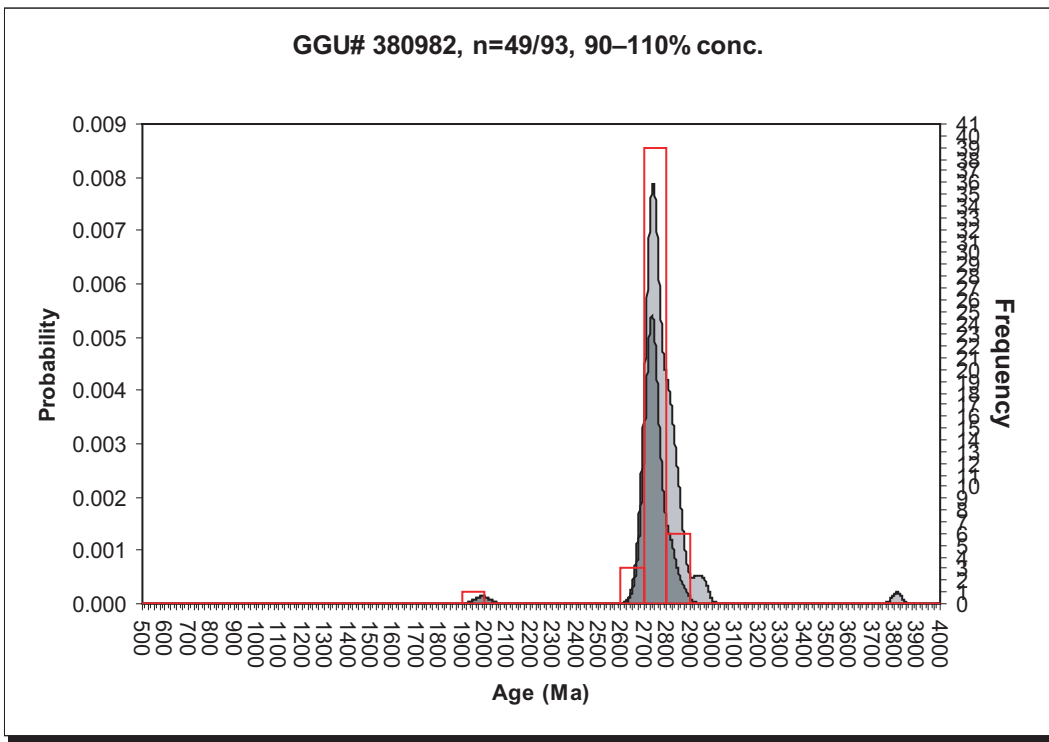
380766



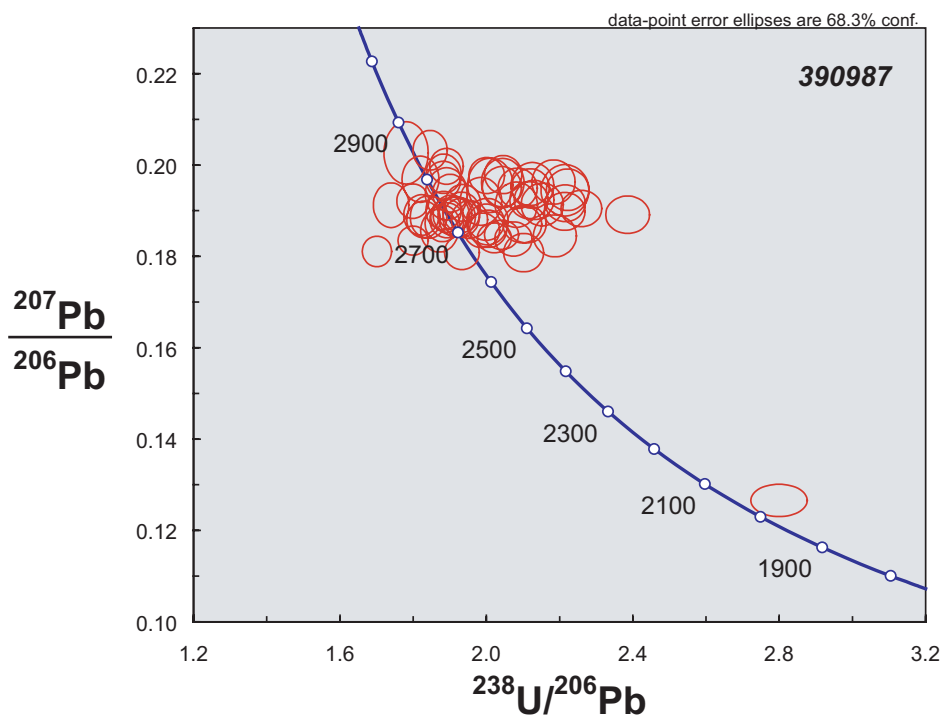
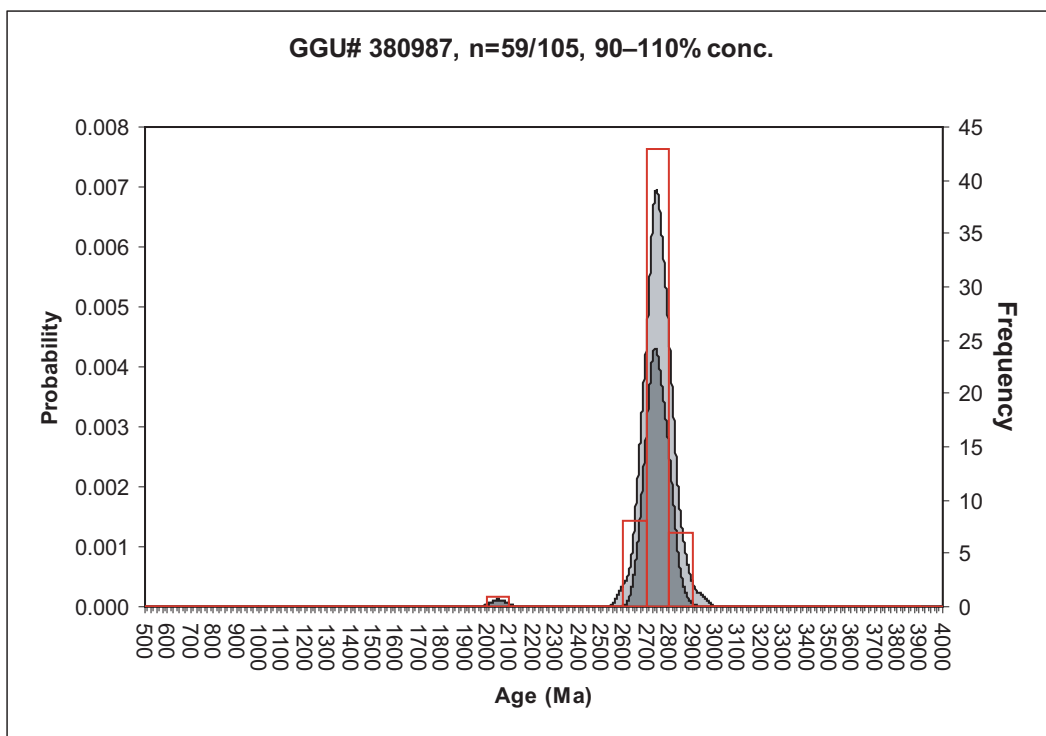
380768



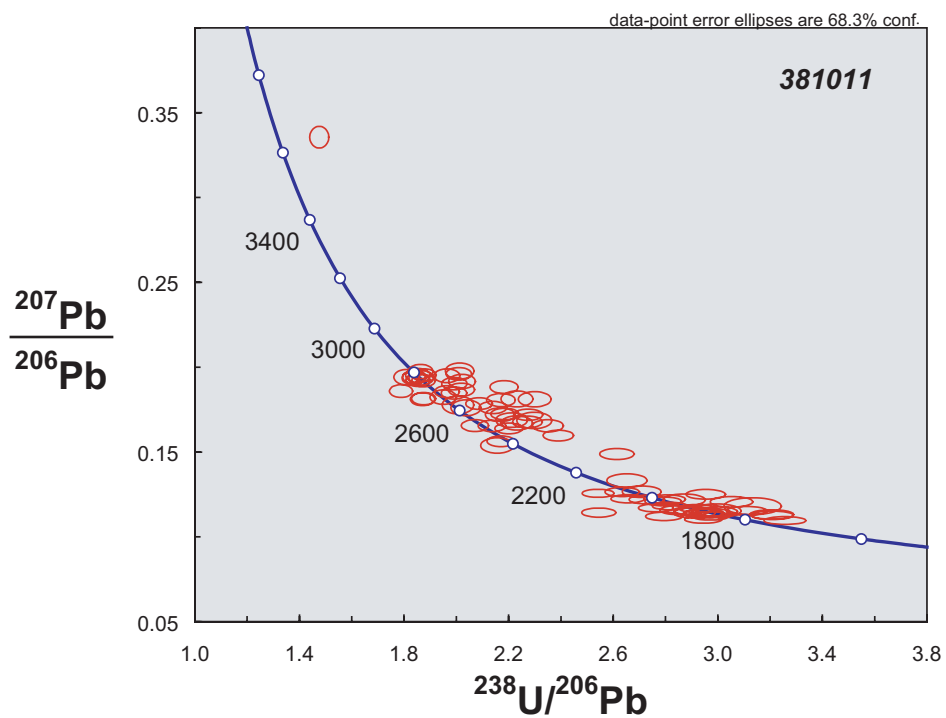
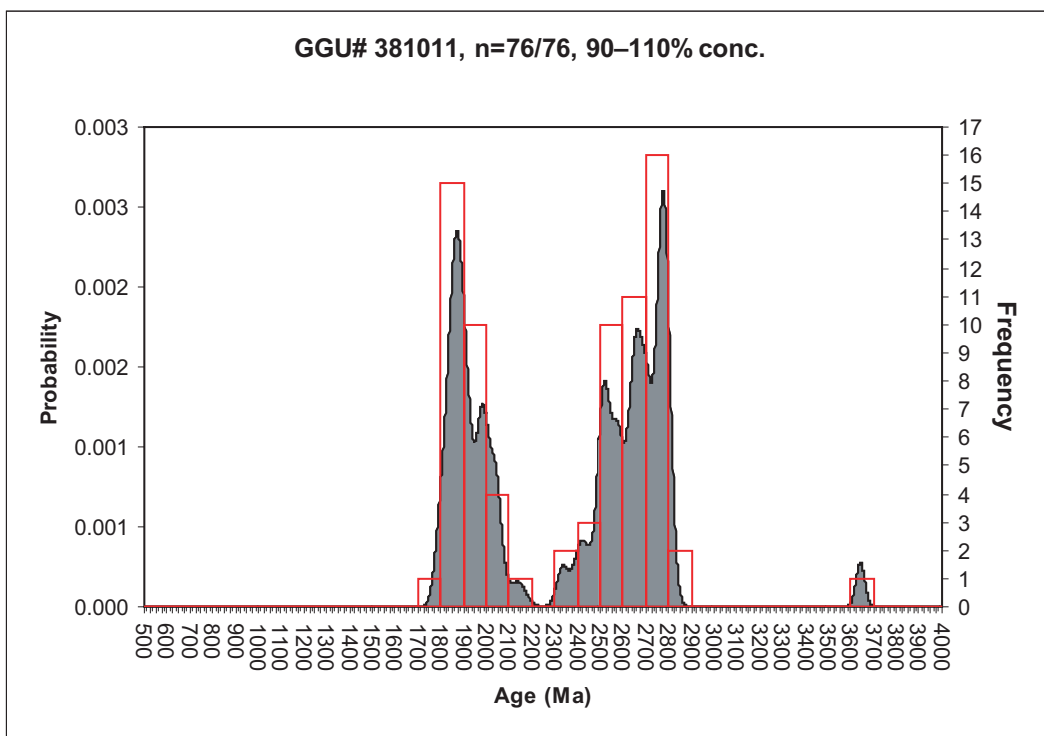
380982



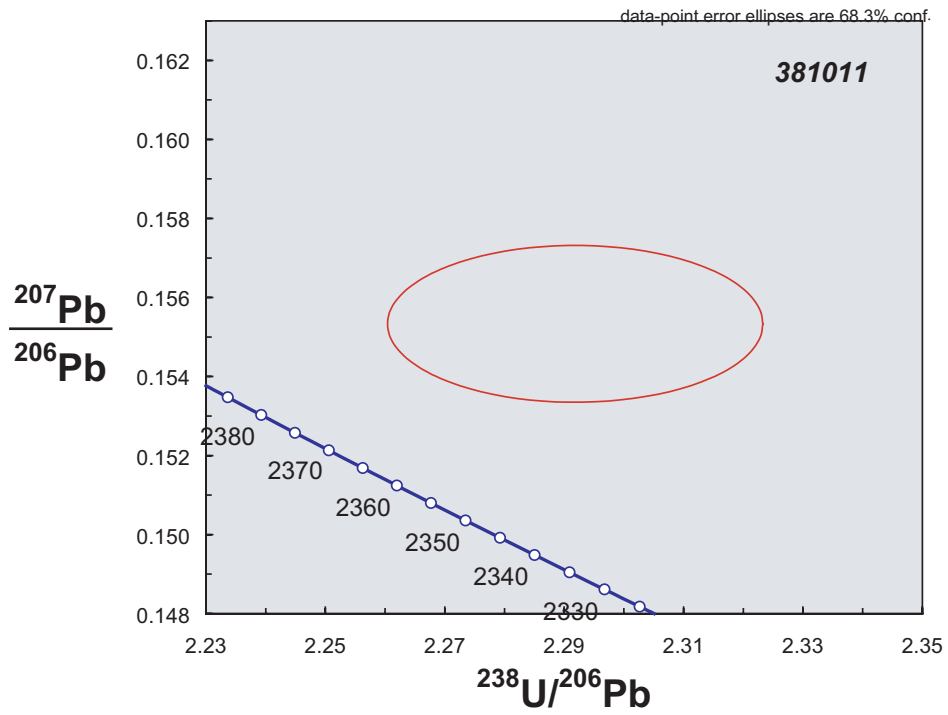
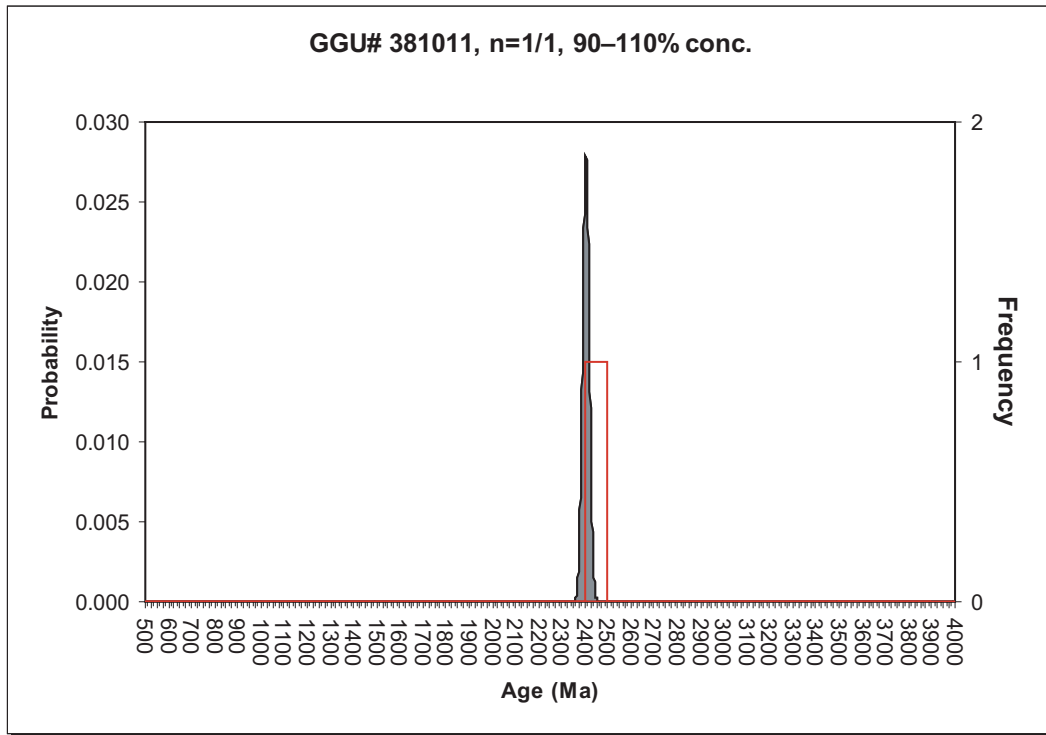
380987



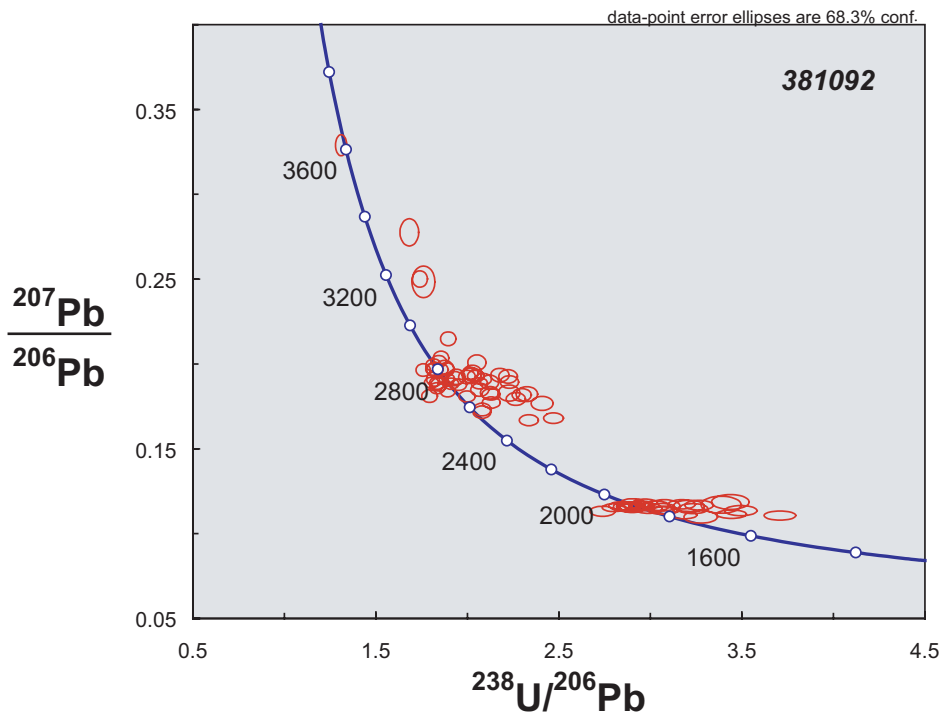
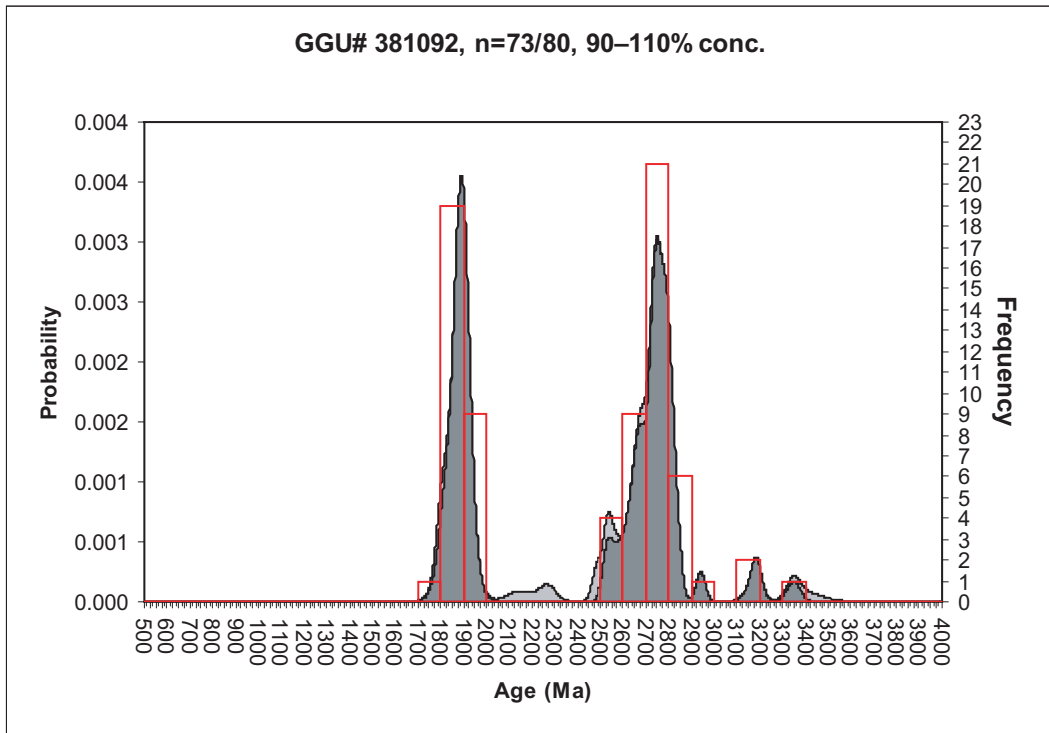
381011



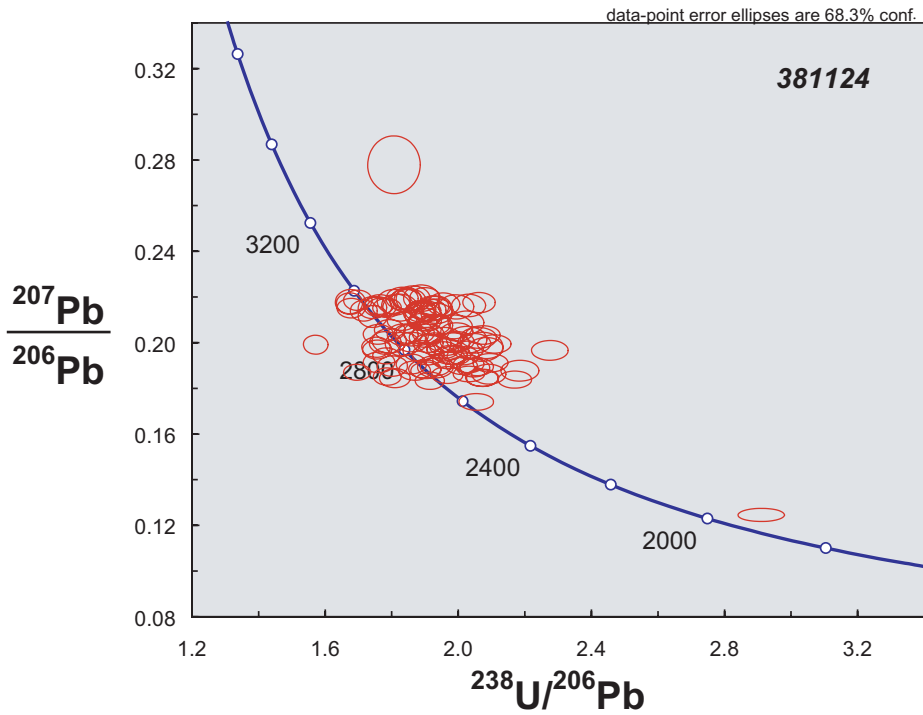
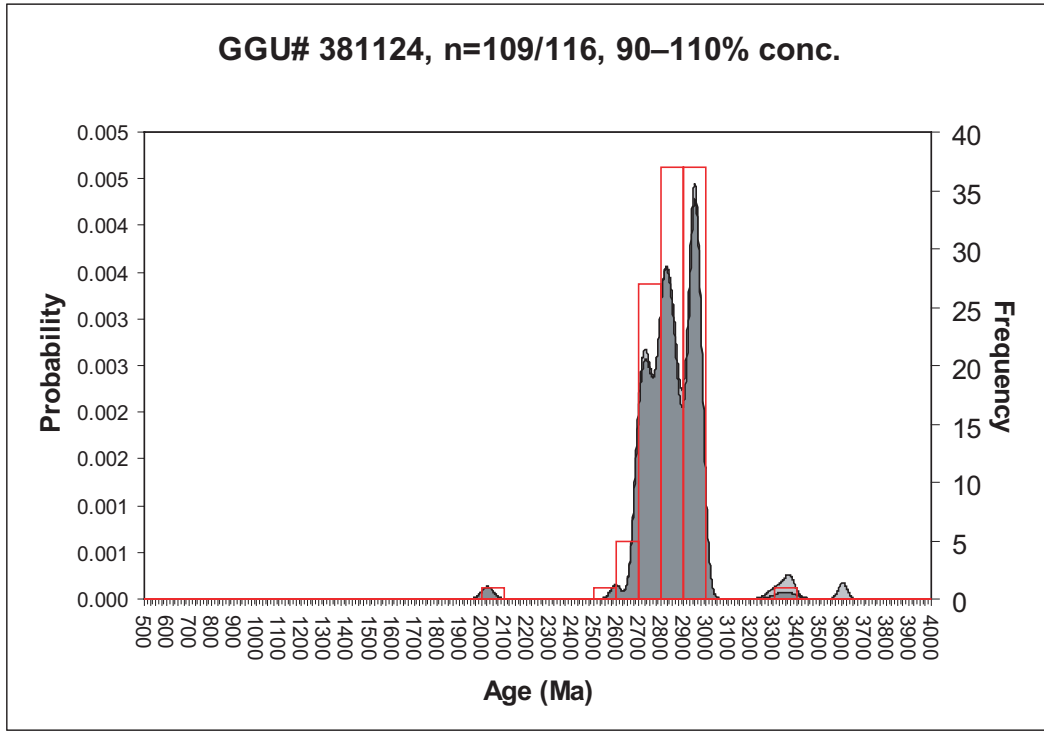
381011



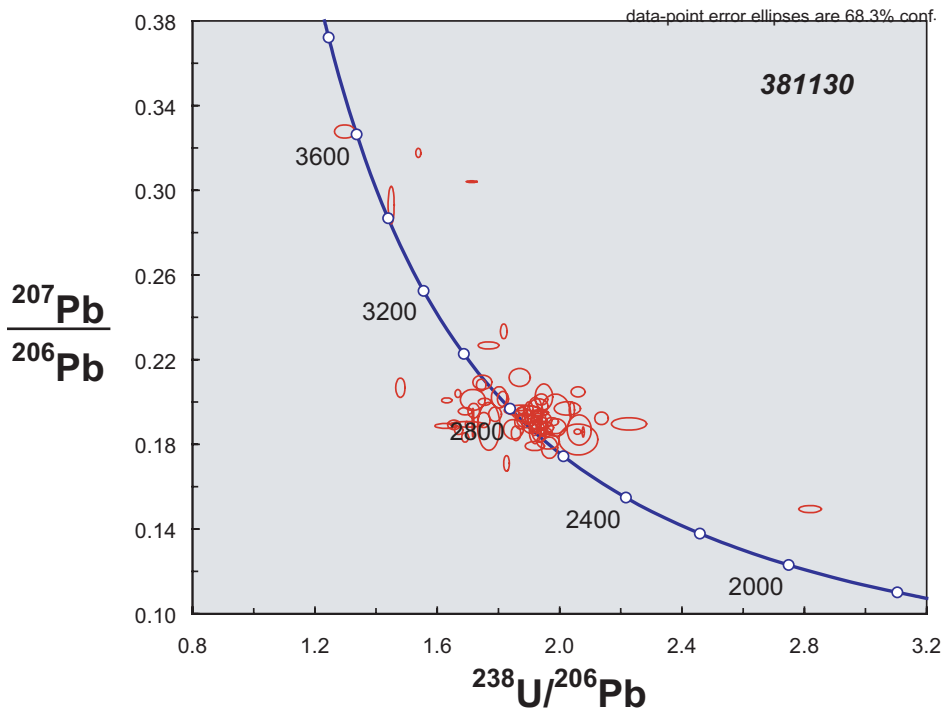
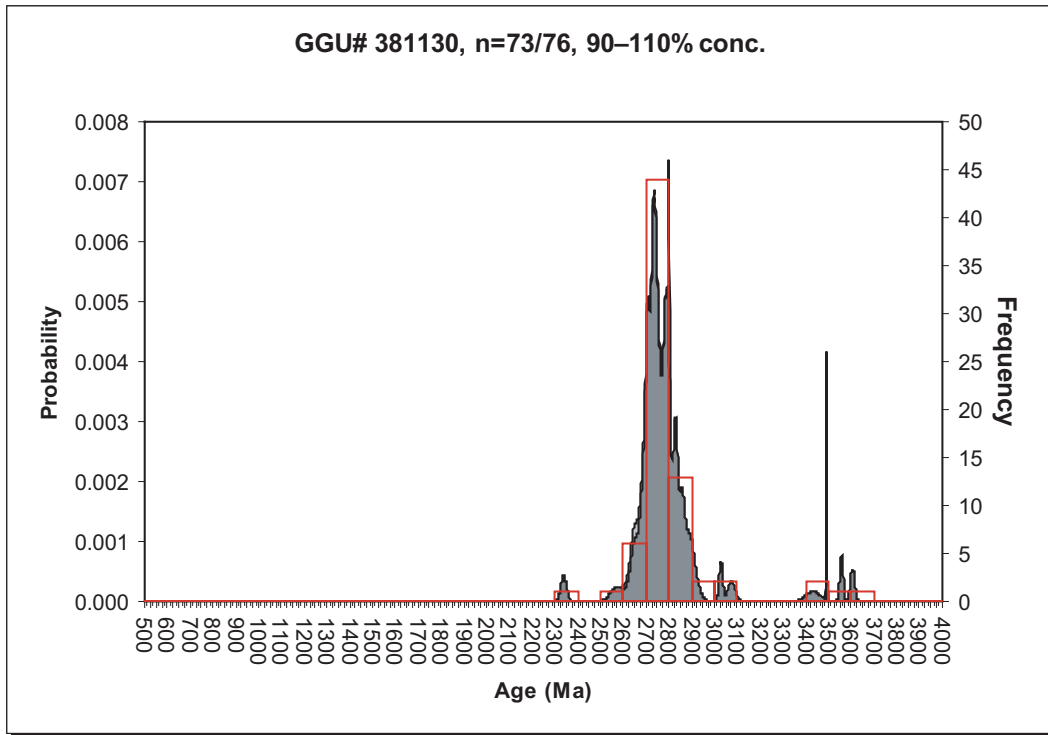
381092



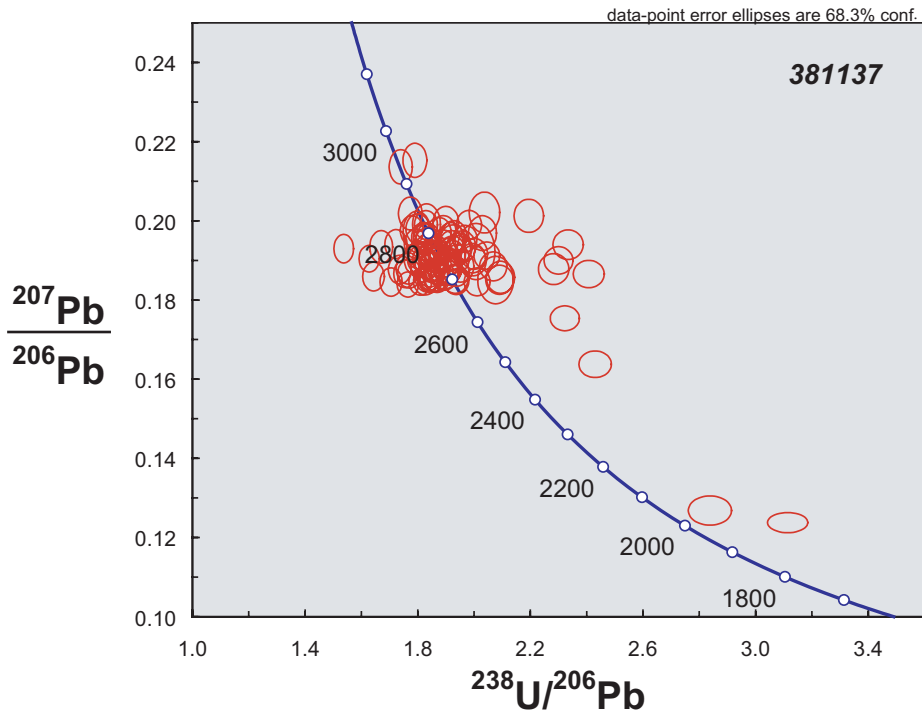
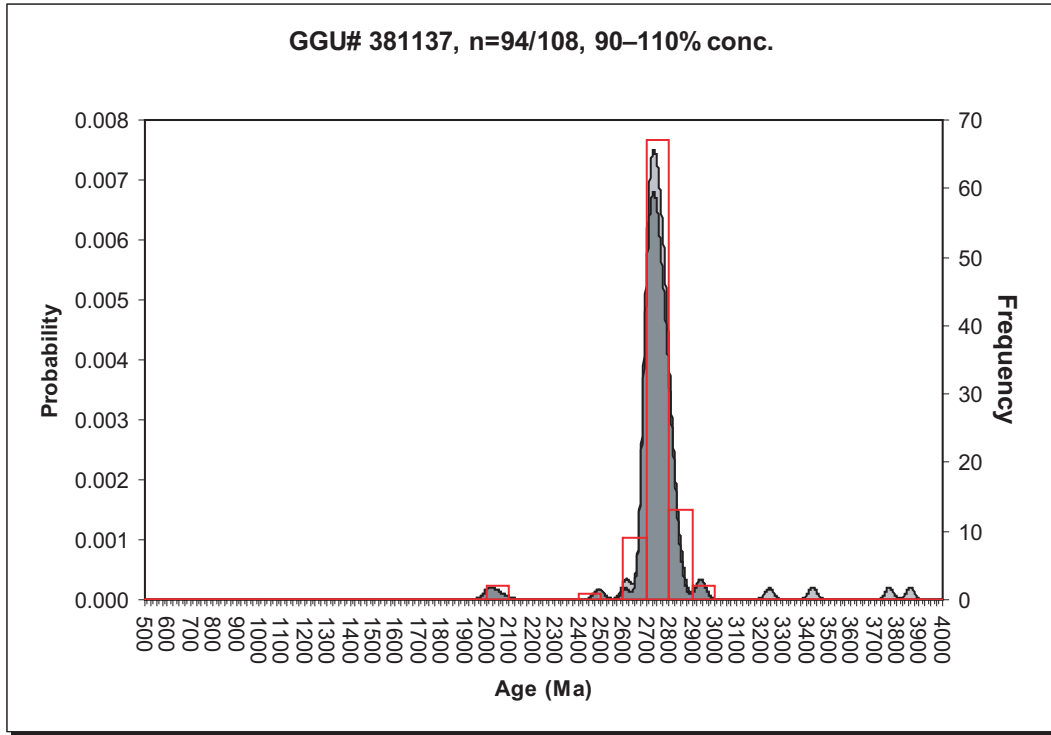
381124



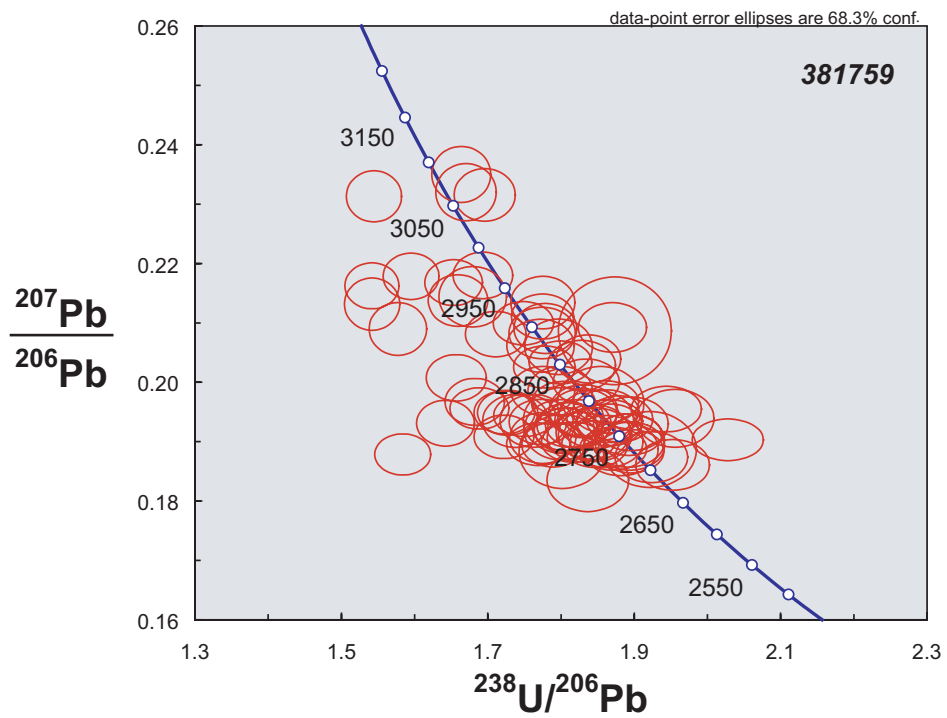
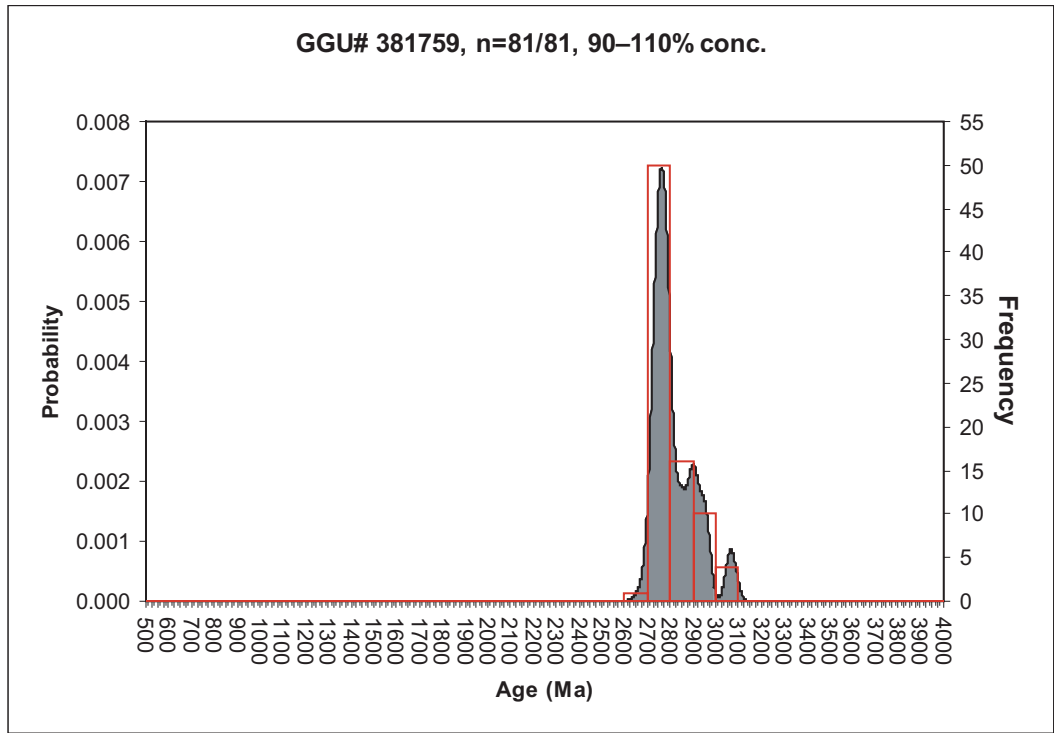
381130



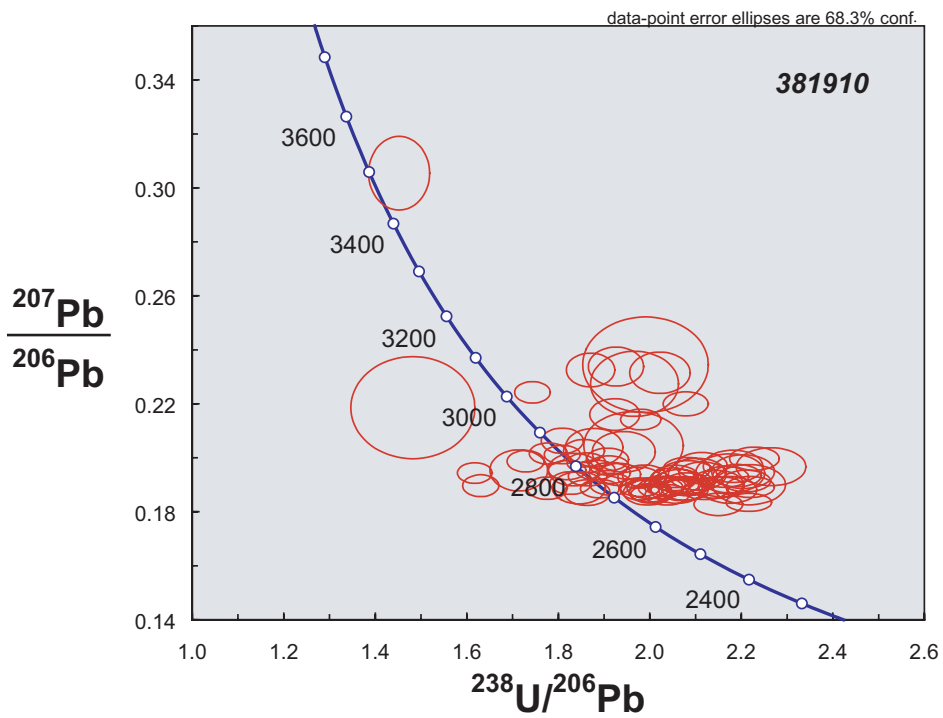
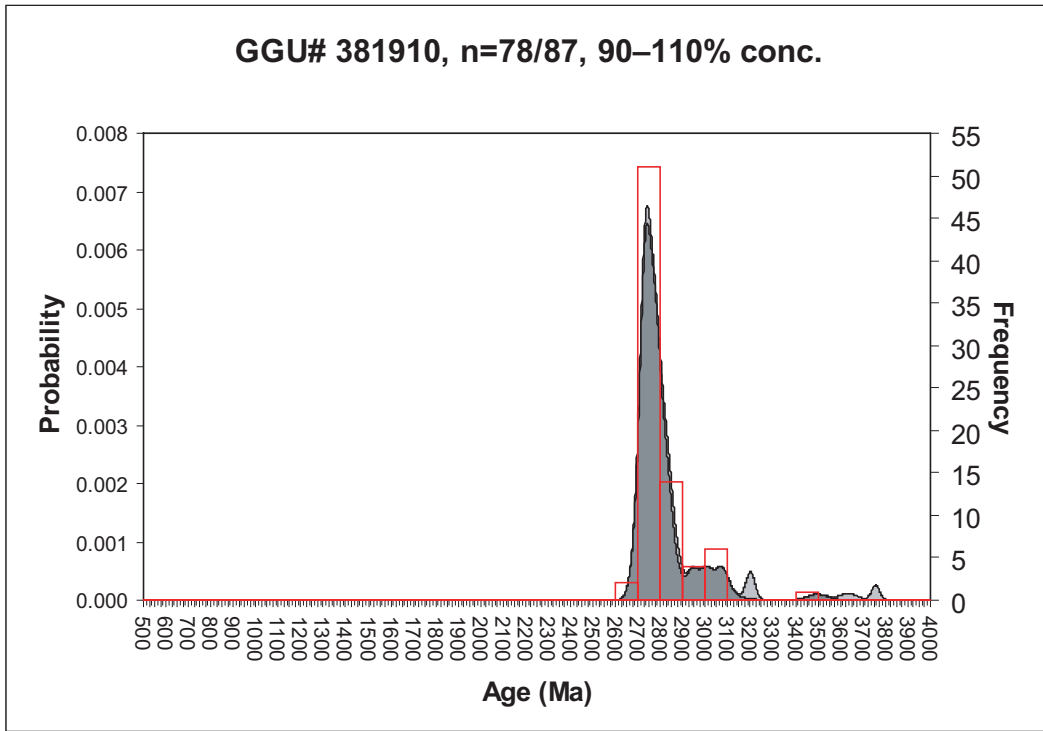
38137



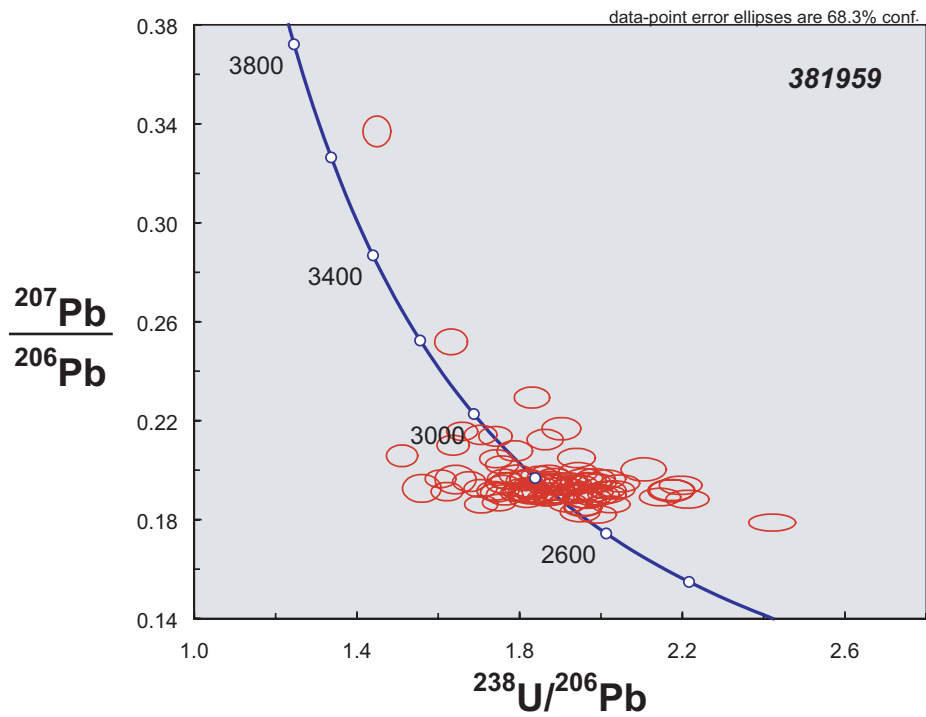
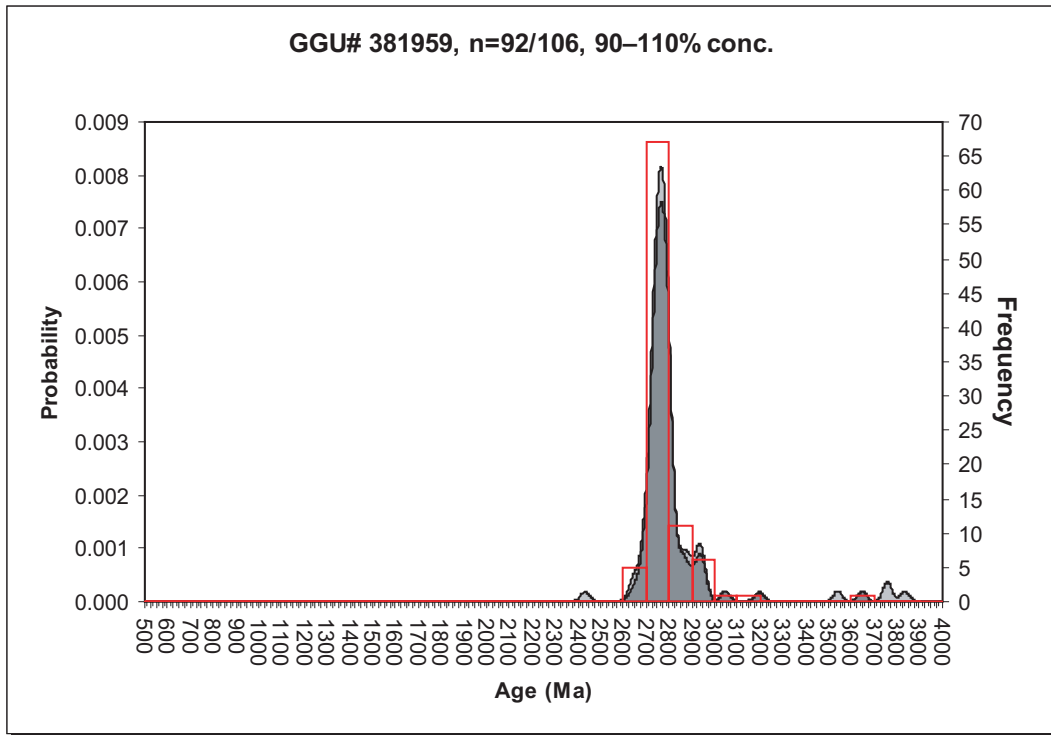
381759



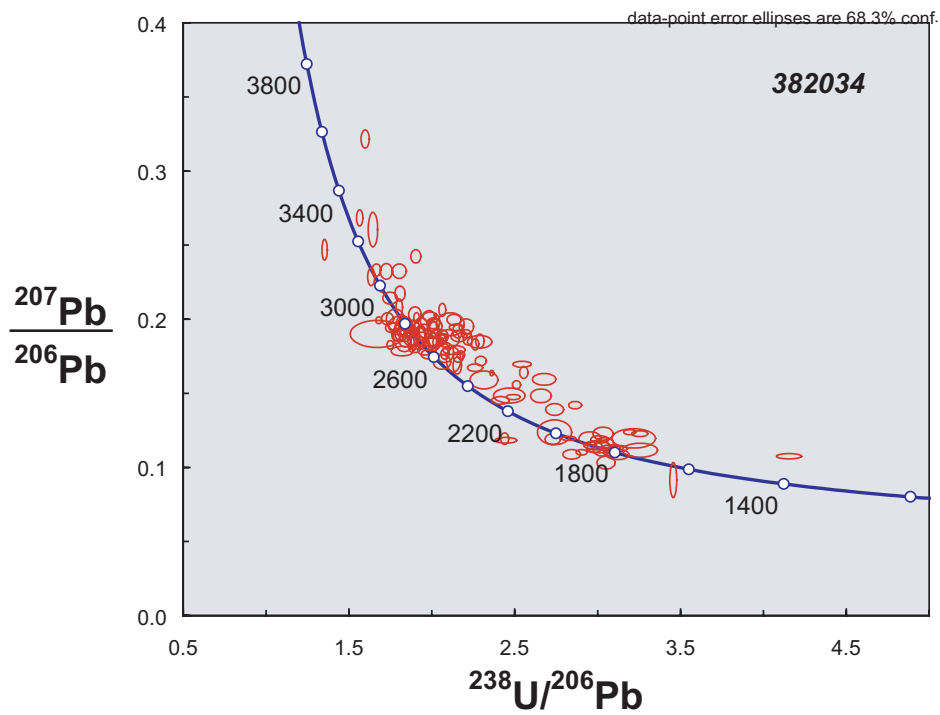
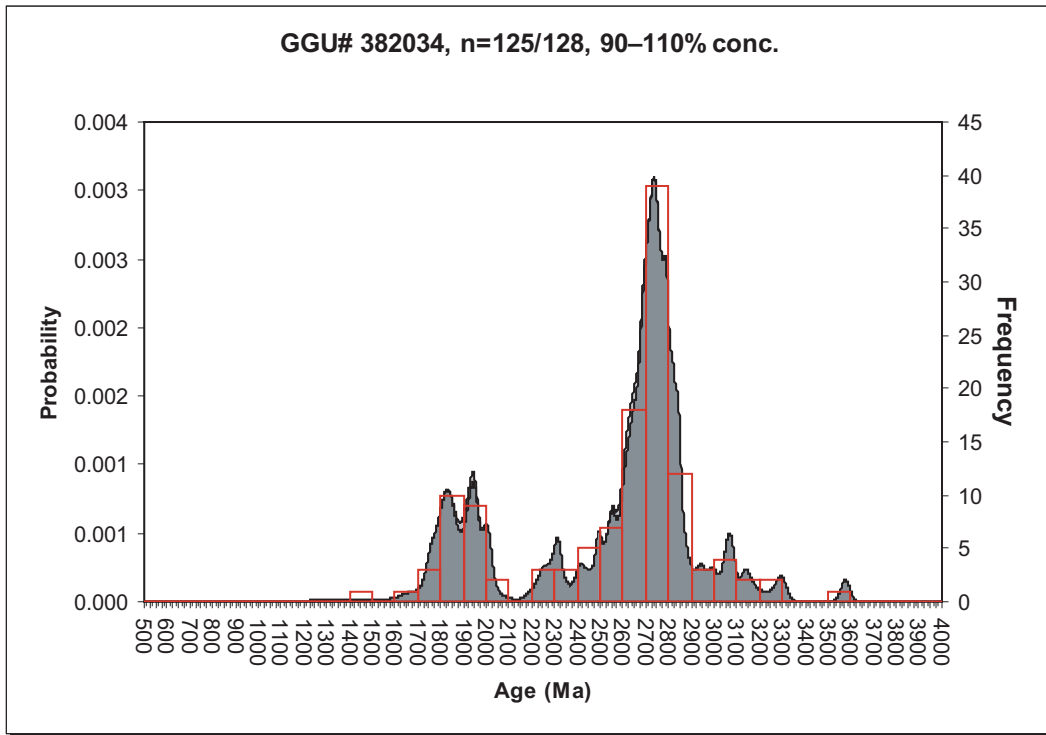
381910



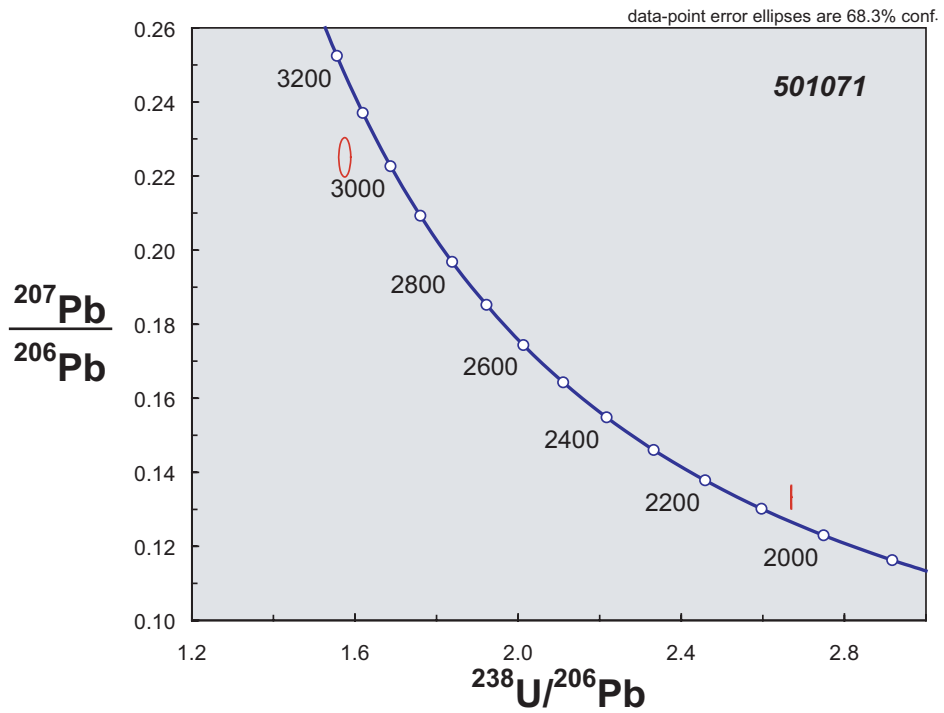
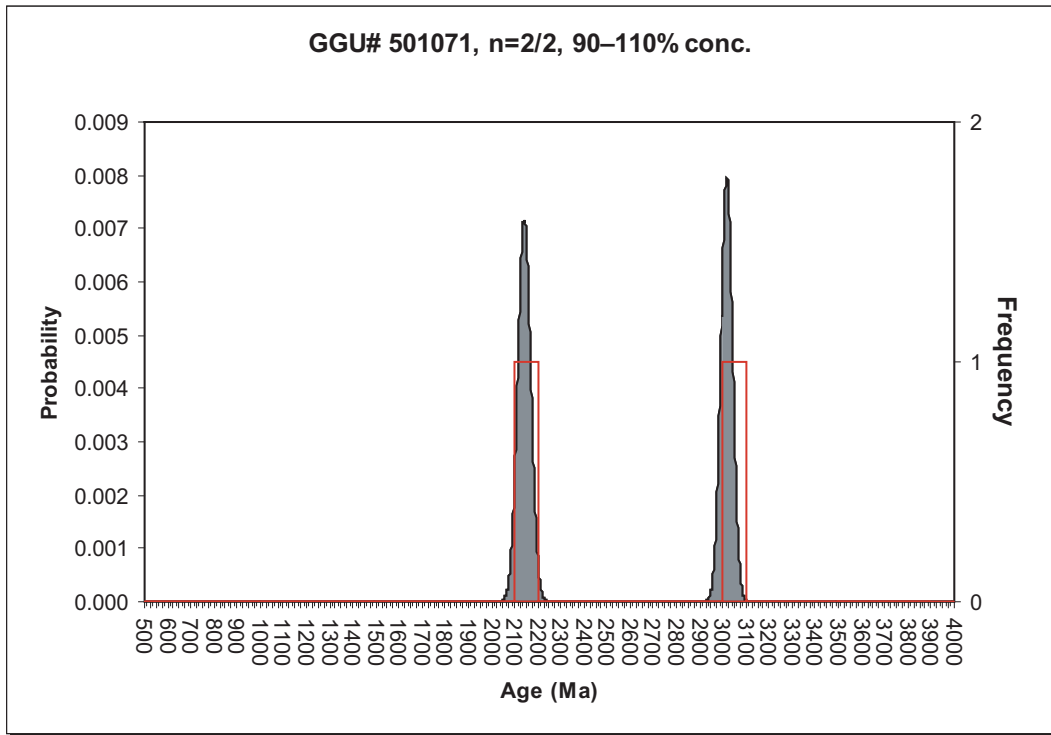
381959



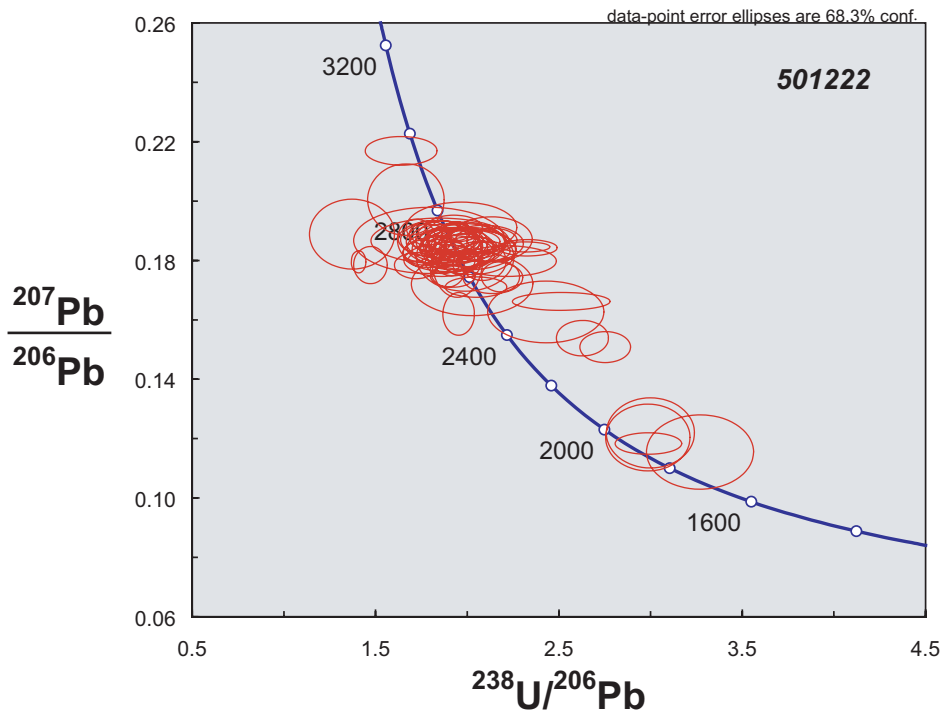
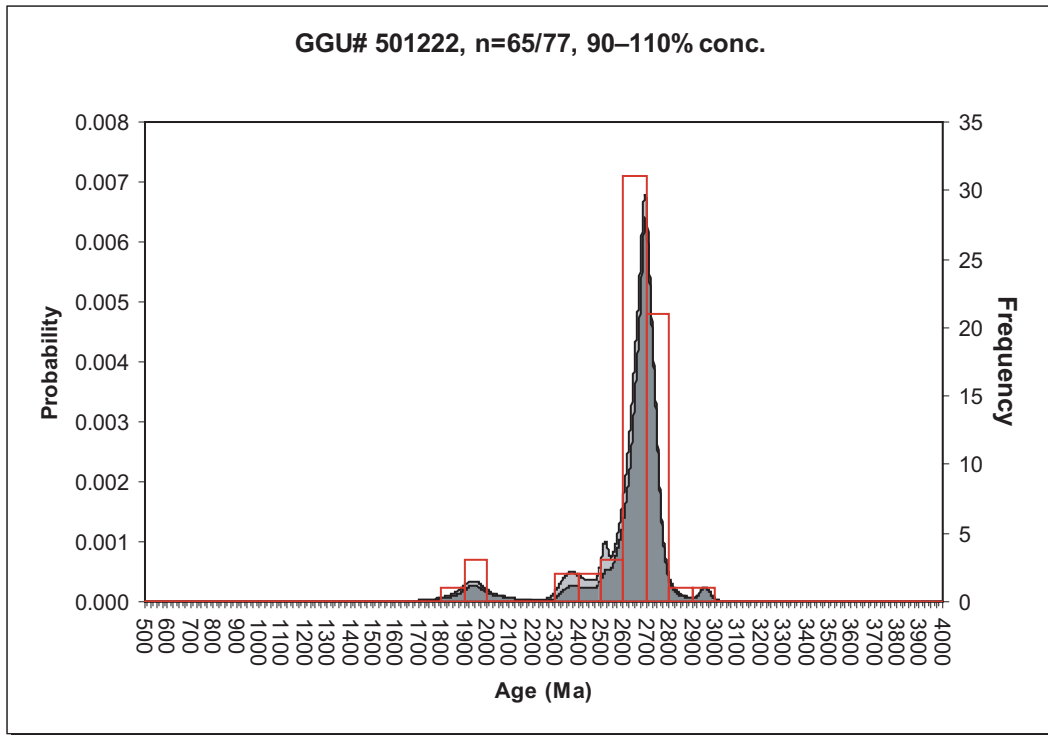
382034



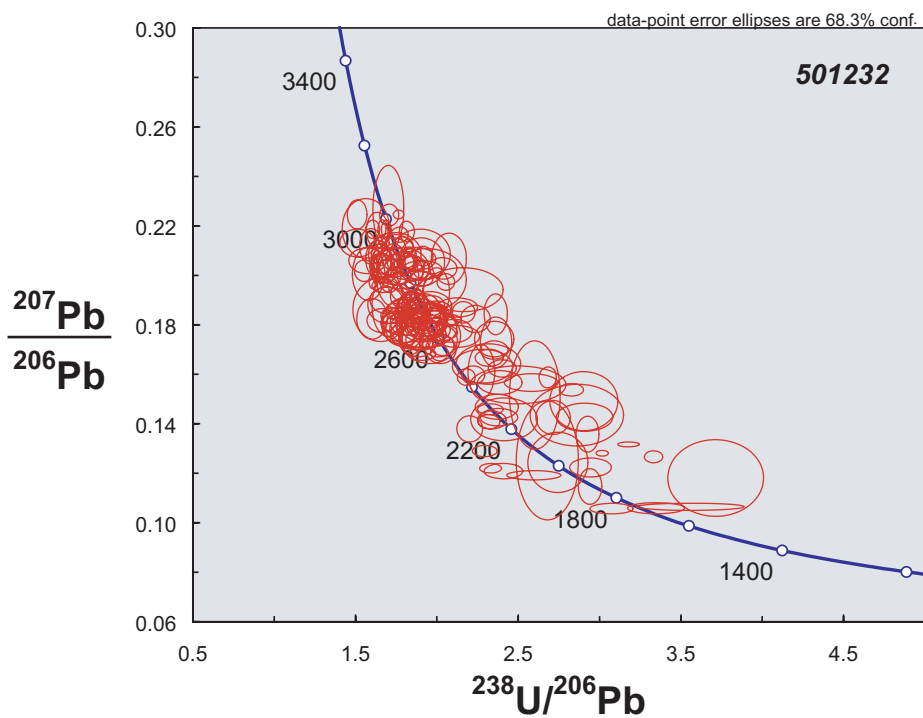
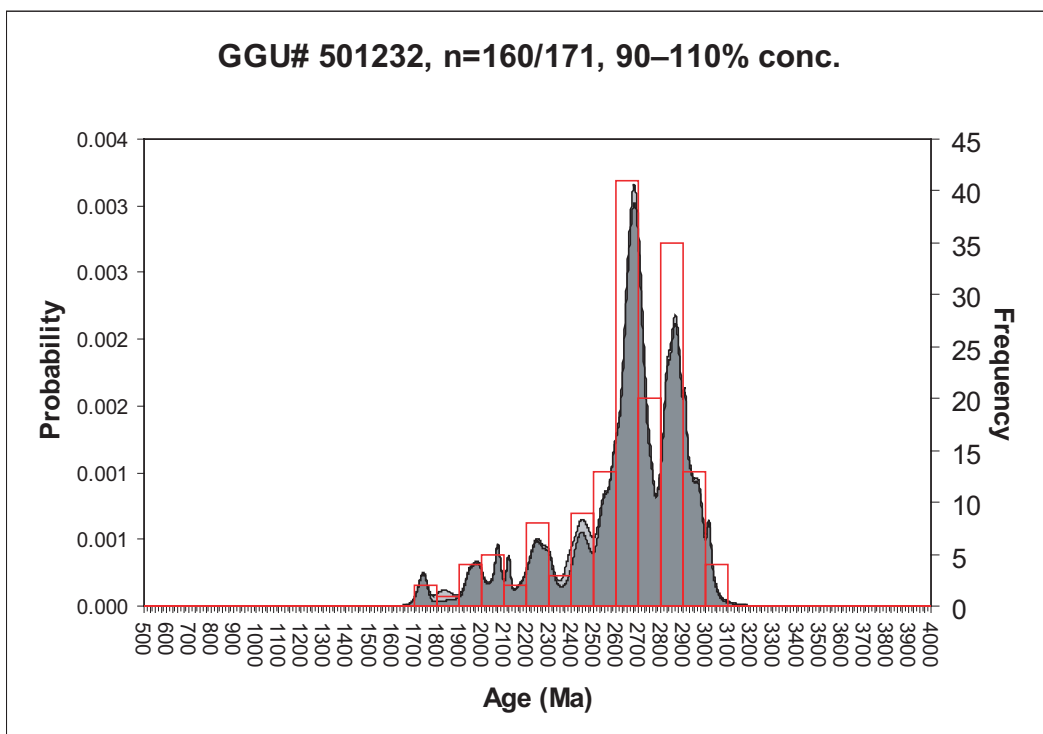
501071



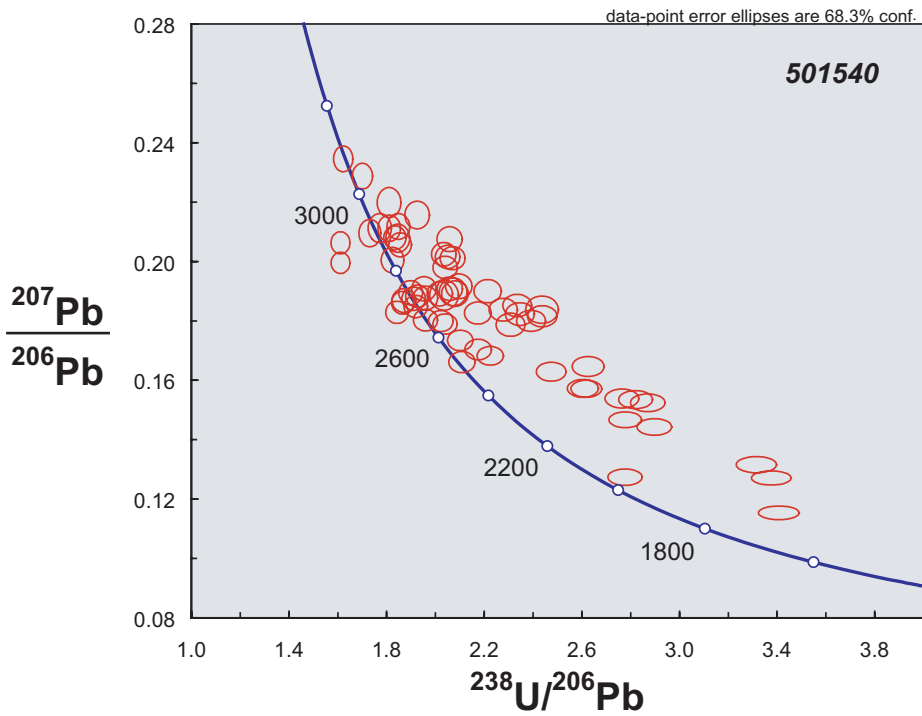
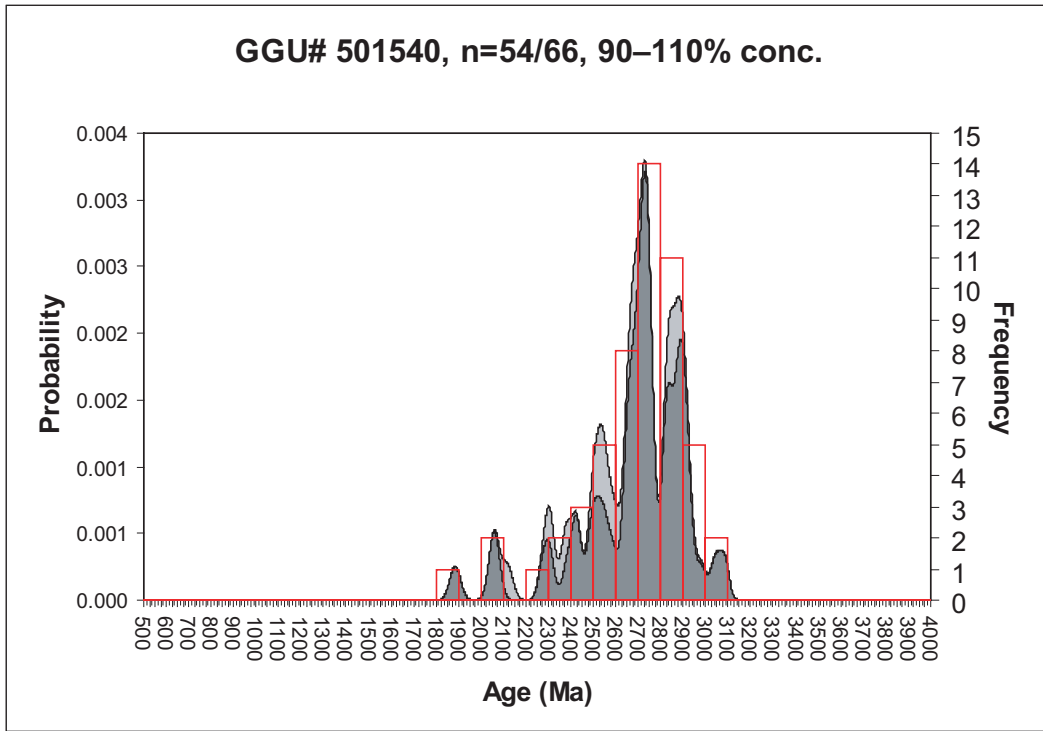
501222



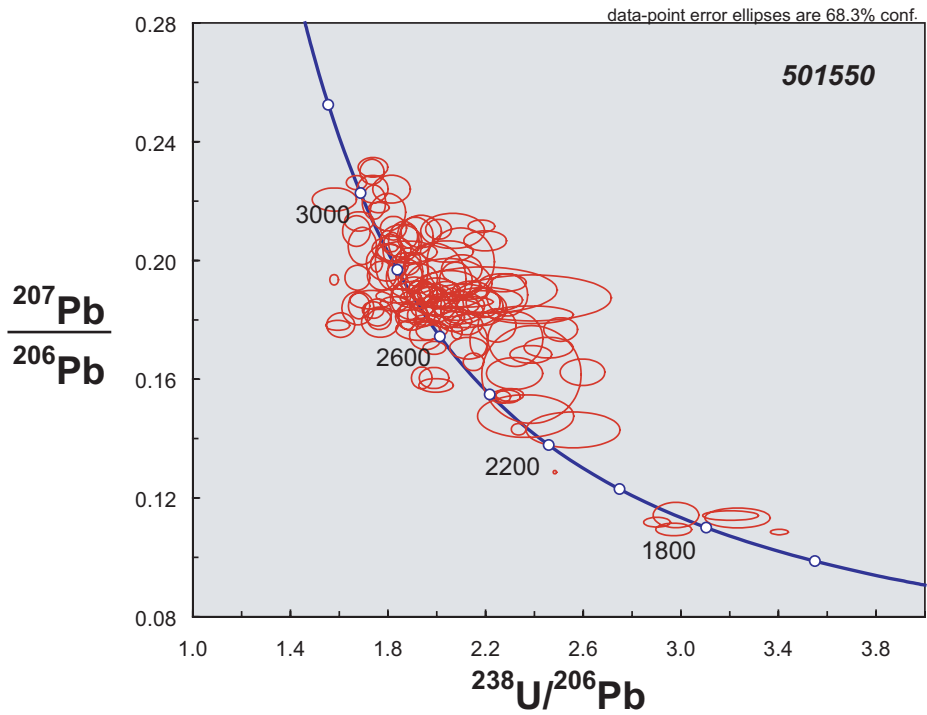
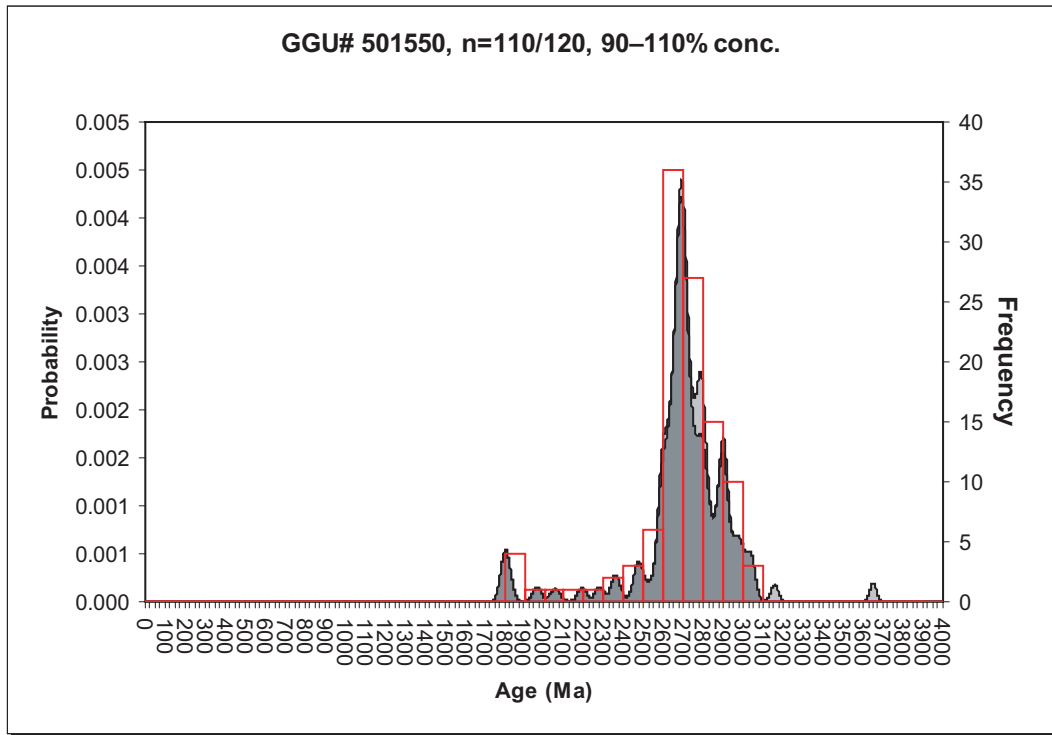
501232



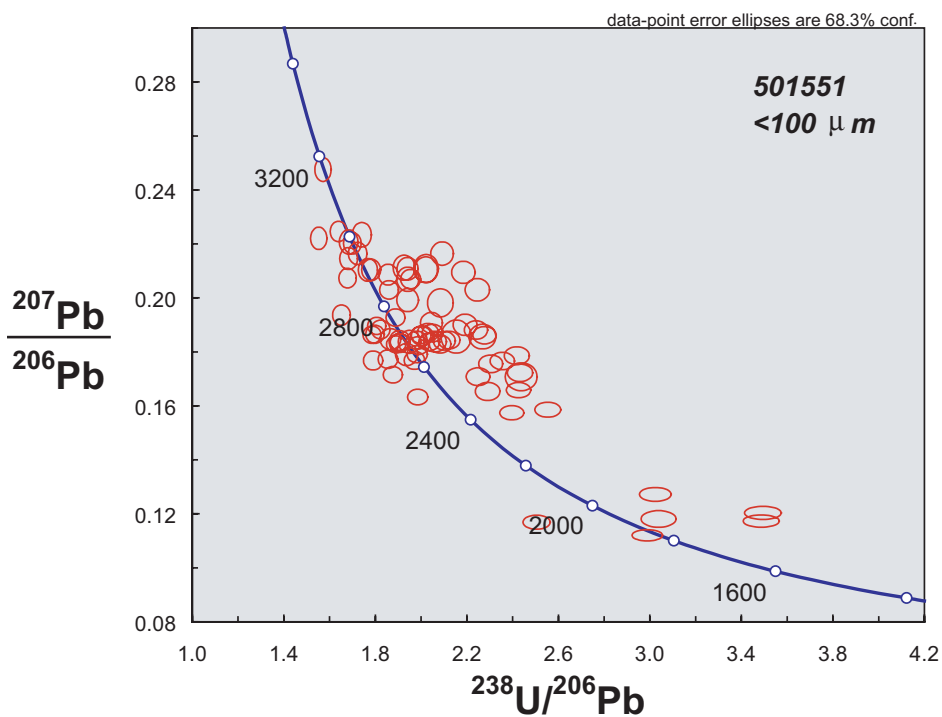
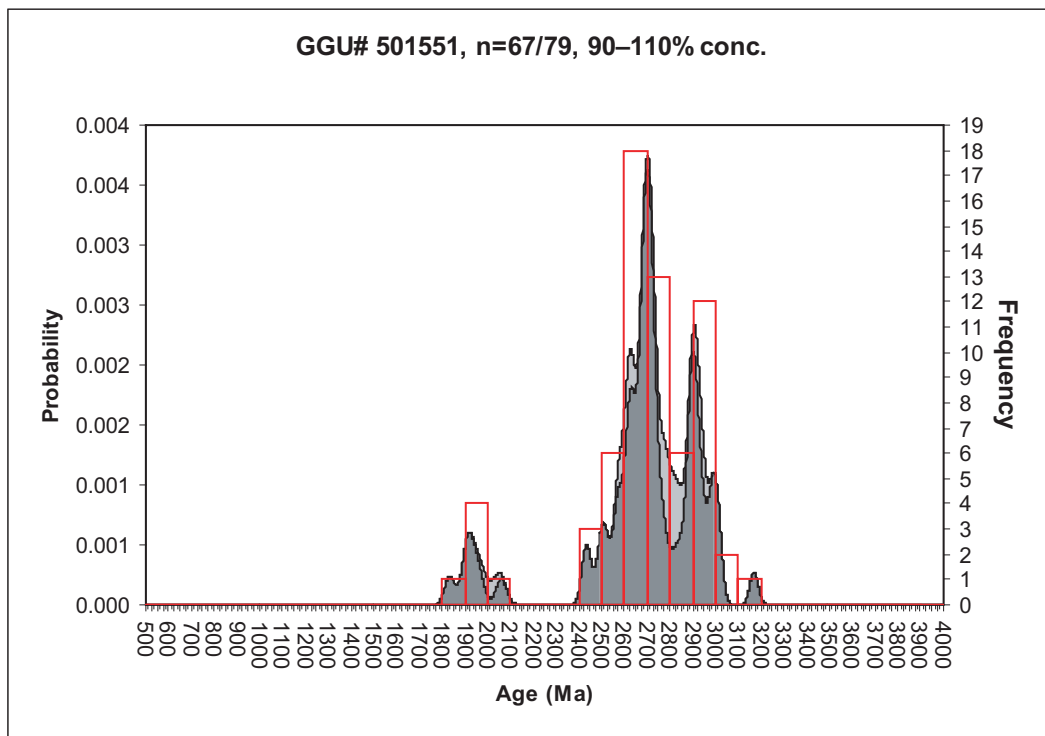
501540



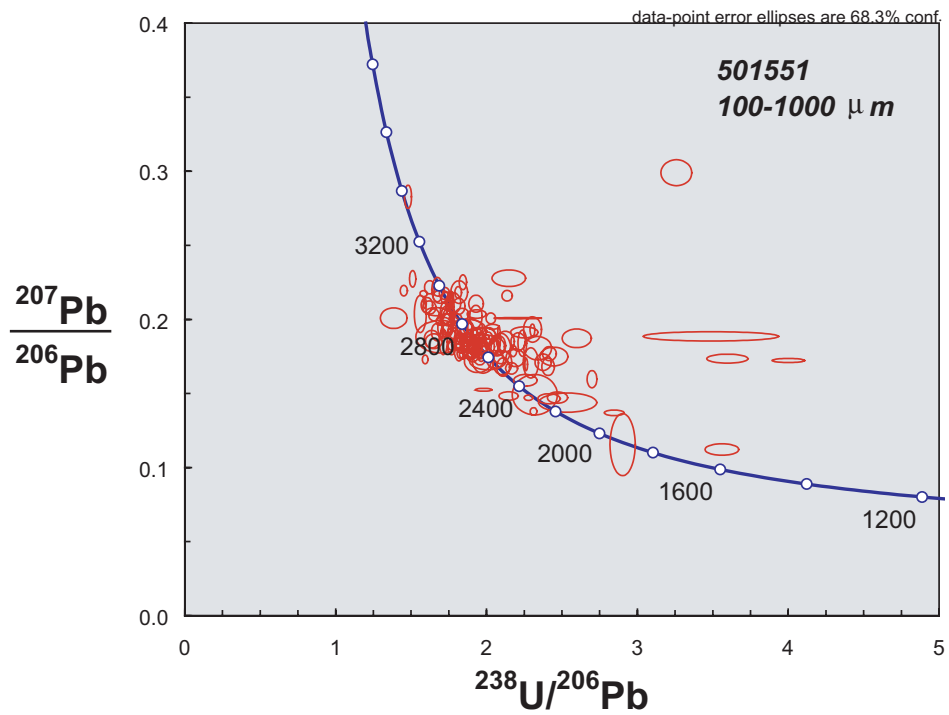
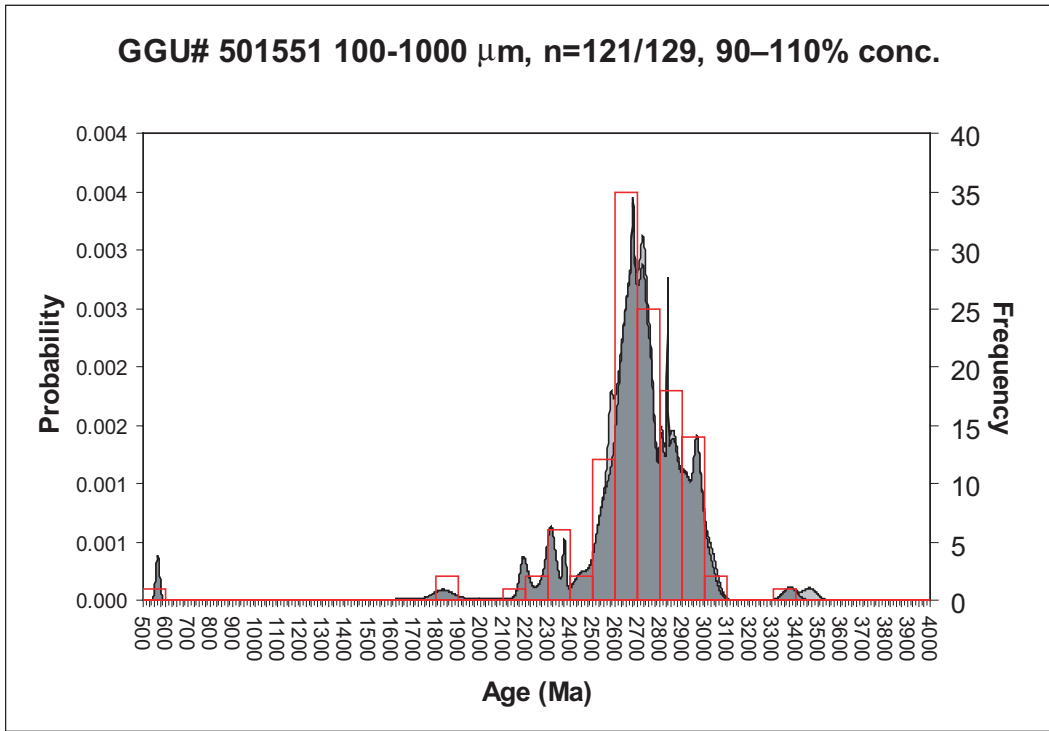
501550



501551

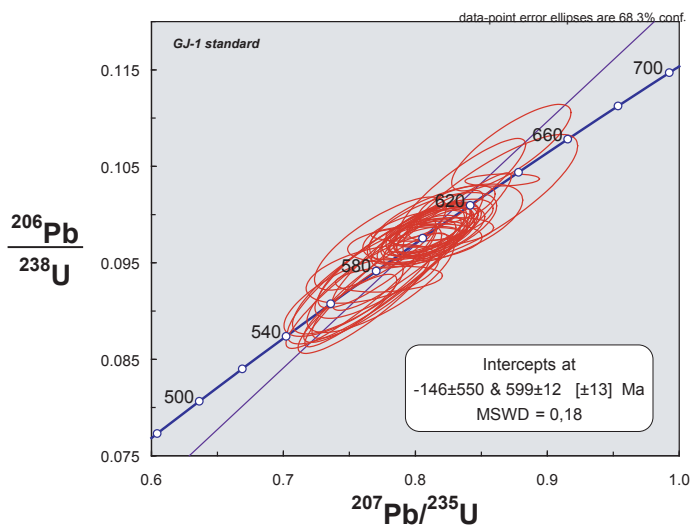
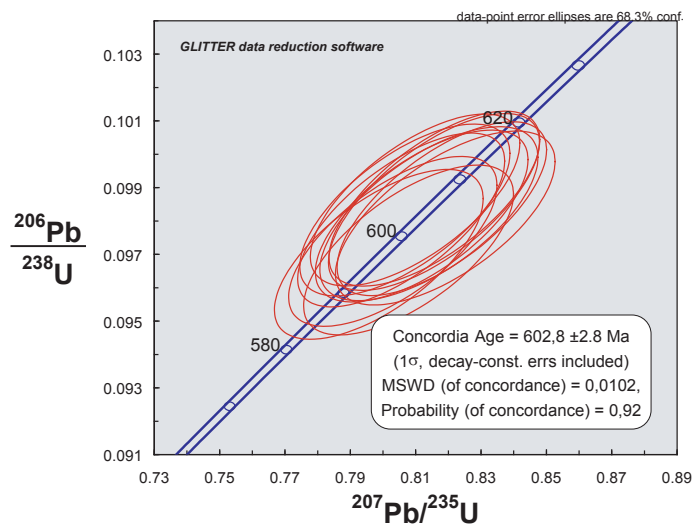
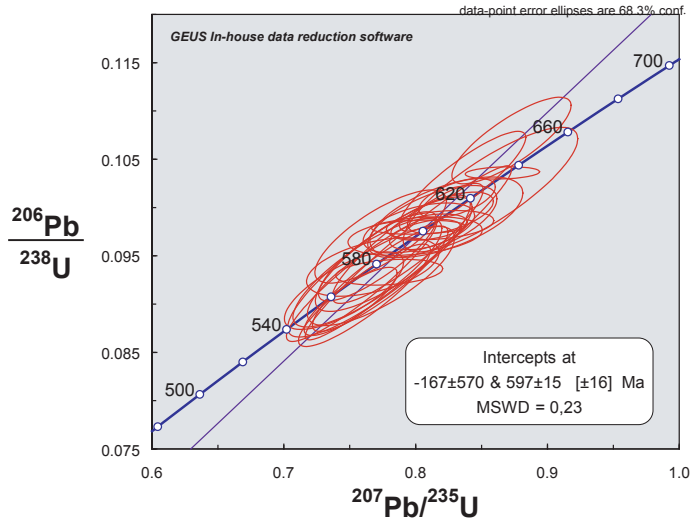


501551



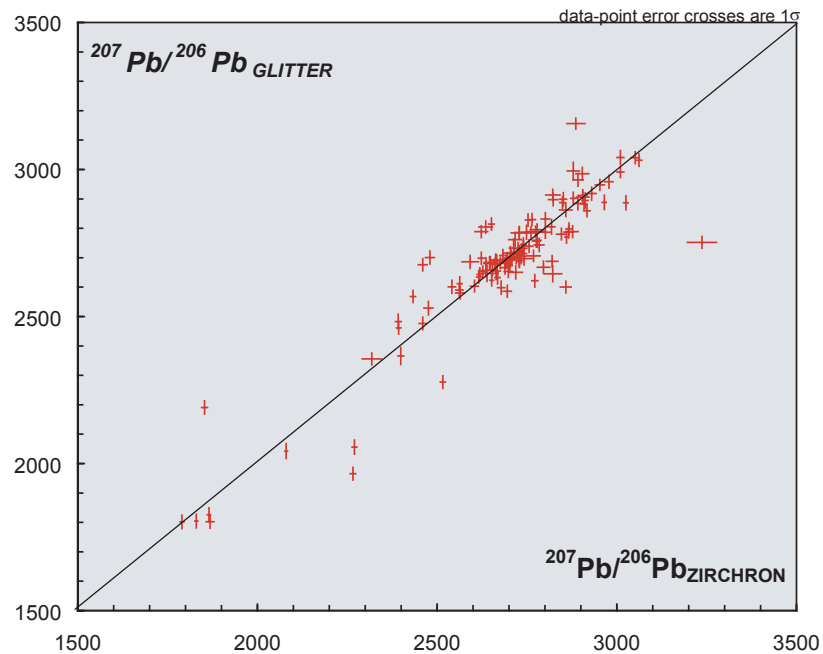
Appendix III – Standard reproducibility

Standard reproducibility of the GEUS primary standard GJ-1.



Appendix IV – Software comparison

Comparison of $^{207}\text{Pb}/^{206}\text{Pb}$ ages for the same data set reduced by the commercially available software GLITTER and the In-house GEUS software ZIRCHRON. The data scatter along a one-to-one slope, which would be expected. The scatter is explained by slightly different interval selections and from the inherent differences in the methodology of the two software packages. GLITTER does not account for common lead as monitored by ^{204}Pb , while ZIRCHRON subtracts any common lead component assuming that the lead was incorporated at the time of zircon crystallisation and that the lead composition conforms with the lead evolution curve of Stacey & Kramers (1975; Earth Planet. Sci. Letters, 26, 207–221).



Appendix V – GIS data representation

The zircon $^{207}\text{Pb}/^{206}\text{Pb}$ age data are available as a GIS-theme from GEUS where age distribution of individual samples is shown as a pie-diagram with linked pdf-files showing the actual age distribution diagram.

